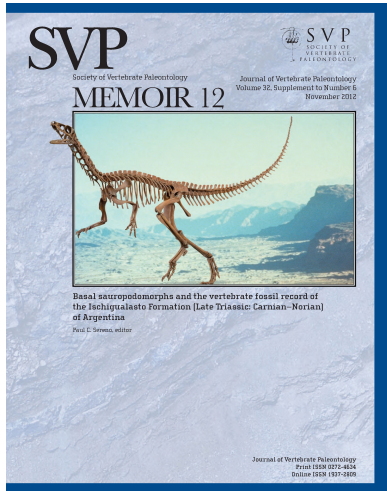


This article was downloaded by: [Society of Vertebrate Paleontology ]

On: 06 November 2013, At: 23:27

Publisher: Taylor & Francis

Informa Ltd Registered in England and Wales Registered Number: 1072954 Registered office: Mortimer House, 37-41 Mortimer Street, London W1T 3JH, UK



## Journal of Vertebrate Paleontology

Publication details, including instructions for authors and subscription information:

<http://www.tandfonline.com/loi/ujvp20>

### Osteology of Eoraptor lunensis (Dinosauria, Sauropodomorpha)

Paul C. Sereno<sup>a</sup>, Ricardo N. Martínez<sup>b</sup> & Oscar A. Alcober<sup>b</sup>

<sup>a</sup> Department of Organismal Biology and Anatomy, and Committee on Evolutionary Biology, University of Chicago, 1027 East 57th Street, Chicago, Illinois, 60637, U.S.A.

<sup>b</sup> Instituto y Museo de Ciencias Naturales, Universidad Nacional de San Juan, San Juan, Argentina, CP5400

Published online: 08 Oct 2013.

To cite this article: Paul C. Sereno, Ricardo N. Martínez & Oscar A. Alcober (2012) Osteology of Eoraptor lunensis (Dinosauria, Sauropodomorpha), Journal of Vertebrate Paleontology, 32:sup1, 83-179, DOI: [10.1080/02724634.2013.820113](https://doi.org/10.1080/02724634.2013.820113)

To link to this article: <http://dx.doi.org/10.1080/02724634.2013.820113>

PLEASE SCROLL DOWN FOR ARTICLE

Taylor & Francis makes every effort to ensure the accuracy of all the information (the "Content") contained in the publications on our platform. However, Taylor & Francis, our agents, and our licensors make no representations or warranties whatsoever as to the accuracy, completeness, or suitability for any purpose of the Content. Any opinions and views expressed in this publication are the opinions and views of the authors, and are not the views of or endorsed by Taylor & Francis. The accuracy of the Content should not be relied upon and should be independently verified with primary sources of information. Taylor and Francis shall not be liable for any losses, actions, claims, proceedings, demands, costs, expenses, damages, and other liabilities whatsoever or howsoever caused arising directly or indirectly in connection with, in relation to or arising out of the use of the Content.

This article may be used for research, teaching, and private study purposes. Any substantial or systematic reproduction, redistribution, reselling, loan, sub-licensing, systematic supply, or distribution in any form to anyone is expressly forbidden. Terms & Conditions of access and use can be found at <http://www.tandfonline.com/page/terms-and-conditions>

## OSTEOLOGY OF *EORAPTOR LUNENSIS* (DINOSAURIA, SAUROPODOMORPHA)

PAUL C. SERENO,<sup>\*1</sup> RICARDO N. MARTÍNEZ,<sup>2</sup> and OSCAR A. ALCOBER<sup>2</sup>

<sup>1</sup>Department of Organismal Biology and Anatomy, and Committee on Evolutionary Biology, University of Chicago, 1027 East 57th Street, Chicago, Illinois, 60637, U.S.A., dinosaur@uchicago.edu;

<sup>2</sup>Instituto y Museo de Ciencias Naturales, Universidad Nacional de San Juan, San Juan, Argentina CP5400, martinez@unsj.edu.ar; oalcober@unsj.edu.ar

**ABSTRACT**—We describe the basal sauropodomorph *Eoraptor lunensis*, based on the nearly complete holotypic skeleton and referred specimens, all of which were discovered in the Cancha de Bochas Member of the Ischigualasto Formation in northwestern Argentina. The lightly built skull has a slightly enlarged external naris and a spacious antorbital fossa with a prominent, everted dorsal margin and internal wall lacking any pneumatic extensions into surrounding bones. The tall quadrate is lapped along its anterior margin by the long, slender ventral process of the squamosal, and the lower jaw has a mid-mandibular joint between a tongue-shaped splenial process and a trough in the angular. All but the posterior-most maxillary and dentary crowns have a basal constriction, and the marginal denticles are larger and oriented more vertically than in typical theropod serrations. Rows of rudimentary palatal teeth are present on the pterygoid. Vertebral centra are hollow, although not demonstrably pneumatized, and all long bones have hollow shafts. The radius and ulna are more robust, the manus proportionately shorter, and the manual unguals less recurved than in the contemporaneous basal theropod *Eodromaeus murphi*. An outstanding feature of the manus of *Eoraptor* is the twisted shaft of the first phalanx of the pollex, which deflects medially the tip of the ungual as in basal sauropodomorphs. The long bones of the hind limb have more robust shafts than those of *Eodromaeus*, although in both genera the tibia remains slightly longer than the femur.

**RESUMEN**—Describimos el sauropodomorfo basal *Eoraptor lunensis* basados en el esqueleto prácticamente completo del holotipo y especímenes referidos, todos ellos descubiertos en el Miembro Cancha de Bochas de la Formación Ischigualasto, en el noroeste de Argentina. El grácil cráneo tiene las narinas externas ligeramente agrandadas, una amplia fosa antorbital con un margen dorsal prominente y evertido, y ausencia de extensiones neumáticas en los huesos circundantes. El alto cuadrado presenta todo su margen anterior solapado por el delgado proceso ventral del escamoso y la mandíbula tiene una junta medial entre un proceso linguoide del esplenial y un canal en el angular. Todas las coronas dentarias y maxilares, menos las más posteriores, tienen una constricción basal y los denticulos marginales son largos y orientados más verticalmente que en el aserrado típico de los terópodos. El pterigoideo tiene filas de dientes palatales rudimentarios. Los centros de las vértebras son huecos, aunque no demostrablemente neummatizados, y todos los huesos largos tienen las diáfisis huecas. El radio y la ulna son más robustos, la mano proporcionalmente corta y los ungueales manuales menos recurvados que en el contemporáneo terópodo basal *Eodromaeus murphi*. Una característica sobresaliente de la mano de *Eoraptor* es la rotación de la primera falange del pulgar, que desvía medialmente la punta del ungueal como en los sauropodomorfos basales. Los huesos largos de las piernas tienen diáfisis más robustas que aquellas de *Eodromaeus*, aunque en ambos géneros la tibia es ligeramente más larga que el fémur.

### INTRODUCTION

Much of the current knowledge about the earliest dinosaurs comes from Late Triassic-aged (Carnian–early Norian) strata of the Ischigualasto Formation in northwestern Argentina (Currie et al., 2009) and the Santa Maria Formation in southeastern Brazil (Langer, 2005). Herrerasaurid theropods, measuring 3–4 m in length, were among the first to be discovered, namely, *Herrerasaurus ischigualastensis* from Argentina (Reig, 1963; Sereno and Novas, 1992, 1994; Sereno, 1994) and *Staurikosaurus pricei* from Brazil (Colbert, 1970; Bittencourt and Kellner, 2009). Recent work in the Ischigualasto Formation of Argentina has added another herrerasaurid, *Sanjuansaurus gordilloi*, to this group (Alcober and Martínez, 2010).

Basal dinosaurs of short body length, 2 m or less, were discovered along with the first herrerasaurids (*Pisanosaurus*; Casamiquela, 1967; Bonaparte, 1976), although more complete remains would not come to light in either Argentina or Brazil until the 1990s. In Argentina, one basal theropod, *Eodromaeus* (Martínez et al., 2011), and three basal sauropodomorphs, *Eoraptor* (Sereno et al., 1993), *Panphagia* (Martínez and Alcober, 2009), and *Chromogisaurus* (Ezcurra, 2010), have been described. Two additional basal sauropodomorphs have been described from

Brazil, *Saturnalia* (Langer et al., 1999, 2007; Langer, 2003) and *Pampadromaeus* (Cabreira et al., 2011).

The holotypic specimen of *Eoraptor lunensis* comprises the single most complete skull and postcranial skeleton of a Carnian-aged dinosaur. During the 1991 Argentine-American Expedition, one of the authors (R.N.M.) lifted its skull from a reddish-gray siltstone outcrop in the lower portion of the Ischigualasto Formation in the Valle de la Luna ('Valley of the Moon') of Ischigualasto Provincial Park (Gore, 1993) (Figs. 1, 2A). The region local to the find is known as Cancha de Bochas ('Field of Balls'), named after the abundant sandstone concretions in the area that weather free as spheroids (Fig. 2D). The skull was completely covered by a layer of gray hematitic cement, except for the labial surface of two maxillary crowns (Fig. 2C). The remainder of the skeleton lay underneath a thin layer of matrix except for the distal one-half of the tail, which had eroded away (Fig. 2B). The following description is based primarily on the holotypic skeleton.

Other, less complete material referred to *Eoraptor lunensis* came to light before and after discovery of the holotypic specimen (Table 1). Some of these specimens provide important information unavailable or poorly exposed in the holotype, such as vertebral morphology obscured by articulation and the complete morphology and articular relations of the distal crus and proximal tarsals. The most important of these was discovered in the wall of

\*Corresponding author.



FIGURE 1. Type locality of *Eoraptor lunensis* in the Ischigualasto Formation at the southern end of the Valle de Luna in a fossiliferous area known as Cancha de Bochas. Photograph taken in 1991 looking south with lava-capped Cerro Morado in the background (photograph by P.C.S.).

the trench during excavation of the holotype and preserves two anterior dorsal vertebrae and most of an articulated right hind limb, none of which was encrusted with the hematitic cement present on the adjacent holotypic skeleton. We discuss several aspects of

TABLE 1. Holotypic and referred material of *Eoraptor lunensis*.

Specimen	Maturity	Description
PVSJ 512 (holotype)	Adult	Skull and articulated skeleton lacking most of left scapulocoracoid, most of left manual phalanges, and caudal vertebrae posterior to caudal vertebra 17
PVSJ 559	Adult	Two anterior dorsal vertebrae, rib shafts, partial right hind limb including a femur lacking the head, tibia, distal one-half of the fibula, astragalus, calcaneum, and metatarsal fragments
PVSJ 745	Subadult	Lower portion of the braincase including the basioccipital and basisphenoid, several partial cervical and dorsal vertebrae, portions of right and left ilia, section of ischial shaft, proximal and distal ends of both femora, proximal end of both tibiae, proximal end of right fibula, and proximal ends of two metatarsals
PVSJ 852	Subadult	Right femur
PVSJ 855	Adult	Right femur
PVSJ 860	Adult	Proximal and distal ends of left femur, distal end of right femur, proximal and distal ends of right tibia, proximal end of left tibia, and proximal end of right fibula
PVSJ 862	Subadult	Proximal end of right humerus, distal ends of both femora, distal end of right tibia, proximal end of right fibula, and right astragalus
PVSJ 876	Adult	Right femur lacking midsection

All specimens come from the Cancha de Bochas Member of the Ischigualasto Formation in the local region known as Cancha de Bochas. PVSJ 559 was found in the wall of the trench around the holotypic skeleton (PVSJ 512) during excavation.

TABLE 2. Blocks composing the holotypic skeleton of *Eoraptor lunensis* (PVSJ 512) after mechanical preparation (see Fig. 4).

Block	Description
1	Skull, proAtlas, atlas, and anterior portion of the axis
2	Axis (posterior portion) and cervical vertebrae 3–8 and associated ribs
3	Cervical vertebra 9, dorsal vertebrae 1 and 2 and associated ribs
4	Right manus
5	Dorsal vertebrae 3–5 and associated ribs, right scapulocoracoid, right forelimb except the manus, and distal left scapular blade
6	Left forelimb
7	Dorsal vertebrae 6–12 and associated ribs, both pubic blades, most of the left hind limb, and some gastralia
8	Articulated series of partial gastralia
9	Dorsal vertebrae 13 and 14 and associated ribs
10	Dorsal vertebra 15, sacrum, caudal vertebrae 1–3 and associated chevrons, associated ribs, both ilia, proximal pubes and ischia, and most of the right hind limb
11	Distal portion of the right pes
12	Distal ischia, distal right femur, and proximal right tibia and fibula
13	Caudal vertebrae 4 and 5 and associated chevrons
14	Caudal vertebrae 6–9 and associated chevrons
15	Caudal vertebrae 10–12 and associated chevrons
16	Caudal vertebrae 13–17 and associated chevrons

cranial and postcranial function in light of the new descriptive and comparative information.

**Institutional Abbreviations**—**AMNH**, American Museum of Natural History, New York, New York, U.S.A.; **MACN**, Museo Argentino de Ciencias Naturales, Buenos Aires, Argentina; **MCZ**, Museum of Comparative Zoology, Harvard University, Cambridge, Massachusetts, U.S.A.; **MOR**, Museum of the Rockies, Bozeman, Montana, U.S.A.; **MWC**, Museum of Western Colorado, Grand Junction, Colorado, U.S.A.; **NHMUK**, The Natural History Museum, London, U.K.; **PVSJ**, Museo de Ciencias Naturales, Universidad Nacional de San Juan, San Juan, Argentina; **UCMP**, University of California, Museum of Paleontology, Berkeley, California, U.S.A.; **USNM**, National Museum of Natural History, Washington, D.C., U.S.A.; **UUVP**, University of Utah, Vertebrate Paleontology Collections, Salt Lake City, Utah, U.S.A.; **YPM**, Yale University, Peabody Museum, New Haven, Connecticut, U.S.A.

## MATERIALS AND METHODS

### Fossil Preparation

The holotypic skeleton of *Eoraptor lunensis* (PVSJ 512) was contained within a single irregular concretion that formed a

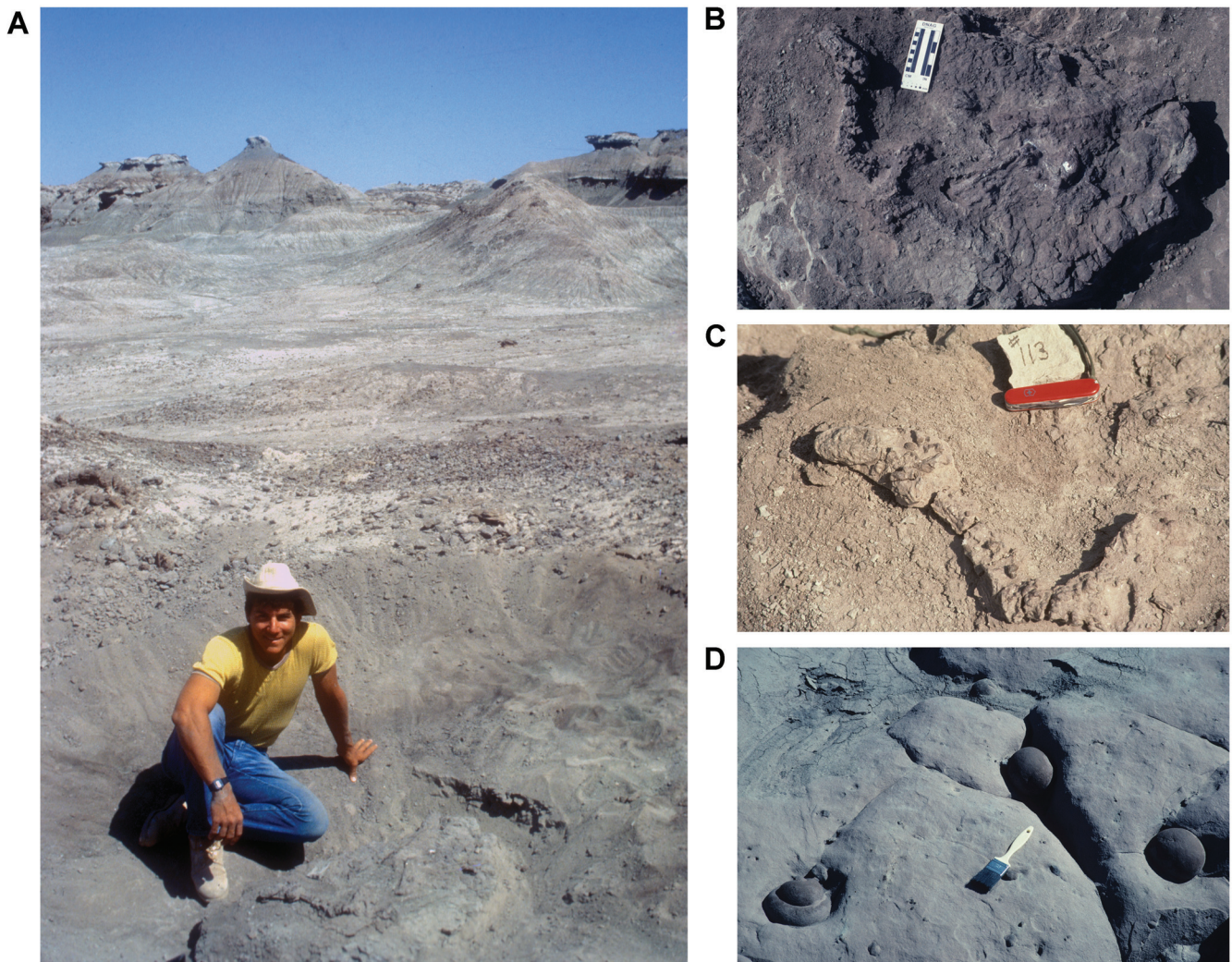


FIGURE 2. Type locality of *Eoraptor lunensis* in the Ischigualasto Formation. **A**, view to the south of the excavation site showing a shallow drainage (by the left hand of P.C.S.) that truncated the tail at midlength. **B**, holotypic skeleton (PVSJ 512) as exposed prior to jacketing. **C**, the skull and neck of the holotypic skeleton (PVSJ 512) encrusted in a hematitic matrix. **D**, spheroidal, hematitic, sandstone concretions weathering out near the type locality in Cancha de Bochas ('field of balls'), Valle de Luna, Ischigualasto.

thin layer over most of the external bone surfaces (Fig. 2B, C). The concretion and surrounding matrix blend together; both are composed of a red-brown, hematitic, muddy siltstone, which was tightly adhered to the beige-colored bone. Although the matrix is calcareous, it was not detectably weakened by topical treatment with strong hydrochloric acid. Preparation, therefore, was accomplished entirely by hand with carbide-tipped dental picks and pneumatic scribes with final cleaning by air abrasives (Fig. 3). The skull and anterior-most end of the cervical column was separated from the remainder of the postcranial skeleton, which was divided into 15 blocks (Fig. 4; Table 2).

#### Anatomical Orientation and Terms

We employ traditional, or 'Romerian,' directional terms over veterinarian alternatives (Wilson, 2006). 'Anterior' and 'posterior,' for example, are used as directional terms rather than the veterinarian alternatives 'rostral' or 'cranial' and 'caudal.' We fol-

low Wilson (1999) and Wilson et al. (2011) regarding terminology for vertebral laminae and fossae, respectively.

#### Computed Tomography

Computed tomographic (CT) scans were taken of the holotypic skull of *Eoraptor lunensis* (PVSJ 512) at the High-Resolution X-ray Computed Tomography Facility at The University of Texas at Austin. Three orthogonal rotations (roll, pitch, yaw) and three orthogonal slice movies (coronal, horizontal, sagittal) are available online ([http://digimorph.org/specimens/Eoraptor\\_lunensis](http://digimorph.org/specimens/Eoraptor_lunensis)). Although the CT imaging provides valuable information on cross-sectional shape and on some internal morphology, discerning the boundaries between bone, tooth, and matrix in many regions of the skull is difficult or impossible.

More useful cross-sectional information was gleaned from breakage surfaces between skeletal blocks (Fig. 4), which provided information on the internal structure of the axial column and many long bones.

A



B



FIGURE 3. Photograph of the skull of *Eoraptor lunensis* (PVSJ 512) after preparation. **A**, lateral view of the right (down) side of skull. **B**, enlarged right lateral view of the snout. Scale bar equals 5 cm in **A** and 2 cm in **B**.

## GEOLOGIC SETTING

### Stratigraphic Position

The Ischigualasto-Villa Unión Basin of northwestern Argentina is part of an extensional rift system that developed within the southern end of South America and southern Africa during an early stage in the breakup of southern Pangaea (Currie et al., 2009). The basin fill comprises a thick nonmarine sequence of Triassic rocks, the Agua de la Peña Group, which includes the mid-Carnian to early Norian Ischigualasto Formation (Fig. 1; see Martínez et al., 2011; Martínez et al., 2013).

The most abundant vertebrate fossils come from the lower two members (La Peña and Cancha de Bochas members), which are well exposed along the southern edge of the basin in a region called the Valle de la Luna. All of the remains of *Eoraptor lunensis* come from the Cancha de Bochas Member in the Valle de la Luna (Fig. 1), which has been radioisotopically dated to the mid-Carnian (ca. 231.4 Ma; Rogers et al., 1993; Martínez et al.,

2011). The holotypic specimen of *Eoraptor lunensis* (PVSJ 512) was found approximately 93 m above the unconformity between the Los Rastros and Ischigualasto formations in an overbank deposit composed of reddish-gray, calcareous and hematitic, muddy siltstone. Referred specimens come from near the same level and area (Table 1; Martínez et al., 2013).

### Associated Fauna

Fossil vertebrates found near *Eoraptor lunensis* within the local area of the Cancha de Bochas include the basal theropod *Herrerasaurus ischigualastensis* (Novas, 1994; Sereno, 1994, 2007a; Sereno and Novas, 1994), the traversodontid cynodont *Exaeretodon argentinus* (Bonaparte, 1966), the carnivorous cynodonts *Ecteninion lunensis* (Martínez et al., 1996), *Problepsodon sanjuanensis* (Martínez and Forster, 1996) and *Probainognathus* sp. (Bonaparte and Crompton, 1994), the dicyodont *Ischigualastia jenseni* (Cox, 1965), the crurotarsan archosaur

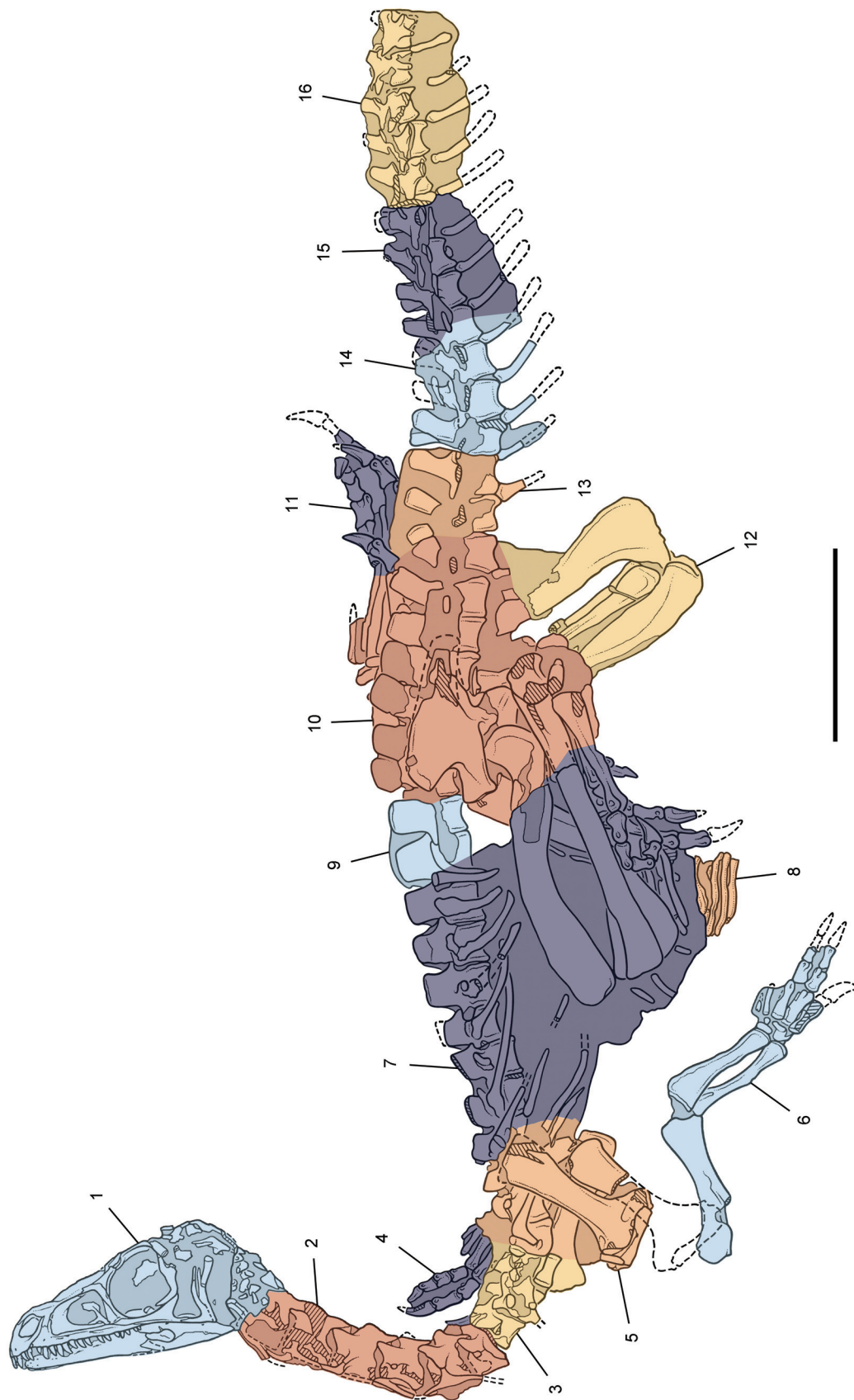


FIGURE 4. Drawing of the skeleton of *Eoraptor lunensis* (PVSJ 512) in left lateral view showing by colored areas the division of the specimen into 16 blocks after mechanical preparation (see Table 2). Dashed line indicates a missing margin; hatching indicates a broken surface; shading indicates matrix. Scale bar equals 10 cm.



FIGURE 5. Photograph of the skeleton of *Eoraptor luanensis* (PVSJ 512) in left lateral view. A small ventral block with several partial gastralia is not included. Scale bar equals 10 cm.





FIGURE 7. Photograph of the skeleton of *Eoraptor lunensis* (PVSJ 512) in right lateral view. Small ventral block with several partial gastralia is not included. Scale bar equals 10 cm.

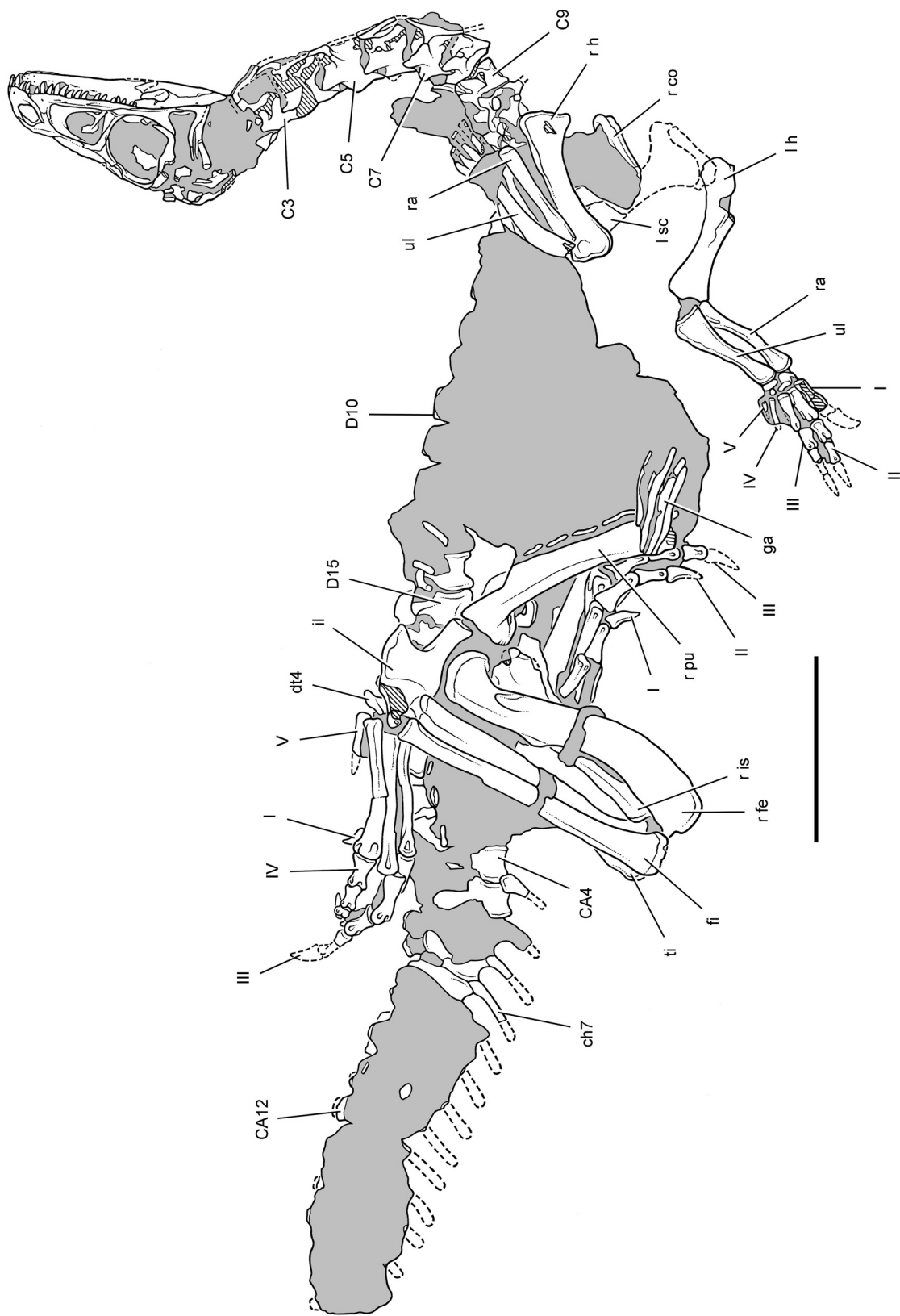


FIGURE 8. Drawing of the skeleton of *Eoraptor lunensis* (PVSJ 512) in right lateral view. Small ventral block with several partial gastralia is not included. **Abbreviations:** I-V, manual and pedal digits I-V; C3, 5, 7, 9, CA4, 12, caudal vertebra 3, 5, 7, 9; CA4, 12, cervical vertebra 4, 12; ch7, chevron 7; co, coracoid; D10, 15, dorsal vertebra 10, 15; dt4, distal tarsal 4; fe, femur; fi, fibula; ga, gastralia; h, humerus; il, ilium; is, ischium; I, left; pu, pubis; r, right; ra, radius; sc, scapula; ti, tibia; ul, ulna. Dashed line indicates a missing margin; hatching indicates a broken surface; shading indicates matrix. Scale bar equals 10 cm.

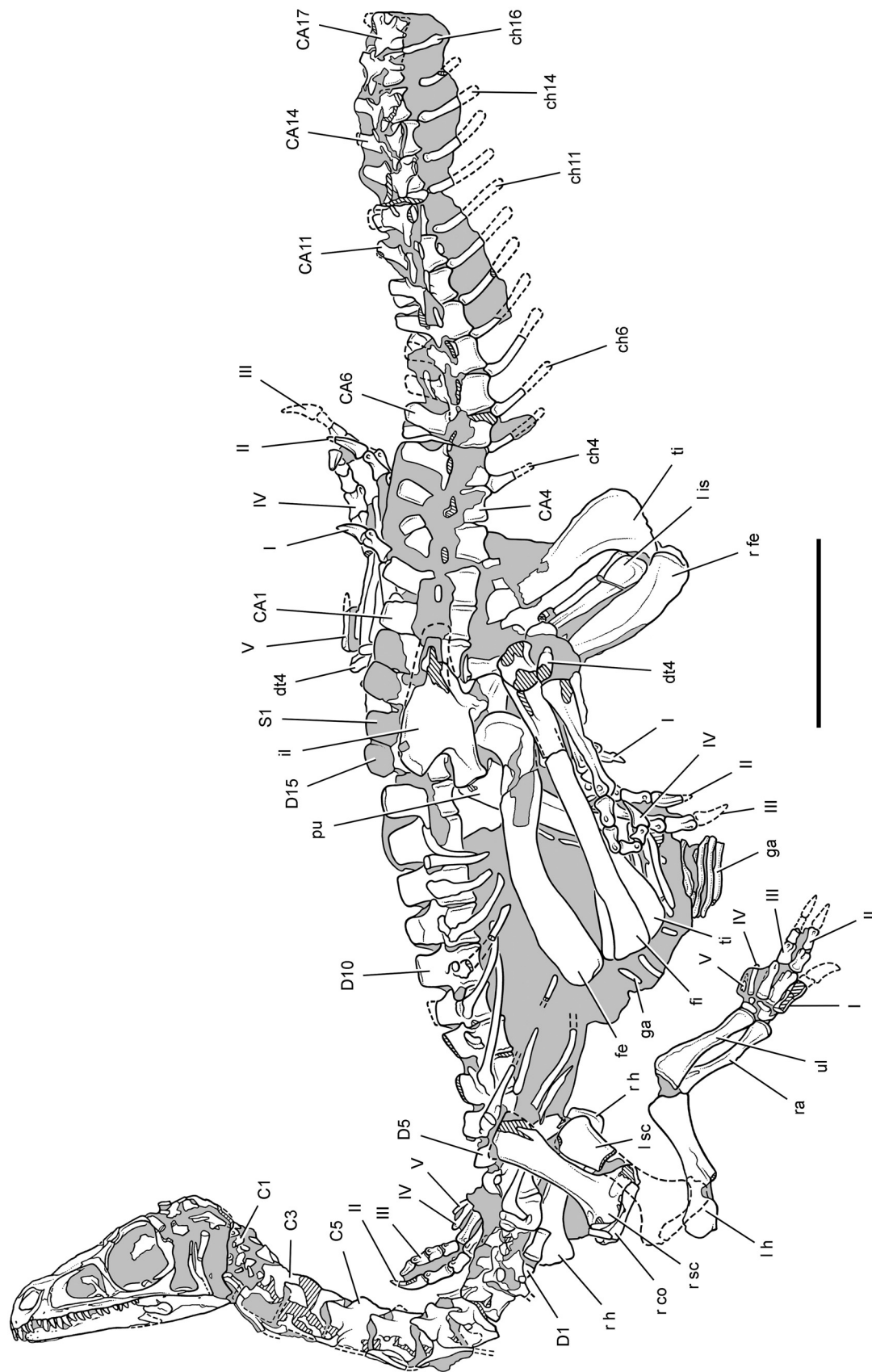


FIGURE 9. Composite drawing of the skeleton of *Eoraptor lunensis* (PVSJ 512) in left lateral view, with information added from the opposite side when bones are obscured by matrix. Small ventral block with several partial gastralia is included. **Abbreviations:** I–V, manual and pedal digits 1–5; **CA1, 3, 5, 6, 11, 14, 17**, cervical vertebra 1, 3, 5; **CA1, 4, 6, 11, 14, 17**, caudal vertebra 1, 4, 6, 11, 14, 17; **ch4, 6, 11, 14, 16**, chevron 4, 6, 11, 14, 16; **co**, coracoid; **D1, 5, 10, 15**, dorsal vertebra 1, 5, 10, 15; **dt4**, distal tarsal 4; **fe**, femur; **fi**, fibula; **ga**, gastralia; **h**, humerus; **il**, ilium; **is**, ischium; **l**, left; **pu**, pubis; **r**, right; **ra**, radius; **ra**, radius; **sc**, scapula; **sc**, scapula; **ti**, tibia; **ul**, ulna. Dashed line indicates a missing margin; hatching indicates a broken surface; shading indicates matrix. Scale bar equals 10 cm.

*Saurosuchus galilei* (Sill, 1974), and abundant remains of the rhynchosaur *Scaphonyx sanjuanensis* (Huene, 1926a). For a complete faunal list, see Martínez et al. (2013).

### Taphonomy

The holotypic skeleton of *Eoraptor lunensis* was buried on its right side (Figs. 2A–C, 4–9). The jaws are tightly opposed, and the skull and neck are flexed dorsally. Both hind limbs are folded close to the body. This configuration suggests that the interspinous ligaments on the dorsal aspect of the cervical column and flexor tendons on the ventral aspect of the hind limbs shortened before burial, as a result of subaerial desiccation, tetanus, or both (Marshall Faux and Padian, 2007). These ligaments and tendons are larger and/or more numerous than those that effect the opposing action on the axial column or hind limb, and so perhaps it is not surprising that they control postmortem movement.

Subaerial exposure prior to burial is also suggested by the poorer preservation of bone surfaces on the left (upper) side of the skeleton. This is particularly apparent in the pelvic girdle and hind limb, which were covered in concretion and could not have been altered by recent erosion. The skull shows similar differential preservation (left/upper side weathered; right/lower side well preserved), but some loss on the upper side is probably the result to surface erosion (Figs. 10–13).

All skeletal elements are preserved in articulation except the right scapula, which was dislocated and rotated from the underside of the carcass to the opposite side of the rib cage (Fig. 9). It is not clear how this dislocation took place, because the associated right forelimb remains close to its anatomical location on the underside of the carcass (Figs. 7, 8). Postmortem scavenging is a weak explanation for this displacement, because no tooth marks nor other signs of selective postmortem movement are discernable. The gastral cuirass, for the most part, is in a position anterior to the distal end of the pubes, and so the trunk cavity appears to have been intact at final interment (Fig. 9).

Although the carcass may have been dehydrated before burial, there are no skin impressions. The carpals, tarsals, and cartilage-covered ends of the long bones are sometimes difficult to distinguish from the matrix. The external surface of the left astragalus, for example, blends into the surrounding matrix. In some cases, the boundaries between bones have been nearly obliterated by postmortem mineralization and recrystallization. The articulated proximal ends of the right tibia and fibula, for example, blend together where they are in contact.

All vertebral centra and long bones are hollow, with extensive internal cavities bounded by thin walls. As a result, some bones have been crushed and flattened after burial. The medullary cavity in the left ulna, for example, has collapsed so that the medial side of the bone is concave rather than convex. Postmortem crushing is strongest in the left forelimb, although many bones have local areas of collapse or brittle fracture.

A very small (3 mm long), subconical, recurved crown is preserved lying against the posterior side of the right posterolateral wing of the parietal at the back end of the skull. The crown does not belong to *Eoraptor* but pertains to an unknown small carnivore. Because the crown does not appear to be transversely compressed or striated, it is unlikely to be from a carnivorous archosaur. Other disarticulated bones from animals larger than *Eoraptor*, such as the crurotarsan archosaur *Saurosuchus*, were also found near the skeleton. Because articulated and disarticulated vertebrate fossils were fairly common in the general area (Cancha de Bochas) where the skeleton of *Eoraptor* was discovered, there is probably no special significance to the proximity of the small tooth and occiput of *Eoraptor*.

A second partially articulated specimen of *Eoraptor* (PVSJ 559) was discovered in the outer wall of the excavation trench around the holotypic skeleton (Fig. 2A). It consists of two anterior dorsal vertebrae, rib shafts, a partial articulated right hind limb including a femur (lacking the head), tibia, distal one-half of the fibula, astragalus, calcaneum, and metatarsal fragments (Table 1).

### Skeletal Maturity

At the time of death, the holotypic skeleton appears nearly mature and may have been approaching maximum adult body size. Most of the bones of the skull are tightly articulated, and the neural arches and centra are fully coossified along the vertebral column. The apparent separation of some neural arches from their respective centra (e.g., anterior cervical vertebrae, mid-caudal vertebrae) is due to postmortem fracturing of the thin lateral wall of the neural canal. The best-preserved and exposed vertebrae include cervical vertebrae 5–7 and 9, dorsal vertebrae 7 and 9, and caudal vertebrae 8 and 11 (Fig. 9). In these vertebrae, the neural arch and centrum are intimately articulated with partial or complete obliteration of the neurocentral suture.

A few sutures, nevertheless, remain open and unfused in the holotypic specimen. These include the neurocentral sutures in the sacral vertebrae, the contact between the sacral ribs and iliac blade ('iliocostal junction'; Wilson, 2011), and the scapulocoracoid suture. The holotypic skeleton (PVSJ 512), thus, may have been a young adult approaching skeletal maturity.

### Adult Body Length

Nearly all of the referred material is very comparable in size; some specimens are slightly larger and others slightly smaller than the holotype (Table 1). The long bones of the partial hind limb found in the trench wall (PVSJ 559) near the holotype are approximately 9% longer (tibial length = 170 vs. 156 mm). The preserved portion of the holotypic skeleton (skull to mid-tail) measures 90 cm in length. Caudal vertebrae 1–17 constitute approximately one-half of tail length, judging from other dinosaurs that do not show caudal elongation or other caudal specializations (e.g., *Plateosaurus*; Huene, 1926b). The anterior one-half of the tail measures 30 cm, suggesting an overall body length of 120 cm for the holotypic skeleton. PVSJ 559, in turn, would measure approximately 130 cm in length.

Although a larger sample size is needed to increase confidence, it may well be that *Eoraptor lunensis*, like the closely related basal sauropodomorphs *Panphagia protos* (Martínez and Alcober, 2009), *Chromogisaurus novasi* (Ezcurra, 2010), and *Pampadro-maeus barberenei* (Cabeira et al., 2011), reached maximum body length at just under 150 cm in length.

## SYSTEMATIC PALEONTOLOGY

DINOSAURIA Owen, 1842

SAURISCHIA Seeley, 1887

SAUROPODOMORPHA Huene, 1932

*EORAPTOR* Sereno, Forster, Rogers, and Monetta, 1993

*EORAPTOR LUNENSIS* Sereno, Forster, Rogers,

and Monetta, 1993

(Figs. 3–93)

**Holotype**—PVSJ 512, articulated skeleton lacking portions of the left side of the skull, caudal vertebrae distal to caudal vertebra 17, most of the left scapula, left coracoid, left manual unguals, and the distal two phalanges of right pedal digit III (Figs. 5–9).

**Type Locality and Horizon**—S31°06'4", W68°54'18", along the northeastern edge of Cancha de Bochas, Valle de la Luna, Ischigualasto Provincial Park, San Juan, Argentina. The skeleton



FIGURE 10. Stereopair of the skull of *Eoraptor lunensis* (PVSJ 512) in right lateral view. Scale bar equals 5 cm.

was located approximately 93 m above the base of the Ischigualasto Formation (Rogers et al., 1993).

**Age**—Mid-Carnian on the basis of a radioisotopic date ( $Ar^{40}/Ar^{39}$ ) not far in section below the type locality (Rogers et al., 1993) and recently recalibrated to 231.4 Ma (Gradstein and Ogg, 2009; Martínez et al., 2011).

**Revised Diagnosis**—Small basal sauropodomorph with the following autapomorphies: premaxilla posterolateral process slender with tongue-shaped distal expansion; nasal with transversely broad, horizontal shelf with a convex lateral margin that overhangs the antorbital fossa; pterygoid process on posterior palate margin that articulates laterally in a synovial socket in the ectopterygoid; narrow premaxilla-maxilla diastema approximately one crown in width; maxillary crowns with a prominent lateral eminence; accessory articular process on the medial aspect of mid-cervical prezygapophyses; extreme hollowing of dorsal centra and neural arches.

*Eoraptor lunensis* can be differentiated from *Panphagia protos* by its shallow neurovascular groove on the lateral aspect of the dentary, less pronounced ridge on the lateral aspect of the surangular, less expanded distal scapular blade (approximately twice neck width), more perpendicular distal border on scapular blade, longer pubic blades (more than four times distal blade width), tibial cnemial crest and opposing proximal condyles more anteroposteriorly expanded, tibial distal end more transversely expanded, and the ascending process and posterior fossa on the astragalus much broader transversely (approximately one-third the width of the astragalus).

*Eoraptor lunensis* can be differentiated from *Chromogisaurus novasi* by the more strongly inturned femoral head, the markedly asymmetrical shape of the fourth trochanter, the tibial cnemial crest and opposing proximal condyles more anteroposteriorly expanded, and the tibial distal end more transversely expanded. Several of these points of distinction may have been influenced by weathering or crushing in *Chromogisaurus novasi*, which is not as well preserved as material pertaining to *Eoraptor lunensis*.

**Referred Specimens**—One referred specimen (PVSJ 559) was found in the wall of the excavation trench approximately 25 cm from the holotypic skeleton. Other specimens (PVSJ 745, 852, 855, 860, 862, 876) were found in the same region (Cancha de Bochas) and include a few braincase elements, some cervical and dorsal vertebrae, two partial hind limbs, and three femora (Table 1). Two specimens, PVSJ 559 and 862, are well preserved and provide the best view of the morphology of the anterior dorsal vertebrae, femur, tibia, fibula, and proximal tarsals.

PVSJ 559 is the most complete referred specimen and thus has the most overlap with other sauropodomorphs from the Ischigualasto Formation. The tibia and astragalus have the broad proportions characteristic of *Eoraptor lunensis* compared with *Panphagia protos*, as differentiated above. The ascending process of the astragalus in PVSJ 559 and 862, for example, constitutes approximately one-third of the width of the bone, unlike the much narrower condition in *Panphagia protos* (Martínez and Alcober, 2009:fig. 9D). The prominent anteromedial corner of the astragalus in both specimens (PVSJ 559, 862) is a

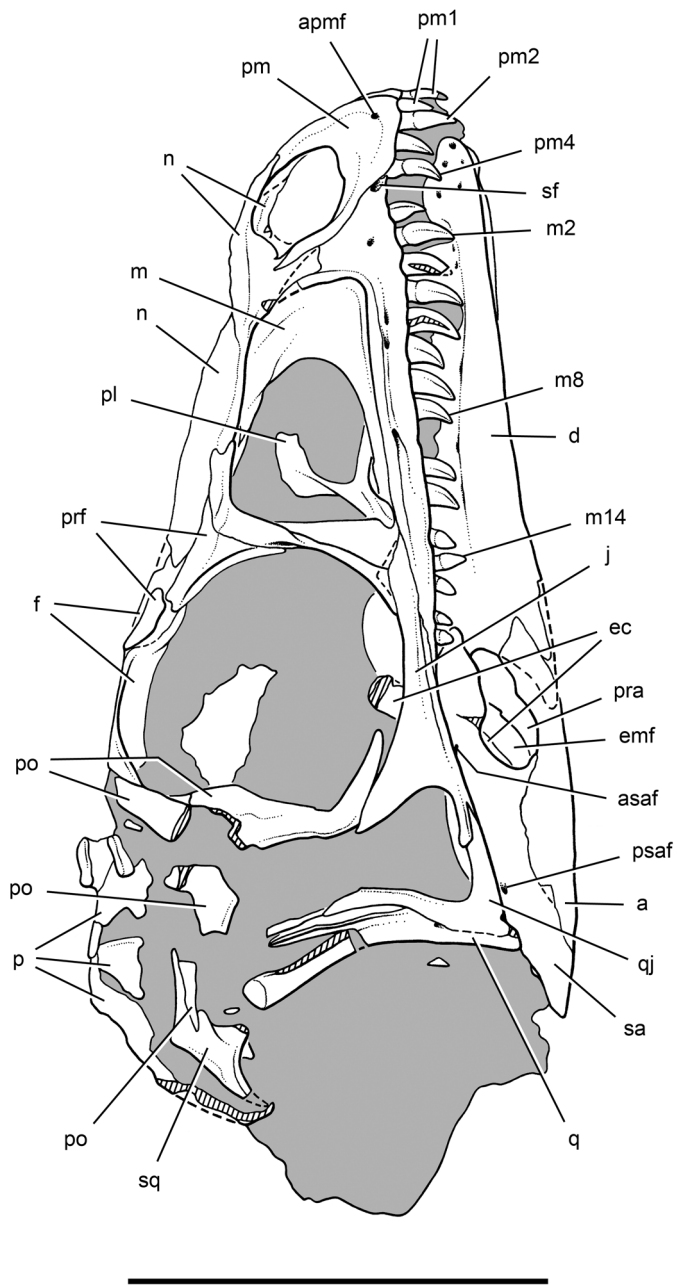


FIGURE 11. Drawing of the skull of *Eoraptor lunensis* (PVSJ 512) in right lateral view. **Abbreviations:** a, angular; apmf, anterior premaxillary foramen; asaf, anterior surangular foramen; d, dentary; ec, ectopterygoid; emf, external mandibular fenestra; f, frontal; j, jugal; m, maxilla; m2, 8, 14, maxillary tooth 2, 8, 14; n, nasal; p, parietal; pl, palatine; pm, premaxilla; pm1, 2, 4, premaxillary tooth 1, 2, 4; po, postorbital; pra, prearticular; prf, prefrontal; psaf, posterior surangular foramen; q, quadrate; qj, quadratejugal; sa, surangular; sf, subnarial foramen; sq, squamosal. Dashed line indicates a missing margin; hatching indicates a broken surface; shading indicates matrix. Scale bar equals 5 cm.

sauropodomorph synapomorphy, but that feature cannot differentiate among sauropodomorph genera within the Ischigualasto Formation.

Referral of the more fragmentary specimens is more tentative (PVSJ 852, 855, 860, 876). The bone most commonly preserved

among these specimens is the femur, which in its entirety or as broken ends does resemble the femur in the holotype. Among other Ischigualasto sauropodomorphs, however, the femur is known only in *Chromogisaurus novasi* and is crushed. So referral of these specimens to *Eoraptor lunensis* on the basis of the femur is not strongly supported and must remain tentative.

## DESCRIPTION

### Skull Overview

The skull of *Eoraptor* is subtriangular in lateral and dorsal views and deeper than wide in posterior view (Figs. 10–19; Table 3). The external naris is slightly enlarged as in other sauropodomorphs, such that its maximum diameter is at least 50% that of the orbit (Fig. 20). The orbit in *Eoraptor* is large relative to skull length. This is viewed here as an allometric consequence of small body size, because it is the usual condition in dinosaurs of comparable size (e.g., *Lesothosaurus*; Sereno, 1991). The sidewalls of the orbit are concave dorsally and posteriorly. In anterior of the skull (Fig. 18), the orbital flange on the postorbital projects laterally.

The sidewall of the skull is occupied by a large antorbital fossa, which does not extend as diverticulae into bordering cranial bones, as commonly occurs in neotheropods (Figs. 21, 22). The ventral margin of the antorbital fossa and anterior end of the snout have neurovascular openings similar to that in basal sauropodomorphs, which include anterior dentary and premaxillary foramina, a subnarial foramen, and a row of foramina on the maxilla that ends in one large foramen that opens posteriorly (Figs. 21–23). The row of foramina ventral to the antorbital region with the posterior-most foramen opening posteriorly characterizes basal sauropodomorphs (e.g., *Plateosaurus*, Galton, 1984; *Masospondylus*, Sues et al., 2004; *Adeopapposaurus*, Martínez, 2009). The lacrimal has only a shallow antorbital invagination and shares the anterodorsal margin of the orbit margin with a relatively large prefrontal, as is common among basal sauropodomorphs (Figs. 24, 25; Sereno, 2007b). The laterotemporal fenestra has a broad, hour-glass shape in lateral view and is bordered posteriorly by slender opposing processes of the squamosal and quadratejugal, as is also

TABLE 3. Measurements (in mm) of the skull of *Eoraptor lunensis* (PVSJ 512).

Dimension	Measurement
Skull length	123
Preorbital skull length	54
Posterior skull height	43
Width of quadrate condyles	10
Transverse width of occiput	(36)
Quadrate height	34
Maximum diameter of external naris	15
Minimum interorbital orbital width	17
Maximum snout width	32
Maximum temporal width	(42)
Vertical diameter of orbit	34
Anteroposterior diameter of orbit	33
Maximum length of antorbital fossa	36
Maximum length of antorbital fenestra	20
Length of upper tooth row	68
Drop in jaw articulation (from maxillary alveolar margin)	7
Maximum height of lower jaw	18
Length of lower jaw	110

Paired structures are measured from the right side. Skull length and posterior skull height were reduced to account for minor displacement of the upper temporal bar and dislocation of the head of the quadrate from the squamosal, respectively. Maximum snout width was increased slightly to account for imbrication of the nasals near the midline. Parentheses indicate estimated measurement.

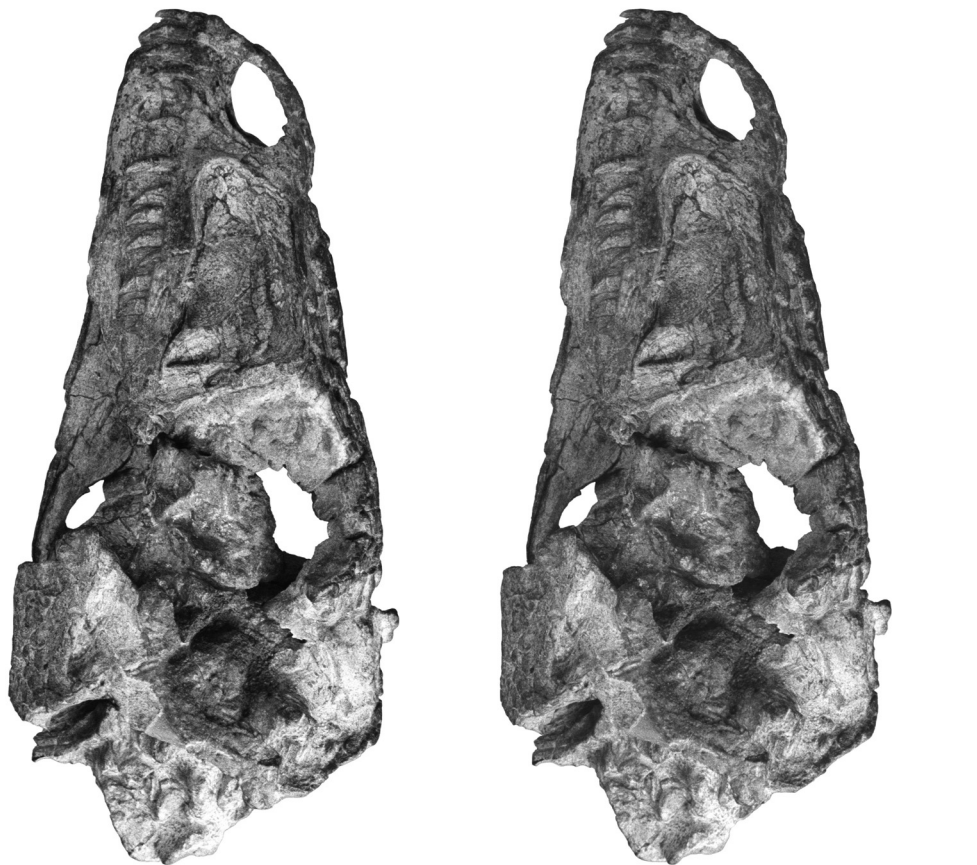


FIGURE 12. Stereopair of the skull of *Eoraptor lunensis* (PVSJ 512) in left lateral view. Scale bar equals 5 cm.

typical of basal sauropodomorphs (Fig. 26; Sereno, 2007b). On the better-preserved right side of the skull, the quadrate is disarticulated from the squamosal. The quadrate cotylus of the squamosal surrounds the quadrate head, unlike the more exposed articulation seen in many theropods (e.g., *Herrerasaurus*; Sereno and Novas, 1994) (Figs. 26, 27).

The dorsal skull roof is more fractured than is either side of the skull (Figs. 14, 15). The fracturing is most pronounced posterior to the orbits, where the roof over the braincase is offset several millimeters to the right. Postmortem transverse compression of the skull is most apparent on the roof of the snout, where the right nasal overlaps the left. The oval supratemporal fossa has a rounded anterior rim, unlike the sharply defined edge and depression in *Herrerasaurus* (Sereno and Novas, 1994).

The palate is transversely compressed and slightly dislodged from its natural articulation with the skull roof and braincase (Fig. 16). Anteriorly, the palatines have been displaced dorsally toward the skull roof, as seen through the left antorbital fenestra (Fig. 21). The dorsal displacement of the palate is greatest at its anterior end, where the footplate of the vomer is lodged against the roof of the nasals within the external naris (Fig. 28). The posterior palate has been transversely compressed, the pterygoids overlapping unnaturally in the midline (Fig. 29). Judging from the gap between the pterygoid and basiptyergoid processes, the palate has slid anteriorly and slightly dorsally away from its natural articulation with the basisphenoid (Figs. 29, 30), with a small amount of displacement in this direction preserved where the right ectopterygoid arches to contact the jugal (Fig. 31).

The occiput and most proximate axial elements are fractured and partially disarticulated, which occurred before or during final burial of the skeleton (Fig. 19). Most of the basioccipital appears to have broken away, leaving a gap along the ventral margin of the foramen magnum.

The lower jaws are preserved in natural articulation against the quadrate condyles on both sides, and the tooth rows are engaged within the snout (Figs. 17, 32). The relationship between the anterior ends of the lower jaws and snout, therefore, is well preserved and quite significant; the lower jaws are noticeably shorter than the upper jaws (Fig. 17), which is not the case in theropod dinosaurs found in the same horizons (e.g., *Herrerasaurus*; Sereno and Novas, 1994:figs. 1F, 5). The midsection and posterior-most tip of the left lower jaw broke away during surface weathering, because the fracture surfaces appear fresh (Figs. 12, 13). That breakage opened the medial aspect of the opposing lower jaw to preparation, where all but the anterior end is exposed (Figs. 33, 34).

No sclerotic ossicles nor any part of the hyoid apparatus is preserved. Although it is possible that the hyoid apparatus was lost during surface erosion, the same cannot be said for the sclerotic ossicles, because the orbits were full of matrix when discovered. Ossified sclerotic rings, which surely were present in life, most likely were lost prior to or during final burial.

The premaxillary and maxillary teeth are preserved on both sides of the skull (Figs. 35–37). Only the base of the prominent third dentary tooth is exposed (Fig. 35B). Recent preparation between the premaxillary teeth has exposed the anterior end of the dentary alveolar margin, showing that the smaller first dentary

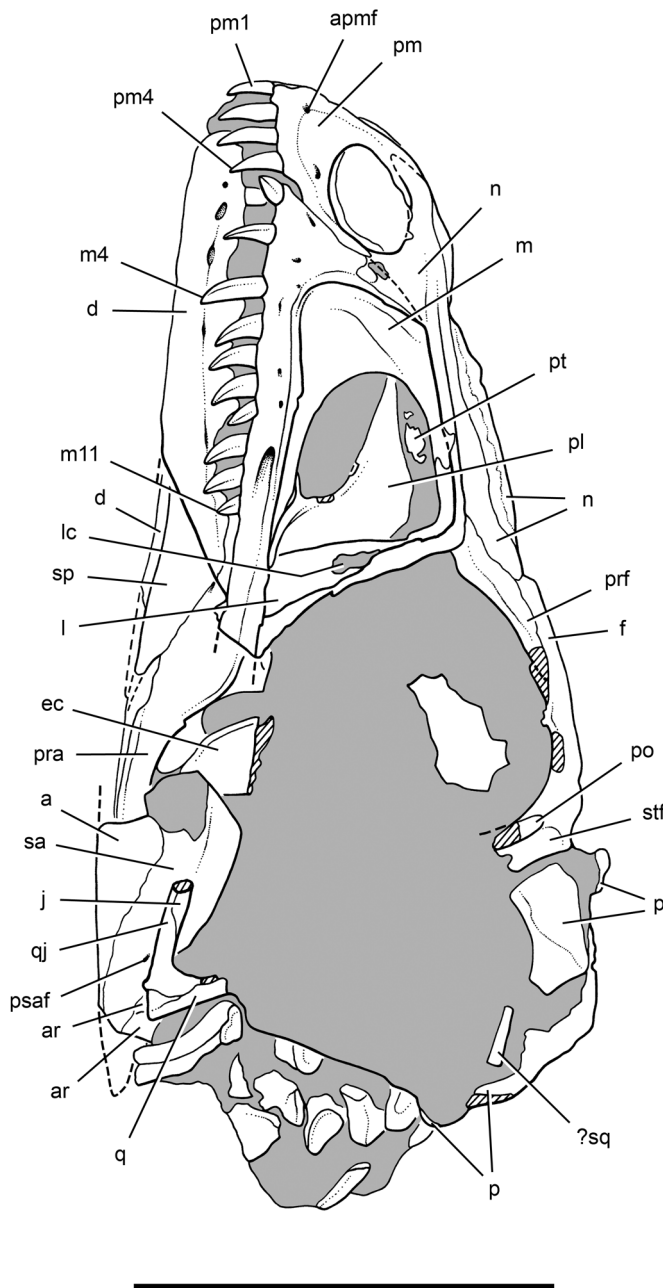


FIGURE 13. Drawing of the skull of *Eoraptor lunensis* (PVSJ 512) in left lateral view. **Abbreviations:** a, angular; apmf, anterior premaxillary foramen; ar, articular; d, dentary; ec, ectopterygoid; f, frontal; j, jugal; l, lacrimal; lc, lacrimal canal; m, maxilla; m4, 11, maxillary tooth 4, 11; n, nasal; p, parietal; pl, palatine; pm, premaxilla; pm1, 4, premaxillary tooth 1, 4; po, postorbital; pra, prearticular; prf, prefrontal; psaf, posterior surangular foramen; pt, pterygoid; q, quadrate; qj, quadratojugal; sa, surangular; sp, splenial; sq, squamosal; stf, supratemporal fossa. Dashed line indicates a missing margin; hatching indicates a broken surface; shading indicates matrix. Scale bar equals 5 cm.

tooth is inset about the space of one alveolus from the anterior end of the dentary, as in *Panphagia* (Martínez and Alcober, 2009) and many basal sauropodomorphs (Sereno, 2007b; Martínez, 2009).

Tiny palatal teeth are preserved on both pterygoids along prominent medial and diagonal ridges (Figs. 38, 39). Palatal teeth

of similar size and distribution were reported in the contemporaneous basal theropod *Eodromaeus* (Martínez et al., 2011). Palatal teeth are not present on the ventrally projecting mandibular flange and would not be visible in lateral view of the cranium (Fig. 40).

### Dorsal Skull Roof

**Premaxilla**—The premaxilla has a subtriangular body that contacts the maxilla medially and ventrally and the nasal dorsally (Figs. 10–15, 18, 23). The body is divided equally into a posterior concave portion that forms the narial fossa and an anterior convex portion that is pierced by neurovascular foramina. The largest foramen, the anterior premaxillary foramen (sensu Sereno, 1991), is located on both sides above the second premaxillary tooth near the ventral margin of the narial fossa (Fig. 23). It opens anteroventrally into the anterior end of the premaxillary body.

Ornithischians such as *Lesothosaurus* (Sereno, 1991) usually have an anterior premaxillary foramen near the anteroventral margin of the narial fossa as in *Eoraptor*. In basal sauropodomorphs such as *Plateosaurus* (Sereno, 2007b) and *Adeopapposaurus* (Martínez, 2009), two or three foramina open into the premaxilla along the posterior side of a bill attachment surface, but these are located outside the narial fossa. In theropods such as *Allosaurus* (Madsen, 1976), a foramen is usually present but located farther dorsally on the floor of the external naris and often on the internal aspect of the premaxilla. There is no foramen in this position in *Eoraptor*. The condition in *Eoraptor* most closely resembles that in many ornithischians.

A second external premaxillary foramen is present only on the left side (Figs. 12, 13). Like the anterior premaxillary foramen, it is located within the narial fossa near its ventral margin. No other openings are visible in lateral view of the premaxilla.

The dorsal (internarial) and posterolateral processes of the premaxilla are very slender in *Eoraptor* (Figs. 12–15, 20). The tapering dorsal process extends distally just beyond the midpoint of the internarial bar, which arches slightly above the adjacent nasal roof of the snout. *Eoraptor* appears to have a simple ‘V’-shaped premaxilla-nasal suture, as opposed to the more complex ‘W’-shaped suture present in most theropods (Figs. 14, 15; Madsen, 1976). Unfortunately, the premaxilla-nasal suture beyond this point cannot be followed with certainty.

The right posterolateral process is completely preserved and articulates against the anterior margins of the right maxilla and nasal, excluding the former from the margin of the external naris (Figs. 20, 22). On the left side of the skull, the distal portion of the left posterolateral process has broken away, exposing a shallow trough for its reception on the nasal. The shape of the distal half of the posterolateral process of the premaxilla is unique. It expands slightly from the narrow midshaft to form a crescent-shaped process.

**Maxilla**—The maxilla articulates with the premaxilla anteriorly, the nasal anteriorly and dorsally, the lacrimal and jugal posteriorly, and the palatine medially (Figs. 10–13, 20–23). Several neurovascular foramina open laterally on the maxilla. Most conspicuous is a series of foramina on the narrow ramus below the antorbital fossa. Most of these are directed anteroventrally, presumably to supply the marginal tissues of the lips. The posterior-most foramen, however, is larger than the others and opens into a groove that passes posteriorly toward the jugal (Fig. 21). The anterior-most foramen is also slightly larger than the others (Fig. 22). The size, location, and direction in which these foramina open is most similar to the condition in basal sauropodomorphs (e.g., *Plateosaurus*, Sereno, 2007b; *Massospondylus*, Sues et al., 2004; *Adeopapposaurus*, Martínez, 2009). The alignment of these foramina strongly suggest that they are interconnected by a canal within the maxilla, although no such passage can be discerned in computed tomographic cross-sections of the skull of *Eoraptor*.

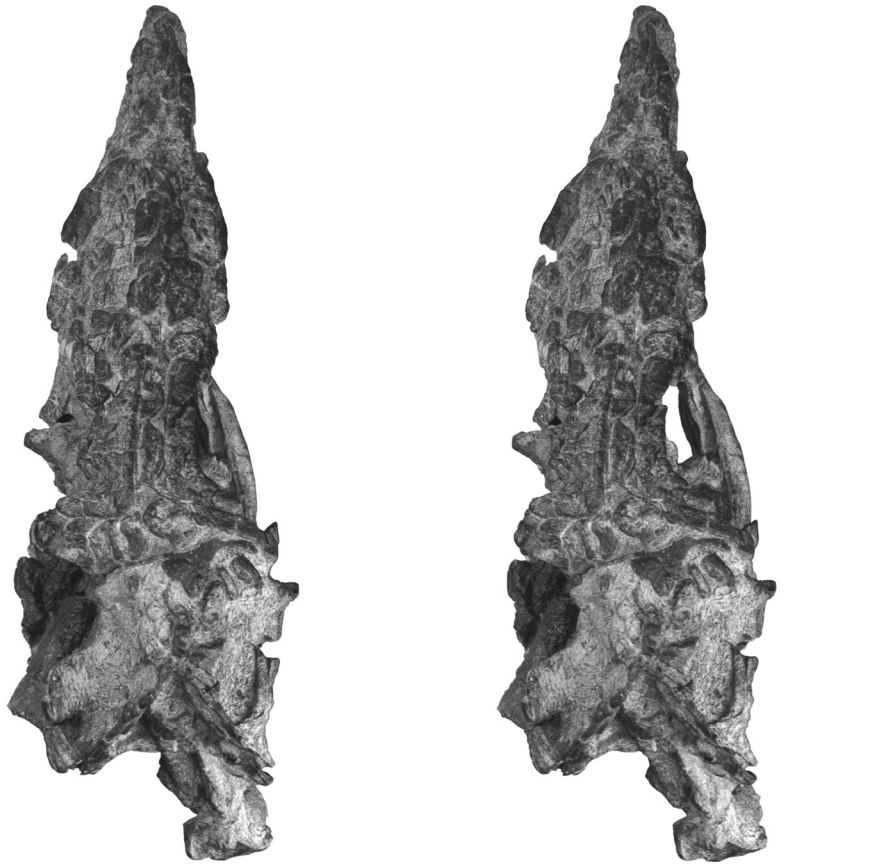


FIGURE 14. Stereopair of the skull of *Eoraptor lunensis* (PVSJ 512) in dorsal view. Scale bar equals 5 cm.

The subnarial foramen is located between the premaxilla and maxilla near the alveolar margin and is best preserved on the right side (Figs. 10–13, 20, 23). Most of the margin of the foramen is formed by a notch in the maxilla (Fig. 23). The foramen passes medially between the maxilla and premaxilla to open ventral to the premaxillary palate, as in basal sauropodomorphs (Serenó, 2007b; Martínez, 2009), *Herrerasaurus* (Serenó and Novas, 1994), and other saurischians that retain this foramen. Another foramen, present only on the left side, is situated near the anterior margin of the maxilla just above the subnarial foramen (Fig. 13). No other openings are present on the maxilla. The anterior extremity of the antorbital fossa, which is well preserved on both sides, does not have a promaxillary fossa or fenestra as occurs in the basal sauropodomorph *Pampadromaeus* (Cabreira et al., 2011), the basal theropods *Herrerasaurus* (Serenó, 2007a) and *Eodromaeus* (Martínez et al., 2011), and the basal ornithischian *Heterodontosaurus* (Serenó, 2012).

*Eoraptor* does not have a ‘subnarial gap,’ or arched diastema, akin to that in coelophysoids (contra Nesbitt et al., 2009). The subnarial foramen, best preserved on the right side (Fig. 23), is bordered by the premaxilla and maxilla and is situated dorsal to a short premaxillary-maxillary diastema. The alveolar margin above the first maxillary tooth curves dorsally, which is matched by a corresponding prominence on the alveolar margin of the articulated dentary (Fig. 23). The axis of the short first maxillary tooth, in addition, is not vertical but rather is

canted slightly anteroventrally toward the diastema, as best preserved on the right side (Figs. 20, 35C, D). Thus, the diastema very likely has functional significance during the procurement or processing of foodstuffs. In computed tomographic coronal cross-section, the slightly enlarged third dentary tooth is positioned near the dorsal expansion in the alveolar margin of the dentary (Fig. 35A, B). We removed matrix from the base of the crown of this tooth, which projects dorsally into the palatal area medial to the maxillary tooth row. In sum, there is a short premaxilla-maxilla diastema with particular relations with adjacent teeth, namely, the first maxillary tooth and the third dentary tooth.

This condition, however, is very different than that in coelophysoid theropods. In coelophysoids, there is no subnarial foramen, and the premaxilla articulates loosely with the maxilla (Tykoski, 2005). The premaxilla lacks the dorsolateral process that articulates on the lateral aspect of the snout present in *Eoraptor*. The better-developed, arched diastema in coelophysoids is open laterally to receive the tip of the dentary tooth, and the posterior premaxillary and anterior maxillary teeth are directed toward one another (Tykoski, 2005; Sereno, 2012:fig. 91). Some confusion may have arisen regarding the condition in *Eoraptor* due to preservational factors on the left side of the skull, where the first maxillary tooth is partially dislodged and points much more strongly anteriorly (Figs. 12, 13). Also, the edges of the premaxilla and maxilla are slightly ajar, which has obscured the ventral rim of the

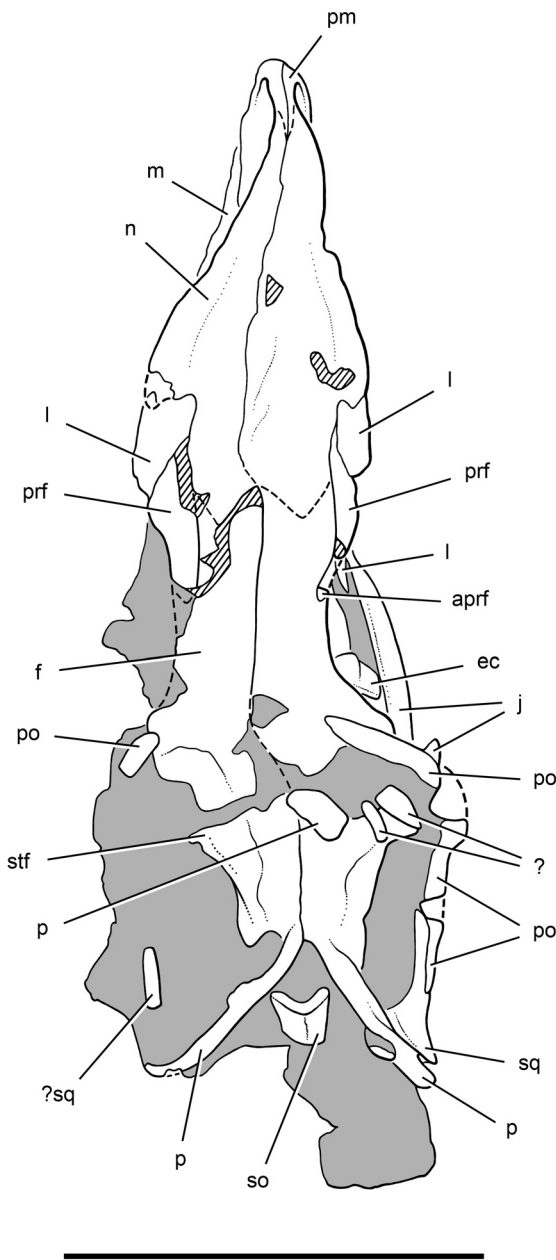


FIGURE 15. Drawing of the skull of *Eoraptor lunensis* (PVSJ 512) in dorsal view. **Abbreviations:** *aprf*, articular surface for prefrontal; *ec*, ectopterygoid; *f*, frontal; *j*, jugal; *l*, lacrimal; *m*, maxilla; *n*, nasal; *p*, parietal; *pm*, premaxilla; *po*, postorbital; *prf*, prefrontal; *so*, supraoccipital; *sq*, squamosal; *stf*, supratemporal fossa. Dashed line indicates a missing margin; hatching indicates a broken surface; shading indicates matrix. Scale bar equals 5 cm.

subnarial foramen. The presence of a subnarial foramen and kinetic premaxilla-maxilla suture in *Eoraptor* has been interpreted correctly in several places (Sereno et al., 1993; Langer and Benton, 2006; Martínez et al., 2011).

The antorbital fossa (Figs. 20–22) is well developed on the maxilla and is much broader anteriorly than in the basal theropod *Herrerasaurus*, which has an unusually narrow fossa. This width of the fossa is considerably narrower dorsal and ventral to the antorbital

fenestra. The anterior rim of the fossa, which forms the anterior portion of the external antorbital fenestra (sensu Witmer, 1997), is slightly everted (Figs. 21, 22, 40A). There is no development of deep pneumatic invaginations or accessory fenestrae or foramina in the antorbital fossa, in contrast to the closely related *Pampadromaeus* (Cabreira et al., 2011) and most tetanuran theropods (e.g., *Allosaurus*; Madsen, 1976). The antorbital fossa, however, is slightly invaginated under the anterior and ventral margins, except above the fourth through sixth maxillary teeth, where the ventral floor of the fossa is visible in lateral view (Fig. 21). The rim of the external antorbital fenestra in this region is lower and sharper than the more everted, rounded form of the remainder of the opening. Only the posterior portion of the rim, thus, resembles the raised relief and rounded cross-sectional profile of the antorbital rim in coelophysoids (e.g., *Coelophysis*).

The surface of the fossa is gently concave anterior to the antorbital fenestra and dorsal to the fourth to seventh maxillary teeth (Figs. 21, 22). Dorsal to this region, the fossa becomes distinctly dorsoventrally convex, as preserved on both sides. The fossa ventral to the antorbital fenestra is narrow and trough-shaped, facing dorsally as much as laterally. In places on both sides of the skull, the surface of the fossa has collapsed into underlying tooth crypts. The ‘D’-shaped inner opening, the internal antorbital fenestra (sensu Witmer, 1997), is some 30% longer than dorsoventrally deep (Fig. 40A).

An articular trough on the posterior ramus of the maxilla accommodates the lacrimal, jugal, and palatine. Of these, the flaring ventral ramus of the lacrimal establishes the broadest contact with the maxilla (Figs. 20, 21, 24). The maxilla-lacrimal suture is overlapped anteriorly by a short prong-shaped process of the palatine, which extends from the posteroventral corner of the antorbital fenestra (Fig. 24). Posteriorly, the maxilla-lacrimal suture is overlapped by the flat, triangular anterior ramus of the jugal.

The posterior ramus of the maxilla tapers to a very slender process that extends posteriorly as far as the posterior border of the orbit (Figs. 10, 11). The process articulates in a slot on the ventral margin of the anterior ramus of the jugal (Fig. 31). The slender maxillary process is completely preserved on the right side, where it lies adjacent to the articular slot on the jugal.

Only a portion of the posterior ramus of the maxilla is visible in medial view. The maxillae articulated with each other proximally by way of anteromedial (= palatal) processes. These processes are exposed in dorsal view, forming the floor beneath the external nares. Judging from the tight articulation of these processes in the midline, the vomer footplate (Fig. 28) may have been located above the position of the second maxillary tooth, as in *Herrerasaurus* (Sereno and Novas, 1994).

**Nasal**—The nasal spans approximately one-half of the length of the skull (Figs. 10–15, 41). It is proportionately shorter than in long-snouted theropods such as *Herrerasaurus* and *Coelophysis*, in which it forms more than one-half of skull length. Sutural contacts of the nasal include the premaxilla, maxilla, lacrimal, prefrontal, and frontal. In lateral view, the internarial bar arches slightly above the sloping margin of the skull roof; crushing has slightly exaggerated the change in angle as the internarial bar joins the roof of the snout on the right side (Fig. 20). This condition is highly reminiscent of that in many basal sauropodomorphs, such as *Plateosaurus*, when this fragile region of the snout has been carefully reconstructed (Sereno, 2007b:fig. 4). The postnarial portion of the nasal is arched gently anteroposteriorly and transversely, with the prominent, overhanging lateral margin of the bone slightly upturned (Figs. 14, 15, 20, 21). The region immediately adjacent to the internarial suture is not as depressed as in *Herrerasaurus*.

The posterodorsal (internarial) process is the most slender process of the nasal (Fig. 23). It tapers in width from a horizontal sheet of bone above the posterior corner of the external naris to

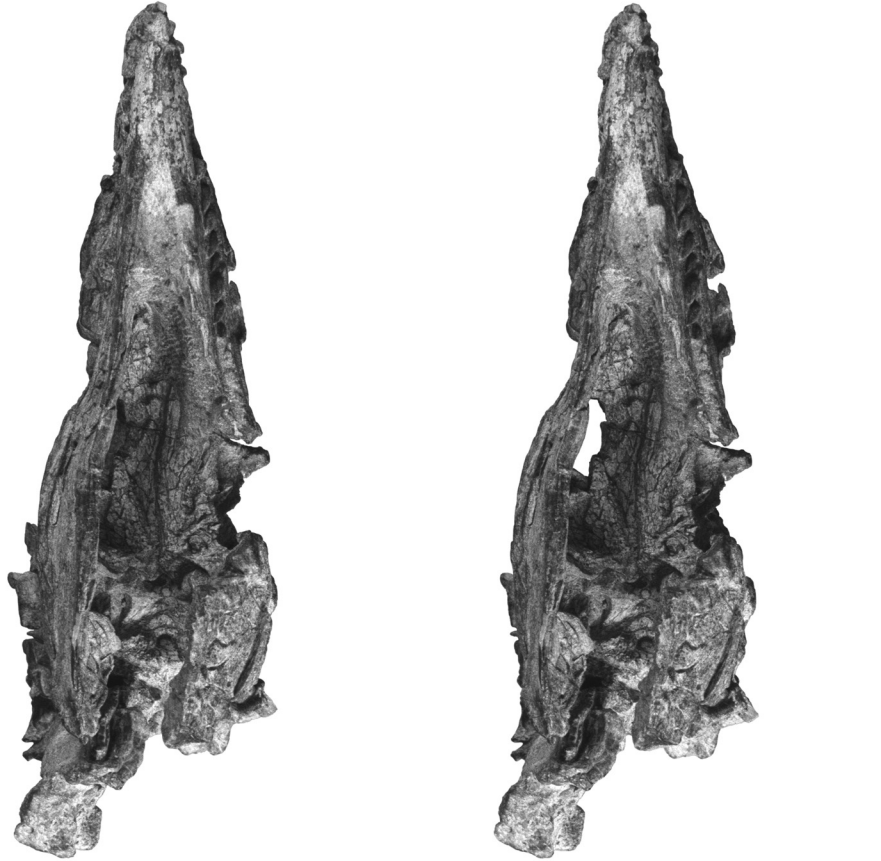


FIGURE 16. Stereopair of the skull of *Eoraptor lunensis* (PVSJ 512) in ventral view. Scale bar equals 5 cm.

a narrow, transversely compressed process at its tip. Near its extremity, the suture with the premaxilla is either fused or obliterated during fossilization. It appears to have a simple 'V'-shaped termination between the premaxillary processes (Figs. 14, 15).

The subtriangular anteroventral process of the nasal forms the posterior margin of the external naris and is overlapped laterally by the posterolateral process of the premaxilla and the maxilla (Fig. 22). The ventral tip of this process rests on the anterior margin of the maxilla just medial to the posterolateral process of the premaxilla. The broad posterior process of the nasal overlaps the frontal but is weathered along its distal margin on both sides (Figs. 14, 15). A portion of the posterior margin of the left nasal appears to be preserved in articulation with the frontal. As best as can be discerned from this specimen, the nasal-frontal suture seems to be similar to that of *Herrerasaurus* and many other theropods (*Allosaurus*; Madsen, 1976), with an anteriorly projecting 'V'-shaped embayment between the posterior ends of the nasals (Fig. 15).

The nasal forms a thin, laterally projecting shelf over the antorbital fossa (Fig. 40A). In dorsal view, the thin shelf flares laterally posterior to the narial region (Fig. 41). A portion of the shelf on the left side was damaged after molding the skull and was replaced with a cast piece.

The lateral margin of the nasal turns medially where it meets the lacrimal, as seen in dorsal view (Figs. 14, 15). Close examination of this margin suggests that the inset suture actually hooks

slightly anteriorly. The nasal, therefore, appears to have a rudimentary posterolateral prong, with the lacrimal inserting between this prong and the rest of the nasal (Langer and Benton, 2006). This is best preserved on the right side, where only the distal tip of the nasal process is broken away. A similar process (posterolateral process of the nasal) is present, but better developed, in many theropods, such as *Ceratosaurus* (MWC 1.1) and *Allosaurus* (Madsen, 1976:pl. 5B). In these theropods, the notch is deeper than in *Eoraptor*, and the nasal process overlaps the lateral side of the lacrimal. The development of at least a rudimentary nasal posterolateral prong also occurs in some basal sauropodomorphs, such as *Plateosaurus* (Sereno, 2007b:fig. 5B), although others show no such development (*Adeopapposaurus*; Martínez, 2009).

**Lacrimal**—The anterior ramus of the 'L'-shaped lacrimal is approximately half as long as the ventral ramus (Figs. 10–13, 20, 21, 24, 25, 40A). The lacrimal is overlapped dorsally by the nasal, medially by the prefrontal, and laterally by the jugal and a hook-shaped process of the palatine. It rests in a trough on the maxilla ventrally and has a 'W'-shaped suture with the maxilla on the wall of the antorbital fossa.

There is no development of pneumatic spaces within the body of the lacrimal as occurs in many large theropods (e.g., *Allosaurus*; Madsen, 1976). The posterodorsal corner of the fossa, however, is slightly invaginated as in *Herrerasaurus* (Sereno and Novas, 1994). That invagination is best developed on the anterior ramus of the lacrimal (Figs. 24, 25).

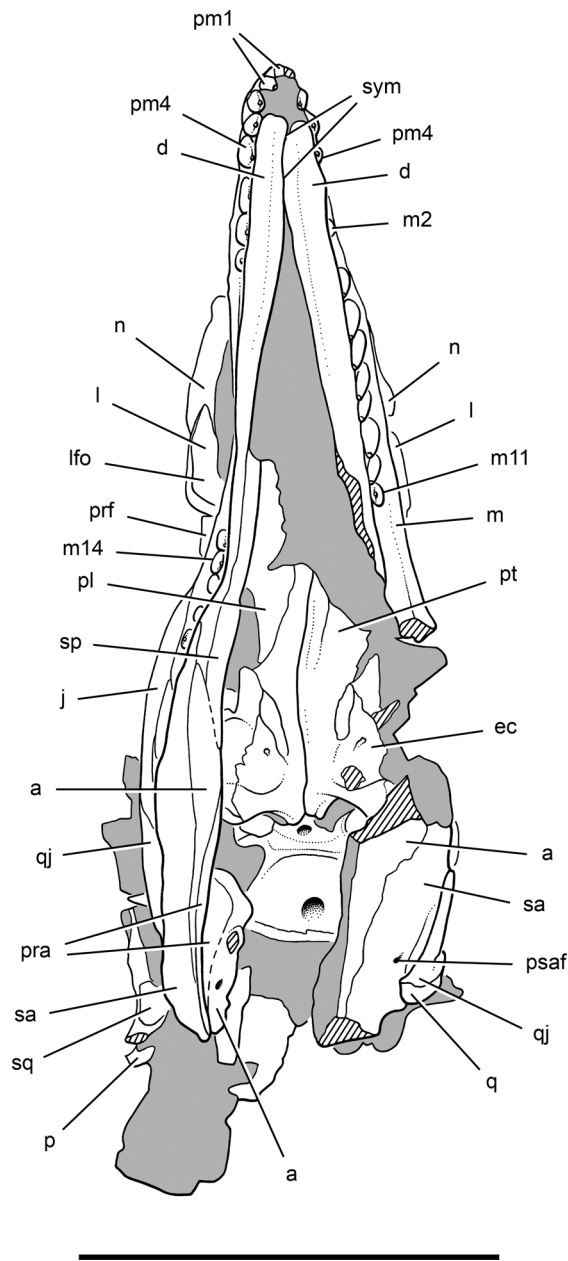


FIGURE 17. Drawing of the skull of *Eoraptor lunensis* (PVSJ 512) in ventral view. **Abbreviations:** a, angular; d, dentary; ec, ectopterygoid; j, jugal; l, lacrimal; lfo, lacrimal fossa; m, maxilla; m2, 11, 14, maxillary tooth 2, 11, 14; n, nasal; p, parietal; pl, palatine; pm1, 4, premaxillary tooth 1, 4; pra, prearticular; prf, prefrontal; psaf, posterior surangular foramen; pt, pterygoid; q, quadrate; qj, quadratojugal; sa, surangular; sp, splenial; sq, squamosal; sym, symphysis. Dashed line indicates a missing margin; hatching indicates a broken surface; shading indicates matrix. Scale bar equals 5 cm.

The orbital surface of the lacrimal, also best preserved on the right side, is narrow ventrally where it forms a rounded orbital rim (Fig. 24). A broad groove midway along the ventral ramus passes dorsally into a large lacrimal foramen, located at approximately one-third of the way along the ventral ramus. Medial to the lacrimal foramen and groove, a narrower groove accommodates the slender tip of the ventral process of the prefrontal.

**Prefrontal**—The ‘L’-shaped prefrontal contacts the nasal anteriorly, the lacrimal laterally, and the frontal posteriorly (Figs. 10–13, 20, 24, 41). The dorsal surface of the prefrontal is gently convex, whereas the orbital surface is concave. Most of the posterior process rests in a deep slot on the lateral side of the frontal. This slotted prefrontal-frontal articulation can be seen in cross-sections of the orbital rim on both sides. The posterior end of the slot in the frontal is well exposed on the right side, where the posterior process of the prefrontal has broken away.

The ventral process narrows dramatically in width as it passes along the medial side of the lacrimal foramen (Fig. 24). The tip of the ventral process appears to be broken away on the right side, where it is exposed. An articular groove on the lacrimal for this process extends along at least two-thirds of the length of the ventral ramus of the lacrimal. The presence of a very slender, elongate ventral process equal to the posterior process in length characterizes many saurischians (*Plateosaurus*, Galton, 1984:fig. 3; *Allosaurus*, UUV 5519, contra Madsen, 1976:pl. 4A, B).

**Frontal**—Sutural contacts of the frontal include the nasal and prefrontal anteriorly and the postorbital and parietal posteriorly, although the exact course of some of these sutures is difficult to discern because of surface weathering and marked fracturing (Figs. 14, 15, 41). Contact between the frontal and the braincase is not exposed. The frontal has a broad articular surface for the nasal anteriorly, partially exposed on the left side and fully exposed on the right. Only the lateral portion of the left nasal-frontal suture is preserved, which is ‘V’-shaped and pointed posteriorly. The prefrontal-frontal suture is exposed on both sides of the skull and has been described in detail above (Fig. 24). The frontal-frontal suture is straight, rather than interdigitating, and forms a butt joint in the midline. The frontal-postorbital suture is most complete on the right side, where the narrow medial process of the postorbital rests in an articular depression on the frontal behind the orbital rim. Posterior to this contact, the surface of the frontal curves ventrally to form most of the anterior wall of the supratemporal fossa. The frontal and parietal have been disarticulated by right lateral movement of the parietals and braincase relative to the rest of the skull. The frontal-parietal suture zigzags from one supratemporal fossa to the other (Figs. 14, 15, 41). A median notch is formed by the paired frontals, into which inserts a median triangular process of the parietals. The form of the suture, such as whether it was interdigitating, cannot be determined.

**Parietal**—The parietal contacts the frontal anteriorly and the squamosal, supraoccipital, and exoccipital-opisthotic posteriorly (Figs. 14, 15, 19, 41). Contact with other portions of the braincase is not exposed. Due to the degree of fracturing, it cannot be determined whether the parietals were fused. On the better-preserved left parietal, a raised sinuous edge seems to mark the medial border of the supratemporal fossa, as is the case in *Herrerasaurus* (Sereno and Novas, 1994). The thin posterolateral wing of the parietal extends from near the midline toward the head of the quadrate. The posterior process of the squamosal, however, separates the parietal and head of the quadrate (Figs. 27, 40A).

**Postorbital**—The triradiate postorbital contacts the frontal medially, the squamosal posteriorly, and the jugal ventrally (Figs. 10, 11, 14, 15, 26, 27). The postorbital probably contacted the parietal and laterosphenoid on the wall of the supratemporal fossa, but this region is too fractured to interpret with confidence. All but the tip of the medial process of the left postorbital has broken away. The right postorbital, on the other hand, is complete but has broken into four pieces, which have drifted apart. By reassembling the pieces, the right postorbital has medial and posterior processes that are subequal in length and a ventral process that is longer (Figs. 10, 11). A crescentic orbital flange extends anteriorly from the central part of the postorbital. The orbital surface of this flange

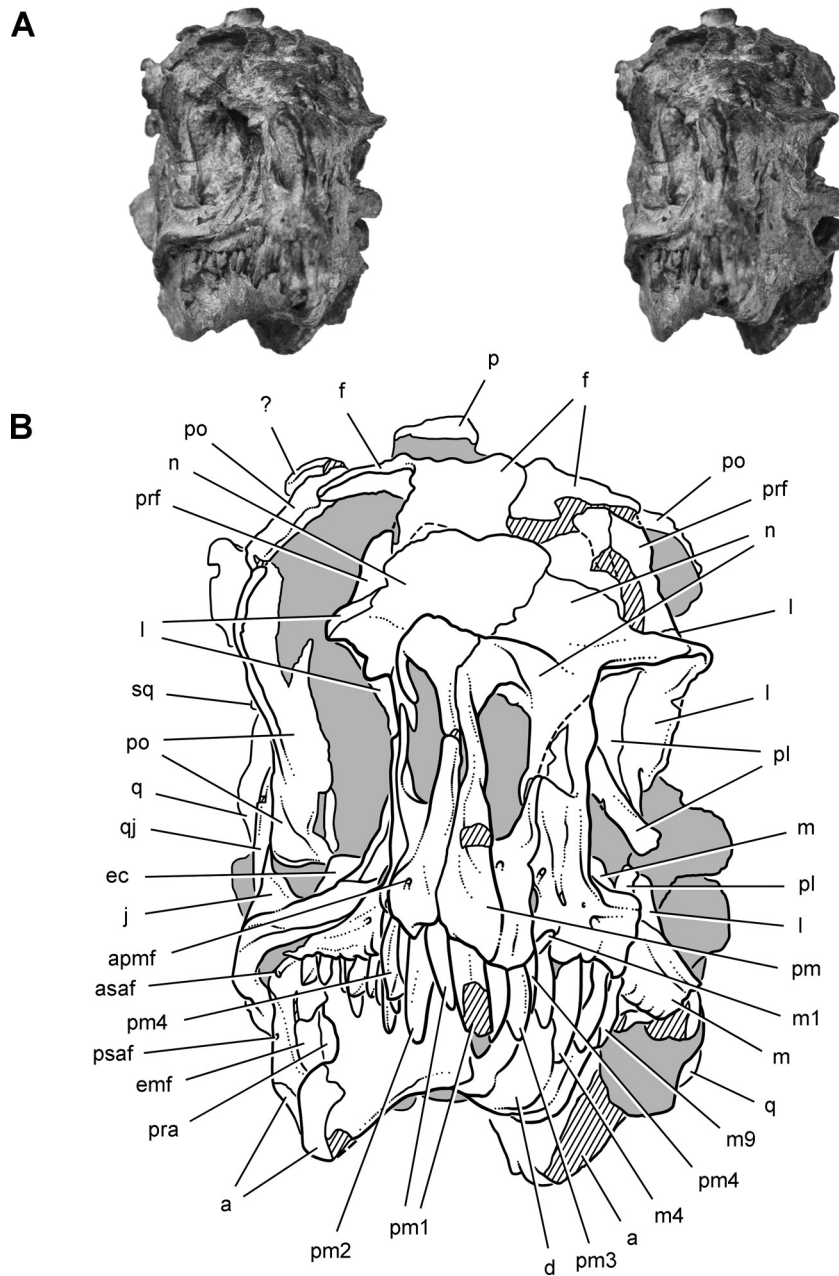


FIGURE 18. Stereopair (A) and drawing (B) of the skull of *Eoraptor lunensis* (PVSJ 512) in anterior view. **Abbreviations:** a, angular; apmf, anterior premaxillary foramen; asaf, anterior surangular foramen; d, dentary; ec, ectopterygoid; emf, external mandibular fenestra; f, frontal; j, jugal; l, lacrimal; m, maxilla; m1, 4, 9, maxillary tooth 1, 4, 9; n, nasal; p, parietal; pl, palatine; pm, premaxilla; pm1-4, premaxillary teeth 1-4; po, postorbital; pra, prearticular; prf, prefrontal; psaf, posterior surangular foramen; q, quadrate; qj, quadratojugal; sq, squamosal. Dashed line indicates a missing margin; hatching indicates a broken surface; shading indicates matrix. Scale bars equal 3 cm in A and 2 cm in B.

and of the medial and ventral processes are concave and partially enclose the orbital cavity, as is well seen in anterior view of the skull (Fig. 18).

The ventral process has a gently concave lateral surface and is subtriangular in cross-section (Fig. 26). At midlength the process is slightly broader anteroposteriorly than transversely. Its relatively robust distal tip curves onto the medial aspect of the jugal. The transversely flattened posterior process inserts into a slot on

the anterior process of the squamosal (Figs. 26, 27). The medial surface of the frontal, is particularly slender compared with that in *Herrerasaurus* (PVSJ 407) and does not participate significantly in the wall of the supratemporal fossa (Figs. 10, 11, 14, 15, 41).

**Squamosal**—The squamosal has four processes, anterior, ventral, posterior, and medial, which collectively contact the postorbital anteriorly, the parietal and exoccipital-opisthotic

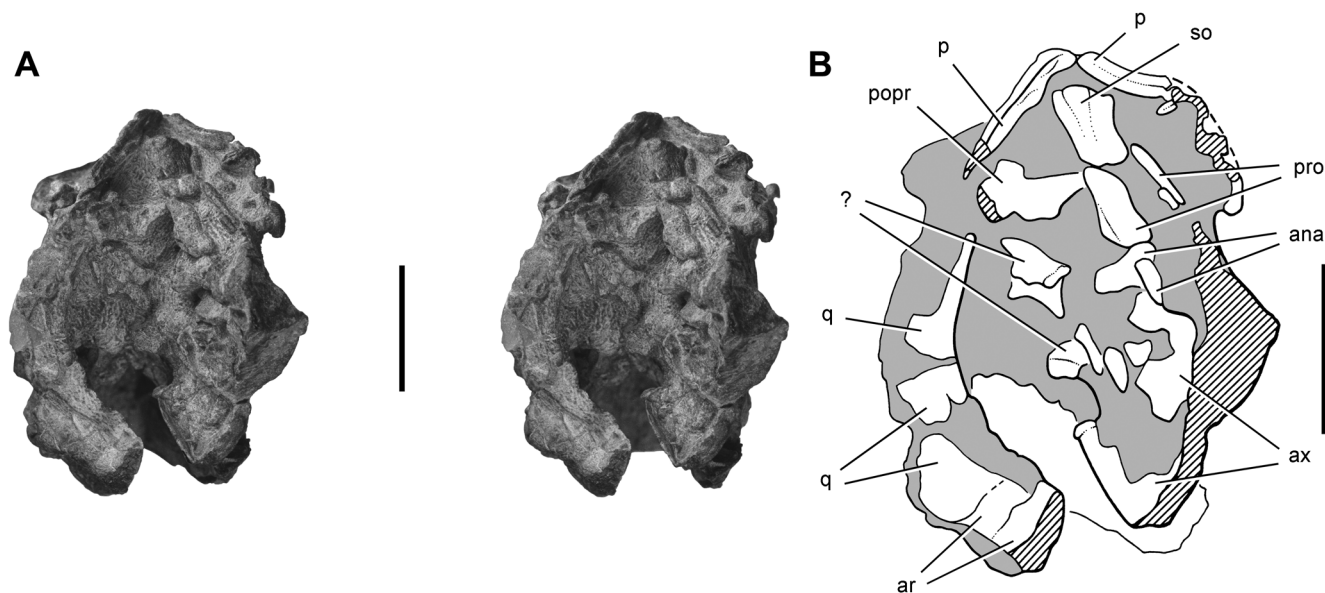


FIGURE 19. Stereopair (A) and drawing (B) of the skull of *Eoraptor lunensis* (PVSJ 512) in posterior view. **Abbreviations:** ana, atlantal neural arch; ar, articular; ax, axis; p, parietal; popr, paroccipital process; pro, proatlas; q, quadrate; so, supraoccipital. Dashed line indicates a missing margin; hatching indicates a broken surface; shading indicates matrix. Scale bars equal 2 cm.

(paroccipital process) posteriorly, and the quadrate and quadratojugal ventrally (Figs. 26, 27). The anterior process is broadest and is missing portions of its thin ventral edge. As in *Herrerasaurus*, it does not appear to expand anteriorly. The medial process, which is only partially exposed, articulates against the posterolateral wing of the parietal. The small posterior process is broken just behind the socket for the quadrate, where it is compressed anteroposteriorly and has a subrectangular cross-section. The posterior surface of the posterior process is flat and articulated against the paroccipital process (Fig. 27). The complete posterior process probably extended distally no more than 2 mm, as suggested by the length of the adjacent posterolateral wing of the parietal.

The ventral process of the squamosal is preserved proximally and distally on the right side (Fig. 26). The base of the process is anteroposteriorly compressed and articulates against the anterior side of the everted lateral process of the quadrate. The slender distal portion of the process is preserved along the anterior margin of the quadrate. Its tip contacts the quadratojugal, passing onto its medial side. The squamosal and quadratojugal, therefore, exclude the quadrate from the border of the laterotemporal fenestra. The slender proportions and length of the ventral process of the squamosal differ markedly from the short, transversely compressed process in many theropods, such as *Herrerasaurus* (Serenó and Novas, 1994). On first inspection, some basal ornithischians, such as *Lesothosaurus*, appear to have a similar slender ventral process. A considerable portion of the process, however, wraps around the quadrate shaft; the ventral process, when fully exposed in *Lesothosaurus*, is transversely compressed and tongue-shaped (Serenó, 1991). *Pampadromaeus* (Cabreira et al., 2011) and other basal sauropodomorphs, in contrast, have a slender ventral process identical to that in *Eoraptor* (Galton, 1984; Sereno, 2007b; Martínez, 2009; Martínez et al., 2011).

The body of the squamosal has a shallow, arcuate laterotemporal fossa on its lateral surface, positioned between the anterior and ventral processes (Fig. 26). The articular cup for the head of the quadrate is unusually deep, as compared with *Herrerasaurus* or

most other saurischians; it is fully exposed on the right side where it has a depth in excess of 2 mm (Fig. 27). The upper portion of the quadrate head would not have been exposed in lateral view (Fig. 40A). In ventral view, the quadrate cotylus is subtriangular, the lateral wall of which has a sagittal orientation (Fig. 27). The long axis of the articular cup has an anteromedial-posterolateral orientation.

**Jugal**—The jugal, best preserved on the right side, has anterior, dorsal, and posterior processes that collectively contact the maxilla, lacrimal, postorbital, quadratojugal, and ectopterygoid (Figs. 10–13, 20, 24, 26, 31, 40A). The forked posterior process of the jugal is the most slender. Unlike *Herrerasaurus* (PVSJ 407) and many other theropods, however, the anterior process that forms the ventral margin of the orbit is narrower than the dorsal process, as in the closely related sauropodomorph *Pampadromaeus* (Cabreira et al., 2011).

The anterior process of the jugal expands at its anterior end, where it overlaps the lacrimal and approaches the tip of the palatine in the posteroventral corner of the antorbital fossa (Fig. 20). There is a low, flat surface on the lacrimal immediately above the anterior end of the jugal, which appears to be an articular surface. If so, it suggests that the dorsal margin of the thin anterior end of the jugal is missing. With its dorsal margin restored accordingly, the anterior process of the jugal would have expanded in dorsoventral height anterior to the orbit, a common and primitive condition among theropods (e.g., *Herrerasaurus*; Sereno and Novas, 1994) and also present in *Pampadromaeus* (Cabreira et al., 2011). A deep slot along the ventral margin of the jugal accommodates the slender posterior process of the maxilla (Figs. 10, 11, 31). The external edge of the slot is swollen and, anteriorly, this rounded edge joins the ventral rim of the antorbital fossa, which has a similar rounded cross-section (Fig. 31). This is the only ornamentation of the jugal in *Eoraptor*, and it closely resembles the condition in *Pampadromaeus* (Cabreira et al., 2011). In *Herrerasaurus*, in contrast, the external surface of the jugal is rugose with a low crest.

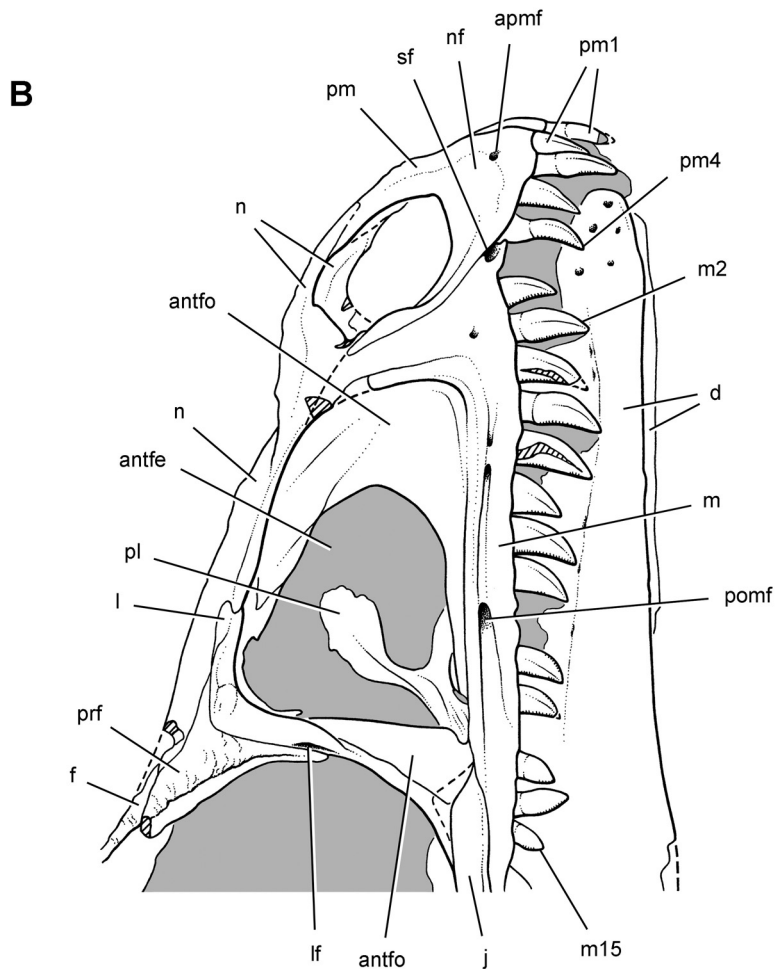


FIGURE 20. Stereopair (A) and drawing (B) of the snout in the skull of *Eoraptor lunensis* (PVSJ 512) in right lateral view. **Abbreviations:** **antfe**, antorbital fenestra; **antfo**, antorbital fossa; **apmf**, anterior premaxillary foramen; **d**, dentary; **f**, frontal; **j**, jugal; **l**, lacrimal; **lf**, lacrimal foramen; **m**, maxilla; **m2**, **15**, maxillary tooth 2, 15; **n**, nasal; **nf**, narial fossa; **pm**, premaxilla; **pm1**, **4**, premaxillary tooth 1, 4; **pl**, palatine; **pmf**, posterior maxillary foramen; **prf**, prefrontal; **sf**, subnarial foramen. Dashed line indicates a missing margin; hatching indicates a broken surface; shading indicates matrix. Scale bars equal 2 cm.

The exposed portion of the dorsal process is short and subtriangular. Its dorsal tip is obscured by overlap of the postorbital. The posterior process is 'V'-shaped and slotted for articulation with the quadratojugal (Fig. 26). The slotted jugal-quadratojugal articulation is constructed, as in *Pampadromaeus* and in other saurischi-

ans; the deeper dorsal prong of the jugal overlaps the quadratojugal laterally, whereas the ventral prong of the jugal wraps around its ventral margin to overlap the quadratojugal medially (right side, PVSJ 512). These posterior processes are subequal in length and terminate midway along the lower temporal bar.

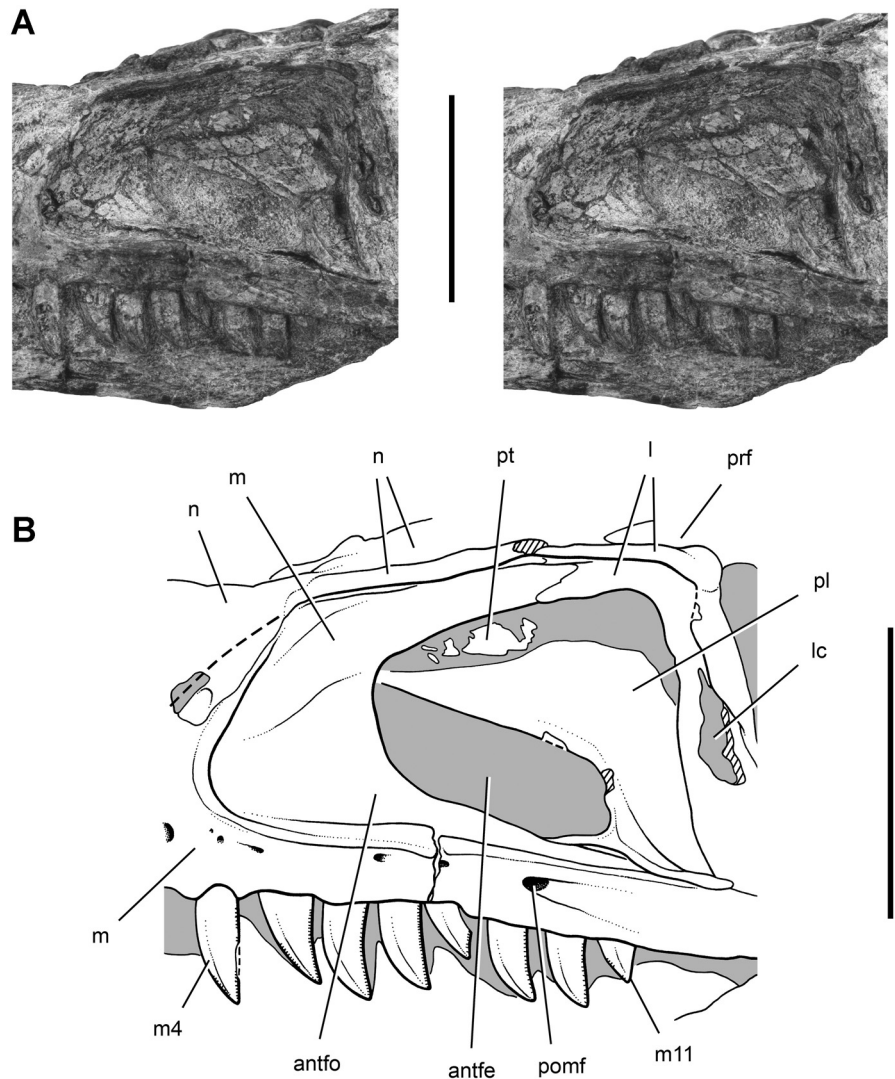


FIGURE 21. Stereopair (A) and drawing (B) of the left antorbital region in the skull of *Eoraptor lunensis* (PVSJ 512) in lateral view. **Abbreviations:** *antfe*, antorbital fenestra; *antfo*, antorbital fossa; *l*, lacrimal; *lc*, lacrimal canal; *m*, maxilla; *m4*, *m11*, maxillary tooth 4, 11; *n*, nasal; *pl*, palatine; *pmf*, posterior maxillary foramen; *prf*, prefrontal; *pt*, pterygoid. Dashed line indicates a missing margin; hatching indicates a broken surface; shading indicates matrix. Scale bars equal 2 cm.

**Quadratojugal**—The ‘L’-shaped quadratojugal is best preserved on the right side (Figs. 10, 11, 26, 32, 40A). The quadratojugal and quadrate appear to be coossified between the jaw articulation and quadrate foramen on the right side, where the former overlaps the latter (Fig. 32). On the left side, in contrast, they are disarticulated and do not appear to have been coossified (Figs. 12, 13). Quadratojugal-quadrate fusion, which is present in *Herrerasaurus* (PVSJ 407), is more commonly reported among theropods than sauropodomorphs (Gilmore, 1920). The dorsal process of the quadratojugal curves onto the anteromedial surface of the lateral flange of the quadrate, where these bones are separate and partially disarticulated. The strap-shaped dorsal process has a relatively uniform width (3 mm) (Fig. 26). Above midheight on the quadrate shaft, the distal end of the dorsal process inserts between the tip of the ventral process of the squamosal and the lateral flange of the quadrate.

The anterior process of the quadratojugal is much shorter than the dorsal process, but has an equivalent maximum width at its proximal end as seen in lateral view. Throughout its length, it is transversely compressed but twists from a vertical orientation near its base to angle dorsomedially-ventrolaterally, where it inserts between the posterior articular processes of the jugal (Fig. 26).

The quadratojugal contributes to the lateral-most edge of the jaw articulation (Figs. 26, 32). A notch on the ventral margin of the quadratojugal separates a tab-shaped posteroventrally directed process that reaches the jaw articulation. The distal extremity of this process and a portion of the quadrate condyle are broken away on the right side (Figs. 26, 32). On the left side, this process appears to oppose the surangular in natural articulation (Figs. 12, 13). The quadratojugal and surangular make only a narrow, restricted contribution to the jaw joint.

#### Palate

The exposed bones of the palate include the quadrate, pterygoid, palatine, ectopterygoid, and vomer (Figs. 16, 17, 28–32, 40A). The epipterygoid, if ossified, is not exposed and is not discernable in computed tomographic cross-sections.

**Quadrate**—The quadrate contacts the squamosal dorsally and anteriorly, the pterygoid medially, the quadratojugal laterally, and the articular and surangular ventrally (Figs. 10–13, 16, 17, 26, 32). The deep articular cotylus in the squamosal for the head of the quadrate (Fig. 27) separates the quadrate from the paroccipital process. The quadrate is taller relative to skull length, and the

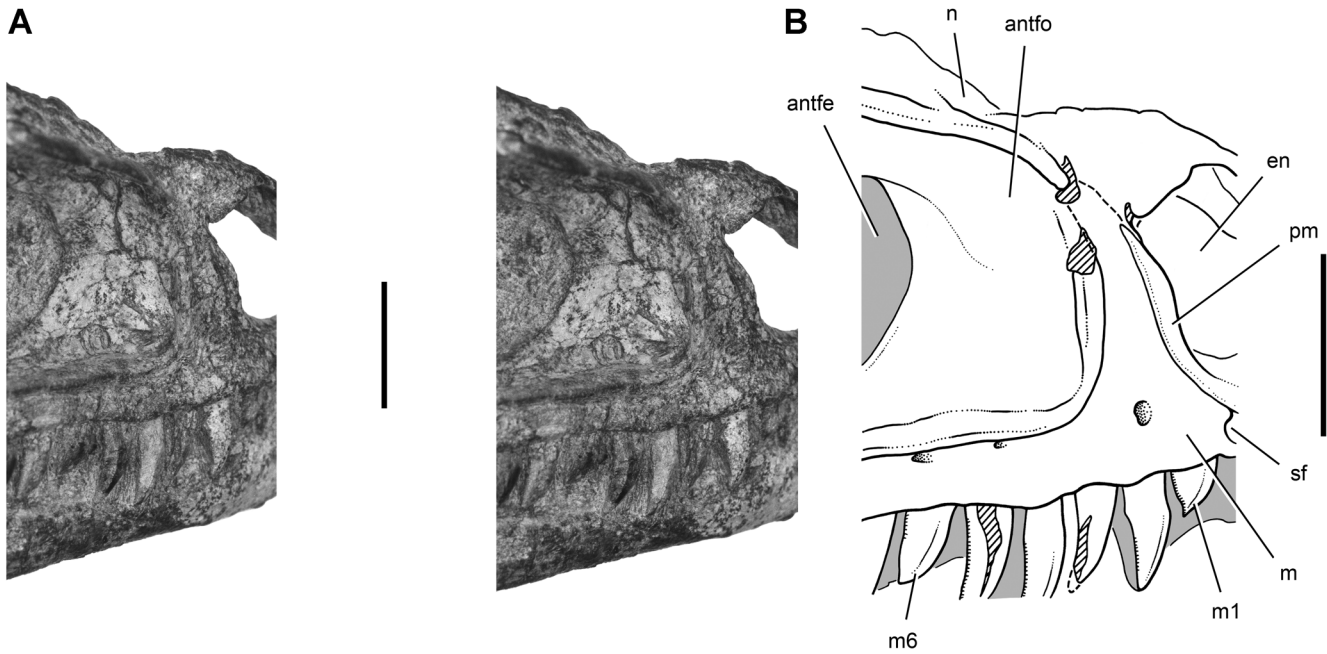


FIGURE 22. Stereopair (A) and drawing (B) of the anterior portion of the right antorbital region of the skull of *Eoraptor lunensis* (PVSJ 512) in right posterolateral view. **Abbreviations:** antfe, antorbital fenestra; antfo, antorbital fossa; en, external nares; m, maxilla; m1, 6, maxillary tooth 1, 6; n, nasal; pm, premaxilla; sf, subnarial foramen. Dashed line indicates a missing margin; hatching indicates a broken surface; shading indicates matrix. Scale bars equal 1 cm.

condyles are narrower than in *Herrerasaurus*. The quadrate shaft is bowed rather than straight in lateral view. With the maxillary tooth row aligned horizontally, the quadrate head is located posterior, rather than anterior, to the jaw articulation (Figs. 10–13).

The quadrate head is subrectangular in lateral view and transversely compressed (Fig. 26). The crescentic lateral flange of the quadrate arches laterally from the shaft, diverging from the quadrate just below the head. In posterior view, a deep notch

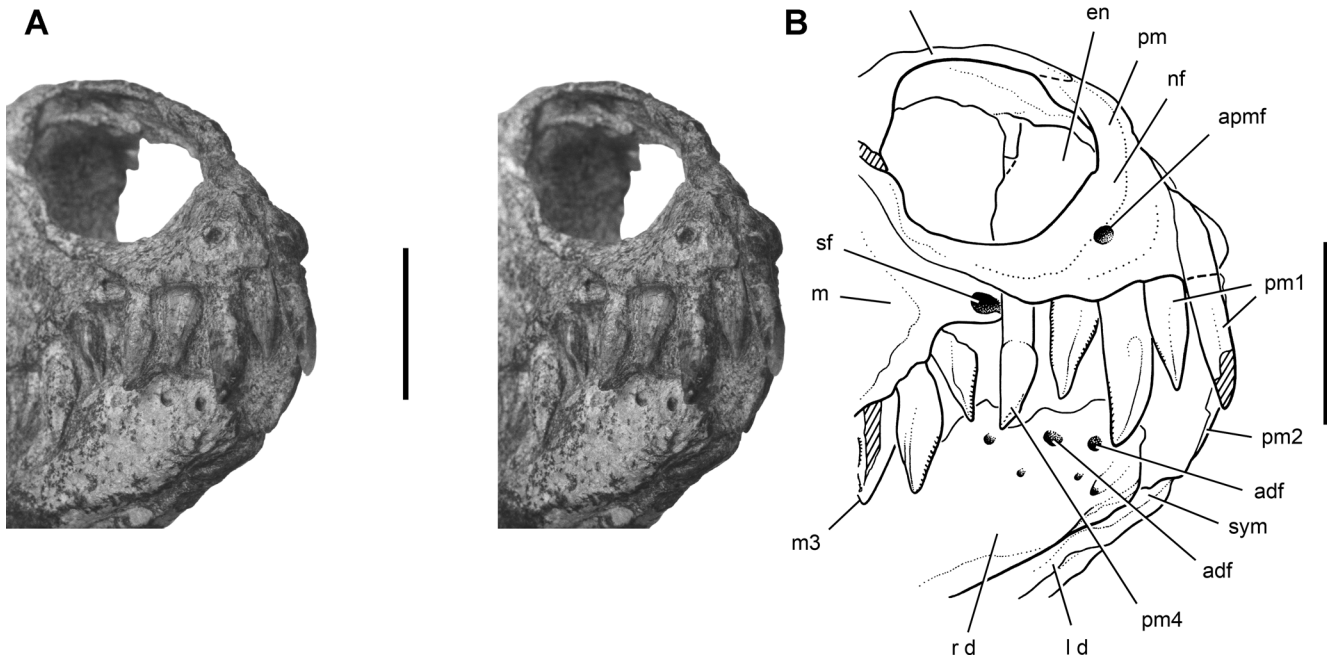


FIGURE 23. Stereopair (A) and drawing (B) of the anterior end of the skull of *Eoraptor lunensis* (PVSJ 512) in right anteroventrolateral view. **Abbreviations:** adf, anterior dentary foramen; apmf, anterior premaxillary foramen; d, dentary; en, external nares; l, left; m, maxilla; m3, maxillary tooth 3; n, nasal; nf, narial fossa; pm, premaxilla; pm1, 2, 4, premaxillary tooth 1, 2, 4; r, right; sf, subnarial foramen; sym, symphysis. Dashed line indicates a missing margin; hatching indicates a broken surface; shading indicates matrix. Scale bars equal 1 cm.

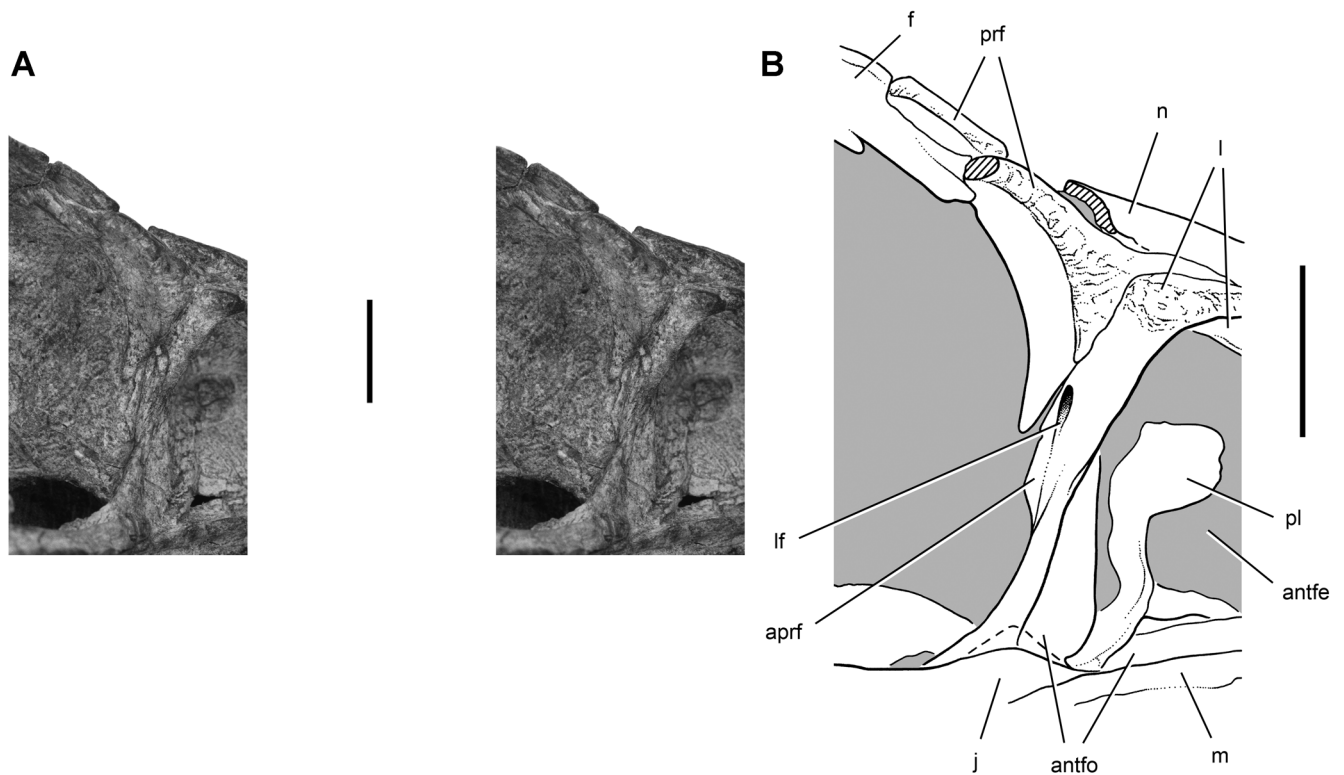


FIGURE 24. Stereopair (A) and drawing (B) of the anterior portion of the right orbit in the skull of *Eoraptor lunensis* (PVSJ 512) in posterolateral view. **Abbreviations:** antfe, antorbital fenestra; antfo, antorbital fossa; aprf, articular surface for the prefrontal; f, frontal; j, jugal; l, lacrimal; lf, lacrimal foramen; m, maxilla; n, nasal; pl, palatine; prf, prefrontal. Dashed line indicates a missing margin; hatching indicates a broken surface; shading indicates matrix. Scale bars equal 1 cm.

ventral to the lateral flange forms most of the margin of the quadrate foramen (Fig. 32). The lateral flange supports both the dorsal process of the quadratojugal and the ventral process of the squamosal along its anterior margin (Fig. 26).

The quadrate condyles are poorly exposed. On the right side, lateral and medial edges of the condyles can be seen on each side of the jaw articulation (Fig. 32). Although small portions of the condyles are missing laterally and medially, their maximum width

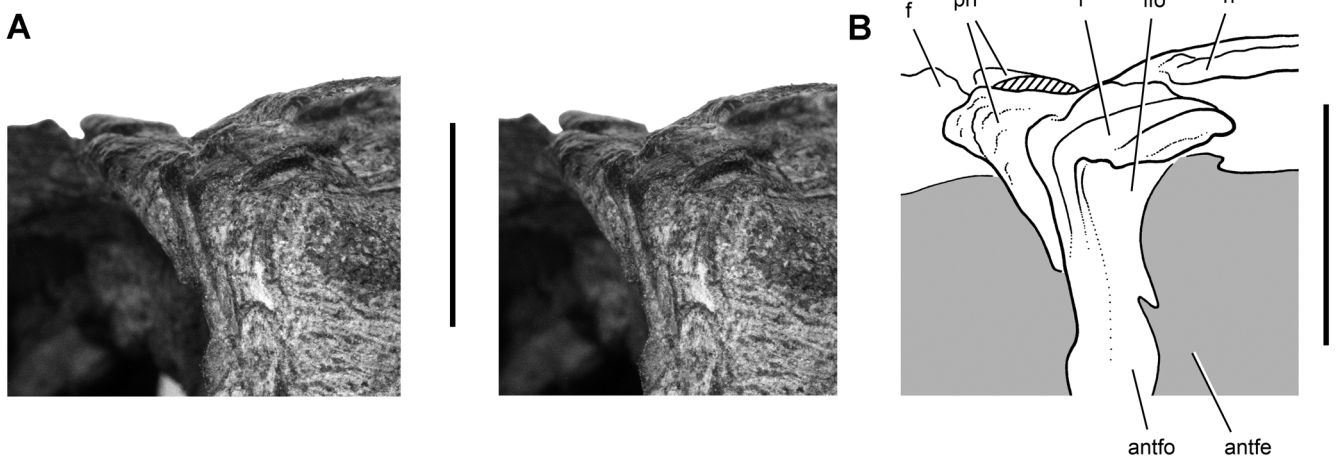


FIGURE 25. Stereopair (A) and drawing (B) of the posterodorsal corner of the right antorbital fossa in the skull of *Eoraptor lunensis* (PVSJ 512) in anterolateral view. **Abbreviations:** antfe, antorbital fenestra; antfo, antorbital fossa; f, frontal; l, lacrimal; lfo, lacrimal fossa; n, nasal; prf, prefrontal. Hatching indicates a broken surface; shading indicates matrix. Scale bars equal 1 cm.

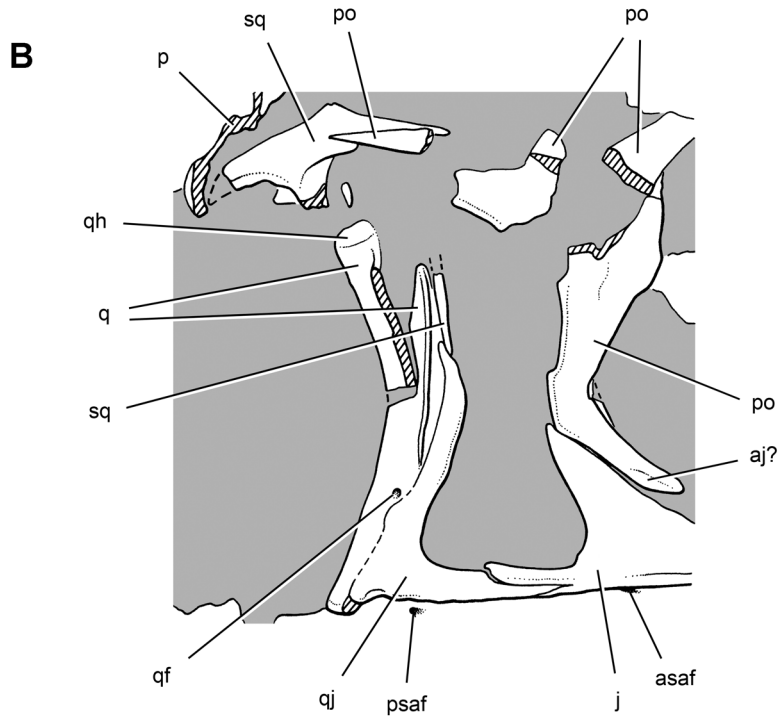
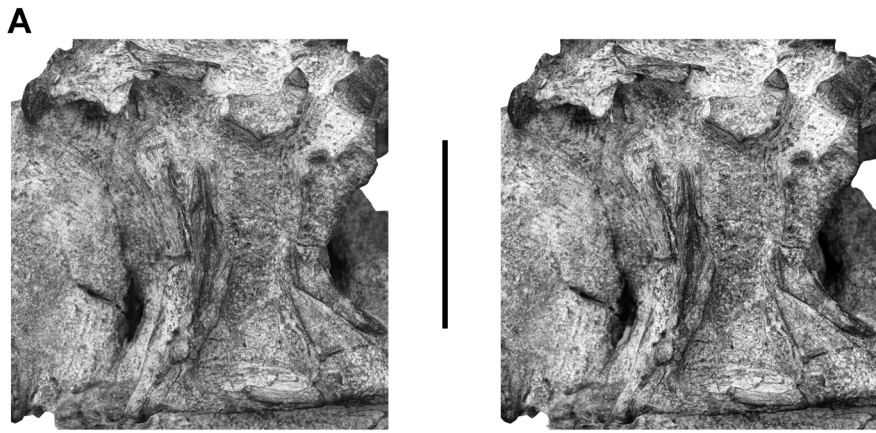


FIGURE 26. Stereopair (A) and drawing (B) of the right laterotemporal region in the skull of *Eoraptor lunensis* (PVSJ 512) in lateral view. **Abbreviations:** aj, articular surface for the jugal; asaf, anterior surangular foramen; j, jugal; p, parietal; po, postorbital; psaf, posterior surangular foramen; q, quadrate; qf, quadrate foramen; qh, quadrate head; qj, quadratojugal; sq, squamosal. Dashed line indicates a missing margin; hatching indicates a broken surface; shading indicates matrix. Scale bars equal 2 cm.

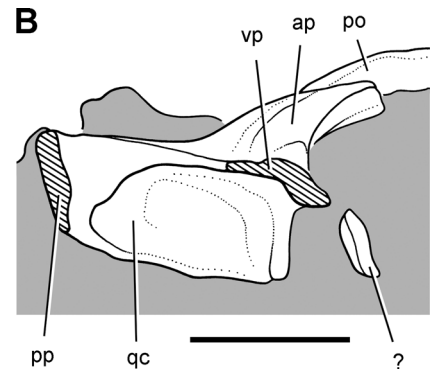
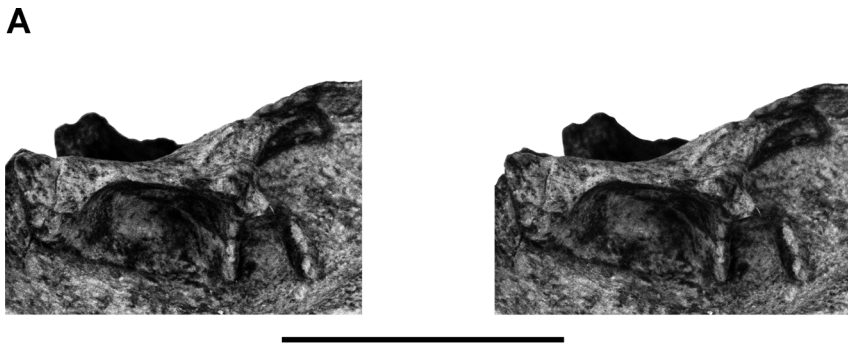


FIGURE 27. Stereopair (A) and drawing (B) of the right squamosal in the skull of *Eoraptor lunensis* (PVSJ 512) in ventral view. **Abbreviations:** ap, anterior process; po, postorbital; pp, posterior process; qc, quadrate cotylus; vp, ventral process. Hatching indicates a broken surface; shading indicates matrix. Scale bars equal 1 cm in A and 5 mm in B.

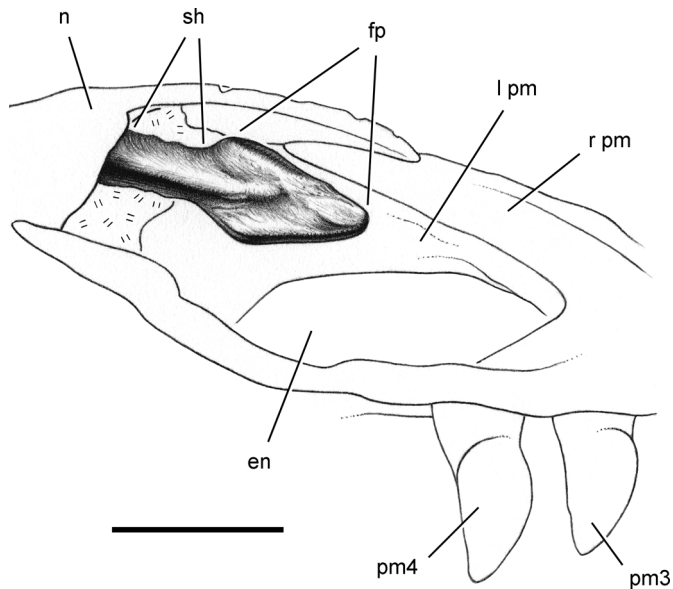


FIGURE 28. Drawing of the anterior end of the vomera in the skull of *Eoraptor lunensis* (PVSJ 512) in ventral view. **Abbreviations:** en, external nares; fp, footplate; l, left; n, nasal; pm, premaxilla; pm3, 4, premaxillary tooth 3, 4; r, right; sh, shaft. Double hatch marks indicate matrix. Scale bar equals 5 mm.

can be measured accurately and only slightly exceeds shaft width. The medial condyle is positioned slightly ventral and anterior to the lateral condyle. Unlike some dinosaurs, including some basal sauropodomorphs (*Plateosaurus*; Sereno, 2007b:fig. 6A), the ventral margin across the condyles is nearly horizontal.

The pterygoid ramus of the quadrate extends from the medial edge of the shaft, as partially exposed on the right side. The ventral edge of the pterygoid ramus curls posteromedially to form a horizontal shelf as in *Herrerasaurus*.

**Pterygoid**—The central portion of the pterygoid is well exposed in ventral view, and a small portion of the anterior ramus is visible through the left antorbital fenestra above the palatine (Figs. 16, 17, 29, 30, 38). Of the three principal rami of the pterygoid (anterior, mandibular, quadrate), only the quadrate ramus is hidden by matrix. The palate has been compressed transversely, which has closed the interpterygoid vacuity, displaced the right pterygoid over the left as were the nasals on the skull roof, and separated the palate and braincase at the basiptyergoid articulation (Fig. 29). In palatal view, the pterygoid overlaps the ventral surface of the palatine, butts against the ectopterygoid laterally, and wraps around the basiptyergoid processes posteriorly.

The anterior ramus of the pterygoid is long, projecting anterodorsally at an angle of about 45° from the basiptyergoid articulation, which is located medial to the posterior border of the orbit. As in other archosaurs, the posterior one-third of the anterior ramus flares to form a ventrally facing subtriangular flange (Fig. 29). The medial margin, exposed on the left pterygoid, is raised in ventral view. More anteriorly, as seen through the antorbital fenestra, this ridge has expanded into a vertical plate, which probably inserts between the posterior ends of the vomera. The lateral edge of the anterior ramus just reaches the border of the postpalatine fenestra, separating the palatine and ectopterygoid (Figs. 29, 30). The pterygoid-ectopterygoid suture courses posteromedially from

the margin of the postpalatine fenestra and, after a short distance, turns posteriorly passing just lateral to a ridge with rudimentary palatal teeth (Fig. 29).

Near the basiptyergoid articulation, the pterygoid-ectopterygoid suture courses across the mandibular ramus of the palate, which projects ventrolaterally into the adductor fossa of the lower jaw (Fig. 30). The pterygoid contribution to this ramus is a distinctive subrectangular strut, which forms the medial one-half of its posterior margin. Proximally, this pterygoid strut is narrow and overhangs the adjacent concave surface of the ectopterygoid (Figs. 29, 30). Distally, the process becomes broader with a concave ventral surface. Its rounded, subrectangular distal end articulates in a deep socket in the ectopterygoid. The end of the strut on the left pterygoid is disarticulated and exposed (Fig. 29). Its rounded, polished appearance and disposition within a deep socket in the ectopterygoid has the appearance of a synovial joint. The basal sauropodomorph *Pampadromaeus* appears to have a similar strut at the posterior end of the pterygoid (Cabreira et al., 2011:fig. 2g). Although more detail is needed for *Pampadromaeus*, this unusual structure of the posterior palate may characterize a subset of basal sauropodomorphs. A very different condition occurs in later-appearing genera, such as *Plateosaurus* (Sereno, 2007b) and *Adeopapposaurus* (Martínez, 2009). In these genera, the pterygoid extends farther laterally to form the posterolateral corner of the mandibular ramus, where it is overlapped either dorsally or ventrally, respectively, by the ectopterygoid. In basal theropods such as *Herrerasaurus* and *Allosaurus*, the pterygoid similarly extends farther laterally and is overlapped dorsally by a thickened, hook-shaped process of the ectopterygoid.

A short pterygoid process is present in *Eoraptor*, which is developed as a subtriangular, wedge-shaped process projects posteriorly near the midline (Figs. 29, 38). It partially encloses the medial aspect of the basiptyergoid articulation.

**Palatine**—The palatine, which is exposed in ventral view on the palate and in dorsal view through the left antorbital fenestra, contacts the pterygoid medially and the maxilla and lacrimal laterally (Figs. 16, 17, 21, 24, 29, 30, 40A). The broad anterior portion of the bone, which has been displaced dorsally on the left side, forms a trapezoidal sheet that angles ventrolaterally away from the midline. Its dorsolateral surface is relatively flat except near its junction with the maxilla, where there is a raised, angular lip along its lateral margin (Figs. 21, 24). This raised lip extends posteriorly as a short, hook-shaped process that overlaps the ventral end of the lacrimal.

In ventral view, the palatine is overlapped along a long, medial contact by the pterygoid (Fig. 29). Laterally, the palatine is sutured to the maxilla along its medial edge in the antorbital fossa, a lateral contact that is lengthened by a slender anterior process (Fig. 21). The palatine forms most of the margin of the postpalatine fenestra but does not reach the ectopterygoid. Unlike many coelurosaurian theropods (e.g., *Tyrannosaurus*; Brochu, 2002), there are no accessory foramina between the palatine and pterygoid.

**Ectopterygoid**—The ectopterygoid is best preserved on the right side, where it contacts the pterygoid and jugal (Figs. 29–31, 33A, B). The lateral process is a dorsoventrally compressed strut that arches from the jugal along the orbital margin to the mandibular flange (Fig. 31). The distal end expands into a flat process, partially exposed under the orbital bar, for articulation with the jugal. The slender posterior process of the maxilla is held within a groove in the jugal and as a result does not contact the ectopterygoid. In palatal view, the ectopterygoid articulates medially against the pterygoid. The anterior portion of the ectopterygoid-ptyergoid suture, which is partially disarticulated on the left side, is straight. More posteriorly, the suture diverges slightly laterally away from the diagonal palatal tooth row on the pterygoid.

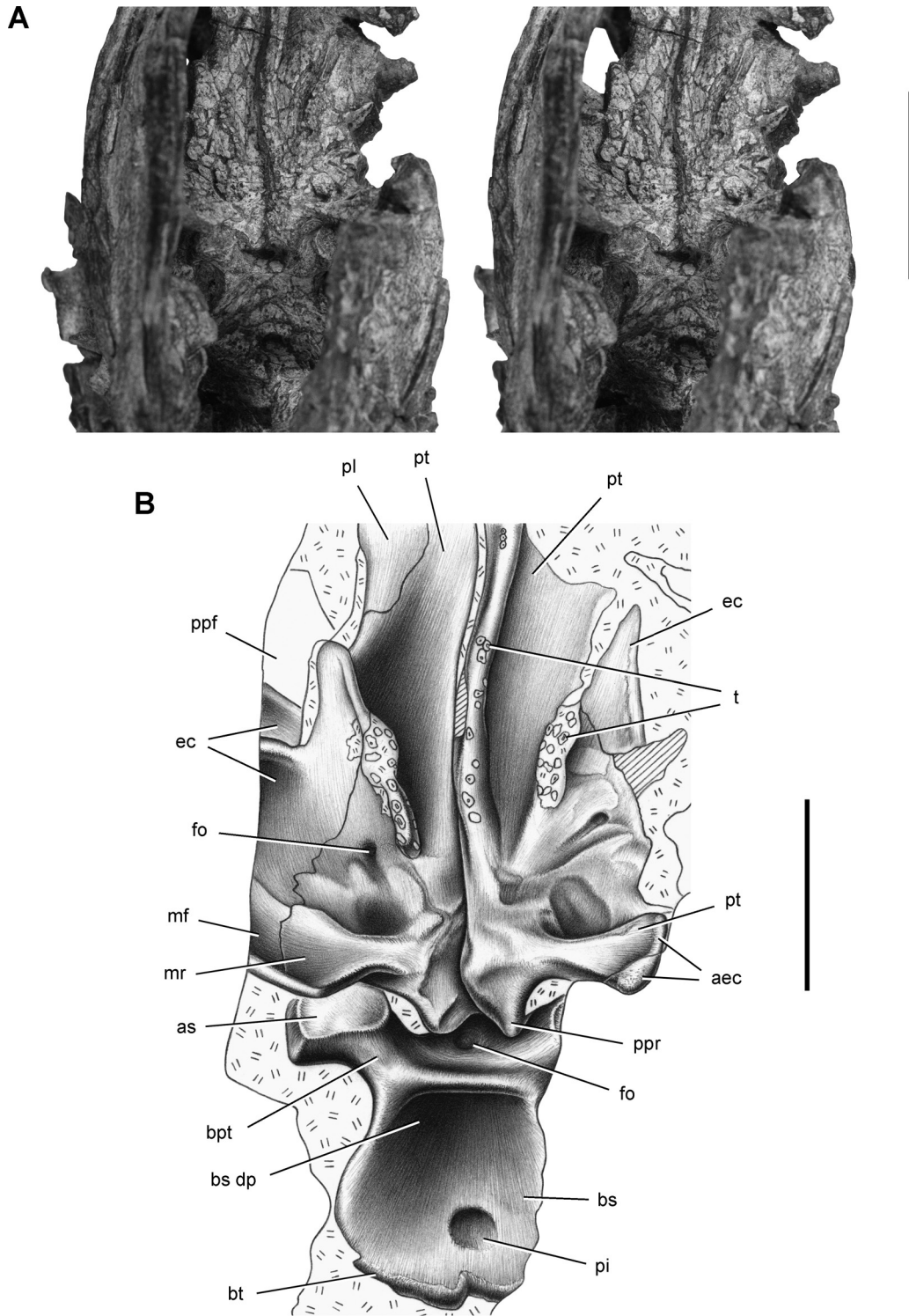


FIGURE 29. Stereopair (A) and drawing (B) of the posterior palate in the skull of *Eoraptor lunensis* (PVSJ 512) in ventral view. **Abbreviations:** aec, articular surface for the ectopterygoid; as, articular surface; bpt, basipterygoid process; bs, basisphenoid; bt, basal tubera; dp, depression; ec, ectopterygoid; fo, foramen; mf, mandibular flange; mr, mandibular ramus; pi, pit; pl, palatine; ppf, postpalatine fenestra; ppr, posterior process; pt, pterygoid; t, tooth. Hatching indicates a broken surface; double hatch marks indicate matrix. Scale bar in A equals 2 cm and in B equals 1 cm.

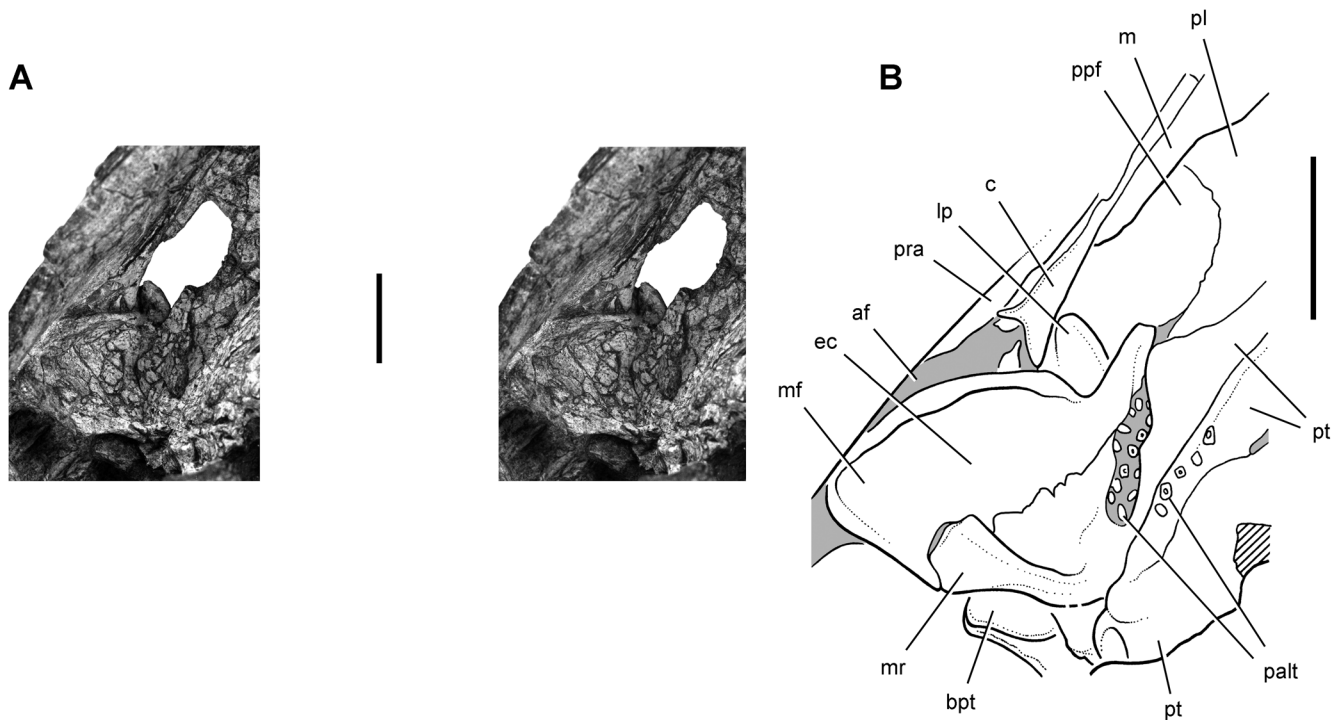


FIGURE 30. Stereopair (A) and drawing (B) of the posterior palate in the skull of *Eoraptor lunensis* (PVSJ 512) in ventromedial view. **Abbreviations:** **af**, adductor fossa; **bpt**, basipterygoid process; **c**, coronoid; **ec**, ectopterygoid; **lp**, lateral process; **m**, maxilla; **mf**, mandibular flange; **mr**, mandibular ramus; **palt**, palatal teeth; **pl**, palatine; **ppf**, postpalatine fenestra; **pra**, prearticular; **pt**, pterygoid. Dashed line indicates a missing margin; hatching indicates a broken surface; shading indicates matrix. Scale bars equal 1 cm.

The mandibular flange is a broad, subtriangular sheet of bone more than one-half of which is formed by the ectopterygoid (Fig. 33A, B). It extends ventrolaterally into the adductor fossa of the lower jaw. The palatal surface of the mandibular flange is gently concave. The shallow concavity, which is not invaginated, is deepest near the anterior and posterior rims formed, respectively, by the ectopterygoid and pterygoid. There is no evidence that this shallow depression housed a pneumatic sac, as is the case in

the invaginated depression present on the ventral aspect of the ectopterygoid in most theropods (e.g., *Tyrannosaurus*; Brochu, 2002).

**Vomer**—The diamond-shaped footplate of the vomer is displaced dorsally and lies on the ventral aspect of the nasals within the narial passage (Fig. 28). The dorsoventrally flattened footplate and the exposed anterior portion of the shaft are coossified as a single element. More posteriorly on the palate, the vomer may



FIGURE 31. Stereopair (A) and drawing (B) of the ventral portion of the right orbit in the skull of *Eoraptor lunensis* (PVSJ 512) in ventromedial view. **Abbreviations:** **ec**, ectopterygoid; **j**, jugal; **l**, lacrimal; **m**, maxilla; **po**, postorbital; **ppf**, postpalatine fenestra. Dashed line indicates a missing margin; hatching indicates a broken surface; shading indicates matrix. Scale bars equal 1 cm.

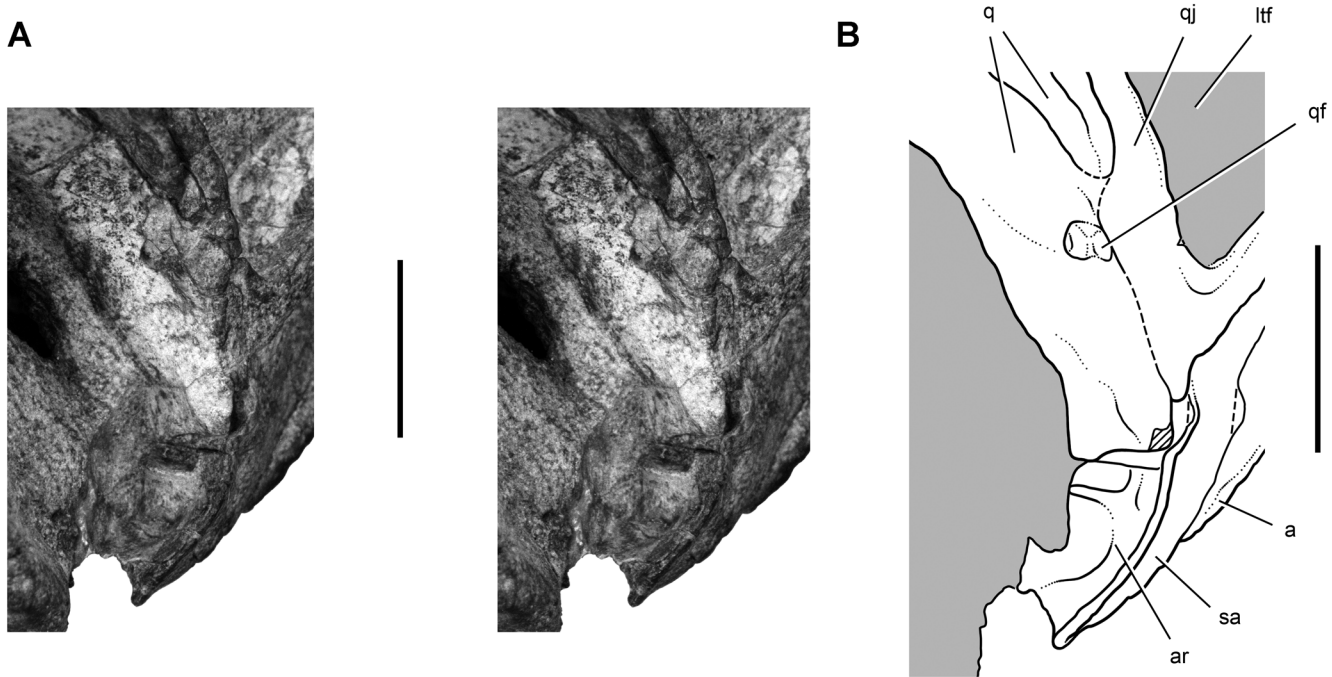


FIGURE 32. Stereopair (A) and drawing (B) of the right jaw articulation in the skull of *Eoraptor lunensis* (PVSJ 512) in posterodorsolateral view. **Abbreviations:** a, angular; ar, articular; lf, laterotemporal fenestra; q, quadrate; qf, quadrate foramen; qj, quadratojugal; sa, surangular. Dashed line indicates a missing margin; hatching indicates a broken surface; shading indicates matrix. Scale bars equal 1 cm.

have diverged as a paired bone, although no further evidence of the form of the vomera can be discerned from computed tomographic cross-sections.

### Braincase

The occiput is fractured into many pieces, which have shifted from their original positions (Fig. 19). The basisphenoid, the only complete exposed bone in the braincase, lies near its natural position posterior to the palate (Fig. 29). Computed tomographic cross-sections unfortunately do not clarify the morphology of the braincase.

**Supraoccipital**—The central portion of the supraoccipital is preserved a few millimeters from its natural articulation with the parietals. Little can be said about its morphology beyond the fact that there is a prominent nuchal eminence or crest for attachment of nuchal ligaments that would have been visible in dorsal view of the skull (Figs. 14, 15), as in *Herrerasaurus* (Sereno and Novas, 1994). There may have been a foramen between the parietal and supraoccipital (Fig. 41). A portion of the lateral margin of the foramen magnum may pertain to the exoccipital-opisthotic, but its identity remains speculative, as do many occipital fragments.

**Basisphenoid**—In ventral view, the basisphenoid has a subquadrate shape (Fig. 29). The central portion of the basisphenoid is concave in ventral view, bounded anteriorly and posteriorly by crests, the former a web of bone between the basiptyergoid processes and the latter the basal tubera. The lateral margins are broadly open rather than enclosed by a bony walls. We identify this shallow structure as a basisphenoid depression (Fig. 29) rather than a ‘basisphenoid fossa,’ the term used to describe the deeper, invaginated structure present in *Eodromaeus* (Martínez et al., 2011) and neotheropods such as *Ceratosaurus* and *Allosaurus*.

The basiptyergoid processes are very robust, pyramidal processes (Fig. 29). These do not resemble the transversely compressed, plate-like processes in *Eodromaeus* (Martínez et al., 2011) or other basal theropods. Rather, they are closer in form to the condition in basal sauropodomorphs such as *Plateosaurus* (Galton, 1984; Sereno, 2007b) and *Adeopapposaurus* (Martínez, 2009). In lateral view, they project below the basal tubera. In posterior view, they project ventrolaterally at approximately 45° from the horizontal. In ventral or lateral view, the processes project much more strongly ventrally than anteriorly. Each process has a distinct shaft proximal to an expanded oval articular end. The broad, wedge-shaped articular surface is fitted to a notch at the posterior end of the pterygoid; a flat surface, constituting one-half of the wedge-shaped articular end, is exposed in ventral view. A small foramen opens on the anterior side of the lamina joining the bases of the basiptyergoid processes (Fig. 29).

The basal tubera are separated in the midline by a very shallow notch and project ventrally as a fan-shaped plate of bone. In the midline dorsal to the notch, a cylindrical pit passes into the body of the basisphenoid (Fig. 29).

### Lower Jaw

The following description is based almost entirely on the well-preserved holotypic right lower jaw (Figs. 10–13, 16, 17, 20, 23, 30, 32, 33A, B, 34, 40B, C). The jaws are preserved in natural articulation. The quadrate condyles on both sides are seated within the respective articular cotyli, and the tooth rows are fully engaged. Given the articulation at the jaw joints, it can be seen that the dentaries do not extend as far anteriorly relative to the premaxillary arcade in *Eoraptor* as is typical in theropods. The tip of the dentary lies adjacent to the third premaxillary tooth on each

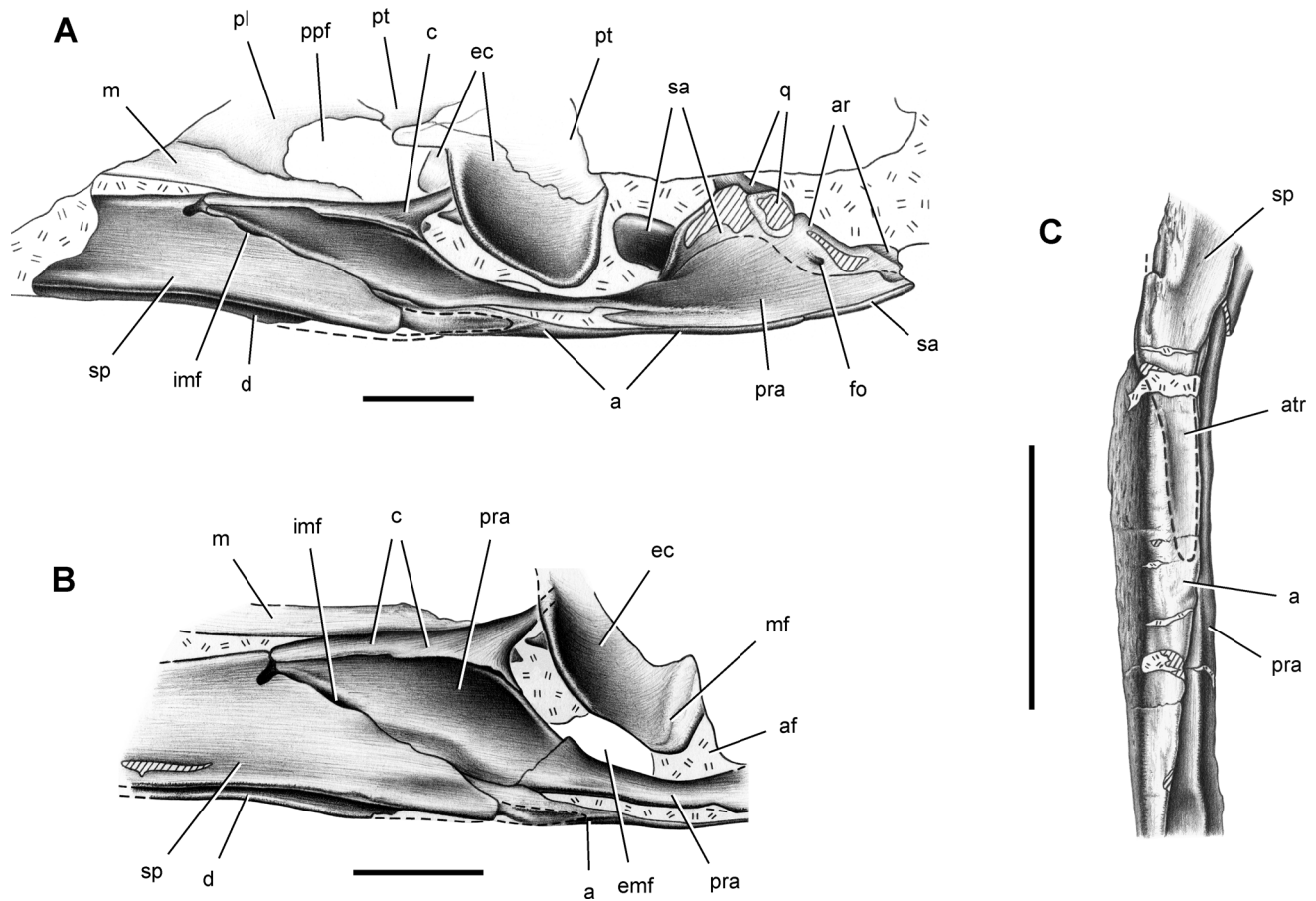


FIGURE 33. Drawings of the lower jaw in the skull of *Eoraptor lunensis* (PVSJ 512). **A**, Posterior two-thirds of the right lower jaw in ventromedial view. **B**, midsection of the right lower jaw in medial view. **C**, midsection of the right lower jaw in ventral view. **Abbreviations:** a, angular; af, adductor fossa; ar, articular; atr, articular trough; c, coronoid; d, dentary; ec, ectopterygoid; emf, external mandibular fenestra; imf, internal mandibular fenestra; fo, foramen; m, maxilla; mf, mandibular flange; pl, palatine; ppf, postpalatine fenestra; pra, prearticular; pt, pterygoid; q, quadrate; sa, surangular; sp, splenial. Dashed line indicates a missing margin; hatching indicates a broken surface; double hatch marks indicate matrix. Scale bars equal 1 cm.

side (Figs. 16, 17, 20). In *Herrerasaurus* (PVSJ 407), in contrast, the dentary tips lie adjacent to the second premaxillary tooth and immediately posterior to the first premaxillary tooth (Sereno and Novas, 1994:fig. 1F). The gap anterior to the dentary ends, we suggest below, may be indicative of the presence in life of a small keratinous lower beak in *Eoraptor*, a condition well described in larger-bodied basal sauropodomorphs (Sereno, 2007b; Martínez, 2009).

**Dentary**—The dentary is the longest and most robust element of the lower jaw (Figs. 10–13, 16, 17, 20, 23, 33A, B, 34, 40B, C). It is proportionately longer than in *Herrerasaurus* (PVSJ 407), constituting more than half of the length of the lower jaw, as measured from the tip to the anterior margin of the mandibular fenestra. Its sutural contacts include the splenial medially and the surangular and angular laterally. The dentary also may contact the coronoid and intercoronoid medially, but this region is obscured by the maxilla. Several neurovascular foramina open along a ventrally curved groove located on the anterior one-half of the dentary near the tips of the anterior maxillary crowns (Figs. 10–13, 20, 40B). This groove is best preserved on the left side, which has an unusually large foramen near its anterior end (Figs. 12, 13). The groove dissipates under the second maxillary tooth. A neurovascular groove of similar form and position is present in *Panphagia*

and *Pampadromaeus* (Martínez and Alcober, 2009; Cabreira et al., 2011).

The anterior one-half of the dentary resembles in some features that of *Herrerasaurus*. In ventral view of the anterior end, the flat facet of the dentary symphysis is exposed on the left side, showing that the symphysis was restricted to a 4-mm section at the anterior end of the dentary ramus (Figs. 23, 40C). The facet is oblique to the sagittal plane, indicating that the dentaries have suffered some transverse compression after burial, as is also the case with the dorsal skull roof and palate. Several additional foramina exit the anterior end of the dentary below the tips of the premaxillary crowns, most notably two large anterior dentary foramina near the alveolar margin (Fig. 23, 40B). This condition closely resembles that in basal sauropodomorphs (*Plateosaurus*, *Adeopapposaurus*), in which the foramina appear to have supported a keratinous bill (Sereno, 2007b; Martínez, 2009).

The posterior one-half of the dentary is plate-like, with a sharp ventral edge that is narrower than the adjacent splenial. The posterior end of the dentary is forked, as preserved on the right side (Figs. 10, 11, 40B). The arched margin between the dorsal and ventral processes of the posterior end is somewhat fragmented but clearly would have formed the anterior margin of the mandibular

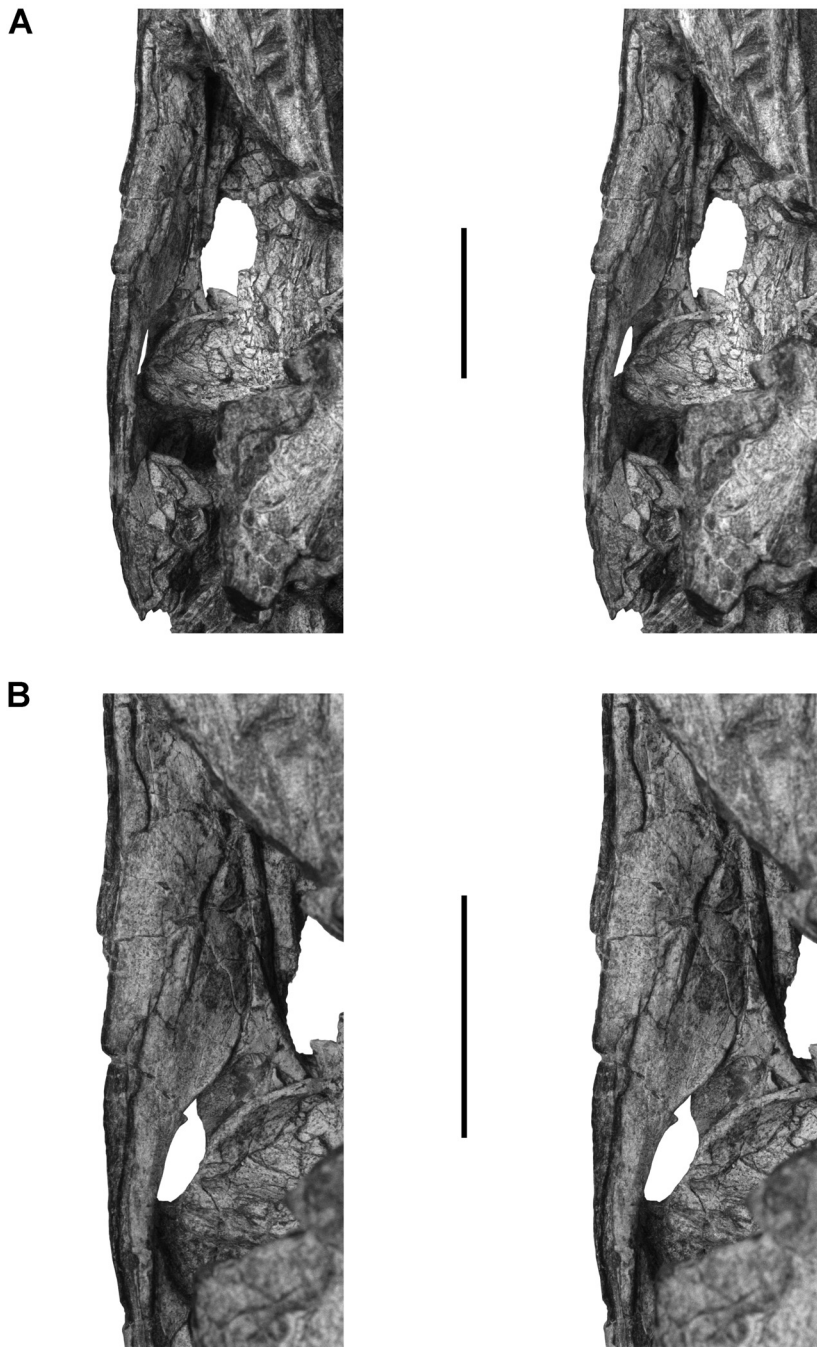


FIGURE 34. Stereopairs of the lower jaw of *Eoraptor lunensis* (PVSJ 512). **A**, posterior two-thirds of the right lower jaw in ventromedial view. **B**, midsection of the right lower jaw in medial view. Scale bars equal 2 cm.

fenestra. The dorsal process may be slightly shorter than the ventral process but is not completely exposed. The ventral portion of the dorsal process is overlapped by the surangular, but whether it fits into a slot in the surangular cannot be determined. Its form, however, differs from the specialized dentary process in *Herrerasaurus* (PVSJ 407), which is very slender, 'T'-shaped in cross-section, and fitted into a narrow slot in the surangular (Sereno and Novas, 1994). The ventral process in *Eoraptor* overlaps the anterior end of the angular (Figs. 10, 11, 40B). The dorsal margin of this process may have broken away, judging from the broad surface on the angular with which it may have articulated.

**Surangular**—The surangular forms the most lateral portion of the jaw articulation, where it contacts the ventral edge of the quadratojugal and the lateral condyle of the quadrate (Figs. 10, 11, 32, 40B, C). Other contacts include the dentary, splenial, and probably the coronoid anteriorly, the angular and prearticular ventrally, and the articular posteriorly. The surangular forms the posterior margin of the external mandibular fenestra. Unlike many derived theropods, such as *Ceratosaurus* and *Allosaurus* (Gilmore, 1920), the coronoid margin of the surangular ventral to the jugal is anteroposteriorly convex in lateral view (Fig. 40B, C), as in *Panphagia* (Martínez and Alcober, 2009). It is also transversely

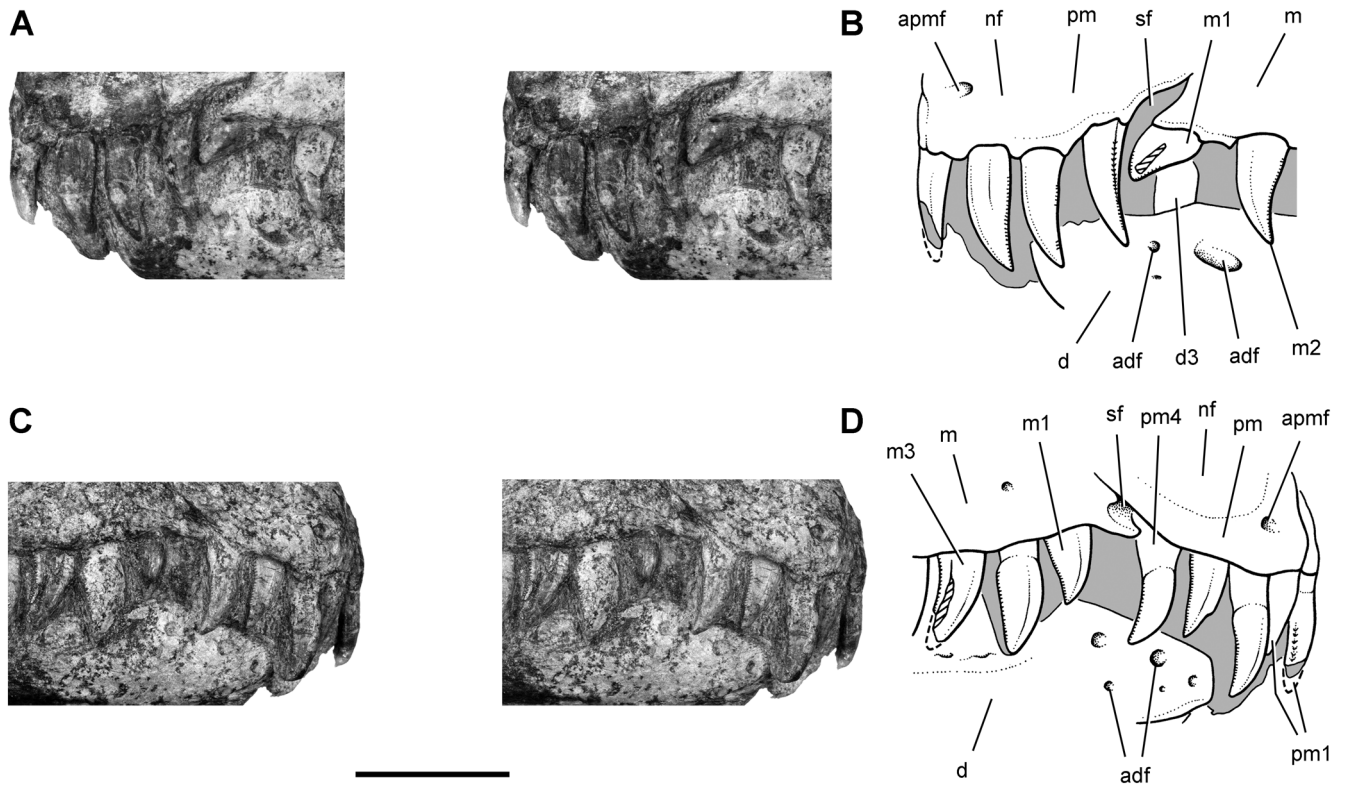


FIGURE 35. Premaxillary and anterior maxillary teeth of *Eoraptor lunensis* (PVSJ 512). Stereopair (A) and drawing (B) of left premaxillary and anterior maxillary teeth in lateral view. Stereopair (C) and drawing (D) of the right premaxillary and anterior maxillary teeth in lateral view. **Abbreviations:** **adf**, anterior dentary foramen; **apmf**, anterior premaxillary foramen; **d**, dentary; **d3**, dentary tooth 3; **m**, maxilla; **m1, 2, 3**, maxillary tooth 1, 2, 3; **nf**, narial fossa; **pm**, premaxilla; **pm1, 4**, premaxillary tooth 1, 4; **sf**, subnarial foramen. Dashed line indicates a missing margin; hatching indicates a broken surface; shading indicates matrix. Scale bar equals 1 cm.

broad and rounded in dorsal view. The surangular ridge anterior to the jaw articulation is very poorly developed in *Eoraptor*, and the small posterior surangular foramen is positioned not far from the jaw articulation (Figs. 10, 11, 40B). In *Herrerasaurus* (PVSJ 407), in contrast, the surangular ridge is developed as a promi-

nent ridge, and the posterior surangular foramen is positioned farther from the jaw articulation. In *Eoraptor*, an additional foramen, the anterior surangular foramen, exits the external surface of the surangular above the external mandibular fenestra. The retroarticular process projects posteriorly, as in the basal sauropodomorphs

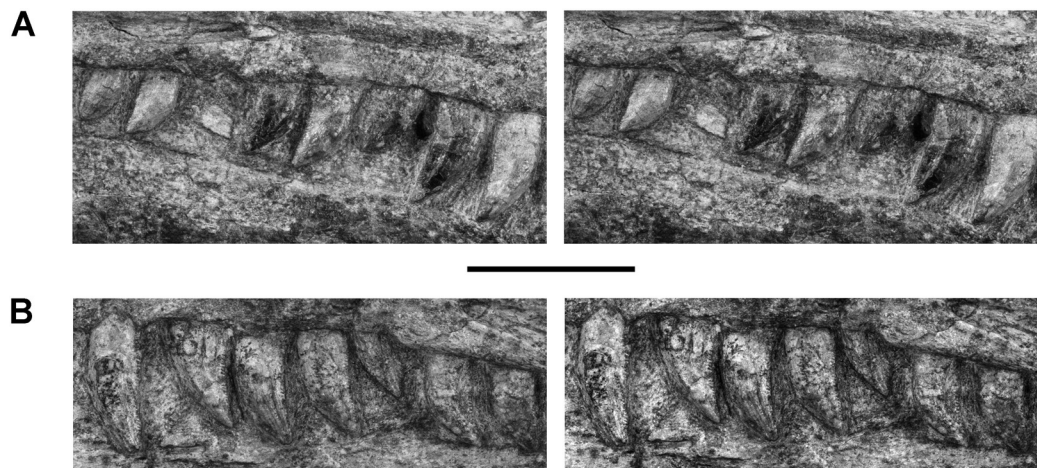


FIGURE 36. Stereopairs of the maxillary teeth of *Eoraptor lunensis* (PVSJ 512). **A**, right middle maxillary teeth 4–11 in lateral view. **B**, left middle maxillary teeth 4–10 in lateral view. Scale bar equals 1 cm.

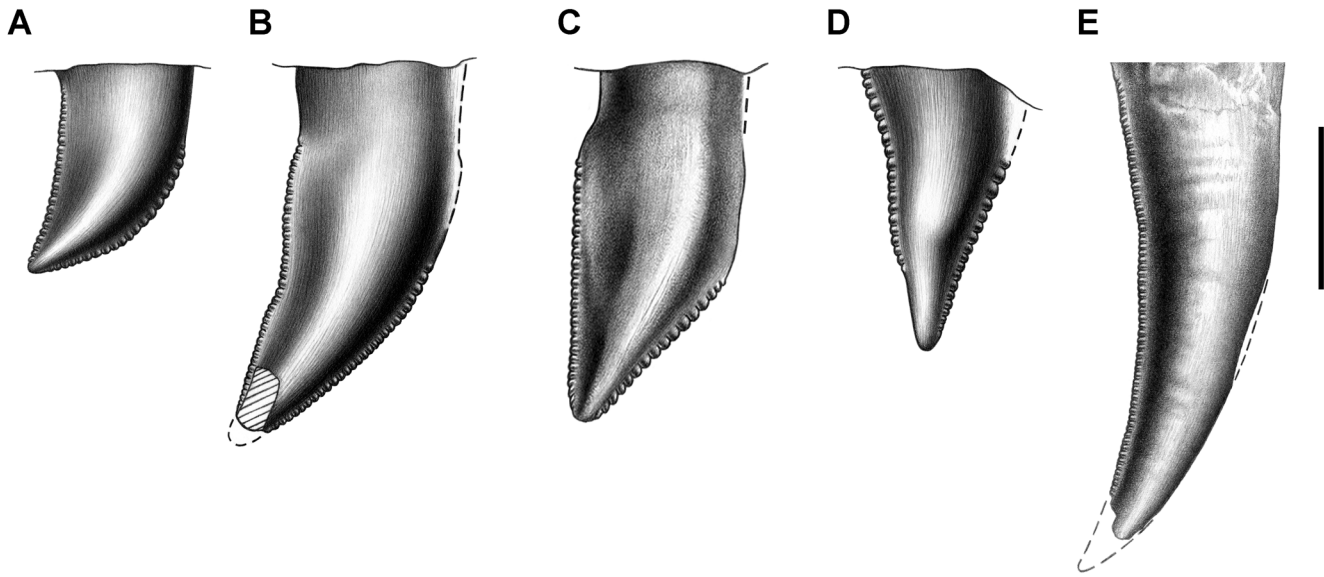


FIGURE 37. Drawings of premaxillary and maxillary teeth of *Eoraptor lunensis* (PVSJ 512) and *Eodromaeus murphi* (PVSJ 561). **A**, posterior maxillary tooth 10 of *Eoraptor lunensis* in right lateral view. **B**, middle maxillary tooth 4 of *Eoraptor lunensis* in right lateral view. **C**, anterior maxillary tooth 2 of *Eoraptor lunensis* in right lateral view. **D**, premaxillary tooth 3 of *Eoraptor lunensis* in right lateral view. **E**, maxillary tooth 3 of *Eodromaeus murphi* in medial view. Dashed line indicates a missing margin; hatching indicates a broken surface. Scale bar equals 3 mm.

*Panphagia* and *Pampadromaeus* (Martínez and Alcober, 2009; Cabreira et al., 2011). It is not upturned as in the basal theropod *Herrerasaurus* (PVSJ 407). An inturned, plate-shaped process of the surangular anterior to the quadrate condyle is partially exposed in medial view (Figs. 33A, 34).

**Angular**—The angular extends from its articulation with the dentary and splenial to a point very near the posterior end of the retroarticular process, where its slender distal tip has broken away (Figs. 10, 11, 32, 33). As in the basal sauropodomorphs *Panphagia* (Martínez and Alcober, 2009) and *Pampadromaeus* (Cabreira et al., 2011), the angular and surangular constitute a smaller proportion of the length of the lower jaw than in *Herrerasaurus*. The angular overlaps the surangular dorsally and articulates in a groove between the surangular and prearticular posteriorly. Anteriorly, the angular is overlapped laterally by the dentary. Its ventral margin curls medially, where there is a shallow, smooth, lanceolate-shaped depression for the posterior tip of the splenial, which has broken away (Fig. 33). The depression for the splenial tip is located on the ventromedial aspect of the angular and forms the concave portion of the concavo-convex splenial-angular articulation characteristic of most theropods. Given the smooth articular surface, it is quite possible that some movement at this articulation was possible. In *Herrerasaurus* (Serenó and Novas, 1994) and *Staurikosaurus* (pers. observ.), in contrast, the splenial-angular joint has the opposite concavo-convex configuration, with an articular fossa on the splenial posterior process.

**Splenial**—The splenial contacts the dentary laterally and the coronoid, prearticular, and angular posteriorly (Figs. 33, 34). In medial view of the lower jaw, the splenial overlaps the prearticular along a long contact. A shallow notch in this border and an adjacent groove along the anterior margin of the prearticular constitute the margins of the small internal mandibular fenestra (Figs. 33A, B, 34), as in *Panphagia* (Martínez and Alcober, 2009). A slightly larger opening is present in larger-bodied basal sauropodomorphs such as *Plateosaurus* (Galton, 1984). In theropods, in contrast, the internal mandibular fenestra is often

proportionately larger, with a deeper notch on the posterior margin of the splenial (e.g., *Tyrannosaurus*; Brochu, 2002). Dorsal to the small internal mandibular fenestra in *Eoraptor*, the thickened dorsal margin of the splenial meets the anterior end of the coronoid. Just below this contact, the splenial margin has a notch; the notch may have an articular function or it may constitute the margin of a small foramen (Figs. 33A, B, 34, 40C). No other foramina are present on the splenial, in contrast to many theropods, which have a splenial notch or foramen or notch near the ventral margin of the bone ('mylohyal foramen' in *Tyrannosaurus*; Brochu, 2002).

The posterior end of the splenial overlaps the angular (Fig. 40C). Although its distal end is broken away on the right side, an articular depression on the ventromedial aspect of the angular shows where the tip would have articulated (Figs. 33C, 34). In *Herrerasaurus* (PVSJ 407) and *Staurikosaurus* (pers. observ.), in contrast, the distal end of the splenial twists onto the ventral aspect of the angular and has a transversely concave, rather than transversely convex, articular surface (Serenó and Novas, 1994).

**Coronoid**—The triradiate coronoid has a short, slender posteroventral process, a longer posterodorsal process, and a much longer anterior process (Figs. 33A, B, 34, 40C). The prearticular provides the main sutural contact, although the coronoid reaches the splenial anteriorly and probably the dentary posterodorsally.

The posteroventral process is anteroposteriorly compressed and has a slot along its ventral margin, into which articulates the thin dorsal edge of the prearticular (Fig. 33B). As preserved on the right side, this articulation is slightly ajar, exposing the opposing articular surfaces. The posterodorsal process is transversely flattened. Its distal tip and contacts are not exposed. The anterior process is also transversely flattened and extends to a common junction with the prearticular and splenial (Fig. 33A, B, 34). This junction of bones on the medial side of the lower jaw is positioned considerably anterior to the contact between the dentary and surangular on the lateral side (Fig. 40C). In neotheropods, in contrast, these medial and lateral articulations are positioned adjacent to one another, functionally dividing the lower jaw into

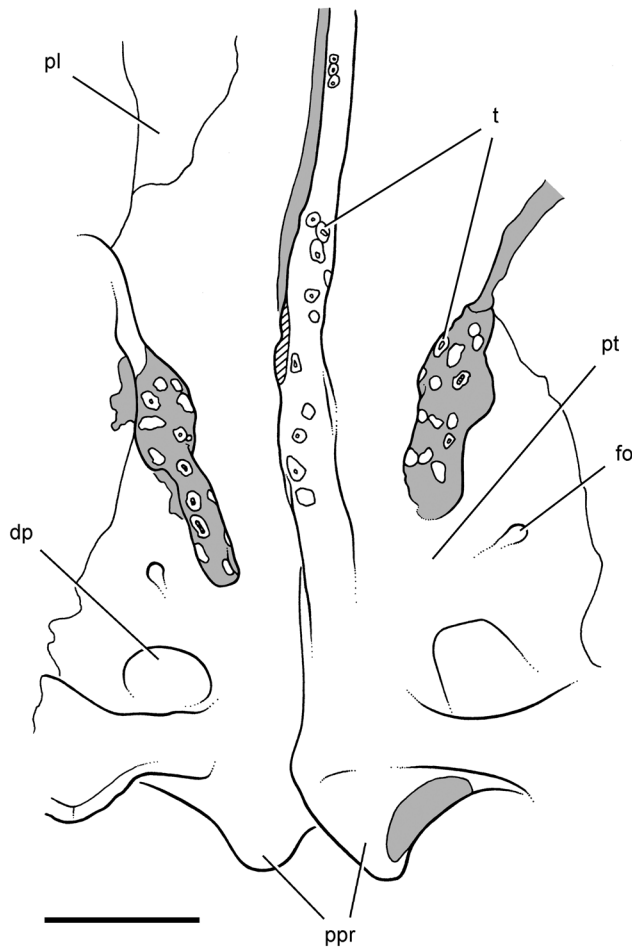


FIGURE 38. Palatal teeth of *Eoraptor lunensis* (PVSJ 512) in ventral view. **Abbreviations:** **dp**, depression; **fo**, foramen; **pl**, palatine; **ppr**, posterior process; **pt**, pterygoid; **t**, tooth. Hatching indicates a broken surface; shading indicates matrix. Scale bar equals 5 mm.

anterior and posterior units, as is well described in *Tyrannosaurus* (Brochu, 2002).

**Intercoronoid**—The presence of an intercoronoid bone anterior to the coronoid cannot be determined in *Eoraptor*, because of the presence of matrix between the anterior ends of the lower jaws. A separate, strap-shaped intercoronoid bone is present just ventral to the alveolar border of the dentary in *Panphagia* (Martínez and Alcober, 2009), similar to the condition in larger-bodied basal sauropodomorphs such as *Plateosaurus* (Brown and Schlaikjer, 1940) and *Adeopapposaurus* (Martínez, 2009). No intercoronoid, however, was reported in the many available skulls of the basal sauropodomorph *Massospondylus* (Sues et al., 2004). Given the phylogenetic proximity of *Panphagia* to *Eoraptor*, it is likely that a slender intercoronoid will eventually be shown to be present (Fig. 40C).

**Prearticular**—The prearticular is an elongate, plate-like bone that extends from the middle of the lower jaw, anteriorly, to the distal end of the retroarticular process, posteriorly (Figs. 33, 34, 40C). It contacts the coronoid dorsally, the splenial and angular ventrally, and the articular posteriorly. The anterior end of the prearticular is tongue-shaped. Its anterior margin has a groove for the internal mandibular opening. A raised lip is developed along a

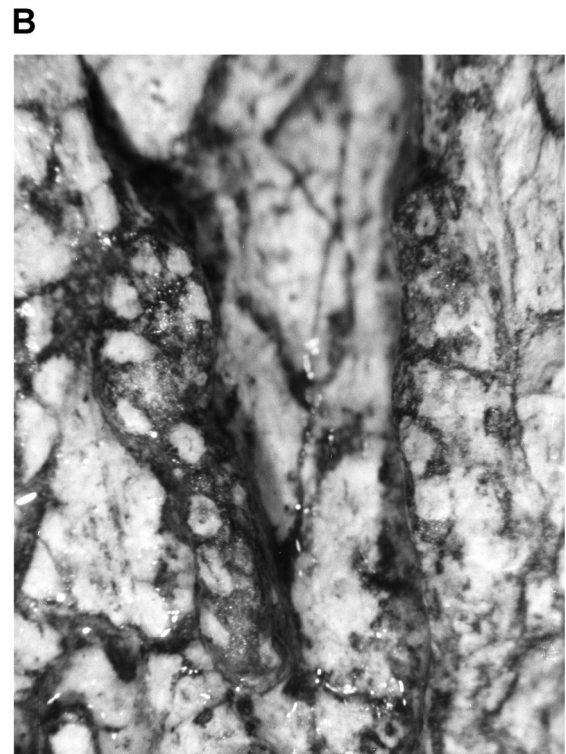
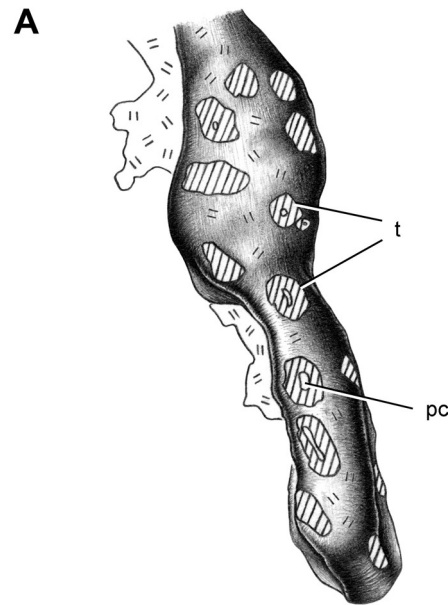


FIGURE 39. Diagonal palatal tooth rows on the right pterygoid of *Eoraptor lunensis* (PVSJ 512) in ventral view. **A**, drawing of pterygoid tooth rows. **B**, photograph of pterygoid tooth rows. **Abbreviations:** **pc**, pulp cavity; **t**, tooth. Hatching indicates a broken or abraded surface; shading and double hatch marks indicate matrix. Scale bars equal 5 mm in **A** and **B**.

portion of its border of the adductor fossa, posterior to which it becomes a narrow shaft 3 mm in height. More posteriorly, it expands as a thin sheet under the articular. As the suture passes near the jaw articulation, the prearticular and articular are coossified. The

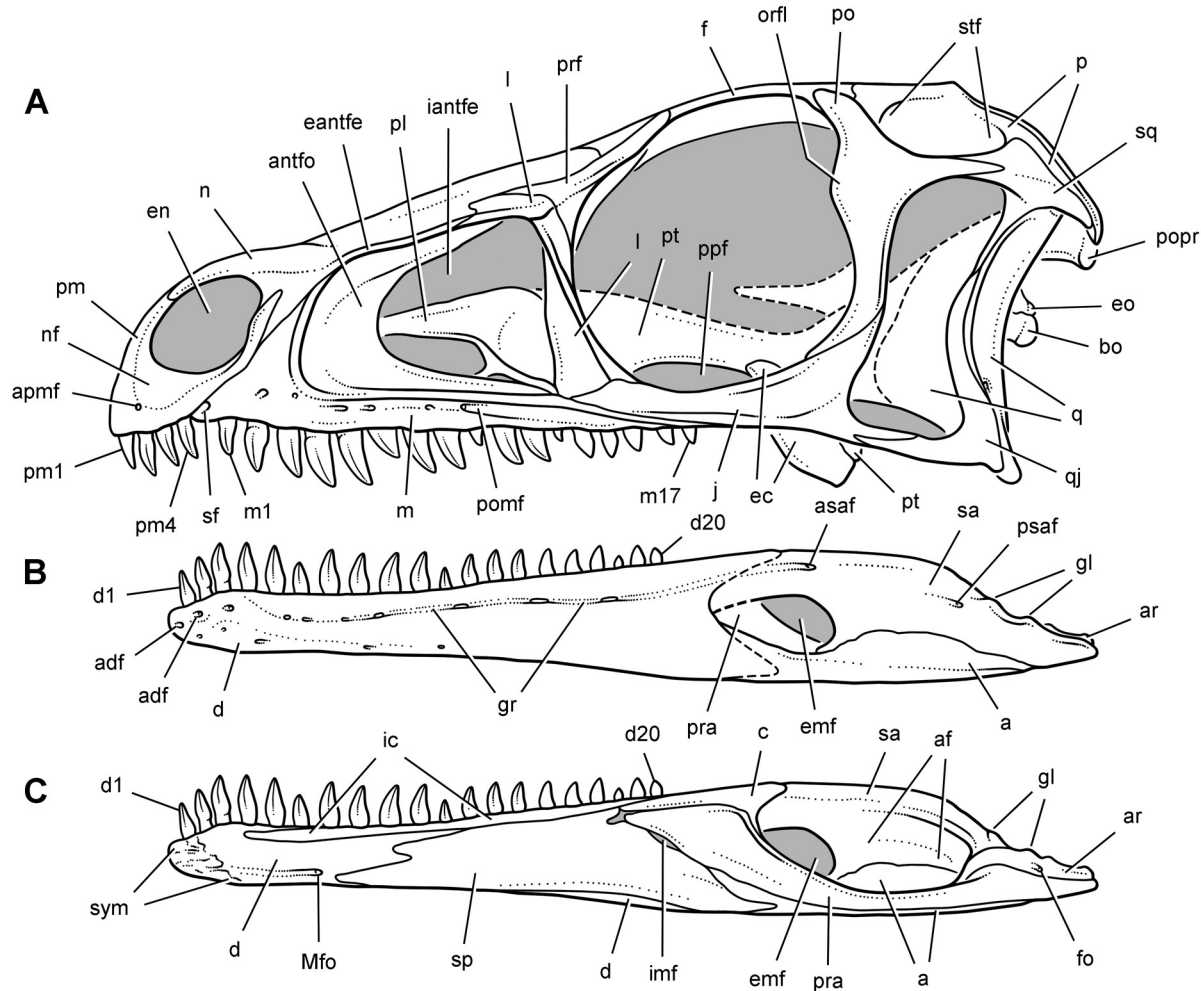


FIGURE 40. Reconstruction of the skull of *Eoraptor lunensis* (PVSJ 512). **A**, cranium in left lateral view. **B**, lower jaw in left lateral view. **C**, lower jaw in medial view. Intercoronoid and most dentary teeth based on *Panphagia protos* (Martínez and Alcober, 2009). **Abbreviations:** a, angular; adf, anterior dentary foramen; af, adductor fossa; antfo, antorbital fossa; apmf, anterior premaxillary foramen; ar, articular; asaf, anterior surangular foramen; bo, basioccipital; c, coronoid; d, dentary; d1, 20, dentary tooth 1, 20; eantfe, external antorbital fenestra; ec, ectopterygoid; emf, external mandibular fenestra; en, external naris; eo, exoccipital; f, frontal; fo, foramen; gl, glenoid; gr, groove; iantfe, internal antorbital fenestra; ic, intercoronoid; imf, internal mandibular fenestra; j, jugal; l, lacrimal; m, maxilla; m1, 17, maxillary tooth 1, 17; Mfo, foramen of Meckel's canal; n, nasal; nf, narial fossa; orfl, orbital flange; p, parietal; pl, palatine; pm, premaxilla; pm1, 4, premaxillary tooth 1, 4; po, postorbital; pomf, posterior maxillary foramen; popr, paroccipital process; ppf, postpalatine fenestra; pra, prearticular; prf, prefrontal; psaf, posterior surangular foramen; pt, pterygoid; q, quadrate; qj, quadratojugal; sa, surangular; sf, subnarial foramen; sp, splenial; sq, squamosal; stf, supratemporal fossa; sym, symphysis. Dashed line indicates bone edge obscured by matrix.

suture is visible again more posteriorly on the retroarticular process (Figs. 33A, 40C).

**Articular**—Non-articular surfaces of the articular are exposed dorsally and medially on the right retroarticular process (Figs. 33A, 34A, 40C). Other surfaces are obscured by the quadrate condyles, surangular, and prearticular. The articular and quadrate form the majority of the jaw joint, which is partially exposed posterior to the right quadrate. Although its exact shape in dorsal view cannot be seen, it can be determined that the long axis of the cotylus is oriented at a right angle to the long axis of the skull, dipping only slightly ventromedially. Posterior to the jaw articulation,

the dorsal surface of the articular is deeply concave. The articular, which appears to be only loosely attached to the enveloping surangular and prearticular, forms the bulk of the retroarticular process. With a subtriangular shape in dorsal, medial, and lateral views, the retroarticular process projects posteriorly and closely resembles that in *Panphagia*, and other basal sauropodomorphs (Galton, 1984; Sues et al., 2004; Sereno, 2007b; Martínez, 2009; Martínez and Alcober, 2009; Cabreira et al., 2011). The basal theropod *Eodromaeus* (Martínez et al., 2011) has a similar retroarticular process, although the process is more upturned and complex in *Herrerasaurus* (Sereno and Novas, 1994). There

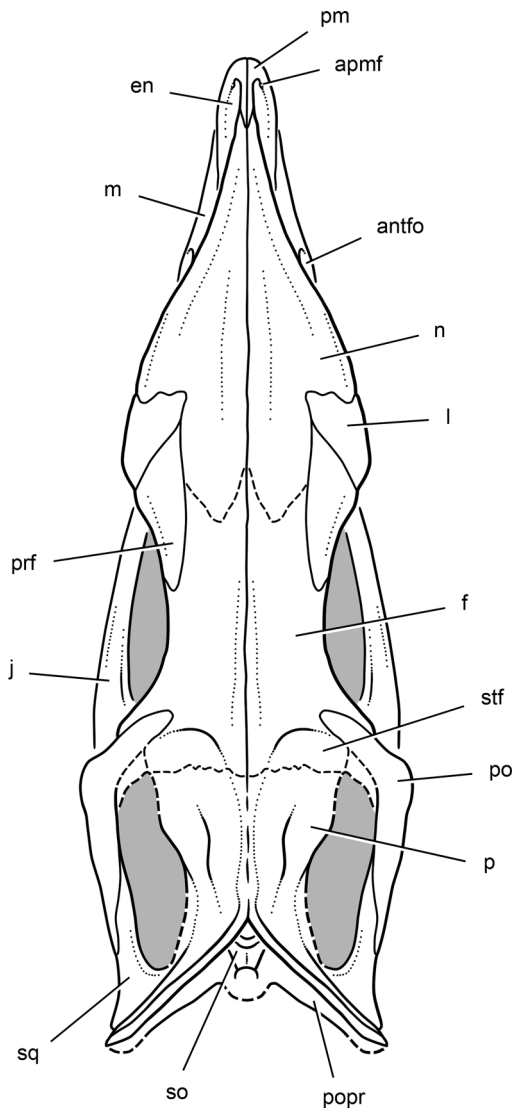


FIGURE 41. Reconstruction of the cranium of *Eoraptor lunensis* (PVSJ 512) in dorsal view. **Abbreviations:** antfo, antorbital fossa; apmf, anterior premaxillary foramen; en, external naris; f, frontal; j, jugal; l, lacrimal; m, maxilla; n, nasal; p, parietal; pm, premaxilla; po, postorbital; popr, paroccipital process; prf, prefrontal; so, supraoccipital; sq, squamosal; stf, supratemporal fossa. Dashed line indicates estimated position of suture or bone edge.

is no development of a pendant medial process on the articular, which characterizes allosauroid theropods (e.g., *Allosaurus*; Gilmore, 1920:fig. 15B).

A foramen that is slightly larger than the posterior surangular foramen opens posteroventral to the jaw articulation on the medial side of the articular (Figs. 33A, 34A, 40C). A groove passes posteroventrally into the foramen, which probably provided passage for a branch of cranial nerve VII.

## Teeth

**General Features**—The tooth rows are most complete on the right side of the skull, which was buried in the sediment when

originally discovered (Figs. 10, 11, 35–37). The tooth rows contain four premaxillary and 17 maxillary teeth. The number of dentary teeth can be estimated from the computed tomography (CT) data of the partial left dentary and from comparison to the closely related genus *Panphagia*. The anterior 14 dentary teeth are preserved in the left dentary. *Panphagia* has 22 or 23 dentary teeth, and the holotypic skull of *Eoraptor* probably had at least 20 dentary teeth. Palatal teeth are also present and restricted to the pterygoid (Figs. 38, 39).

The first tooth in the upper tooth row is situated at the anterior extremity of the premaxilla near the midline; there is no gap between the anterior-most teeth in each premaxilla. The last tooth in the upper tooth row, the 17th maxillary tooth, is situated under the orbit (Figs. 10, 11, 40A). Extension of the tooth row under the orbit is the primitive condition for saurischians, retained in basal sauropodomorphs such as *Plateosaurus* and in basal theropods such as *Herrerasaurus* and ceratosaurians (Tykoski and Rowe, 2004). The last tooth in tetanurans, in contrast, is located at the anterior margin of the orbit (Gauthier, 1986).

The upper tooth row in *Eoraptor* is interrupted by the presence of a short diastema between the premaxilla and maxilla that is roughly equivalent to the width of a single tooth (Figs. 35, 40A). Tooth size decreases adjacent to the diastema; the last premaxillary crown and first maxillary crown are distinctly smaller than adjacent crowns. Computed tomographic cross-sections suggest that the third dentary tooth, the base of which has been exposed on the left side (Fig. 35A, B), is slightly enlarged and positioned opposite the diastema.

Preparation between the premaxillary teeth reveals that the small first dentary tooth is inset about the length of one alveolus from the anterior end of the ramus. Retraction of the first dentary tooth to accommodate a lower keratinous bill is a feature present in *Panphagia* and other basal sauropodomorphs (Sereno, 2007b; Martínez, 2009). At first, it appears that *Pampadromaeus* does not exhibit similar retraction of the first dentary tooth, given the position of the first tooth in the preserved dentary and skull reconstruction (Cabreira et al., 2011:fig. 2). A close-up photograph, however, shows that the first tooth is dislodged anteriorly from its alveolus (Cabreira et al., 2011:fig. S4). That first alveolus, seen in lateral view as a concave dip in the alveolar margin, is clearly inset from the end of the dentary, which is marked by several neurovascular foramina.

Fully exposed premaxillary and anterior maxillary crowns (Figs. 35–37) have a similar crown profile to that in basal sauropodomorphs, such as *Panphagia* (Martínez and Alcober, 2009), *Pampadromaeus* (Cabreira et al., 2011), *Adeopapposaurus* (Martínez, 2009), and *Plateosaurus* (Galton, 1984). All teeth in the upper tooth rows appear to have a basal constriction and all but the posterior-most crowns are gently recurved. In erupting teeth, the basal constriction and eminence may be obscured by the alveolar margin, because the upper part of the crown appears more similar in profile to that common among theropods. The constriction is weakest just posterior to the center of the maxillary tooth row around maxillary tooth 10 (Fig. 37A). The small, subtriangular posterior maxillary crowns have lost any recurvature and have a shape in lateral view resembling primitive ornithischian cheek teeth (Figs. 10, 11, 20). Whether the basal constriction is present in dentary crowns cannot be determined, although such is likely given the matching form of the dentary teeth in *Panphagia* (Martínez and Alcober, 2009), *Pampadromaeus* (Cabreira et al., 2011), and *Saturnalia* (Langer et al., 1999).

Another feature of the dentition of *Eoraptor* is the presence of a rounded eminence on the lateral side of the upper crowns (Figs. 35–37). This rounded eminence is well preserved along the entire upper tooth row on the left side of the skull (Figs. 35A, B, 36B). Some of the crowns in the right maxillary tooth row

have been crushed flat. All crowns appear to exhibit this eminence, which is also present in *Panphagia* (Martínez and Alcober, 2009) and *Pampadromaeus* (Cabreira et al., 2011). Even the short posterior-most maxillary teeth have a bulbous lateral crown surface. In premaxillary and anterior maxillary teeth, the eminence is offset toward the anterior crown margin, which is offset medial to the posterior margin. A similar eminence could not have been present on the medial crown surfaces because many of the maxillary crowns lie flat against the dentary.

The crowns have marginal denticles at a density of about six per millimeter on both anterior and posterior margins (Fig. 37). The denticles along the mesial margin are present only on the distal two-thirds of the crown margin and extend farther toward the base of the crown on the distal margin. This asymmetry in marginal ornamentation is also the case in *Panphagia* (Martínez and Alcober, 2009:fig. 5) as well as in the crowns of many theropods (Norell and Makovicky, 1999). Our use of the term 'denticle,' rather than 'serration,' for the marginal crown structures in *Eoraptor* is somewhat arbitrary, because they appear to be intermediate in size and orientation between the larger, subconical, obliquely inclined denticles in basal sauropodomorphs such as *Plateosaurus* and the smaller, wedge-shaped, perpendicular serrations in many theropods and in the caniniform crowns of heterodontosaurid ornithischians (Serenó, 2012). The denticles in *Panphagia*, *Pampadromaeus*, and *Saturnalia* appear similar but are in need of further detailed comparison.

A general replacement pattern is apparent in the maxillary tooth rows in *Eoraptor*, judging from the erupted crowns; internal details are not visible in the available computed tomographic scan. Every third position in the maxillary tooth rows is either vacant or has a tooth undergoing eruption. In the left maxillary tooth row, these include the third, fifth, eighth, and 11th tooth positions (Figs. 12, 13). In the right maxillary tooth row, these include the third, sixth, ninth, and 12th tooth positions (Figs. 10, 11). This pattern is not as clear in the premaxillary teeth or in the most posterior maxillary teeth, and the eruption pattern in the dentary tooth rows is not exposed or visible in computed tomographic images.

**Premaxillary Teeth**—Of the four premaxillary teeth, the first has the straightest crown and the second and third are the largest (Figs. 35, 40A). All have denticulate crown margins. The alveolar margin on the premaxilla slopes slightly anteroventrally, increasing the effective length of the premaxillary crowns relative to those in the maxilla as in *Pampadromaeus* (Cabreira et al., 2011). The eight crowns in the premaxillary dental arcade project ventrally around the more rounded, bulbous ends of the dentaries. In anterior view of the skull, the maxillary teeth are tucked just out of sight behind the premaxillary arcade (Fig. 18).

**Maxillary Teeth**—Maximum tooth size occurs in the fourth or fifth position in each maxillary tooth row, posterior to which tooth size decreases (Figs. 10, 11, 36, 40A). The maxillary tooth row extends farther posteriorly than the opposing dentary tooth row, as is common among herbivorous and carnivorous basal saurischians. The posterior end of the maxillary tooth row diverges laterally, following the curve of the jugal. The tooth crypts for the maxillary teeth fill the body and posterior ramus of the maxilla, which as a consequence has collapsed in places from postmortem transverse compression.

**Palatal Teeth**—Rudimentary palatal teeth are present on two prominent ridges on the pterygoid. The parasagittal tooth row, which is exposed only on the left pterygoid, has approximately 30 teeth. The diagonal row has approximately 20 teeth. The number of palatal teeth is approximately 100 teeth. (Figs. 38, 39).

Palatal teeth of similar size and location have been described in the basal theropod *Eodromaeus* (Martínez et al., 2011). In the basal sauropodomorph *Pampadromaeus* (Cabreira et al., 2011), only the medial row was described, although it is very easy to

lose either of these rudimentary tooth rows during preservation or preparation. It now appears likely that both branches of Saurischia (Theropoda, Sauropodomorpha) originally retained rudimentary palatal teeth on the pterygoid. There are no teeth on the palatine or on the footplate of the vomer. Whether there were any teeth more posteriorly on the vomer cannot be determined.

The palatal teeth in *Eoraptor* are similar in form. They are subcylindrical without apparent recurvature and have a subcircular or oval cross-section, the smaller crowns often the more subcircular. They vary in diameter from just under 1.0 mm to approximately 0.5 mm and have a maximum height of approximately 2 mm. Thus, compared with a maxillary tooth from the middle of the tooth row, the palatal teeth are one-third to one-sixth the mesiodistal diameter and about one-third or less the height of the crown.

None of the crowns have complete apices, and so the form of the crown tip remains unknown. It is unlikely that all of the tips of the palatal teeth could have been lost during preparation of the holotypic cranium, which was accomplished under high-power magnification. More likely, some or all of the tips of the palatal teeth, which surmount prominent palatal ridges, were lost from abrasion during feeding. At  $\times 50$  magnification, the palatal teeth do not appear to have an external enamel layer. They appear to be made solely of dentine with a central pulp cavity (Fig. 39).

On the ridge near the medial margin of the pterygoid, the palatal teeth appear to be distributed in a single row (Fig. 38). Tooth size is smallest anteriorly and gradually increases in size posteriorly. The most anterior teeth exposed near the midline are positioned under the anterior margin of the orbit.

The teeth on the diagonal ridge on the pterygoid do not appear to be distributed randomly (Figs. 38, 39). Multiple rows appear to be present, with longitudinal alignment of teeth best preserved on the right side and side-by-side alignment best preserved on the left side. Thus, it appears there may be as many as 10 teeth in a single row based on the left side and as many as three subparallel rows based on the right side. Matrix was left between the teeth in each diagonal tooth area for support.

## Postcranial Skeleton Overview

The postcranial description of *Eoraptor* is based largely on the holotypic postcranial skeleton (PVSJ 512), which was divided into 15 blocks that were left in articulation (Fig. 4; Table 2). Only critical portions of the right manus have been disarticulated to better understand the morphology and function of digit I (Figs. 75, 76). No specimen preserves caudal vertebrae or even centra distal to caudal vertebra 17 (Fig. 9). There are no clavicles, sternal plates, or sternal ribs. Ossified sternal plates and sternal ribs are unlikely to have been present in *Eoraptor*, given the high level of articulation of the skeleton and the completeness of the pectoral girdles, forelimbs, and gastral cuirass. Although the same is true for the absence of ossified clavicles, it is possible these elements may have been lost, given some postmortem movement of the pectoral girdles. Ossified clavicles have been recorded in members of all three major clades of dinosaurs (Ornithischia, Saurpodomorpha, Theropoda) (Bryant and Russell, 1993).

The most important referred specimen for this description is PVSJ 559, which includes two largely disarticulated and uncrushed anterior dorsal vertebrae and a partially articulated right hind limb (Table 1). These elements provide important information on the axial column and the anatomy and articulation between the bones of the hind limb. The skeletal silhouette of *Eoraptor lunensis*, nonetheless, is based on the holotypic skeleton, as the bones it lacks have yet to be recovered in referred material (Fig. 93). Measurements of the postcranial skeleton are in Tables 4–11; comparative measurements and ratios can be found in Tables 12 and 13.

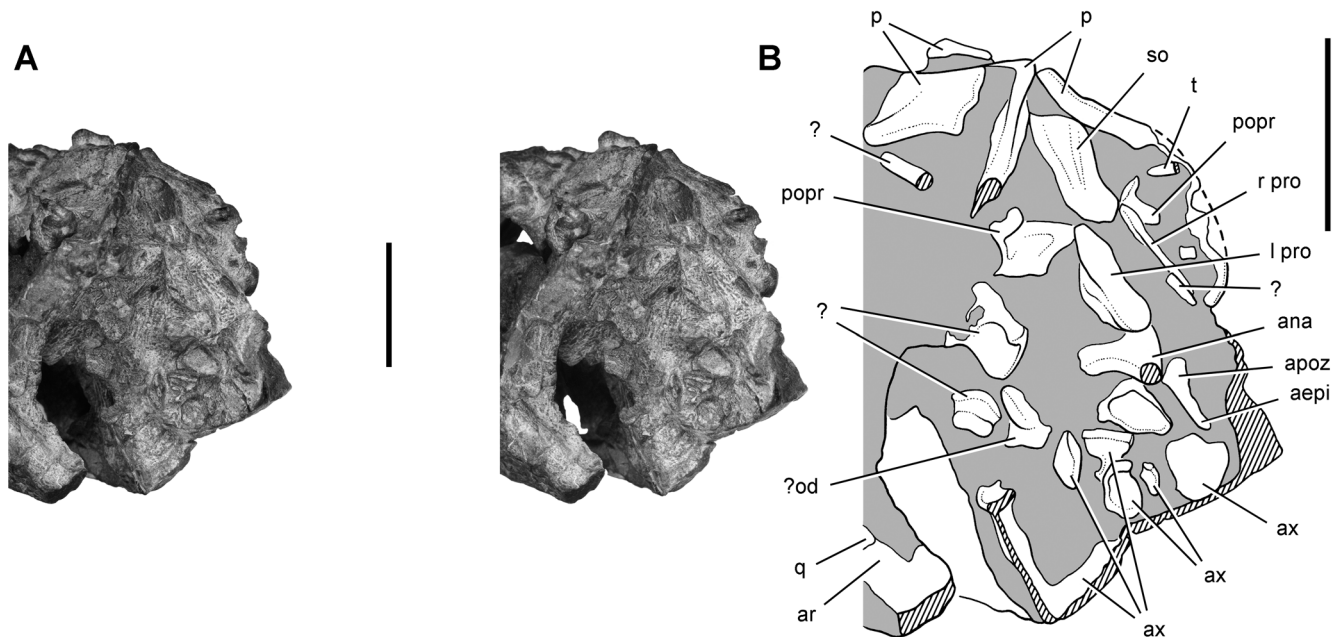


FIGURE 42. Stereopair (A) and drawing (B) of the proatlas, atlas, and fragments of the axis of *Eoraptor lunensis* (PVSJ 512) in dorsolateral view. **Abbreviations:** *aepi*, atlantal epiphysis; *ana*, atlantal neural arch; *apoz*, atlantal postzygapophysis; *ar*, articular; *ax*, axis; *l*, left; *od*, odontoid; *p*, parietal; *popr*, paroccipital process; *pro*, proatlas; *q*, quadrate; *r*, right; *so*, supraoccipital; *t*, tooth. Dashed line indicates a missing margin; hatching indicates a broken surface; shading indicates matrix. Scale bars equal 2 cm.

### Axial Skeleton

The axial column is complete from the proatlas to mid-caudal vertebra 17 (Fig. 9; Tables 4–6). The remainder of the tail had eroded away by the time the skeleton was discovered (Fig. 2A, B). *Eoraptor* has nine cervical, 15 dorsal, three sacral, and an unknown number of caudal vertebrae (Figs. 9, 93; Table 5). The cervical vertebrae are broken and eroded anteriorly (Fig. 42). Postaxial cervical vertebrae are well exposed on their right (down) side (Figs. 43–48). Dorsal vertebrae are best exposed on their left (up) side (Figs. 5, 6, 51, 52A). A disarticulated pair of anterior dorsal vertebrae (first and second dorsal vertebrae) in a referred specimen (PVSJ 559) provides useful information unavailable in the articulated column of the holotype (Fig. 50). The three sacral vertebrae have been prepared and exposed largely in dorsal view. Particular attention was paid to the form and articular relations of the first sacral rib (Fig. 53). Caudal vertebrae are best exposed on their left (up) side (Figs. 5, 6, 55–59).

**Proatlas**—The proatlas consists of a pair of plate-shaped ossifications of the neural arch that articulate between the occiput and the atlas. They are preserved near their natural positions, the left side more completely exposed (Fig. 42; Table 4). The broad dorsal surface of the element has a gentle sigmoid shape, and in lateral view it appears subtriangular. The prezygapophysis is longer, thinner, and more pointed than the postzygapophysis and is preserved

in articulation with the rim of the foramen magnum. The postzygapophysis overlaps the atlantal prezygapophysis. The short lateral process curves ventrally, partially enclosing the neural canal.

*Eoraptor* is the only early basal sauropodomorph in which the proatlas is known. The proatlas is also preserved in the contemporaneous theropods from Ischigualasto, *Herrerasaurus* (Sereno and Novas, 1994) and *Eodromaeus* (Martínez et al., 2011). In *Herrerasaurus* (PVSJ 407), the proatlas is flatter, with little development of a lateral process (Sereno and Novas, 1994). The proatlas is also preserved in *Allosaurus* (MOR 660), *Deinonychus* (MOR 747), and an increasing number of non-avian theropods.

**Atlas**—The left atlantal neural arch is preserved in lateral view near its natural position (Fig. 42; Table 4). The triradiate neural arch has a short prezygapophysis that contacts the proatlas, and a longer, broader postzygapophysis that articulates with the axis. The postzygapophysis and a long, posteriorly projecting epiphysis have separated from the anterior portion of the neural arch, exposing a cylindrical cross-section (Fig. 42). In *Herrerasaurus* (Sereno and Novas, 1994:fig. 11), the neural arch has a more slender form and the posterior extension that contains the postzygapophysis is plate-shaped rather than cylindrical. The location of the atlantal intercentrum and rib is uncertain.

**Axis**—The best-preserved portions of the axis are the pre- and postzygapophyses and the ventral margin of the centrum (Fig. 42). An odontoid process may be preserved, fused to a portion of the axial centrum. An adjacent concave articular surface may represent a portion of a fused axial intercentrum. A ventral keel is present on the axial centrum.

The subtriangular prezygapophysis faces dorsolaterally and is similar to that in *Herrerasaurus* (Sereno and Novas, 1994:fig. 11), except that it is flat rather than slightly convex. The postzygapophyses and base of the neural spine are also very similar. The postzygapophyses flare laterally from the neural arch in

TABLE 4. Measurements (in mm) of the left proatlantal and atlantal neural arches of *Eoraptor lunensis* (PVSJ 512).

Dimension	Measurement
Proatlas, maximum length	12
Proatlas, maximum width	4
Atlas, maximum length of neural arch	13

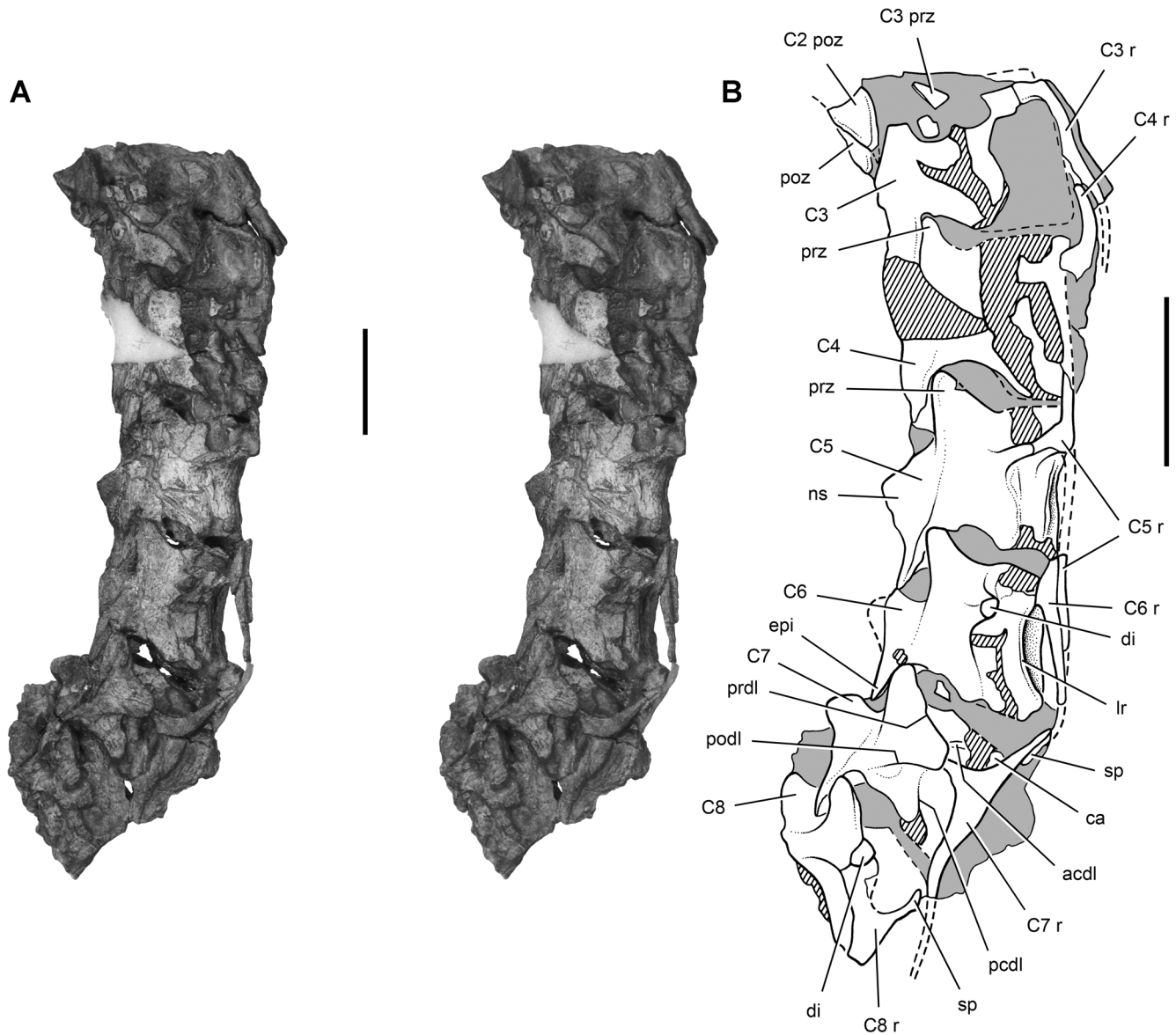


FIGURE 43. Stereopair (A) and drawing (B) of cervical vertebrae 2–8 of *Eoraptor lunensis* (PVSJ 512) in right lateral view. **Abbreviations:** **acdl**, anterior centrodiapophyseal lamina; **C2–8**, cervical vertebrae 2–8; **ca**, capitulum; **di**, diapophysis; **epi**, epipophysis; **lr**, lateral ridge; **ns**, neural spine; **pcdl**, posterior centrodiapophyseal lamina; **podl**, postzygodiapophyseal lamina; **poz**, postzygapophysis; **prz**, prezygapophysis; **r**, rib; **sp**, spine. Dashed line indicates a missing margin; hatching indicates a broken surface; shading indicates matrix. Scale bars equal 2 cm.

dorsal view and extend posteriorly as epipophyses, the tips of which have been broken off. The postzygapophyseal facet is subtriangular, as in *Herrerasaurus* (PVSJ 407). Although there is a small, subtriangular fossa between the postzygapophyses, a horizontal interpostzygapophyseal lamina is not present as in *Herrerasaurus* (Sereno and Novas, 1994), which floors the fossa bridging between the medial edges of the postzygapophyses.

**Postaxial Cervical Vertebrae**—The entire postaxial series is preserved in articulation (Figs. 43–49; Table 5). The first nine presacral vertebrae are regarded as cervical vertebrae, based on the form and position of their rib articulations and the form of their

associated ribs (see below). The centra of cervical vertebrae 3 and 4 are flattened and fragmented (Fig. 43). Their neural arches, however, are more intact and can be used to assess the relative lengths of their centra.

As in *Herrerasaurus* (PVSJ 407), centrum length increases gradually from the axis to the fourth and fifth cervical vertebrae, after which it decreases dramatically (Table 5). There is approximately a 30% reduction in the length of the middle to posterior cervical centra and an even greater reduction in the distance between pre- and postzygapophyses of the neural arch. In lateral view, middle cervical centra (C5, C6) are parallelogram-shaped;

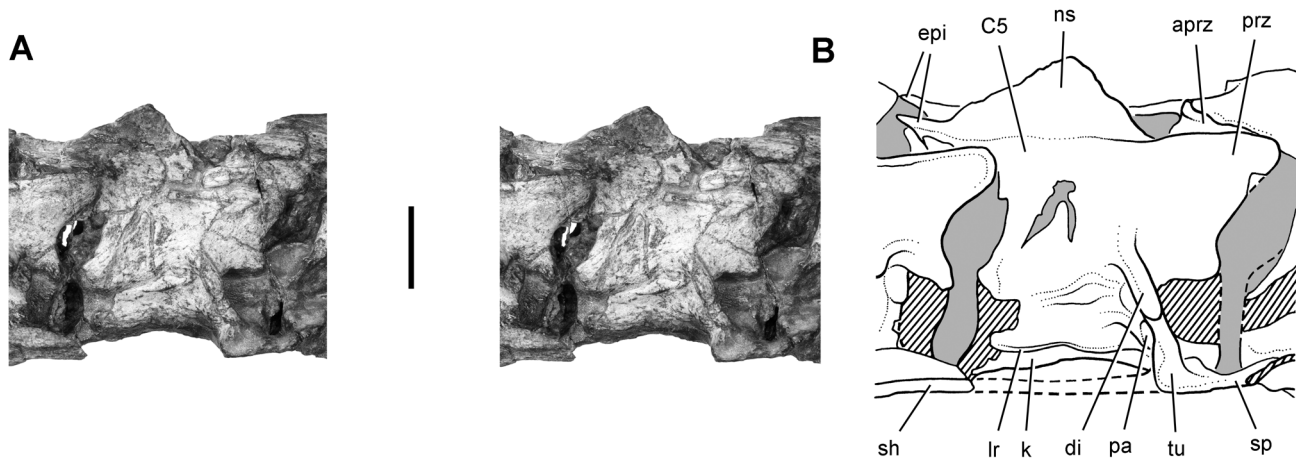


FIGURE 44. Stereopair (A) and drawing (B) of cervical vertebra 5 of *Eoraptor lunensis* (PVSJ 512) in right lateral view. **Abbreviations:** aprz, accessory prezygapophyseal process; C5, cervical vertebra 5; di, diapophysis; epi, epiphysis; k, keel; lr, lateral ridge; ns, neural spine; pa, parapophysis; prz, prezygapophysis; sh, shaft; sp, spine; tu, tuberculum. Dashed line indicates a missing margin; hatching indicates a broken surface; shading indicates matrix. Scale bars equal 1 cm.

the anterior face is elevated when the posterior face is oriented vertically (Figs. 43, 44). This shape is also present in the seventh and eighth cervical centra. The ninth cervical centrum shows no elevation of the anterior face, but rather it is weakly trapezoidal (Fig. 47). The shapes and lengths of the cervical centra indicate that the ninth cervical vertebra functioned as a transi-

tional link between the dorsal series and the rising cervical series (Fig. 49).

In cross-section, the presacral vertebrae are extremely hollow (Fig. 52). The neural canal is enlarged and extends dorsally into the neural arch. A thin horizontal septum divides the neural canal from the internal cavity of the centrum. The lateral walls of the

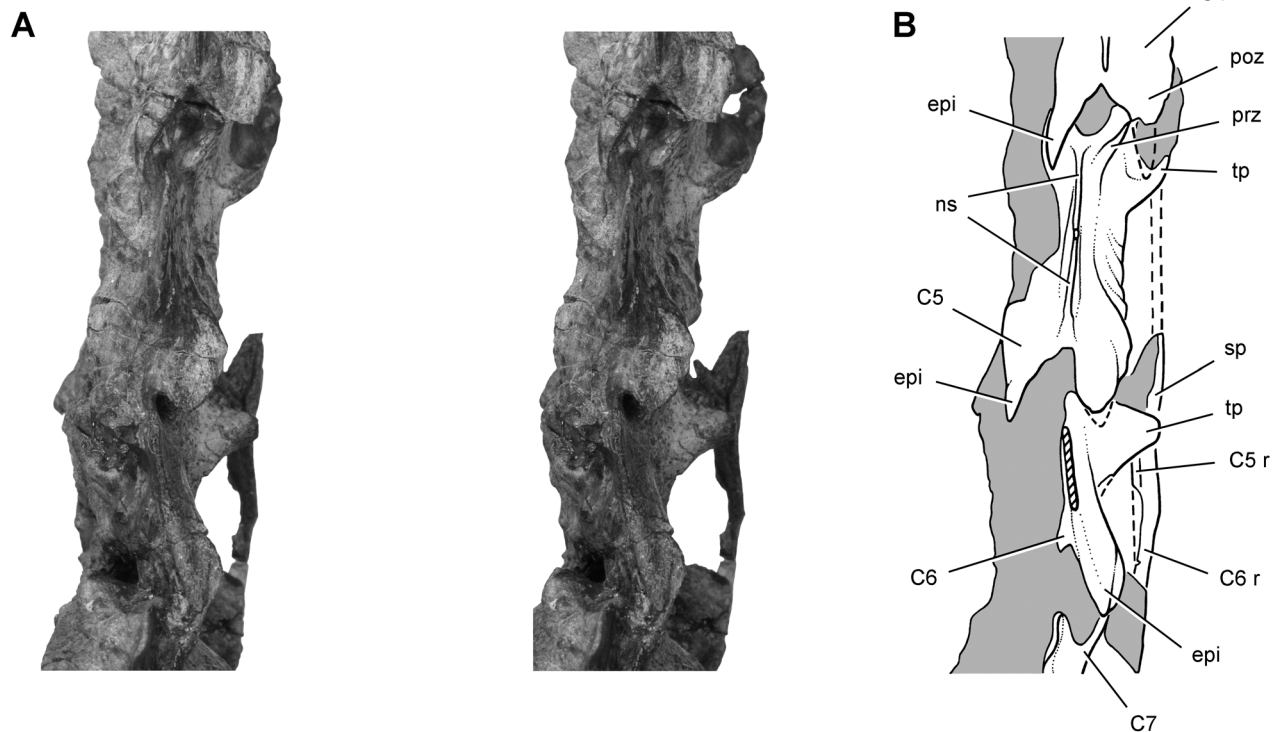


FIGURE 45. Stereopair (A) and drawing (B) of cervical vertebrae 5 and 6 of *Eoraptor lunensis* (PVSJ 512) in dorsal view. **Abbreviations:** C4–7, cervical vertebrae 4–7; epi, epiphysis; ns, neural spine; poz, postzygapophysis; prz, prezygapophysis; r, rib; sp, spine; tp, transverse process. Dashed line indicates a missing margin; hatching indicates a broken surface; shading indicates matrix. Scale bar equals 2 cm.

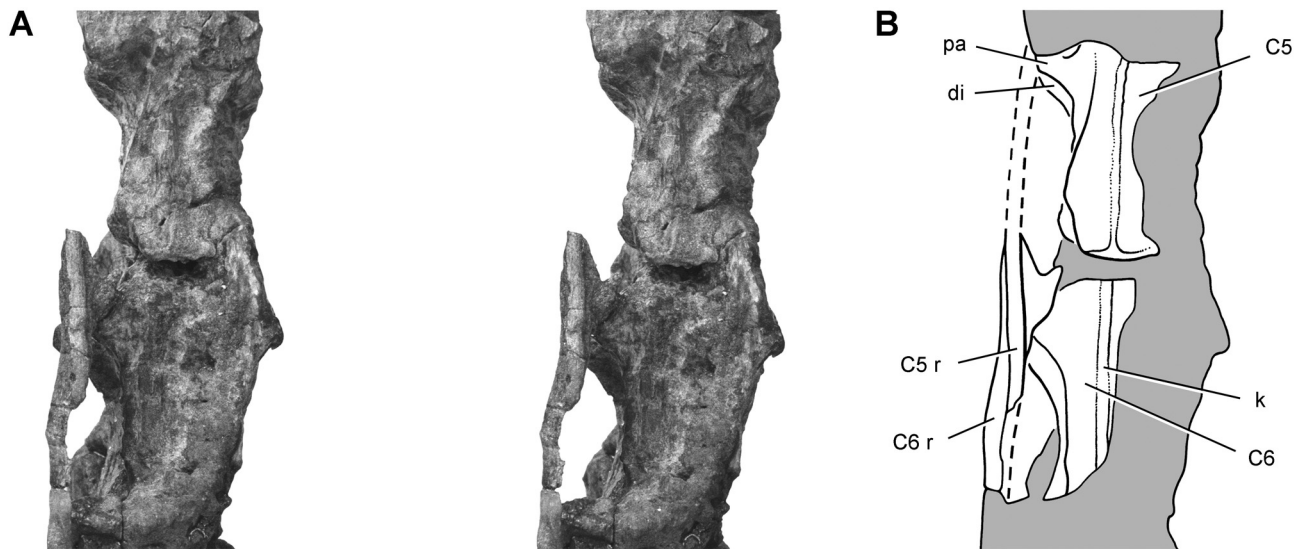


FIGURE 46. Stereopair (A) and drawing (B) of cervical vertebrae 5 and 6 of *Eoraptor lunensis* (PVSJ 512) in ventral view. **Abbreviations:** C5, 6, cervical vertebra 5, 6; di, diapophysis; k, keel; pa, parapophysis; r, rib. Dashed line indicates a missing margin; shading indicates matrix. Scale bar equals 2 cm.

centrum are very thin; the anterior and posterior articular faces are relatively thicker. Although the cervical vertebrae are hollow, there are no invaginated pneumatic openings in any part of the axial column in *Eoraptor*, in contrast to *Eodromaeus* (Martínez et al., 2011).

The sides of the centra posterior to the parapophyses are concave. On the fifth and sixth cervical vertebrae, a crest is present on the ventrolateral margin of the centrum opposite the rib shaft (Fig. 43, lr). It is strongest in the sixth cervical vertebra, where it extends the length of the centrum from the parapophysis to the posterior rim. A similar crest may have been present in anterior cervical vertebrae, as occurs in *Herrerasaurus* (Serenó and Novas, 1994:fig. 11), but the sidewalls of the centra are not preserved. The crest is absent in the seventh through the ninth cervical vertebra. A low ventral keel is present on the axis and on all other cervical vertebrae preserving this region (C5–C9). It is lost abruptly in the first dorsal vertebra (Fig. 48). In a referred specimen (PVSJ 559), the first two dorsal vertebrae maintain a ventral keel (Fig. 50). Anterior and posterior faces of the cervical centra are moderately concave throughout the series.

In the fifth and sixth cervical vertebrae, the parapophysis is developed as a dorsoventrally compressed strut projecting ventrolaterally from just behind the rim of the centrum (Figs. 43, 44). In more posterior cervical vertebrae, the parapophysis shortens in length, broadens in area of attachment, and moves dorsally onto the side of the centrum just below the neurocentral junction. In the ninth cervical vertebra, the parapophysis is represented by a raised welt of considerable size on the anterior rim of the centrum. The most anterior diapophyses that are preserved are also on the fifth and sixth cervical vertebrae, where they are developed as ventrolaterally projecting processes. In the fifth cervical vertebra, the process is slender and subcylindrical (Fig. 44). In the sixth cervical vertebra, the base of the process is considerably broader and dorsoventrally compressed. This trend continues in the seventh cervical vertebra, in which the entire process is flattened (Fig. 43). In the posterior-most cervical vertebra (C9), the end of the diapophysis is more robust, with an oval articular surface (Figs. 47, 48).

A cross-pattern involving four laminae around the diapophysis first appears in rudimentary form in the seventh cervical vertebra, in which the transverse process is stronger and dorsoventrally flattened (Fig. 43). These include the pre- and postzygodiapophyseal laminae above, which connect the diapophysis to the zygapophyses, and the anterior and posterior centrodiaapophyseal laminae below, which connect the diapophysis to the dorsal corners of the centrum (Wilson, 1999). In the preceding vertebra, laminae extend anteriorly and posteriorly from the base of the diapophysis but dissipate before reaching another vertebral structure. In the ninth cervical, the laminae are well developed and fully exposed (Figs. 47, 48). The anterior centrodiaapophyseal lamina is lower in relief than the others. It eventually disappears in the dorsal column, as the parapophysis approaches the diapophysis (Fig. 47).

Except for a single prezygapophysis on the third cervical vertebra, which is disarticulated from the axial postzygapophysis, the articular facets between the cervical neural arches are visible only in articulation (Fig. 43). In the third cervical vertebra, the oval prezygapophyseal facet is relatively flat. The axial postzygapophysis suggests that the articulation angled ventromedially at about 20° from the horizontal. More posteriorly in the cervical series, the inclination of the zygapophyseal articulation increases, and the articular surface becomes transversely arched (Fig. 43). The zygapophyseal articulation between the eighth and ninth cervical vertebrae, which is visible in cross-section, is inclined at more than 50° from the horizontal and has a gentle transverse flexure of the articular surface.

An unusual accessory articular process arises from the medial side of the base of the prezygapophysis in the middle cervical vertebrae, and it is present in at least the fifth and sixth cervical vertebrae (Fig. 44). It is flattened transversely, and its articular surface is inclined anteroventrally, with a similar, although not identical, orientation as the principal prezygapophyseal articular facet. It articulates near the posteromedial margin of the postzygapophysis. This accessory prezygapophyseal process in middle cervical vertebrae has not been described before. It may be unique to *Eoraptor*, although there is little comparative

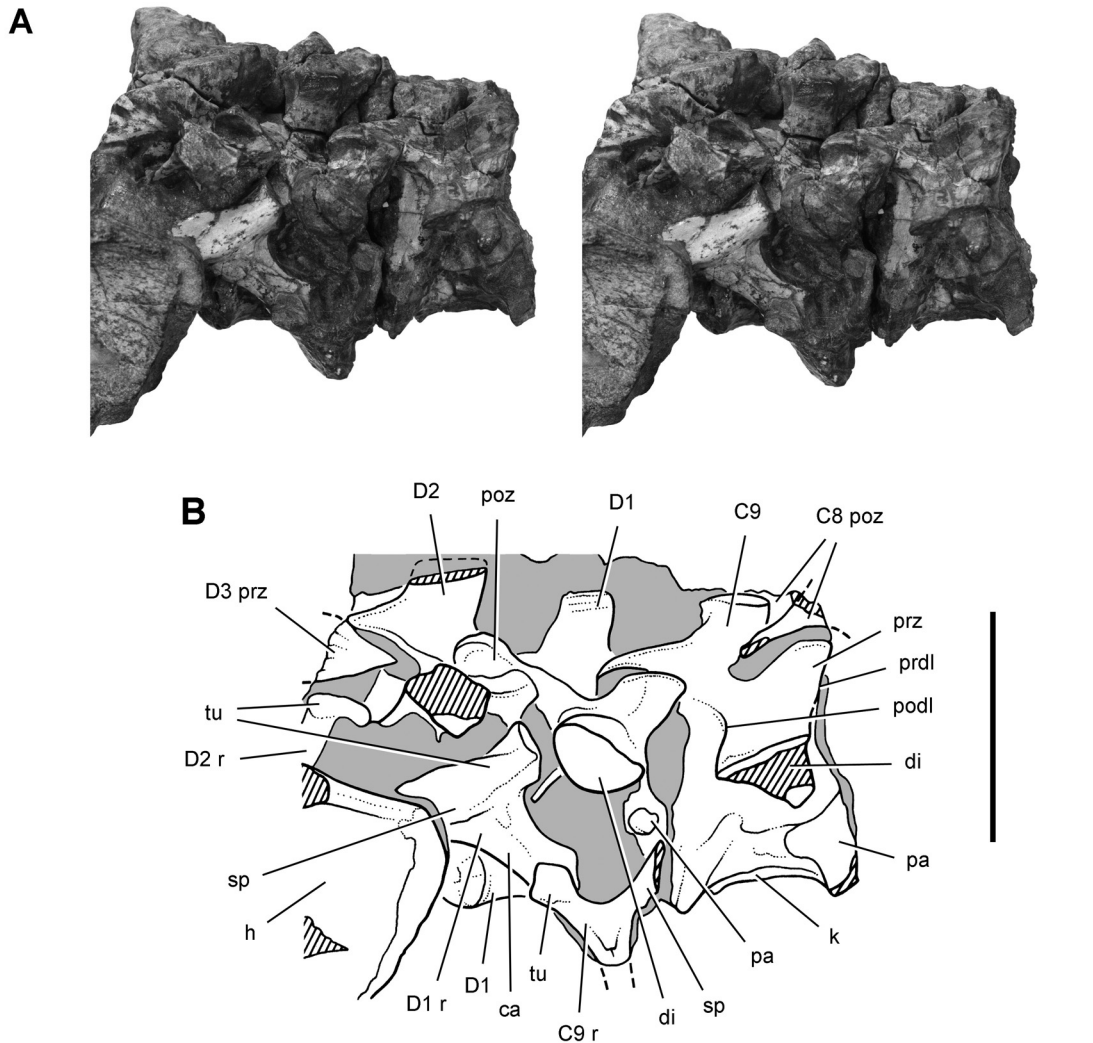


FIGURE 47. Stereopair (A) and drawing (B) of cervical vertebra 9 and dorsal vertebrae 1 and 2 of *Eoraptor lunensis* (PVSJ 512) in right lateral view. **Abbreviations:** C8, 9, cervical vertebra 8, 9; ca, capitulum; D1–3, dorsal vertebrae 1–3; di, diapophysis; h, humerus; k, keel; pa, parapophysis; podl, postzygodiapophyseal lamina; poz, postzygapophysis; prdl, prezygodiapophyseal lamina; prz, prezygapophysis; r, rib; sp, spine; tu, tuberculum. Dashed line indicates a missing margin; hatching indicates a broken surface; shading indicates matrix. Scale bars equal 2 cm.

information in other basal sauropodomorphs such as *Panphagia*, *Pampadromaeus*, and *Saturnalia*. In *Panphagia*, a cervical vertebra originally described as the eighth (Martínez and Alcober, 2009:fig. 6B) corresponds better with the fourth or fifth cervical vertebra in *Eoraptor*, given the elongate proportions of the centrum, the low, elongate profile of the neural spine, the narrow proportions of the transverse process, and the anteroventral position of the diapophysis. It does not have the accessory prezygapophyseal process.

The postzygapophyses have larger articular surfaces than corresponding prezygapophyses and extend slightly beyond the edges of the latter in articulation (Fig. 45). Prominent prong-shaped epiphyses are present on the atlantal neural arch, the axis, and the third through the fifth cervical vertebrae. Weak epiphyses are present on the sixth cervical vertebra, and they are absent in more posterior cervical vertebrae (Figs. 43, 49).

The neural spines are lower throughout the cervical series in *Eoraptor* than in *Herrerasaurus* (Sereno and Novas, 1994:fig. 12). On the third and probably also the fourth cervical vertebra, the spine is developed as a low crest (Fig. 43). In the fifth cervical vertebra, the spine is subtriangular and very thin (Fig. 44). In the sixth vertebra, the spine is broken but was probably developed much as in the preceding vertebra. The neural spine has a more restricted base in the seventh and eighth vertebrae, but not until the ninth vertebra does the spine take the form of a thickened, subrectangular strut (Figs. 43, 44, 47, 49). All spines are erect rather than angled posterodorsally. Unlike *Herrerasaurus* (Sereno and Novas, 1994:fig. 11B), none of the cervical vertebrae have a deep fossa between the postzygapophyses and the base of the spine. Unlike *Eodromaeus*, there is no development of cervical pleurocoels or their posterior extension as an external groove or trough (Martínez et al., 2011:fig. 2B).

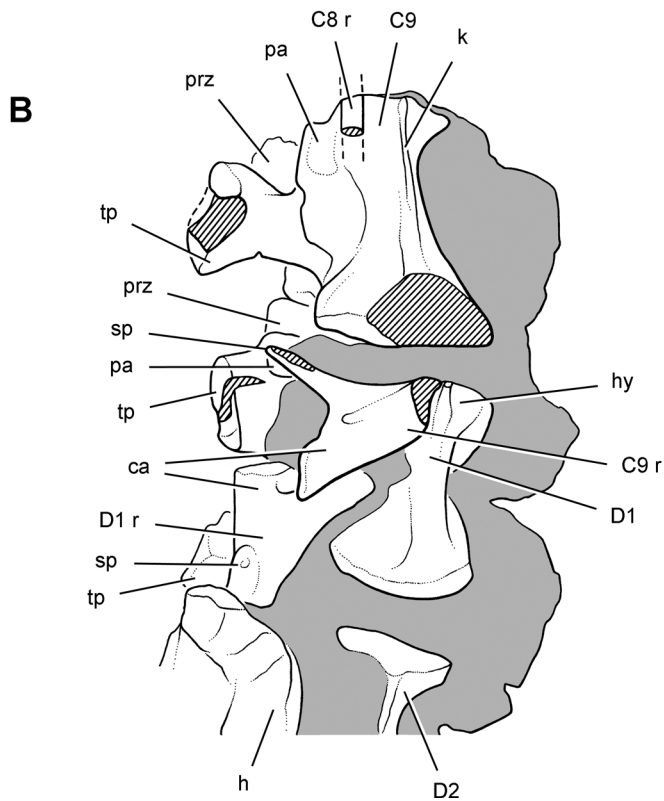
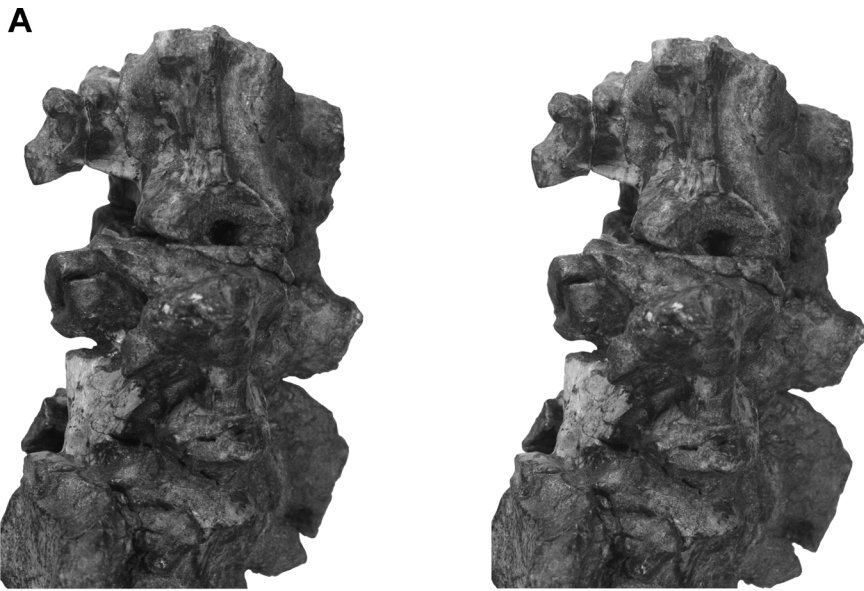


FIGURE 48. Stereopair (A) and drawing (B) of cervical vertebra 9 and dorsal vertebrae 1 and 2 of *Eoraptor lunensis* (PVSJ 512) in ventral view. **Abbreviations:** C8, 9, cervical vertebra 8, 9; ca, capitulum; D1, 2, dorsal vertebra 1, 2; h, humerus; hy, hypapophysis; k, keel; pa, parapophysis; prz, prezygapophysis; r, rib; sp, spine; tp, transverse process. Dashed line indicates a missing margin; hatching indicates a broken surface; shading indicates matrix. Scale bars equal 2 cm.

**Dorsal Vertebrae**—There are 15 dorsal vertebrae (Figs. 47, 48, 50–52; Table 5). The form of the centrum, transverse process, neural spine, and corresponding rib change dramatically between the last cervical (C9) and first dorsal vertebrae (Figs. 47, 48, 50A). The shorter centrum of the first dorsal vertebra has a prominent hypapophysis (Fig. 48); the parapophysis has shifted dorsally to straddle the neurocentral suture (Fig. 50A); the transverse process is very robust and elevated (Figs. 47, 48, 50A); the neural spine is deeper than broad (Figs. 47, 50A); and the rib is approximately

twice the size of that associated with the ninth cervical vertebra (Fig. 48).

The length of the centra in the dorsal series gradually becomes longer in the first six dorsal vertebrae, after which length stabilizes at around 20 mm. The centra are spool-shaped with gently concave anterior and posterior faces. The first dorsal has a well-developed, wedge-shaped hypapophysis extending below the anterior articular face (Figs. 48, 50). The second dorsal may also have a very rudimentary hypapophysis, but the centrum is not completely

TABLE 5. Measurements (in mm) of postatlantal vertebrae of *Eoraptor lunensis* (PVSJ 512).

Vertebra	Centrum length	Centrum height (posterior)	Interzygapophyseal length <sup>†</sup>	Neural spine height (maximum)	Neural spine length (maximum)
C2	—	—	24	—	—
C3	—	—	27	—	—
C4	24	10	30	—	—
C5	24	10	32	6	12
C6	23	11	28	—	—
C7	20	(11)	27	7	8
C8	18	—	21	7	7
C9	17	12	20	4	6
D1	17	12	20	8	5
D2	16	(12)	—	—	—
D3	16	—	—	—	—
D4	17	—	—	10	11
D5	(19)	—	—	11	11
D6	20	—	—	10	13
D7	20	14	—	10	15
D8	21	15	—	10	17
D9	20	14	—	11	(17)
D10	21	14	—	14	17
D11	22	15	—	13	17
D12	23	15	—	13	17
D13	21	15	—	14	17
D14	20	15	—	16	18
D15	18	15	—	16	17
S1	(19)	—	—	16	17
S2	(19)	—	—	16	17
S3	20	(15)	—	17	17
CA1	17	—	—	16	16
CA2	20	—	—	20	13
CA3	22	15	—	22	13
CA4	20	(15)	—	22	12
CA5	20	(14)	—	21	11
CA6	21	14	—	21	12
CA7	20	14	—	—	—
CA8	19	13	—	—	—
CA9	19	13	—	15	9
CA10	18	13	—	15	9
CA11	18	13	—	14	9
CA12	17	12	—	11	7
CA13	17	12	—	11	7
CA14	17	12	—	9	7
CA15	17	12	—	9	9
CA16	17	11	—	6	7
CA17	20	10	—	—	—

Interzygapophyseal length given only for the axis to the first dorsal vertebra. Neural spine length was measured from the neural arch just above the zygapophyses to the distal end of the spine. Parentheses indicate estimated measurement; dash indicates unknown measurement. **Abbreviations:** C, cervical; CA, caudal; D, dorsal; S, sacral.

<sup>†</sup>Excluding epipophysis.

exposed (Fig. 48). Both have a low ventral keel in PVSJ 559 (Fig. 50A, D).

As in the cervical vertebrae, invaginated pneumatic openings are not present anywhere on the centrum, despite the fact that the vertebrae are extremely hollow. In cross-sections of the sixth and 13th dorsal vertebrae, for example, the neural canal expands ventrally into the upper one-half of the centrum (Fig. 52C). The lower one-half of the centrum is separated from the neural canal by a thin septum. The external walls of the centrum do not exceed 1 mm in thickness. Small internal pockets in the neural arch are also visible in a cross-section through the zygapophyseal region of the 14th dorsal vertebra (Fig. 52B).

The parapophysis is located on the anterodorsal corner of the centrum in the first and second dorsal vertebrae but shifts onto the neural arch posteroventral to the prezygapophysis by the fifth or sixth dorsal vertebra (Figs. 50, 51). In the eighth dorsal vertebra, the parapophysis is developed as a stout cylindrical process 4 mm long. It is positioned on the anterior side of the diapoph-

ysis, which is longer (1 cm). The diapophysis is robust, cylindrical, and upwardly directed in the anterior dorsal vertebrae. Starting with a length of 5 mm in the first dorsal, the diapophysis achieves a length of more than 10 mm in the third and fourth dorsal vertebrae, where it is dorsoventrally compressed. The diapophyses decrease in length to about 4 mm posterior to the ninth dorsal vertebra (Fig. 51). As far posteriorly as the 12th dorsal vertebra, the diapophysis is positioned posterodorsal to the parapophysis and is substantially longer than the former; the articulating two-headed ribs confirm this observation. The processes of the 13th dorsal vertebrae are not well exposed. In the 14th and 15th dorsal vertebrae (Fig. 52A), the parapophysis is located on the anteroventral aspect of the diapophysis, which has increased in length to approximately 10 mm.

The angle of the zygapophyseal articulation decreases across the dorsal series from more than 50° above the horizontal in the first dorsal vertebra to less than 20° in the 14th dorsal vertebra (Fig. 52). A hyposphene-hypantrum articulation appears abruptly

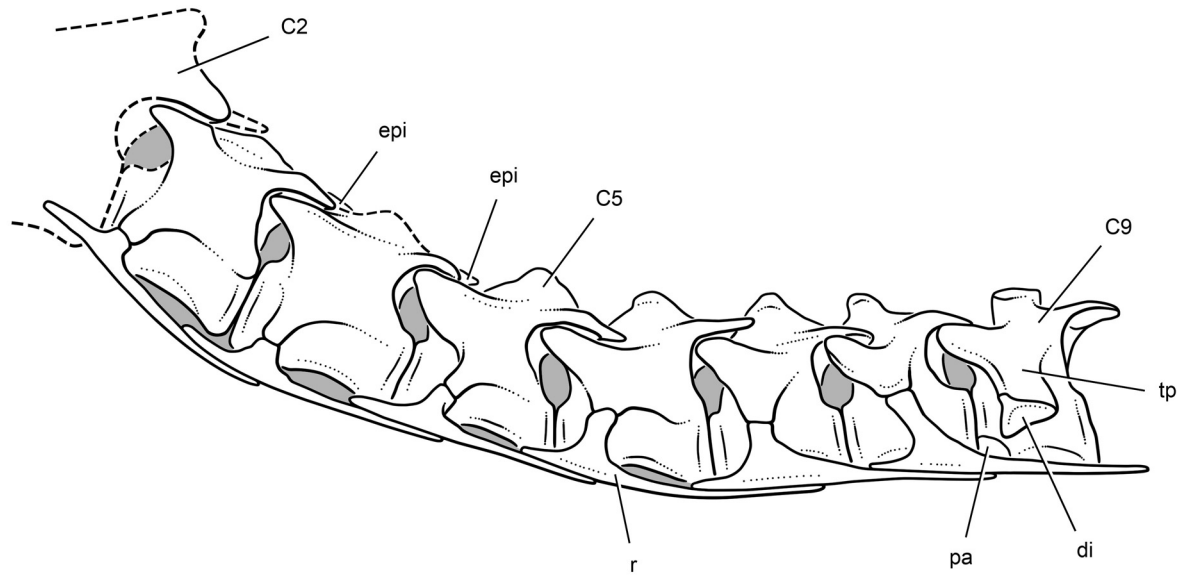


FIGURE 49. Reconstruction of cervical vertebrae 2–9 and cervical ribs 3–8 of *Eoraptor lunensis* (PVSJ 512). **Abbreviations:** C2, 5, 9, cervical vertebra 2, 5, 9; di, diapophysis; epi, epiphysis; pa, parapophysis; r, rib; tp, transverse process. Dashed line indicates a missing margin.

in the second dorsal vertebra, where a descending medial lip on the postzygapophysis is present (Fig. 50B). A cross-section of the postzygapophyses of the 14th dorsal vertebra shows a strongly flexed articular surface and presence of a hyposphene (Fig. 52A, B). Hyposphene-hypantrum articulations in the dorsal series in *Eoraptor*, thus, were likely present posterior to the first dorsal vertebra.

The cross-pattern of laminae around the diapophysis that characterizes the posterior cervical vertebrae (pre-, postzygodiapophyseal laminae; anterior and posterior centrodiaepophyseal laminae) are present in the anterior dorsal vertebrae (Fig. 50A, B). The elevated parapophysis engages the anterior centrodiaepophyseal lam-

ina in the first dorsal, which becomes the paradiapophyseal lamina (Fig. 50A). There is no centroparapophyseal lamina extending from the parapophysis anteroventrally to the centrum. The four aforementioned laminae separate three fossae, which are best developed in the anterior dorsal vertebrae (Fig. 50A, B). From anterior to posterior, these are the prezygapophyseal centrodiaepophyseal, centrodiaepophyseal, and postzygapophyseal centrodiaepophyseal fossae (Wilson et al., 2011:fig. 5). The neural arch laminae decrease in strength posteriorly along the dorsal series. Pre- and postzygodiaepophyseal laminae are absent in the 13th and 14th dorsal vertebrae (Fig. 52), in contrast to the condition in *Herrerasaurus*, in which the cross-pattern is maintained throughout the dorsal series (Novas, 1994:fig. 1).

The neural spines are plate-like throughout the dorsal series, never exceeding 2 mm in width (Fig. 51). There is no development of spine tables or distal thickenings of any sort. The first dorsal vertebra has a subrectangular neural spine that is taller than wide (7 mm by 5 mm, respectively) (Fig. 47, 50A). This is actually the narrowest neural spine in the entire vertebral column; the posterior-most cervical spine is second narrowest, with a width of 6 mm (Table 5). Anteroposterior spine width increases in more posterior dorsal vertebrae, measuring 8 mm in the second dorsal vertebra and 11 mm in the fourth dorsal vertebra. Spine width increases more rapidly than spine height, so that all dorsal spines except the first are broader than tall. A typical middle dorsal spine measures 17 mm in width and 15 mm in height. A small triangular spinoprezygapophyseal fossa is present at the base of the spine facing anteriorly and a deeper spinopostzygapophyseal fossa is present between the postzygapophyses facing posteriorly.

**Sacral Vertebrae**—There are three vertebrae that attach to the ilium and, by this criterion, are regarded as sacral vertebrae (Figs. 53, 54; Table 5). Their configuration is very similar to that in *Eodromaeus* and *Herrerasaurus*. The posterior two have very broad attachments to the iliac blade and clearly represent the primordial tetrapod pair (Romer, 1956). These two vertebrae are not coossified, as is clear from exposure of the ventral aspect of the

TABLE 6. Measurements (in mm) of the chevrons of *Eoraptor lunensis* (PVSJ 512).

Chevron number	Proximodistal length
2	(20)
3	—
4	(30)
5	(33)
6	(34)
7	(35)
8	(32)
9	(29)
10	(28)
11	(27)
12	(26)
13	(25)
14	(24)
15	(23)
16	(22)
17	—

Chevron number corresponds with the number of the anterior of the two caudal vertebrae with which it articulates (i.e., chevron 2 articulates between caudal vertebrae 2 and 3). Parentheses indicate estimated measurement; dash indicates unknown measurement.

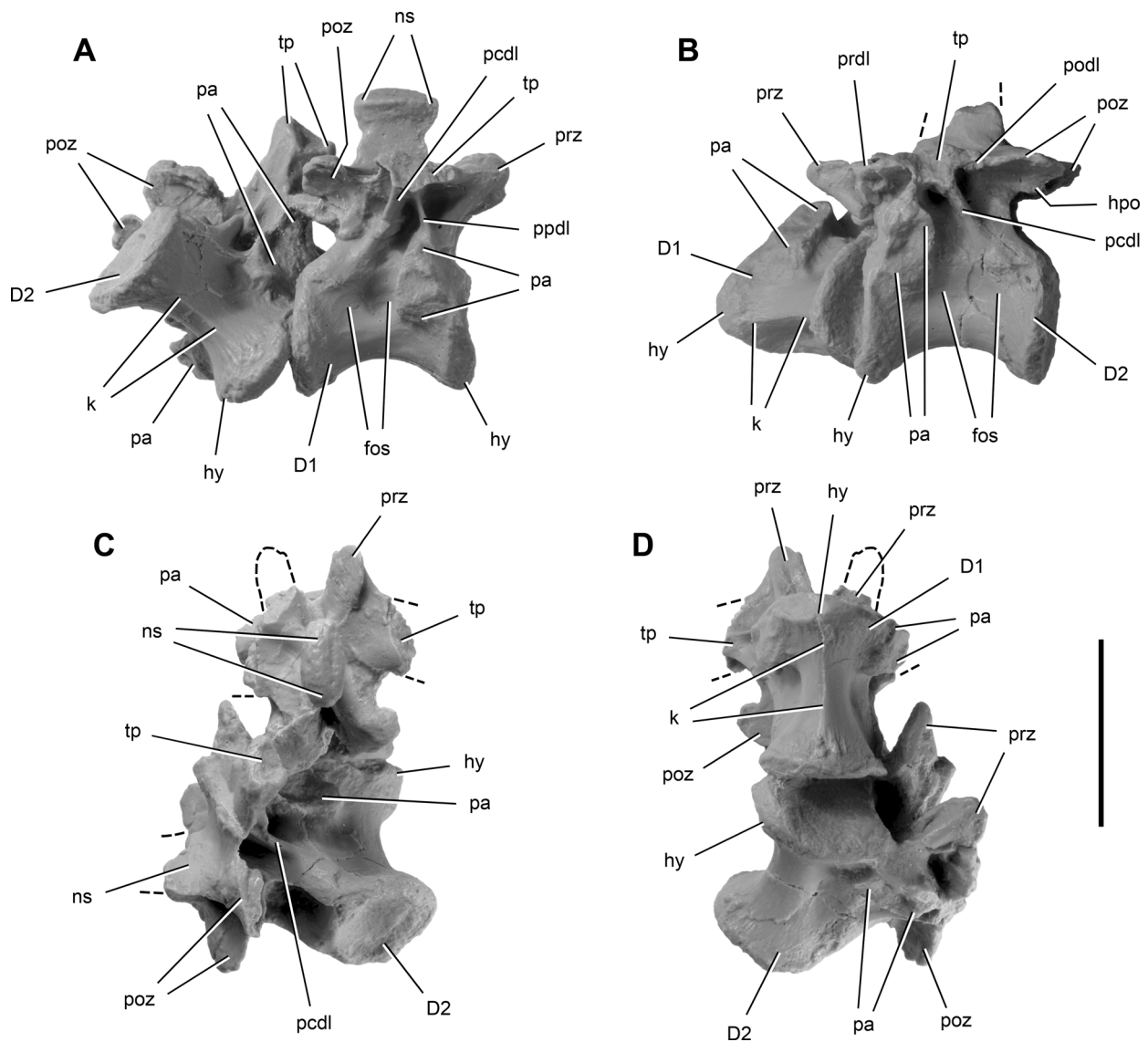


FIGURE 50. Dorsal vertebrae 1 and 2 of *Eoraptor lunensis* (PVSJ 559). **A**, dorsal vertebra 1 in right lateral view. **B**, dorsal vertebra 2 in left lateral view. **C**, dorsal vertebra 1 in dorsal view. **D**, dorsal vertebra 1 in ventral view. **Abbreviations:** D1, 2, dorsal vertebra 1, 2; fos, fossa; hpo, hyposphene; hy, hypapophysis; k, keel; ns, neural spine; pa, parapophysis; pcdl, posterior centrodiapophyseal lamina; podl, postzygodiapophyseal lamina; poz, postzygapophysis; ppdl, paradiapophyseal lamina; prdl, prezygodiapophyseal lamina; prz, prezygapophysis; tp, transverse process. Dashed line indicates a missing margin. Scale bar equals 2 cm.

third sacral centrum, although individually the neural arches and ribs of all sacral vertebrae are fused.

In the holotype (PVSJ 512), the sacrum has been sheared anteroposteriorly; the left pelvic girdle is positioned posterior to the right, and the attachment of the right sacral transverse processes are slightly ajar. Despite this distortion, the position of the sacral transverse processes relative to the ilium on each side appears to have been maintained. On both sides, for example, the third sacral vertebra has a broad attachment to the brevis shelf, and this is the expected location of this attachment judging from other basal archosaurs with two or three sacral vertebrae. It is likely, therefore, that the first sacral vertebra attached to the preacetabular process of the ilium, as preserved on the right side of the sacrum (Fig. 53C).

The third sacral vertebra has a strongly parallelogram-shaped centrum with ventral offset of the posterior face. The neural spine of the third sacral vertebra is subquadrate. The strap-shaped transverse process of the first sacral vertebra is truncated along a straight edge distally, which is located adjacent to the distal end of the preacetabular process of the ilium. The truncated form of the end of the rib strongly suggests that it attached the ilium at an angle similar to that preserved on the right side (Fig. 54). The transverse processes of the second and third sacral vertebrae are much broader and attach to the iliac blade above the acetabulum and along the brevis shelf, respectively.

The length of the sacral centra, the low-angle articulation of the sacral zygapophyses (as seen between the first and second

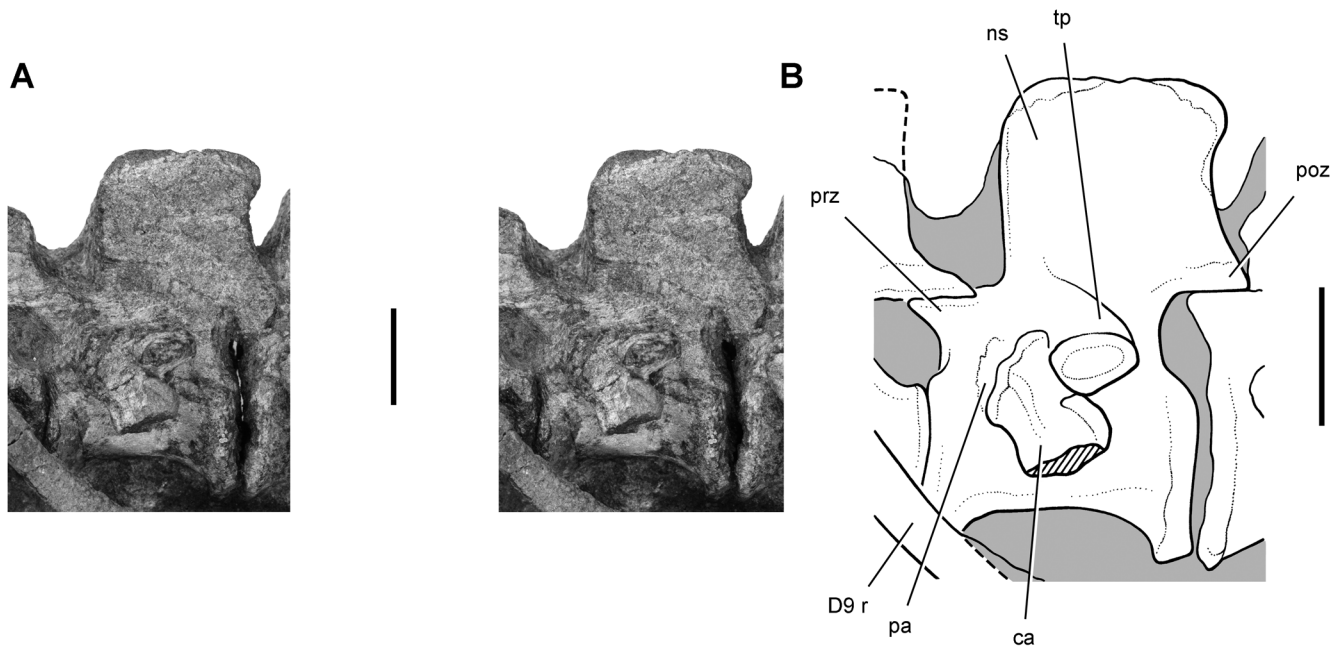


FIGURE 51. Stereopair (A) and drawing (B) of dorsal vertebra 10 of *Eoraptor lunensis* (PVSJ 512) in left lateral view. **Abbreviations:** ca, capitulum; D9, dorsal vertebra 9; ns, neural spine; pa, parapophysis; poz, postzygapophysis; prz, prezygapophysis; r, rib; tp, transverse process. Dashed line indicates a missing margin; hatching indicates a broken surface; shading indicates matrix. Scale bars equal 1 cm.

sacral vertebrae), and the plate-shaped, subquadrate neural spines are similar to the condition in the posterior dorsal vertebrae.

The sacral ribs are completely coossified with the sacral transverse processes (Figs. 53, 54). The first sacral transverse process

and rib form a slender, dorsoventrally flattened strut that is preserved in place, projecting from high on the neural arch toward the anterior end of the preacetabular process (Fig. 53C). The truncated end is shaped to articulate the preacetabular process of the ilium. The narrow form and elevated position on the neural arch of

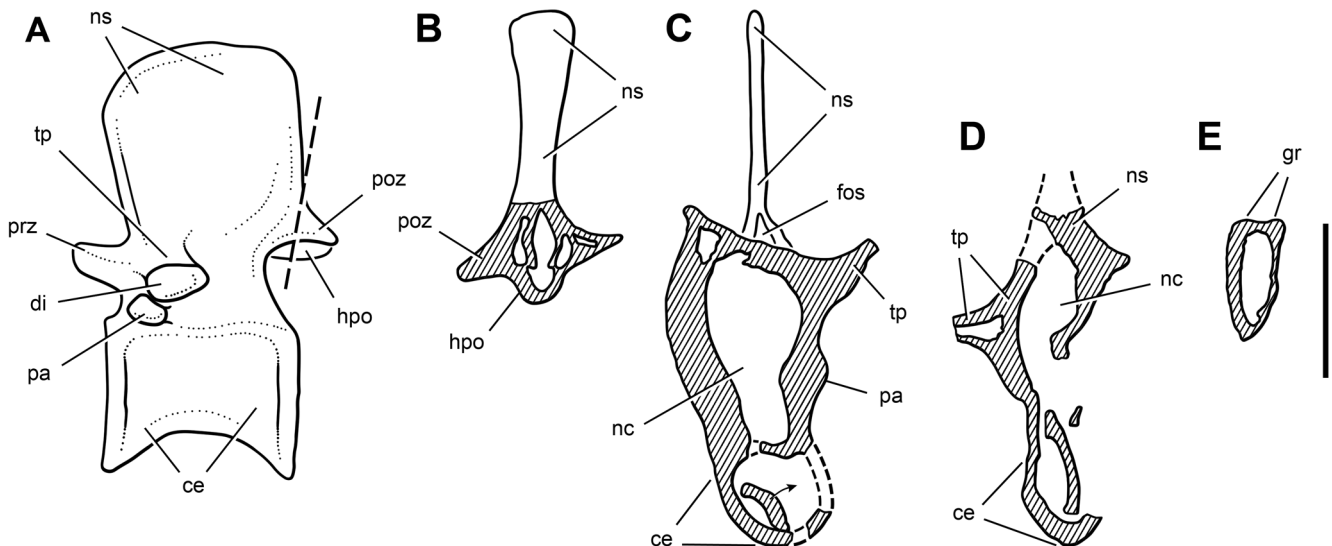


FIGURE 52. Reconstruction of dorsal vertebra 14 and cross-sections (observed on breakage planes) through several vertebrae and a chevron in *Eoraptor lunensis* (PVSJ 512). **A**, reconstruction of dorsal vertebrae 14 in left lateral view (dashed line indicates cross-section in B). **B**, cross-section of dorsal vertebra 14 through the posterior aspect of the neural spine and zygapophyses as seen in posterior view. **C**, cross-section through dorsal vertebra 13 anterior to the neural spine as seen in anterior view. **D**, cross-section through caudal vertebra 9 anterior to the neural spine as seen in posterior view. **E**, cross-section through the shaft of chevron 12 (anterior toward top of page) as seen in distal view. **Abbreviations:** ce, centrum; di, diapophysis; fos, fossa; gr, groove; hpo, hyposphene; nc, neural canal; ns, neural spine; pa, parapophysis; poz, postzygapophysis; prz, prezygapophysis; tp, transverse process. Dashed line in A indicates cross-section shown in B; hatching in B-E indicates a broken surface. Scale bar equals 1 cm in B-D and 5 mm in E.

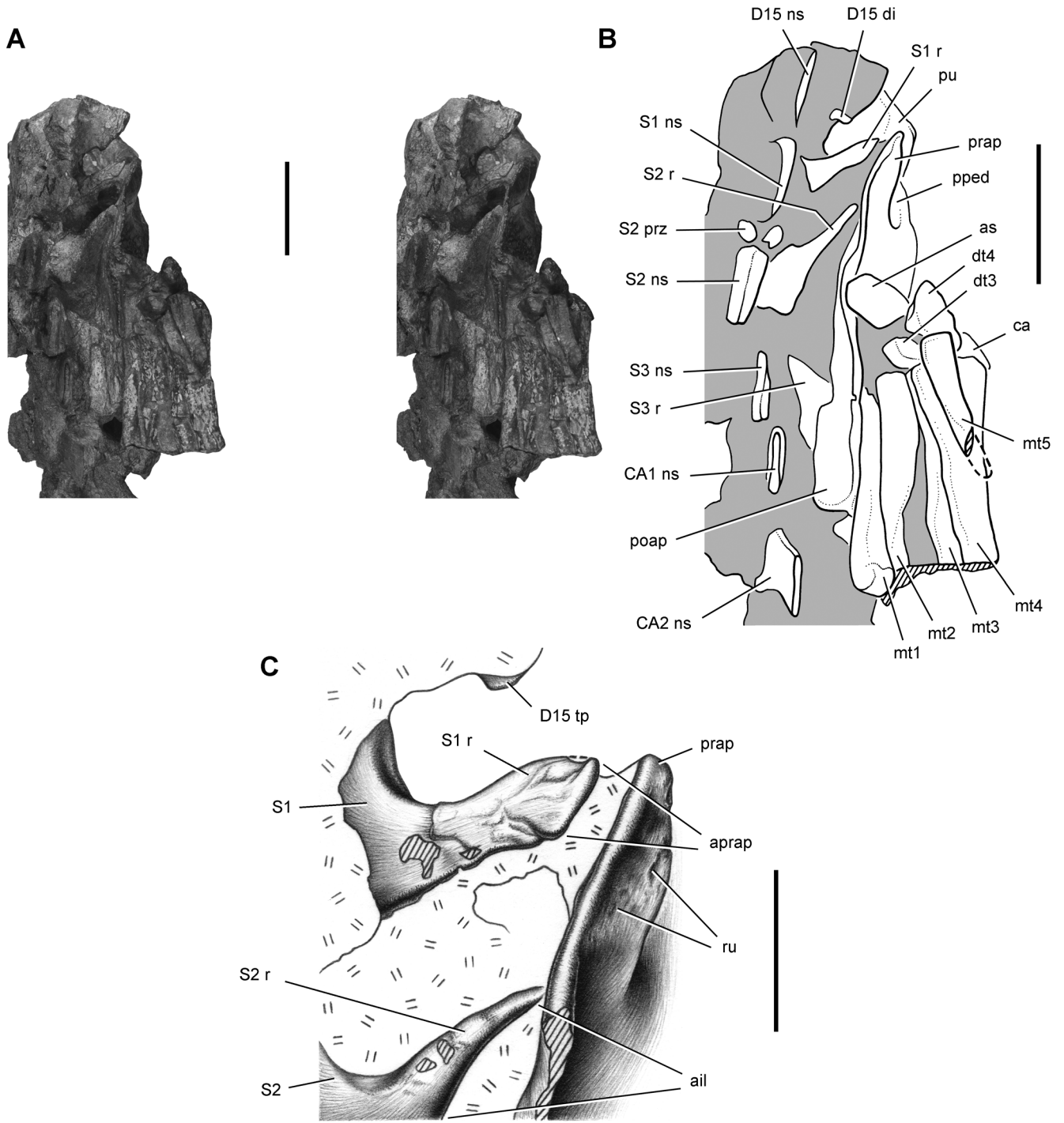


FIGURE 53. Stereopair (A) and drawing (B) of sacral vertebrae and ribs and magnified drawing of the first sacral vertebra and rib (C) of *Eoraptor lunensis* (PVSJ 512) in dorsal view. **Abbreviations:** ail, articular surface for the ilium; aprap, articular surface for the preacetabular process; as, astragalus; ca, calcaneum; CA1, 2, caudal vertebra 1, 2; D15, dorsal vertebra 15; di, diapophysis; dt3, 4, distal tarsals 3, 4; mt1–5, metatarsals 1–5; ns, neural spine; poap, postacetabular process; pped, pubic peduncle; prap, preacetabular process; prz, prezygapophysis; pu, pubis; r, rib; ru, rugosity; S1–3, sacral vertebrae 1–3; tp, transverse process. Dashed line indicates a missing margin; hatching indicates a broken surface; double hatch marks and shading indicate matrix. Scale bars equal 3 cm in A and B and 1 cm in C.

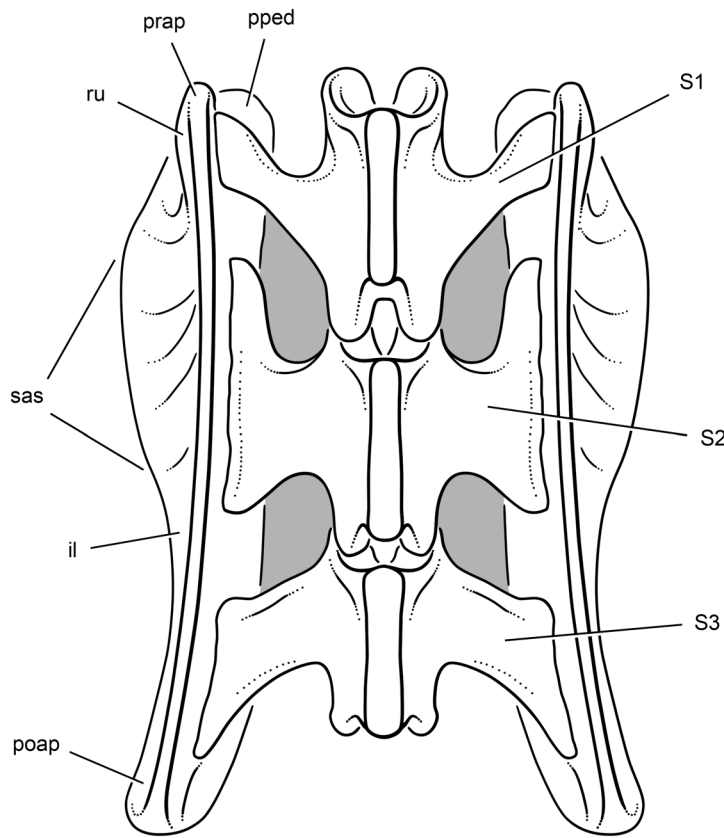


FIGURE 54. Reconstruction of the sacrum and right and left ilia of *Eoraptor lunensis* (PVSJ 512) in dorsal view. **Abbreviations:** **il**, ilium; **poap**, postacetabular process; **pped**, pubic peduncle; **prap**, preacetabular process; **ru**, rugosity; **S1–3**, sacral vertebrae 1–3; **sas**, supraacetabular crest.

the first sacral transverse process and rib suggest that the rib was previously free as the most distal of dorsal ribs and subsequently was incorporated into the sacrum.

The transverse processes and ribs of the second and third sacral vertebrae are fan-shaped in dorsal view, with more robust distal attachment surfaces than the first. The transverse process and rib of the second sacral vertebra contacts the ilium above the acetabulum; and those of the third sacral vertebra contact the ventromedial margin of the postacetabular process.

**Caudal Vertebrae**—The first 17 caudal vertebrae and the prezygapophyses of the 18th caudal vertebrae are preserved in articulation (Figs. 9, 55–59; Table 5). The last preserved caudal vertebra in *Eoraptor* (CA17) is unmodified, with a strong neural spine, small zygapophyses that angle at about 50°, strut-shaped transverse processes, and a long chevron (Fig. 58). Because more distal caudal vertebrae are not known in the holotypic or referred material (Table 1), the form of the distal half of the tail cannot be determined by direct observation in *Eoraptor* at this time. Some distal caudal vertebrae are known for the closely related genera *Panphagia* (Martínez and Alcober, 2009:fig. 6H) and *Pampadromaeus* (Cabreira et al., 2011:fig. 1). In neither case are the centra or prezygapophyses lengthened, so it is probable that the distal tail was similar in *Eoraptor*. A stiffened distal tail with elongate centra and lengthened prezygapophyses characterizes *Herrerasaurus* (Novas, 1994), *Eodromaeus* (Martínez et al., 2011), and nearly all neotheropods. In basal theropods, such as *Herrerasaurus* and *Eodromaeus*, the elongate prezygapophyses that stiffen the tail first appear in the caudal series between caudal vertebrae 20–25, posterior to the last preserved vertebra in *Eoraptor* (CA17).

The spool-shaped caudal centra become more transversely pinched than the dorsal centra, starting with the second caudal vertebrae. The centra of sacral vertebra 3 and anterior caudal vertebrae 1 and 2 are parallelogram-shaped, such that the posterior face is lowered, which lowers the axis of the tail (Fig. 9). In anterior or posterior view, the gently concave faces of the caudal centra have a subtriangular shape due to the narrowness of the ventral half of the centrum and the transverse breadth of the spacious neural canal. In cross-section, the caudal centra show the same hollowed condition that is present in presacral cross-sections (Fig. 52). As seen in the ninth caudal vertebra, the neural canal fills the neural arch from the top of the centrum to the base of the neural spine (Fig. 52D). A thin septum may have been present flooring the canal, as in the dorsal vertebrae. The centrum is solid near the articular ends but is extremely hollow in between. The sidewalls of the ninth caudal vertebra, for example, are less than 1 mm thick. It is not surprising, therefore, that local areas of the caudal column have collapsed.

The first caudal centrum is shorter than the adjacent third sacral and second caudal vertebrae (Fig. 9; Table 5), its parallelogram-shaped centrum offsetting slightly ventrally the remainder of the tail. In the second caudal vertebra, centrum length returns to that typical of the dorsal and sacral vertebrae (20 mm), and this length is maintained through the seventh caudal vertebra. Centrum length decreases gradually in the eighth through the 17th caudal vertebra. Because centrum height decreases somewhat faster than centrum length in the caudal series, the middle caudal centra have progressively longer proportions (Fig. 59).

The transverse processes are very well developed throughout the anterior and middle caudal vertebrae and are always about

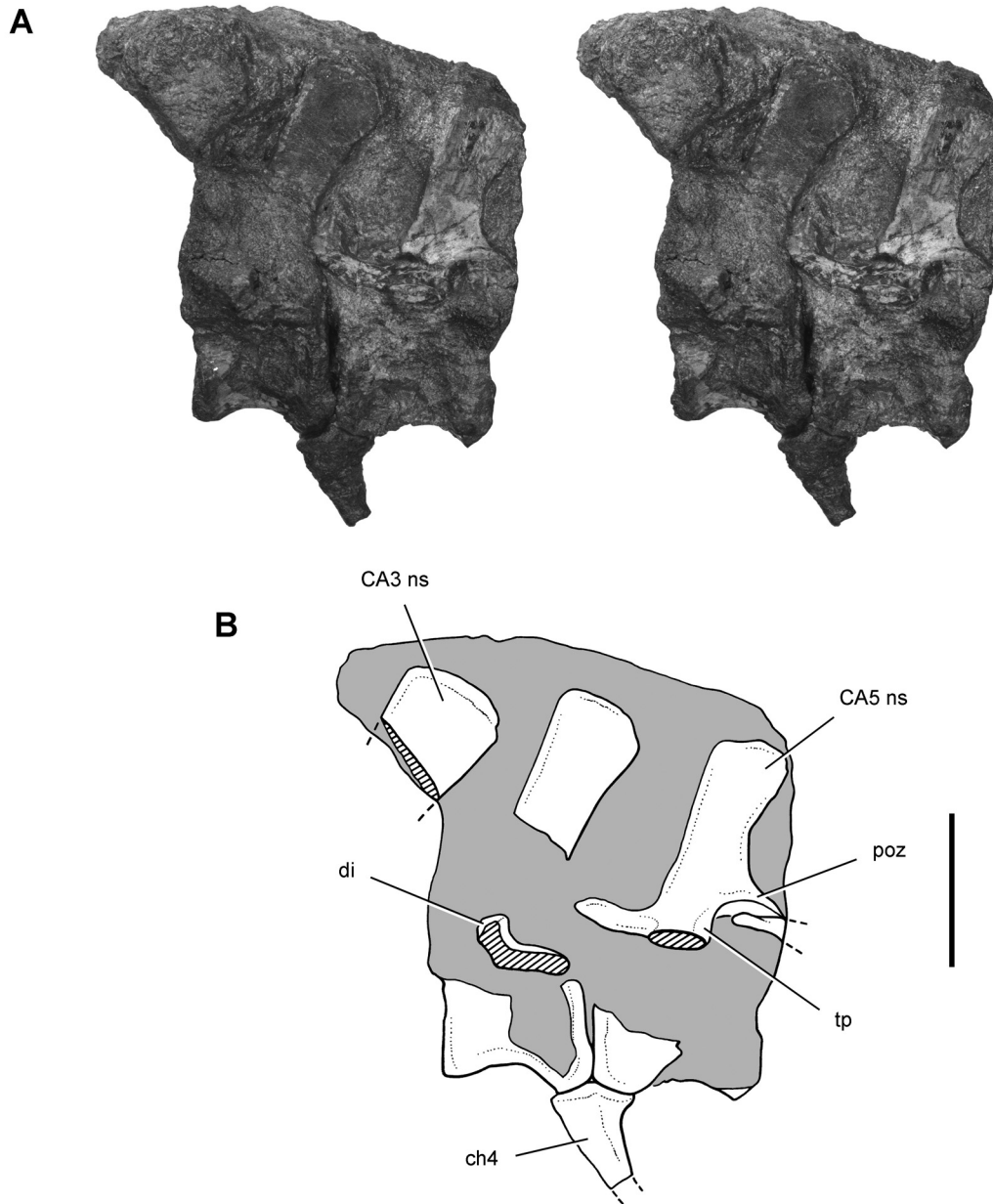


FIGURE 55. Stereopair (A) and drawing (B) of caudal vertebrae 3–5 of *Eoraptor lunensis* (PVSJ 512) in left lateral view. **Abbreviations:** CA3, 5, caudal vertebra 3, 5; **ch4**, chevron 4; **di**, diapophysis; **ns**, neural spine; **poz**, postzygapophysis; **tp**, transverse process. Dashed line indicates a missing margin; hatching indicates a broken surface; shading indicates matrix. Scale bars equal 2 cm.

20% longer than the neural spines (Figs. 9, 59). In the first and second caudal vertebrae, the transverse processes appear to angle posterolaterally, which avoids contact with the postacetabular process of the ilium. In the fifth caudal vertebra, the transverse process is blade-shaped and expands from a narrow proximal end (6 mm) to a broad distal end (12 mm) (Fig. 55). Transverse processes of this general shape are present until the 14th or 15th caudal vertebra, in which they are subrectangular (Figs. 57, 58). The transverse processes in the succeeding two vertebrae are noticeably narrower.

In the fifth caudal vertebra, the zygapophyses articulate at an angle of 50–60°, and this orientation is maintained throughout the middle caudal vertebrae (Figs. 55–58). The neural spines are proportionately much taller in the anterior caudal vertebrae than in the dorsal and sacral vertebrae. In the fifth caudal vertebra, for example, the neural spine is 9 mm wide at its narrowest point above the base and 21 mm tall (Fig. 55). Because neural spine height decreases more rapidly than spine width, spine proportions become progressively broader in the mid-caudal vertebrae. The spine of the 13th caudal vertebra is 10 mm tall

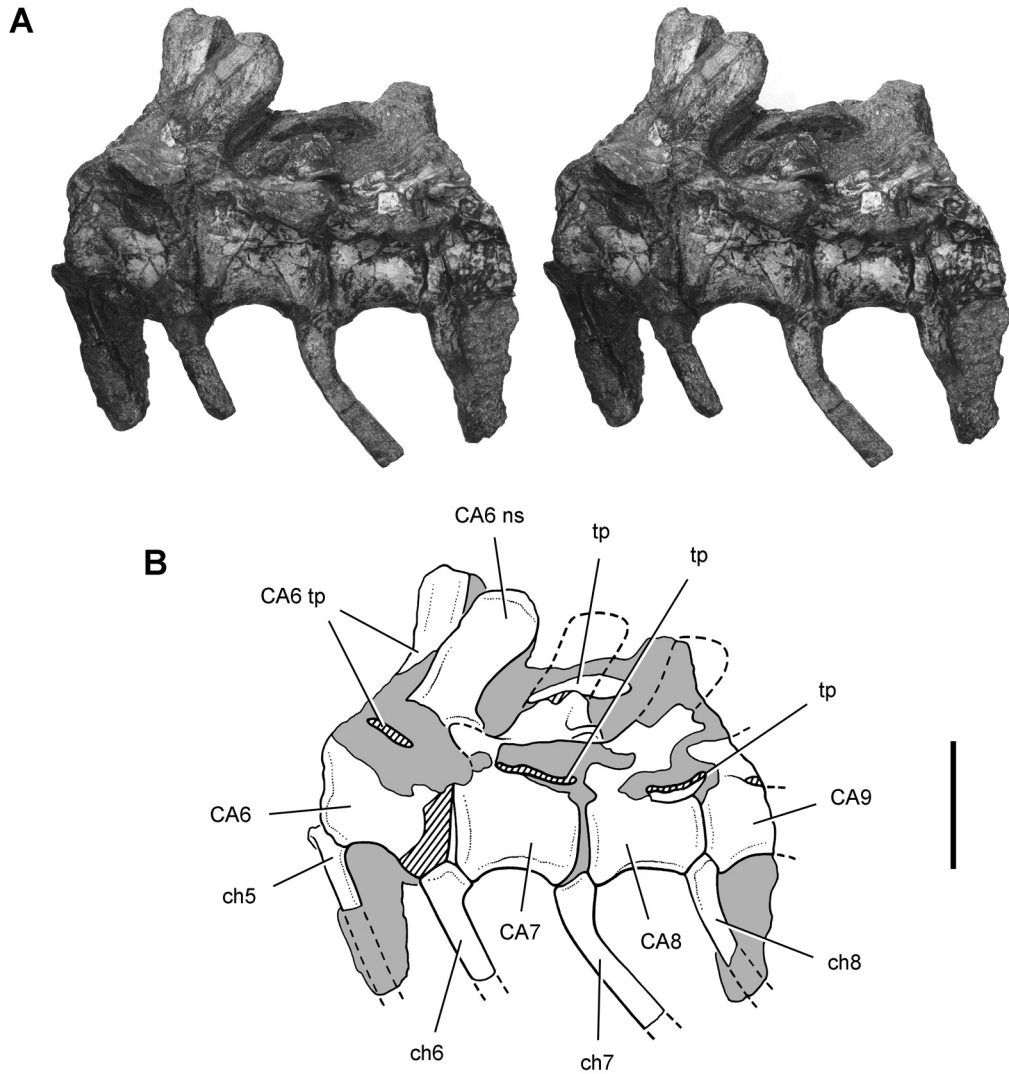


FIGURE 56. Stereopair (A) and drawing (B) of caudal vertebrae 6–9 of *Eoraptor lunensis* (PVSJ 512) in left lateral view. **Abbreviations:** CA6–9, caudal vertebrae 6–9; ch5–8, chevrons 5–8; ns, neural spine; tp, transverse process. Dashed line indicates a missing margin; hatching indicates a broken surface; shading indicates matrix. Scale bars equal 2 cm.

and 7 mm wide, and by the 17th caudal vertebra, spine height and width appear to be subequal (Fig. 58). The best-preserved neural spines (CA4, 5, 10, 13) show that the increase in distal width of the spine is due to a tab-shaped expansion along the posterior margin. The anterior margin of the caudal neural spines, in contrast, is straight. The axis of the spine in lateral view is inclined posterodorsally at approximately 20° from the vertical in all preserved caudal vertebrae.

**Presacral Ribs**—With the exception of the atlantal rib, the presacral ribs are preserved near their natural articulation with the vertebral column (Fig. 9). Most of the ribs, however, remain in the matrix, and none is completely exposed. Some of the cervical ribs appear to be fused to the vertebrae, whereas others are clearly disarticulated (Fig. 43).

Portions of the ribs of the second through the fourth cervical vertebrae are exposed on the left side of the cervical series

(Figs. 43, 44). As in more posterior cervical ribs, the rod-shaped shafts of the anterior cervical ribs are directed posteriorly and overlap the ventral aspect of the succeeding rib. This overlap is enhanced by a long, anteriorly projecting spine (Fig. 60A) that is first preserved in the fourth cervical rib. The cervical rib shafts, thus, form a structurally continuous rod aligned parallel to the cervical centra.

The fifth and seventh cervical ribs are nearly completely exposed and provide more complete information on the form of middle cervical ribs (Figs. 44, 60A). Anteriorly, there are three prominent processes set at nearly right angles to one another. A long, pointed spinous process projects anteriorly beyond the anterior end of its respective centrum. It has sharp dorsal and ventral margins, a crescentic cross-section, and articulates ventrolaterally with the shaft of the next anterior rib. The tuberculum and capitulum of the seventh cervical rib are well exposed

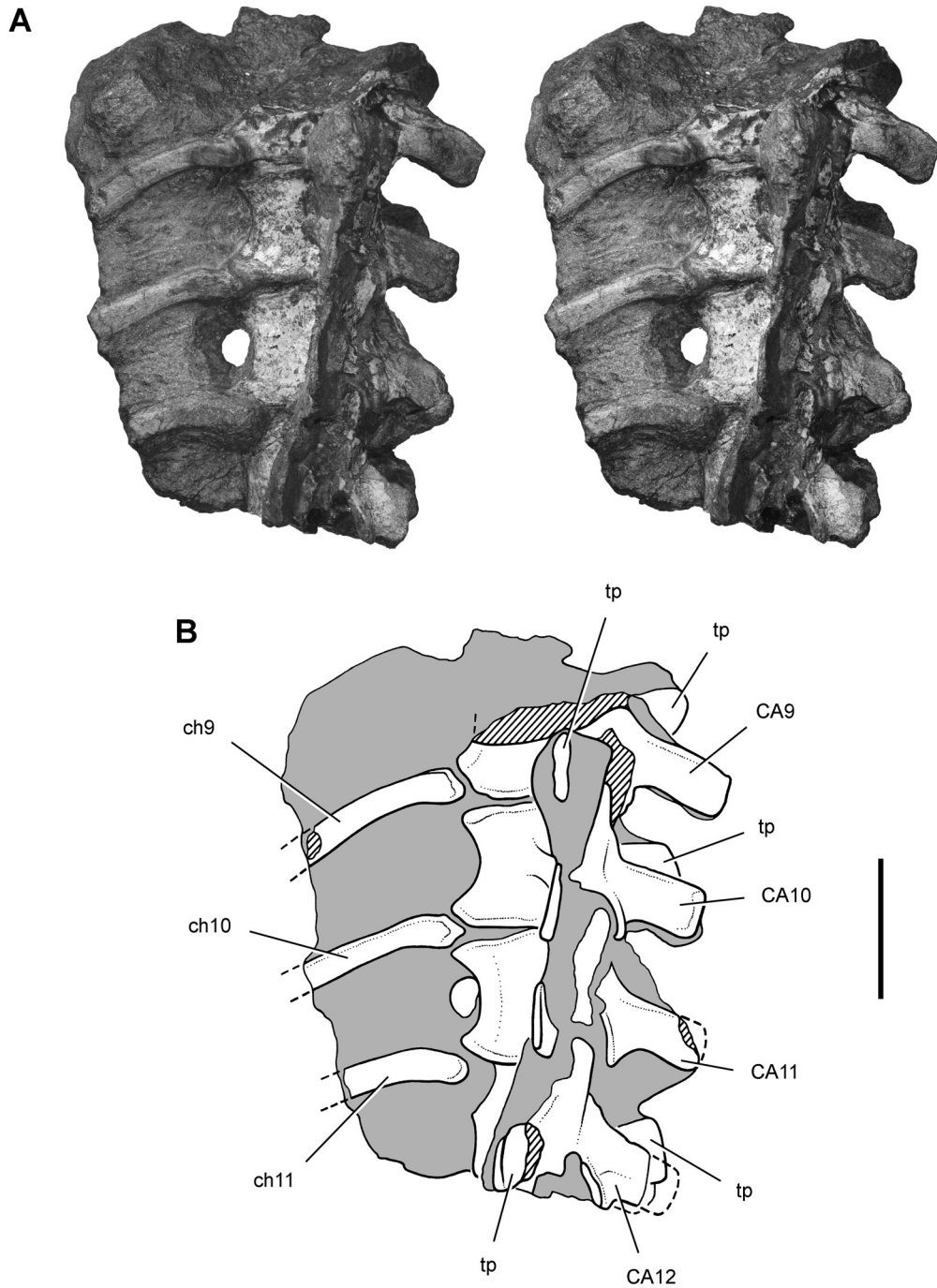


FIGURE 57. Stereopair (A) and drawing (B) of caudal vertebrae 9–12 of *Eoraptor lunensis* (PVSJ 512) in left lateral view. **Abbreviations:** CA9–12, caudal vertebrae 9–12; ch9–11, chevrons 9–11; tp, transverse process. Dashed line indicates a missing margin; hatching indicates a broken surface; shading indicates matrix. Scale bars equal 2 cm.

(Fig. 60A). The capitulum is broader than the tuberculum and projects medially and somewhat anterodorsally. The tuberculum is narrower and is directed dorsomedially toward the diapophysis. The rib spine and shaft are offset ventrolateral to the ventral margin of the cervical centra. The distal portion of the rib shaft is flattened and has a subrectangular cross-section. The broad

articular surface of the shaft faces dorsomedially, and the shaft extends posteriorly to the end of the next vertebra, as shown by an articular scar on the shaft of the sixth cervical rib for the shaft of the fifth cervical rib. Thus, the tip of the fifth cervical rib overlaps the midshaft of the sixth cervical rib, which overlaps the spinous process of the seventh cervical rib (Fig. 49).

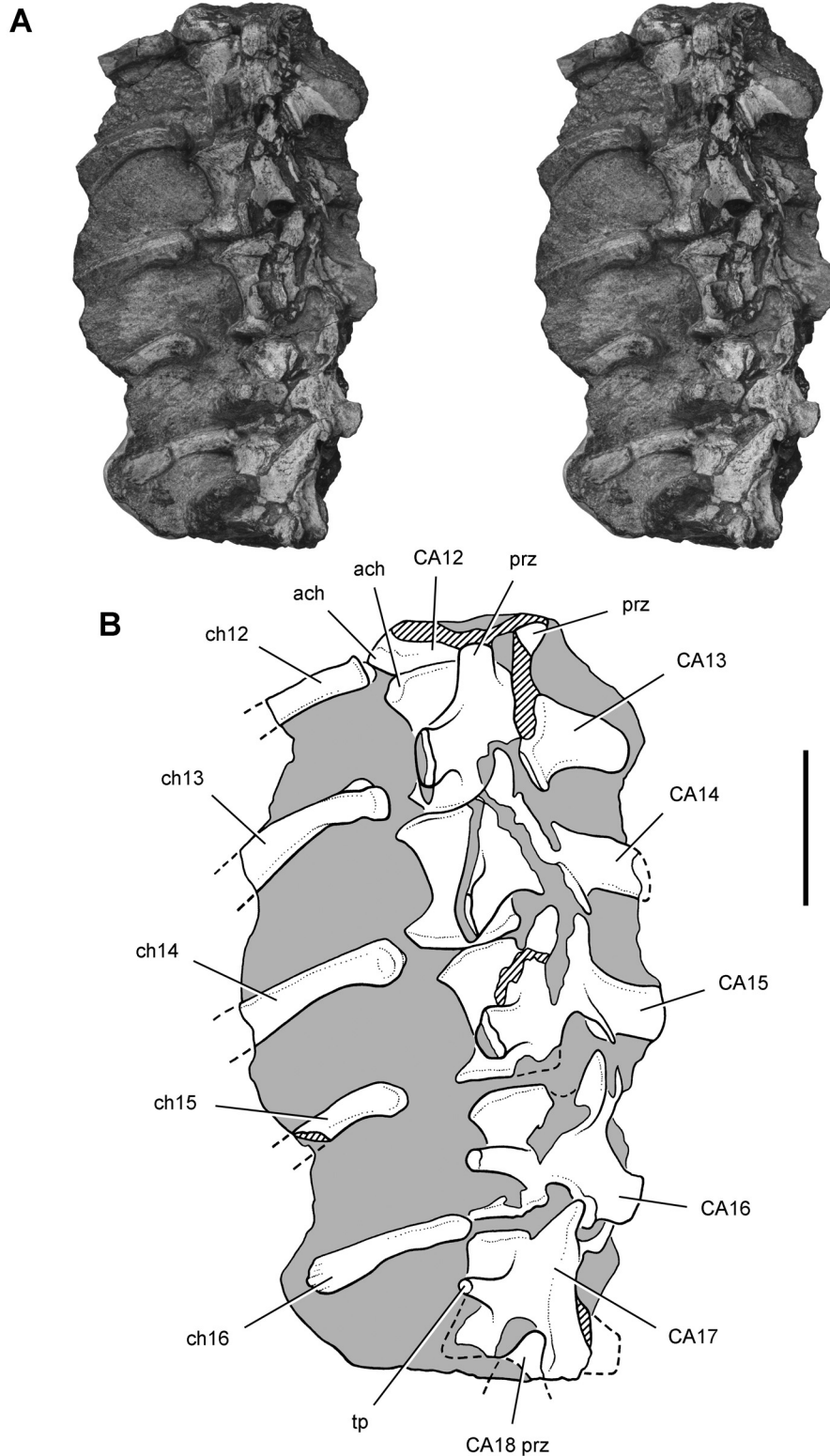


FIGURE 58. Stereopair (A) and drawing (B) of caudal vertebrae 13–17 of *Eoraptor lunensis* (PVSJ 512) in left lateral view. **Abbreviations:** ach, articular surface for chevron; CA12–18, caudal vertebrae 12–18; ch12–16, chevrons 12–16; prz, prezygapophysis; tp, transverse process. Dashed line indicates a missing margin; hatching indicates a broken surface; shading indicates matrix. Scale bars equal 2 cm.

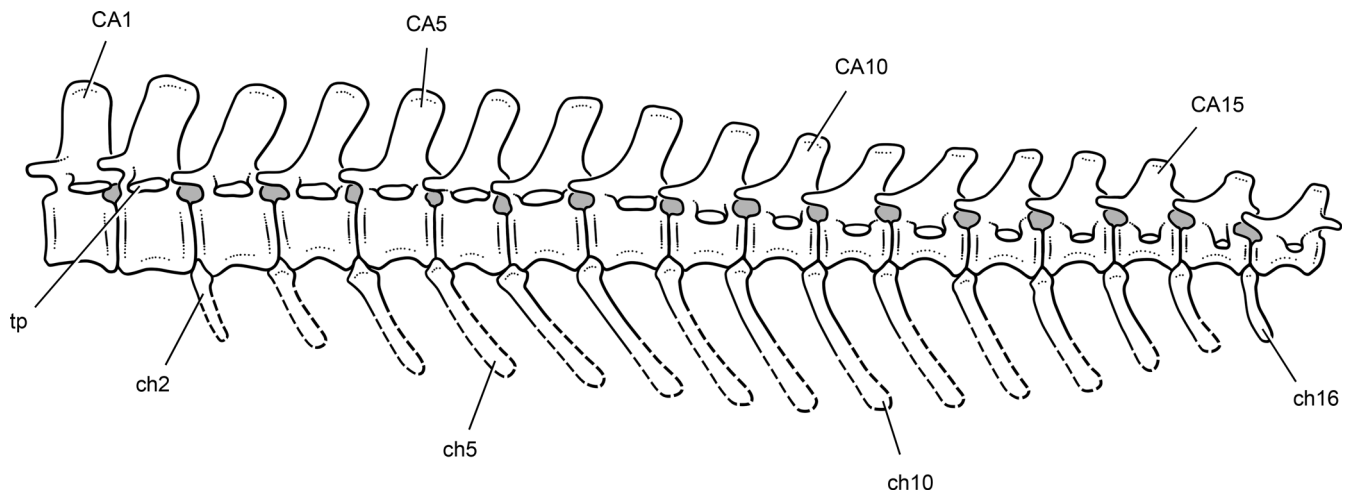


FIGURE 59. Reconstruction of caudal vertebrae 1–17 and chevrons 2–16 of *Eoraptor lunensis* (PVSJ 512) in left lateral view. **Abbreviations:** CA1, 5, 10, 15, caudal vertebra 1, 5, 10, 15; ch2, 5, 10, 16, chevron 2, 5, 10, 16; tp, transverse process. Dashed line indicates a missing margin.

The spinous process of the eighth cervical rib is narrower and flatter and only about one-half the length of that of the seventh cervical rib (Fig. 43). The capitulum is longer and points more strongly anteriorly than medially. The ninth cervical rib, which is dislocated ventrally, has a low, short spine as in the preceding rib, and its shaft is triangular, rather than a quadrangular, cross-section (Fig. 60B).

The first dorsal rib is approximately twice the diameter and length of the last cervical rib, which may indicate that it was the first rib that attached to a cartilaginous sternum (Fig. 60B). The form of the rib also differs. The spine, for example, is reduced to a

low ridge. The capitulum is much longer than the tuberculum, and both lie in nearly the same plane as the proximal shaft of the rib (Fig. 60B).

The fourth dorsal rib measures approximately 95 mm (tuberculum to shaft end) and may be the longest in the rib cage. The fifth dorsal rib is shorter (approximately 90 mm), as are more posterior ribs such as the seventh (approximately 70 mm) and 14th (less than 30 mm). The capitulum remains long in the first five dorsal ribs because the distance between the diapophysis and parapophysis remains the same. Although the parapophysis moves dorsally from the centrum onto the neural arch in the anterior dorsal vertebrae,

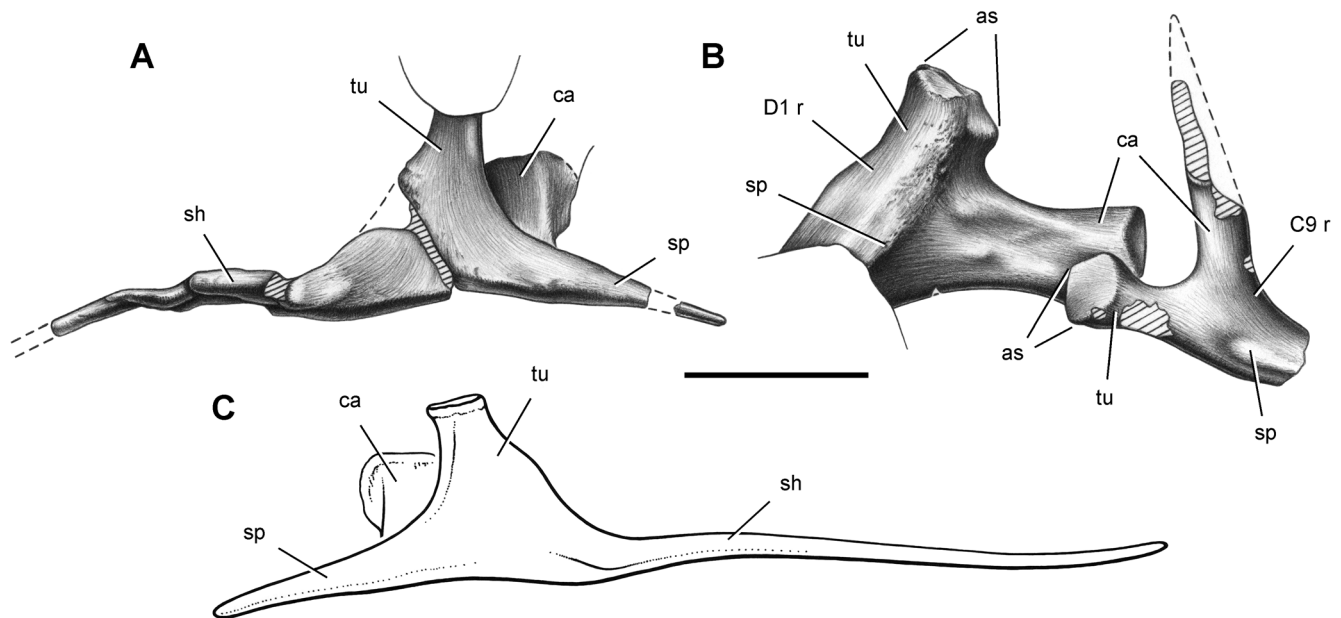


FIGURE 60. Posterior cervical and anterior dorsal ribs of *Eoraptor lunensis* (PVSJ 512). **A**, seventh cervical rib in right lateral view. **B**, proximal ends of ninth cervical and first dorsal ribs in right lateral view. **C**, reconstruction of seventh cervical rib in left lateral view. **Abbreviations:** as, articular surface; C9, cervical vertebra 9; ca, capitulum; D1, dorsal vertebra 1; r, rib; sh, shaft; sp, spine; tu, tuberculum. Dashed line indicates a broken surface. Scale bar equals 1 cm in **A** and **B**.

the transverse process increases in length. In the mid-dorsal vertebrae (D8–12), however, the transverse process becomes shorter and, as a result, the capitulum is reduced to the length of the tuberculum (Fig. 51).

**Chevrons**—In the following description, chevrons are identified according to the vertebra with which they share their primary (anterior) articulation (Figs. 55–59; Table 6). There are no chevron facets between caudal vertebrae 1 and 2; the first chevron base is preserved in place articulating with well-developed facets between caudal vertebrae 2 and 3. Thus, the most anterior chevron is identified as the chevron 2, because it articulates between the second and third caudal vertebrae (Fig. 59).

The chevron of the second caudal vertebra is incomplete distally but appears to be only about two-thirds the length of succeeding chevrons (Figs. 9, 59). All succeeding chevrons are longer than the neural spines of their associated caudal vertebrae. Furthermore, because the height of the caudal neural spines decreases along the caudal column more rapidly than the length of the chevrons, the more posterior chevrons are longer relative to their associated caudal neural spines. Thus, anterior chevrons are approximately 40% longer than their associated neural spines, whereas posterior chevrons are more than twice as long. The chevrons increase in length distally along the proximal column, reaching a maximum in the chevron of the seventh caudal vertebra (Table 6). Distal to this chevron, length decreases gradually. Several of the tips of the chevrons projected beyond the concretion that encased the skeleton and were eroded away.

The proximal ends of the chevrons are strongly concave in anterior or posterior view, which corresponds with the narrow proportions of the ventral margin of the caudal centra. The major articular facet occurs on the anterior side of the base and is oriented at a high angle to the axis of the proximal end of the chevron (Fig. 56). The smaller posterior facet, in contrast, is located at a very low angle to the axis of the shaft. At least in the middle caudal vertebrae, the asymmetry of the proximal facets reflects the posterior inclination of the chevron. The principal chevron facet on the posterior margin of the 14th and 15th caudal centra has nearly vertical orientation and projects below the opposing facet on the 15th and 16th caudal centra, respectively (Fig. 58). This arrangement of facets accommodates a posteroventrally inclined approach by the chevron.

The saddle-shaped proximal articular end encloses the hemal canal in all anterior and middle caudal chevrons. A trough passes distally from the oval opening of the hemal canal along the anterior and posterior margins of the base of the chevron. Incipient anterior processes are developed to each side of the hemal canal in anterior caudal chevrons and appear in lateral view as little more than a bend in the anterior margin of the chevron.

The shafts of the chevrons are transversely compressed throughout their lengths. In lateral view, the shafts narrow in width before slowly expanding toward the distal blade. At its narrowest width in lateral view, the shaft bends distinctly posteriorly, so that the blade of the chevron is oriented at an angle approximately 30° from the axis of the caudal column. All of the chevron shafts narrow in width before expanding toward the blade, and there is no discernible trend along the caudal series in the angle of the bend in the shaft. Surprisingly, the shaft and blade of each chevron are hollowed; a transversely compressed cavity, sometimes with some spongy bone infilling, extends down the shaft and into the lobed-shaped end of each chevron, as seen in many cross-sections (Fig. 52E).

**Gastralia**—Rows of gastralia are preserved on both sides of the skeleton near the distal end of the pubes (Fig. 9). The best-preserved section includes five elements that arch over the distal ends of the pubic blades, as seen in right lateral view of the skeleton. In left lateral view, more gastralia are visible in the same re-

gion anterior to the left pes (Figs. 7, 8). Nothing can be said about their number or arrangement as an articulated cuirass. Preparation of these slender rods was very difficult, because the boundary to surrounding matrix was not always distinct. They measure approximately 1–2 mm in diameter. Circular and oval cross-sections are visible. It is entirely possible that two elements are present to each side of the midline, although no such articulation can be distinguished.

### Pectoral Girdle

The scapula and coracoid are best preserved on the right side (Figs. 9, 61–64; Table 7). On the left side, only the distal end of the scapular blade is preserved. Clavicles were not found in the holotypic skeleton and may not have been ossified in *Eoraptor*, as discussed above. Alternatively, they may have been lost, because the right scapulocoracoid has moved from its original position to the opposite side of the specimen and because most of the left scapulocoracoid is not preserved.

**Scapula**—The form of the scapula in *Eoraptor* more closely resembles the condition in basal sauropodomorphs such as *Saturnalia* (Langer et al., 2007) than that in basal theropods or ornithischians (Figs. 61–63, 64A, B). With the long axis of the scapular blade held vertically, the scapular glenoid is shallow and faces posteroventrally and slightly laterally. The margin between the rim of the glenoid and the blade is concave in lateral view, which differs from the convex margin in *Herrerasaurus*.

The neck of the scapular blade is proportionately broader than in the strap-shaped blade in *Herrerasaurus* (Sereno, 1994) or the narrow-necked but more expanded distal blades in *Eodromaesus* (Martínez et al., 2011), *Tawa* (Nesbitt et al., 2009), and heterodontosaurids (Sereno, 2012). The blade, nonetheless, is proportionately more elongate compared with neck width than in *Panphagia*

TABLE 7. Measurements (in mm) of the pectoral girdle, humerus, ulna, and radius of *Eoraptor lunensis* (PVSJ 512).

Dimension	Measurement
<b>Scapula</b>	
Maximum length	81
Maximum proximal width (lip of glenoid to acromion)	40
Depth of glenoid	7
Blade length	61
Blade proximal end (neck), minimum width	13
Blade distal end, width	27L
<b>Coracoid</b>	
Maximum length	22
Maximum width (posterior process to acromion)	37
<b>Humerus</b>	
Maximum length	85
Maximum proximal width	28
Maximum distal width	23
Deltpectoral crest length	37
Transverse shaft diameter	11
Minimum shaft diameter	6
<b>Ulna</b>	
Maximum length	64
Maximum proximal width	14
Maximum distal width	9
Minimum shaft diameter	6
<b>Radius</b>	
Maximum length	63
Maximum proximal width	(10)
Maximum distal width	8
Minimum shaft diameter	6

Paired structures are measured from the right side except as indicated (L, left). Parentheses indicate estimated measurement.

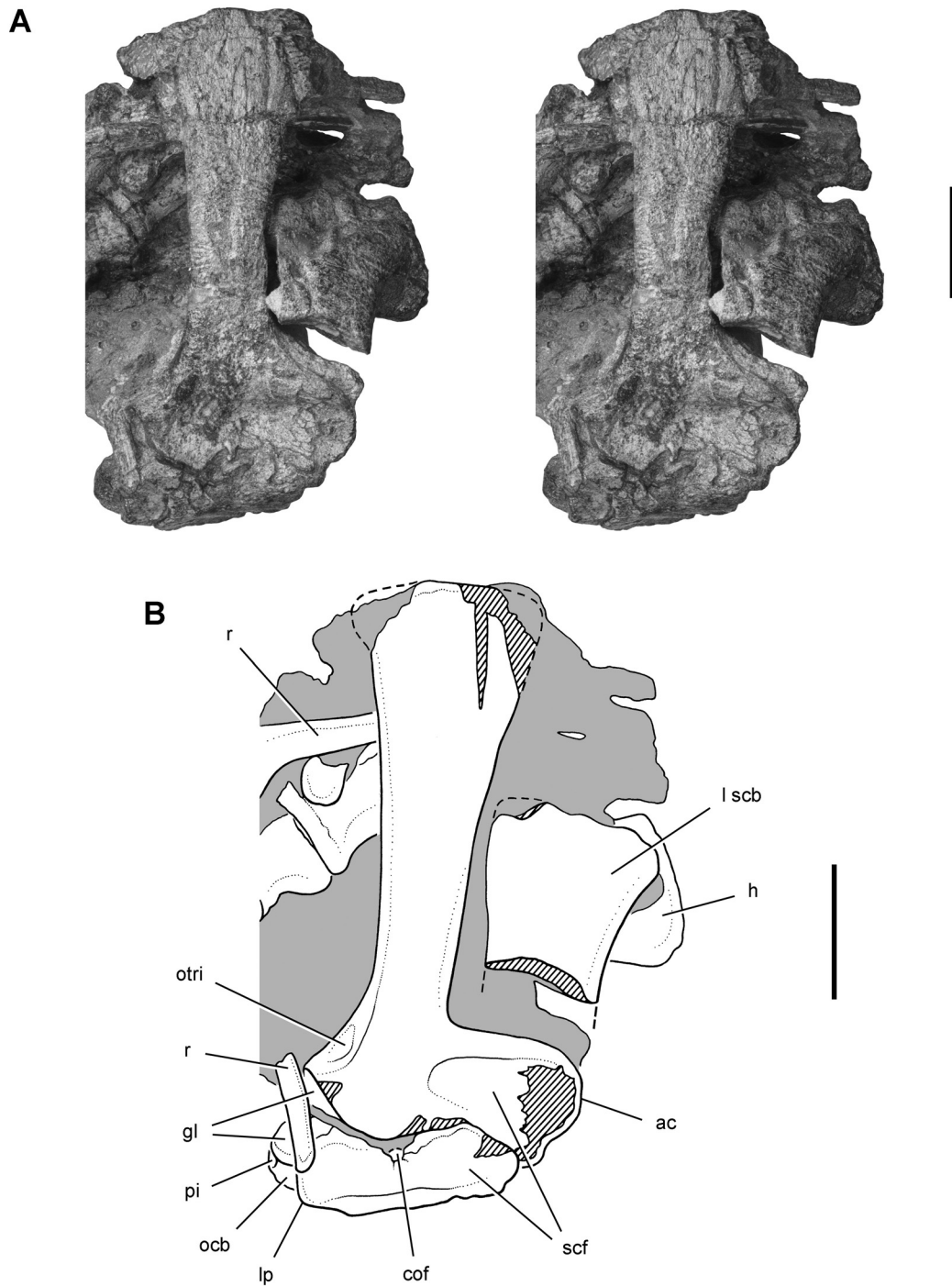


FIGURE 61. Stereopair (A) and drawing (B) of the right scapulocoracoid of *Eoraptor lunensis* (PVSJ 512) in lateral view. **Abbreviations:** **ac**, acromion; **cof**, coracoid foramen; **gl**, glenoid; **h**, humerus; **l**, left; **lp**, lateral process; **ocb**, origin of *m. coracobrachialis*; **otri**, origin of *m. triceps longus*; **pi**, pit; **r**, rib; **scb**, scapular blade; **scf**, scapulocoracoid fossa. Dashed line indicates a missing margin; hatching indicates a broken surface; shading indicates matrix. Scale bars equal 2 cm.

(Martínez and Alcober, 2009) and *Saturnalia* (Langer et al., 2007), in which blade length is less than 2.5 times neck width. The posterior margin of the scapular blade is more rounded than the anterior margin, and as in *Herrerasaurus* (Sereno, 1994), the blade

follows a gentle sigmoid curve in posterior view. At the distal end of the blade, the posterior corner has a tab-shaped extension (Fig. 64B). The distal end of the blade has an approximately symmetrical profile, whereas in *Panphagia* (Martínez and Alcober, 2009)

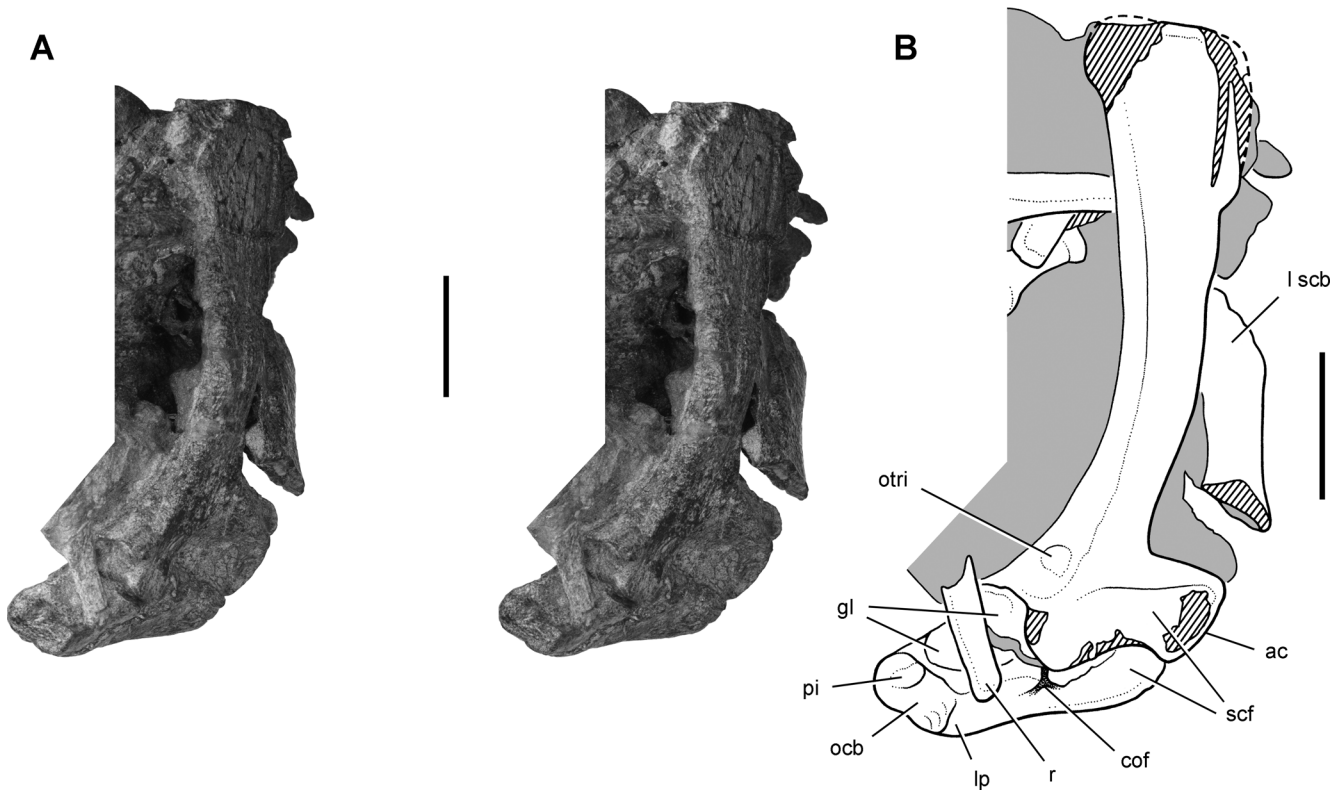


FIGURE 62. Stereopair (A) and drawing (B) of the right scapulocoracoid of *Eoraptor lunensis* (PVSJ 512) in posterolateral view. **Abbreviations:** **ac**, acromion; **cof**, coracoid foramen; **gl**, glenoid; **l**, left; **lp**, lateral process; **ocb**, origin of m. coracobrachialis; **otri**, origin of m. triceps longus; **pi**, pit; **r**, rib; **scb**, scapular blade; **scf**, scapulocoracoid fossa. Dashed line indicates a missing margin; hatching indicates a broken surface; shading indicates matrix. Scale bars equal 2 cm.

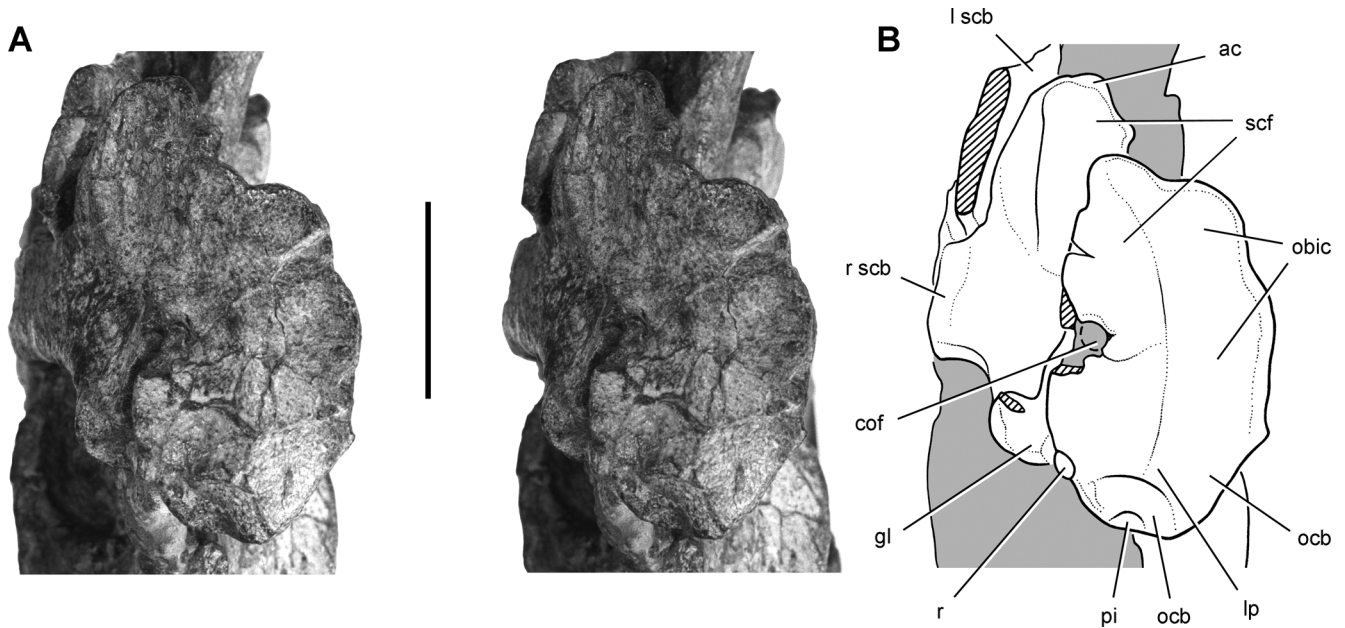


FIGURE 63. Stereopair (A) and drawing (B) of the right coracoid of *Eoraptor lunensis* (PVSJ 512) in ventral view. **Abbreviations:** **ac**, acromion; **cof**, coracoid foramen; **gl**, glenoid; **l**, left; **lp**, lateral process; **obic**, origin of m. biceps; **ocb**, origin of m. coracobrachialis; **pi**, pit; **r**, right or rib; **rscb**, scapular blade; **scf**, scapulocoracoid fossa. Dashed line indicates a missing margin; hatching indicates a broken surface; shading indicates matrix. Scale bar equals 2 cm.

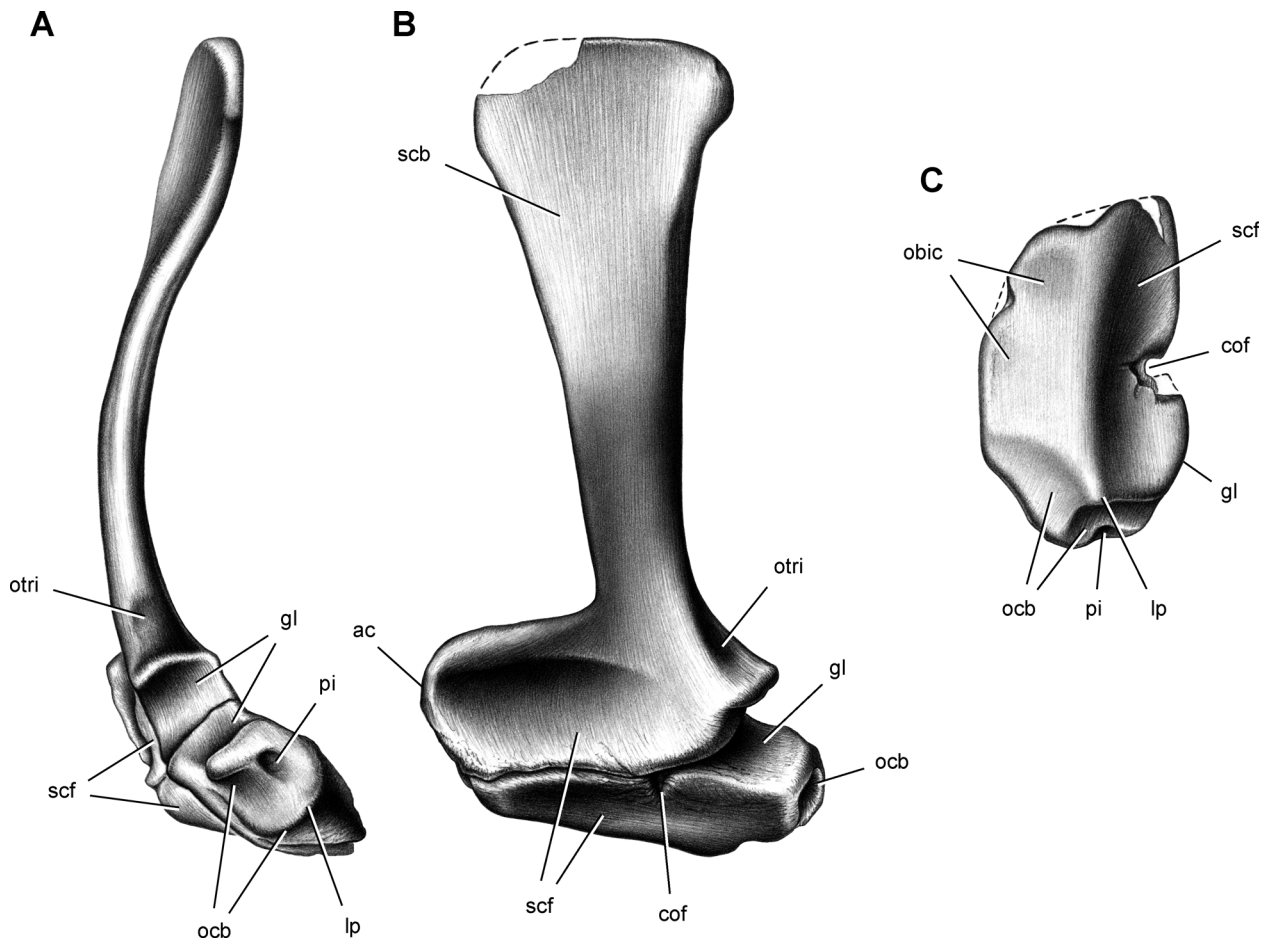


FIGURE 64. Reconstruction of the left scapulocoracoid of *Eoraptor lunensis* (PVSJ 512) in posterior (A), lateral (B), and ventral (C) views. **Abbreviations:** ac, acromion; cof, coracoid foramen; gl, glenoid; lp, lateral process; obic, origin of m. biceps; ocb, origin of m. coracobrachialis; otri, origin of m. triceps longus; pi, pit; scb, scapular blade; scf, scapulocoracoid fossa. Dashed line indicates a missing margin.

and *Saturnalia* (Langer et al., 2007) the anterior corner of the blade is considerably shorter than the posterior corner. *Eoraptor* has an oval depression on the lateral aspect of the acromion, which may have served as an attachment area for supracoracoideus musculature.

**Coracoid**—Relative to the scapula, the coracoid in *Eoraptor* (Figs. 61–63, 64C) is smaller than in *Herrerasaurus* and *Eodromaeus* (Martínez et al., 2011) and slightly smaller than in *Saturnalia* (Langer et al., 2007). In ventral view, the coracoid is oval, with a height about twice its breadth (Fig. 64C). The strongly arched external surface can be divided into three discrete areas—dorsal, ventral, and anterior. These surfaces meet at a sharp corner, here termed the lateral process. The dorsal surface comprises the upper one-half of the coracoid. It is gently concave anteroposteriorly and has been regarded in theropods as the area of insertion of the supracoracoideus muscle (Raath, 1977; Langer et al., 2007). A deep notch along the border nearest the scapula forms most of the margin of the coracoid foramen.

The ventral surface comprises most of the ventral one-half of the coracoid and is deflected medially along a well-marked angle that joins the lateral process (Fig. 64C). This surface, in turn, is divided by a subtle bend into two gently concave surfaces, anterior and posterior, which have been regarded in theropods as the areas

of insertion of the deltoideus and coracobrachialis longus muscles, respectively (Raath, 1977).

The posterior surface of the coracoid is subquadrate and deeply concave. It is commonly regarded as the area of insertion for the coracobrachialis brevis muscle (Raath, 1977; Langer et al., 2007). A marked pit is present near its medial margin, and the most posterior corner of this surface, the posterior process, is blunt and rounded (Fig. 64C), as in *Saturnalia* (Langer et al., 2007) and other basal sauropodomorphs. In most theropods, in contrast, the posterior corner is developed as a prominent hook-shaped process (e.g., *Herrerasaurus*; Sereno, 1994). The partially exposed medial surface of the coracoid is dorsoventrally concave. The coracoid glenoid equals the scapular glenoid in size but faces somewhat more laterally.

#### Forelimb

**Humerus**—The proximal end of the humerus is most complete on the right side, although the articular end is weathered (Figs. 65, 66, 67A–C; Table 7). The broad, plate-shaped proximal end closely resembles that in *Herrerasaurus* (Sereno, 1994). The head is developed as a modestly rounded expansion situated in the middle of the proximal end on its posterior aspect

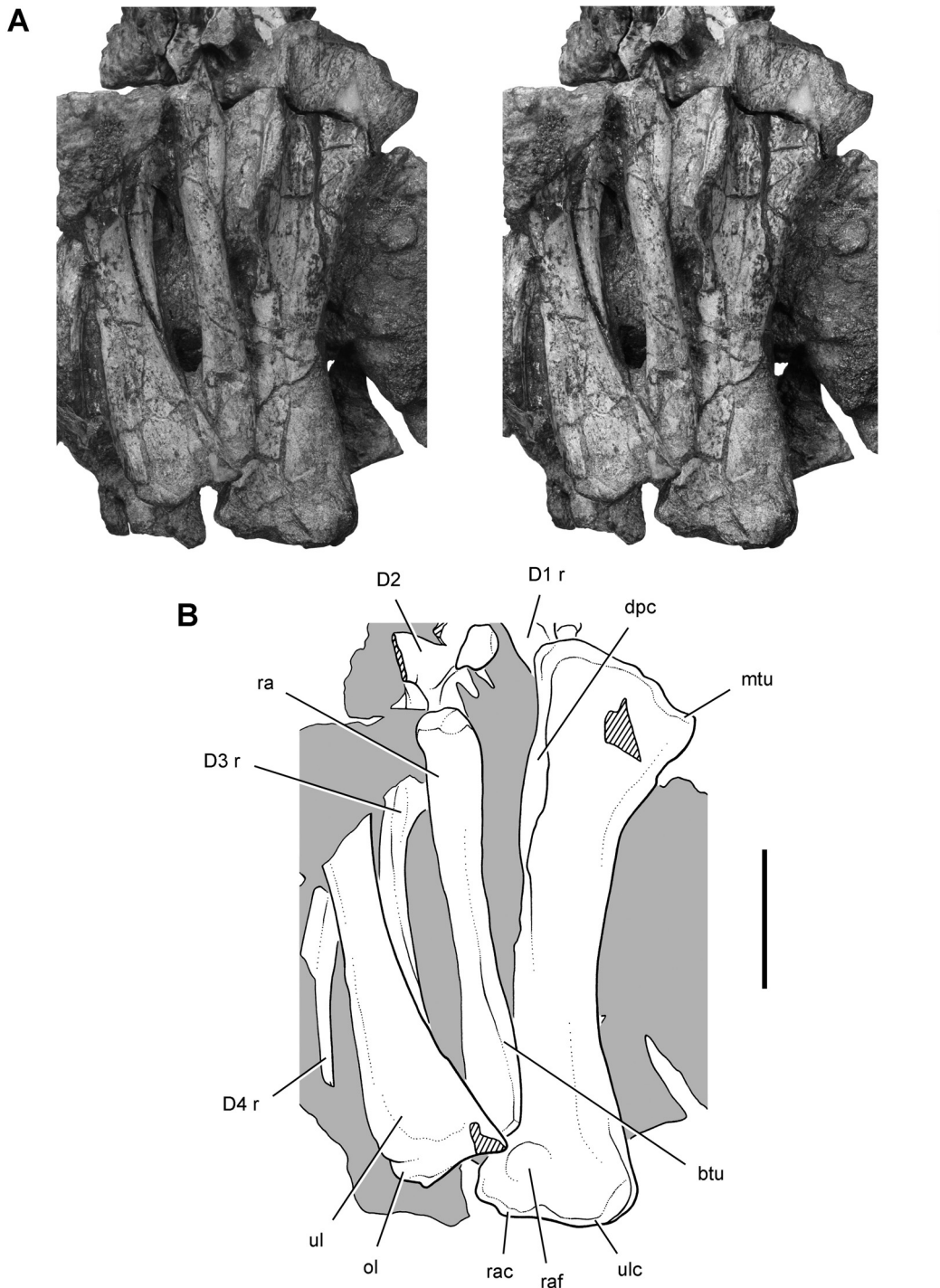


FIGURE 65. Stereopair (A) and drawing (B) of right humerus, radius, and ulna of *Eoraptor lunensis* (PVSJ 512) in anteromedial view. **Abbreviations:** **btu**, biceps tubercle; **D1–4**, dorsal vertebra 1–4; **dpc**, deltopectoral crest; **mtu**, medial tuberosity; **ol**, olecranon; **r**, rib; **ra**, radius; **rac**, radial condyle; **raf**, radial fossa; **ul**, ulna; **ulc**, ulnar condyle. Hatching indicates a broken surface; shading indicates matrix. Scale bars equal 2 cm.

(Fig. 61). A medial tuberosity is present but is less prominently developed and lower in position than that in *Herrerasaurus* (Serenó, 1994). It is unlikely that the more subtle expression of these features in *Eoraptor* is simply a correlate of small body size or immaturity, because these features are prominently expressed in

subadult specimens of *Herrerasaurus* (MACN 18.060; Reig, 1963) that are closer in size to the largest specimens of *Eoraptor*. The deltopectoral crest is developed as a curved flange that extends along the proximal 45% of the humerus. Its external margin is directed about 75° away from a transverse axis through the distal

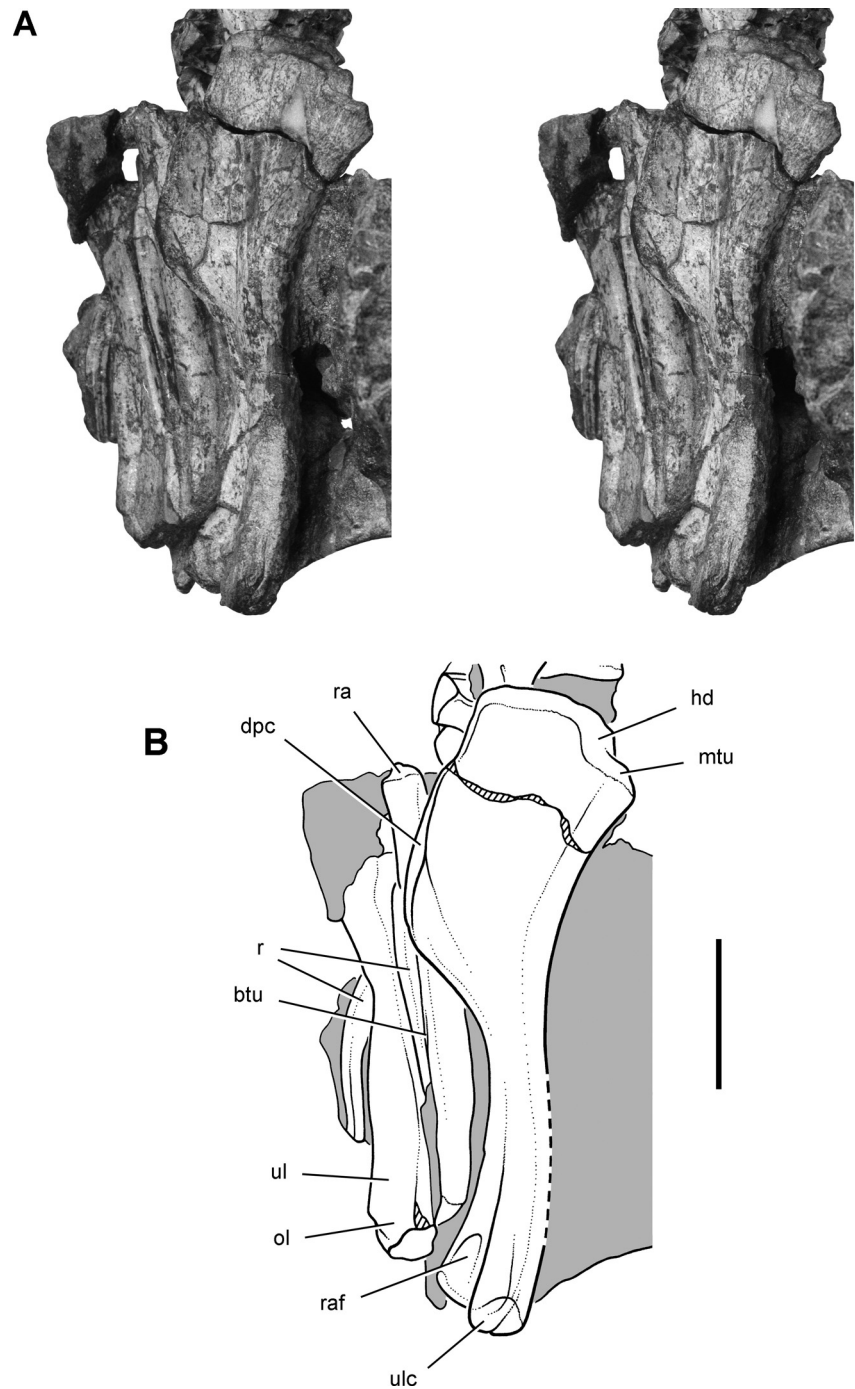


FIGURE 66. Stereopair (A) and drawing (B) of right humerus, radius, and ulna of *Eoraptor lunensis* (PVSJ 512) in medial view. **Abbreviations:** **btu**, biceps tubercle; **dpc**, deltopectoral crest; **hd**, head; **mtu**, medial tuberosity; **ol**, olecranon; **r**, rib; **ra**, radius; **raf**, radial fossa; **ul**, ulna; **ulc**, ulnar condyle. Dashed line indicates a missing margin; hatching indicates a broken surface; shading indicates matrix. Scale bars equal 2 cm.

condyles. The external margin of the crest is thickest in its middle third, tapering to a thin edge before joining the shaft.

The shafts of both humeri have been flattened postmortem. Neither seems to have been strongly bowed, as occurs in some theropods (e.g., *Tawa*, Nesbitt et al., 2009; *Dilophosaurus*, Welles, 1984). Rather, the shaft seems to follow a gentle sinuous curve in lateral view and is straight in anterior view as in *Saturnalia* (Langer et al., 2007).

The distal end of the humerus is divided into a transversely convex radial and ulnar condyles. In anterior view, the radial condyle does not round as far proximally onto the shaft as in *Herrerasaurus* (Sereno, 1994; fig. 4A), but it is situated distal to a radial fossa as in the latter species. The distal end is more generalized than that in *Herrerasaurus* because it lacks the well-developed entepicondyle, ectepicondyle, and associated pits that characterize the latter species. It most closely resembles

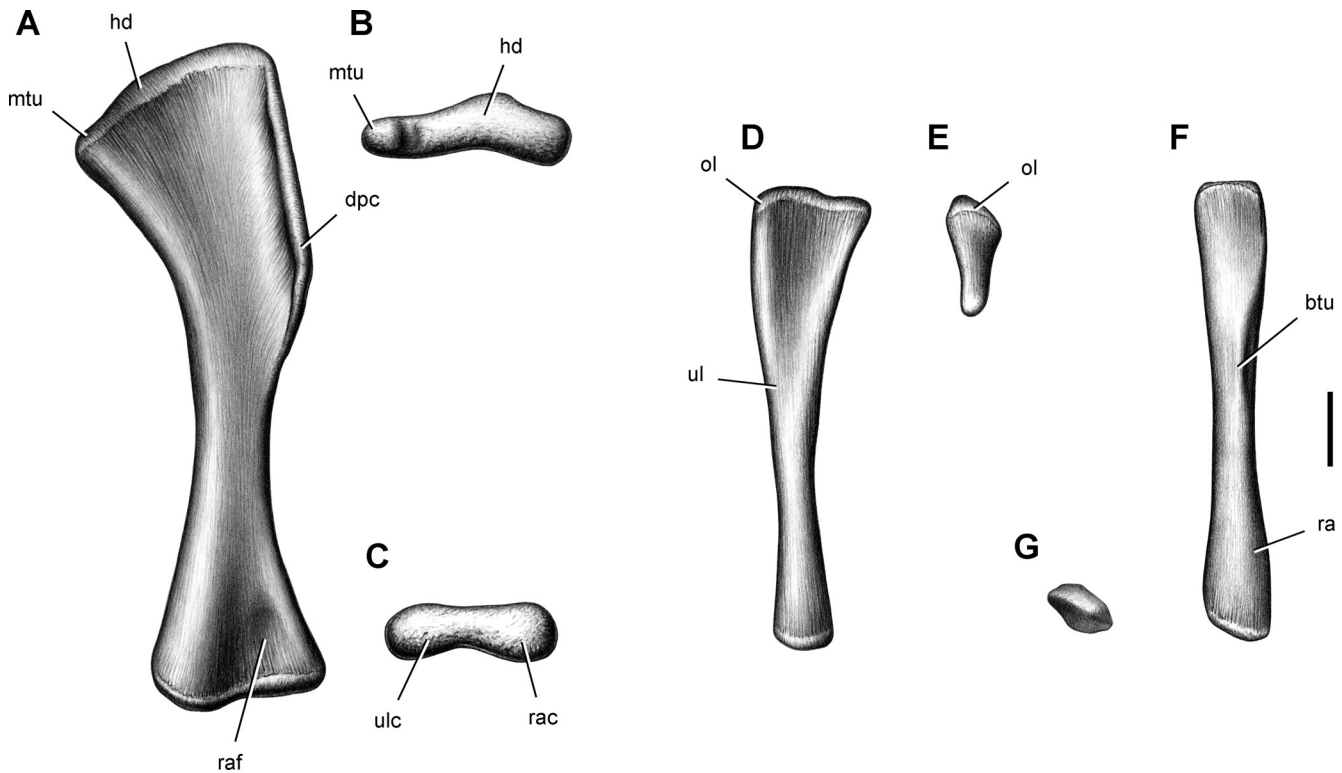


FIGURE 67. Reconstruction of the left humerus, ulna and radius of *Eoraptor lunensis* (PVSJ 512). Humerus in anterior (A), proximal (B), and distal (C) views (anterior toward bottom of page). Ulna in medial (D) and proximal (E) views. Radius in medial (F) and distal (G) views (anterior toward bottom of page). **Abbreviations:** btu, biceps tubercle; dpc, deltopectoral crest; hd, head; mtu, medial tuberosity; ol, olecranon; ra, radius; rac, radial condyle; raf, radial fossa; ul, ulna; ulc, ulnar condyle.

*Saturnalia* in these regards (Langer et al., 2007), although the deltopectoral crest and distal condyles do not expand as far from the shaft. In general, the humerus and other long bones of the forelimb are more robust in *Saturnalia*, which is probably not due to its somewhat larger (ca. 30%) maximum body size.

**Ulna**—The three-dimensional shape of the proximal articular surface of the ulna cannot be reconstructed with confidence due to severe flattening of both ulnae (Figs. 65, 66, 67D, E). In lateral view, the olecranon process is very low and rounded, unlike the proximally prominent process in *Saturnalia* (Langer et al., 2007) and in the theropods *Herrerasaurus* (Sereno, 1994) and *Eodromaeus* (Martínez et al., 2011). In either lateral or medial view, the proximal articular surface is oriented almost at a right angle to the shaft axis (Figs. 65, 67D).

Relative to the length of the ulna, the shaft appears to be proportionately more robust than that in *Saturnalia* or *Herrerasaurus*, although some of the apparent width is due to flattening of the shaft, which has an elliptical cross-section. Flattening of the ulnar shafts has removed most of their natural twist, such that the transverse axes of both proximal and distal ends lie in nearly the same plane. The shaft of the ulna was not in contact with that of the radius, as is clear from the positions of these bones in both forelimbs (Figs. 8, 65, 66). A substantial interosseous space is present. In theropods such as *Herrerasaurus* (Sereno, 1994) and *Eodromaeus* (Martínez et al., 2011), in contrast, the shafts of the ulna and radius are in contact for much of their length.

The distal end of the ulna is slightly expanded transversely and appears to have a simple transversely convex surface for articulation with the carpus, as in *Saturnalia* and *Eodromaeus*. In *Her-*

*rerasaurus*, in contrast, the distinctive distal articular surface of the ulna rounds onto the anterior side of the distal end (Sereno, 1994).

**Radius**—The better-preserved right radius is best exposed in medial view (Figs. 65, 66, 67F, G). Its proximal end appears to be flattened transversely, with an anteroposteriorly convex articular surface. The cylindrical shaft is smooth and lacks the prominent biceps tubercle present in *Herrerasaurus* (Sereno, 1994:figs. 6–8). The slightly smaller, subcylindrical distal end is transversely convex and similar to that in *Saturnalia* (Langer et al., 2007). In *Herrerasaurus*, in contrast, the distal end is squared, with a gently concave distal articular surface.

**Carpus**—The carpus is poorly preserved (Fig. 68). Throughout the skeleton, postmortem weathering and diagenesis more strongly affected cartilage-covered articular surfaces than periosteum on bone shafts, and the carpus is no exception. Although it is clear that several elements are present, their margins are often indistinct. Drawings were made under magnification, using water or acetone to enhance color differences. The left carpus is the better preserved of the two (Fig. 68B). On the right side, only the lateral carpals are preserved and are difficult to distinguish from fragments of the distal end of the right ulna (Fig. 68A).

The left carpus may preserve the radiale and ulnare, two large ossifications distal to the radius and ulna, respectively (Fig. 68B). Both appear to have a tabular shape. The bone tentatively identified as the radiale appears to be tipped, its broader surface facing ventrally. Its ventral margin may be fused via diagenesis to a smaller distal element, which could represent an enlarged distal carpal 1, as occurs in many basal sauropodomorphs, such as *PlatEOSaurus* (Sereno, 2007b). In the right carpus, there are several

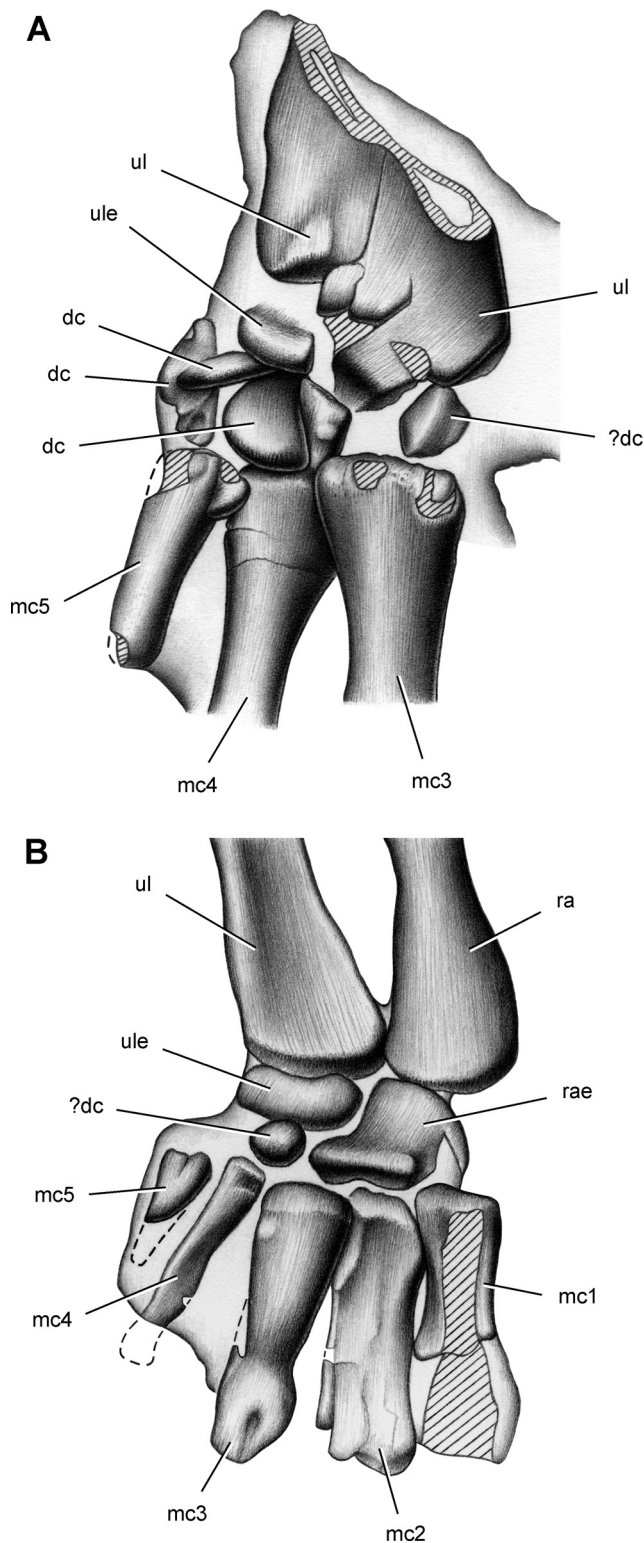


FIGURE 68. Drawings of right and left carpi of *Eoraptor lunensis* (PVSJ 512). **A**, right carpus in dorsal view. **B**, left carpus in ventral view. **Abbreviations:** **dc**, distal carpal; **mc1–5**, metacarpals 1–5; **ra**, radius; **rae**, radiale; **ul**, ulna; **ule**, ulnare. Dashed line indicates a missing margin; hatching indicates a broken surface; light shading indicates matrix. Scale bars equal 1 cm.

TABLE 8. Measurements (in mm) of the right manus of *Eoraptor lunensis* (PVSJ 512).

Bone	Maximum length
Digit I	
Metacarpal 1	14
Phalanx 1	14
Ungual	14
Digit II	
Metacarpal 2	20
Phalanx 1	12
Phalanx 2	12
Ungual	14
Digit III	
Metacarpal 3	21
Phalanx 1	10
Phalanx 2	9
Phalanx 3	8
Ungual	(12)
Digit IV	
Metacarpal 4	16
Digit V	
Metacarpal 5	10

Ungual length is measured perpendicular to a chord across the proximal articular end. Parentheses indicate estimated measurement.

tabular ossifications proximal to metacarpals 4 and 5 (Fig. 68A). The proximal ossification is largest and probably represents the ulnare, whereas the more distal ossifications probably represent distal carpals.

From the available information in the holotype, the carpus in *Eoraptor* is composed of at least six ossifications and possibly more (Fig. 73D). There is some suggestion that distal carpal 1, the most medial distal carpal, is larger than the others. In larger-bodied basal sauropodomorphs such as *Massospondylus*, distal carpal 1 overlaps distal carpal 2 (Sereno, 2007b). The carpus in *Eoraptor* appears to have been well ossified and is composed of more than three elements. Beyond these two observations, there is no special similarity to the well-ossified carpus in *Herrerasaurus* (Sereno, 1994) or *Eodromaeus* (Martínez et al., 2011). Nor is there any similarity to the carpus in the more derived tetanuran theropods, which is characterized by an enlarged semilunate carpal proximal to metacarpals 1 and 2 (Ostrom, 1969; Sullivan et al., 2010).

**Metacarpus**—Because the left metacarpals have been crushed dorsoventrally (Fig. 68B), the following description is based mainly on the right metacarpals, which are completely exposed in dorsal and proximal views and partially exposed in ventral and distal views (Figs. 69–74). Although crushed and less complete, the left metacarpals retain important information on carpal-metacarpal and intermetacarpal articular relations.

*Eoraptor* retains all five manual digits, as in several other basal saurischians and ornithischians (e.g., Sereno, 2007b; Martínez, 2009; Sereno, 2012). In all dinosaurs except sauropods and hadrosauroids (Sereno, 1997), the lateral digits of the manus (digits IV, V) and their respective metacarpals are reduced relative to the three inner digits (digits I–III; Table 8). In *Eoraptor* and *Eodromaeus*, metacarpals 4 and 5 are more strongly developed relative to metacarpals 1–3 than they are in the theropods *Herrerasaurus* (Sereno, 1994:fig. 15) or *Tawa* (Nesbitt et al., 2009). In the first two genera, for example, metacarpal 4 is longer than metacarpal 1, whereas the reverse is true in *Herrerasaurus* and other theropods that retain metacarpal 4. All five metacarpals, as well as the bones of the forearm and the phalanges, have somewhat stouter proportions in *Eoraptor* than in *Eodromaeus* or *Herrerasaurus* (Figs. 9, 67, 73).



FIGURE 69. Stereopair of right manus of *Eoraptor lunensis* (PVSJ 512) in dorsolateral view. Scale bar equals 2 cm.

The proximal ends of the metacarpals have flat intermetacarpal articular surfaces, which indicate that the metacarpal bases were bound together by ligaments that limited their movement (Figs. 69–73). In proximal view, the bases of the metacarpals articulate to form an arch (Fig. 73B), which can be restored to its probable natural curve (Fig. 73C). Overlap of the bases of the metacarpals in an arched configuration in proximal view may be plesiomorphic for Dinosauria. The manus of the basal ornithischian *Lesothosaurus diagnosticus*, for example, also shows an overlapping, arched condition comparable to that in *Eoraptor*. A new reconstruction of the *Lesothosaurus* metacarpus is given here, based on the single known, partially articulated manus for this early ornithischian (Fig. 77; Table 14). Complete preparation and more detailed study of this manus are warranted.

The articulation of the bases of the metacarpals in *Eodromaemus* (Martínez et al., 2011), *Herrerasaurus* (Serenó, 1994:fig. 15), and most neotheropods is distinctive; the bases of the major metacarpals (1–4) are dorsoventrally deep and wedge-shaped in proximal view, with flat intermetacarpal surfaces. A similar condition has arisen in heterodontosaurid ornithischians, which have block-shaped metacarpal bases (Serenó, 2012). The condition in *Eoraptor* is more generalized, showing some overlap of metacarpals along an arch but not the more compact configuration seen in neotheropods and heterodontosaurids.

Metacarpal 1 is particularly stout (Fig. 76). It is shorter and slightly broader than metacarpals 2 and 3, as in *Herrerasaurus* (Serenó, 1994:fig. 11) and *Eodromaemus* (Martínez et al., 2011). In proximal view, the triangular articular surface is broader than deep and is transversely convex (Fig. 73B, C). The base of metacarpal 1, as preserved in the left manus (Fig. 68B), is clearly inset proximally into the carpus relative to the base of metacarpal 2, as characterizes many larger-bodied basal sauropodomorphs (Serenó, 2007b). The proximal one-third of the shaft articulates

against metacarpal 2, as preserved in the left metacarpus. The remainder of the shaft is dorsoventrally flattened. In dorsal view, a shallow dorsal extensor depression that is present to accommodate the intercondylar process of the proximal phalanx is present proximal to the lateral distal condyle (Figs. 70, 71, 73A, D, 74, 76). The distal condyles are strongly asymmetrical; the deeper and broader lateral distal condyle extends farther distally. In dorsal view, a transverse axis through the distal condyles is offset approximately 20–25° from the perpendicular to the long axis of the bone (Figs. 70, 73A, D, 76). The offset of 30° in *Herrerasaurus* is similar (Serenó, 1994:fig. 14A). The distal condyles are also rotated approximately 20° relative to the base, such that the lateral collateral ligament pit is more broadly exposed in dorsal view (Figs. 70, 73A, D, 74). In *Herrerasaurus*, this rotation is somewhat greater (approximately 30°).

The proximal articular surface of metacarpal 2 is deeper than broad, the opposite of the proportions of metacarpal 1 (Figs. 69, 71, 73B, 74). Much of the proximal articular surface of the right metacarpal 2 is broken away. The remainder of metacarpal 2 is very similar to that in *Herrerasaurus*, except that the shaft is straight rather than bowed ventrally. Medial and lateral sides of the proximal end of the shaft are flattened for articulation against metacarpals 1 and 3, respectively, the former contact occurring in a vertical plane and the latter contact with metacarpal 2 overlapping metacarpal 3 (Figs. 72, 73) as in *Herrerasaurus* (Serenó, 1994). At midlength the shaft is dorsoventrally compressed before it expands toward the distal condyles. Dorsally, there is a shallow dorsal extensor depression for the dorsal intercondylar process of the proximal phalanx (Figs. 70, 71, 73A, D, 74). This articular depression is shifted slightly toward the lateral side of the distal end of the metacarpal as in *Herrerasaurus* (Serenó, 1994), suggesting that hyperextension of the phalanges would have deflected digit II toward digit III. The partially exposed distal condyles of metacarpal 2 are deeper than in *Herrerasaurus*. In dorsal view, the lateral

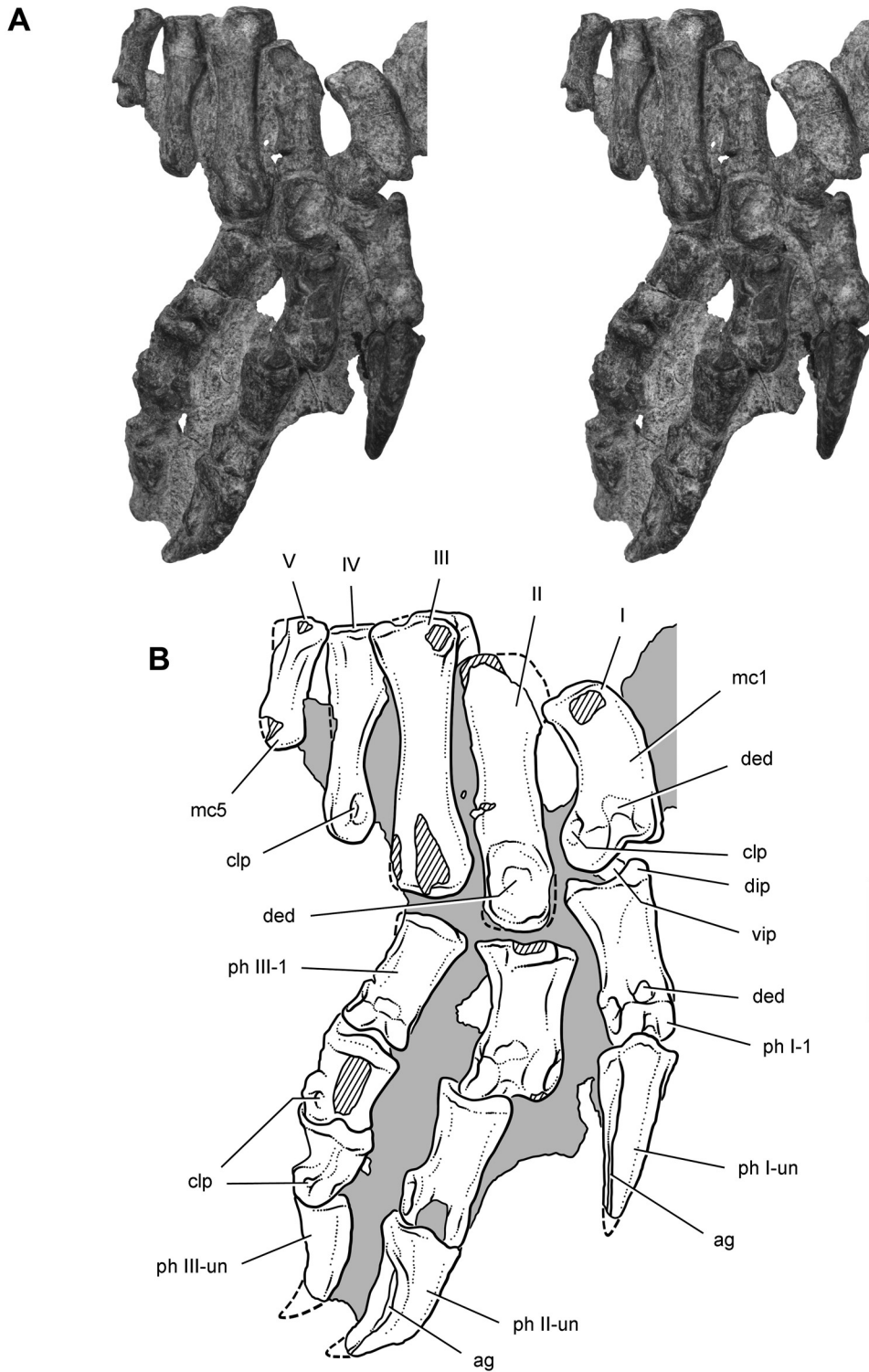


FIGURE 70. Stereopair (A) and drawing (B) of right manus of *Eoraptor lunensis* (PVSJ 512) in dorsal view. **Abbreviations:** I–V, manual digits I–V; ag, attachment groove for unguis; clp, collateral ligament pit; ded, dorsal extensor depression; dip, dorsal intercondylar process; mc1, 5, metacarpal 1, 5; ph, phalanx; un, unguis; vip, ventral intercondylar process. Dashed line indicates a missing margin; hatching indicates a broken surface; shading indicates matrix. Scale bar equals 2 cm in A and 1 cm in B.

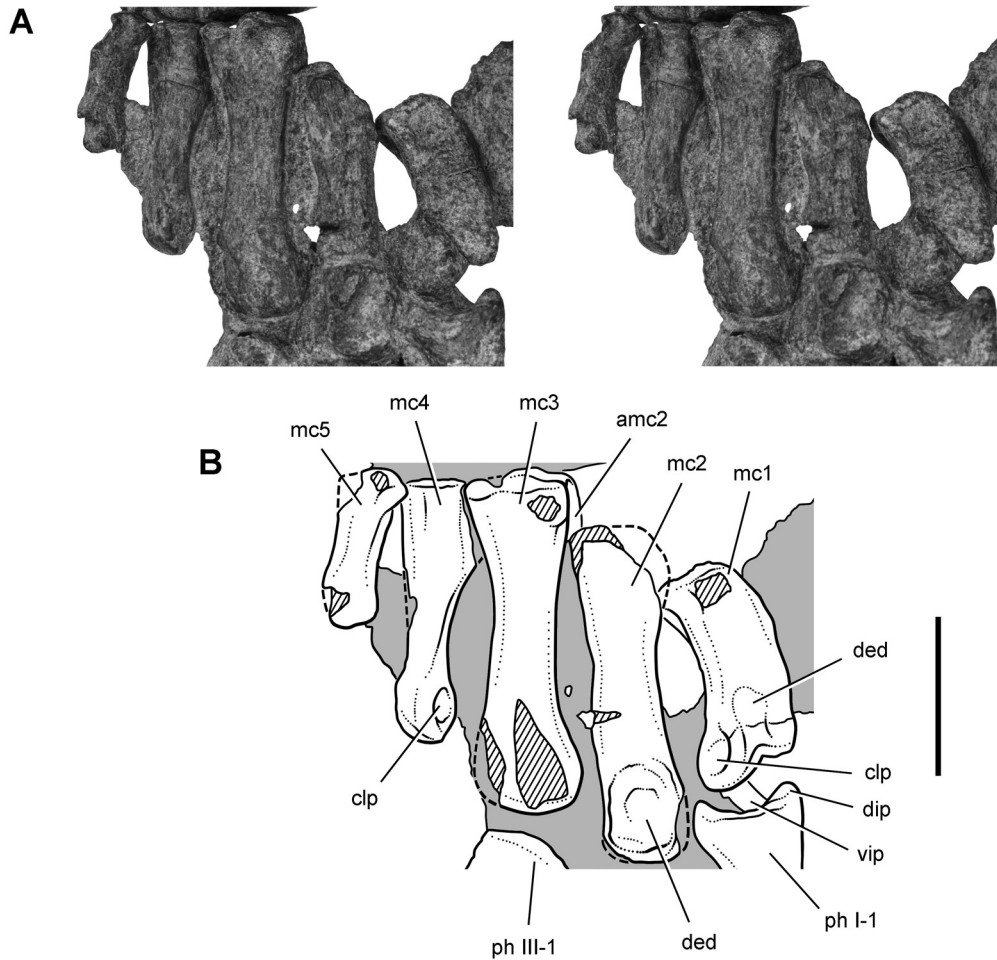


FIGURE 71. Stereopair (A) and drawing (B) of the right metacarpals of *Eoraptor lunensis* (PVSJ 512) in dorsal view. **Abbreviations:** I, III, manual digit I, III; **amc2**, articular surface for metacarpal 2; **clp**, collateral ligament pit; **ded**, dorsal extensor depression; **dip**, dorsal intercondylar process; **mc1–5**, metacarpals 1–5; **ph**, phalanx; **vip**, ventral intercondylar process. Dashed line indicates a missing margin; hatching indicates a broken surface; shading indicates matrix. Scale bars equal 1 cm.

distal condyle was probably larger than the medial, judging from the shape of the opposing articular surface on the proximal phalanx. In ventral view, only the medial distal condyle projects from the matrix, which suggests that the distal condyles are rotated about the long axis of the metacarpal as in metacarpal 1 (Figs. 72, 74). A similar size differential and rotation is present at the distal end of metacarpal 2 in *Herrerasaurus* (Sereno, 1994:fig. 14B).

Metacarpal 3 is slightly longer than metacarpal 2. Its proximal end is gently convex rather than concave as in *Herrerasaurus* (PVSJ 373; Sereno, 1994). The shape of the proximal articular surface also appears to be opposite that of *Herrerasaurus*—broader than deep (Fig. 73B, C). The proximal end, however, has been affected by crushing on the ventral side of the metacarpal base. After restoration, the subquadrate shape of the articular surface remains transversely broader than deep, the opposite of the condition in *Herrerasaurus* (Sereno, 1994). In *Eoraptor*, metacarpal 3 has a more slender midshaft than metacarpal 2, whereas in *Herrerasaurus* they are subequal. In dorsal view of the distal end, the surface is damaged (Fig. 71). A dorsal extensor depression, if present, would have been small and shallow (Fig. 73A, D). In ventral view, the distal condyles are not fully exposed (Fig. 72).

The ventral margin of the medial condyle, however, projects from the matrix, with no exposure of the lateral condyle. This suggests that the distal condyles are rotated in the same direction as in metacarpals 1 and 2, as in *Herrerasaurus*.

Metacarpal 4 is shorter than metacarpals 2 and 3 but longer than metacarpal 1 (Figs. 69–73). In proximal view, the subtriangular articular surface is broader than deep (Fig. 73B, C). Even with some depth added as a correction for crushing, the proximal articular end is not quite as deep as that in *Herrerasaurus*. A single, undivided distal articular condyle is present as in *Herrerasaurus*. In *Eodromaeus*, in contrast, metacarpal 4 has divided distal condyles (Martínez et al., 2011).

In dorsal view of the proximal end, a large triangular facet on the medial side articulates against the posterior aspect of metacarpal 3 (Figs. 71, 72). The shaft has a subtriangular cross-section, with a flattened medial surface facing metacarpal 3 and a rounded lateral edge. There is some torsion in the shaft opposite to that in metacarpals 1–3 and opposite to that in metacarpals 1–4 in *Herrerasaurus*. The distal end, which is broader dorsoventrally than wide transversely, is rotated both by torsion in the shaft of the bone and by its position on the metacarpal arch, such that

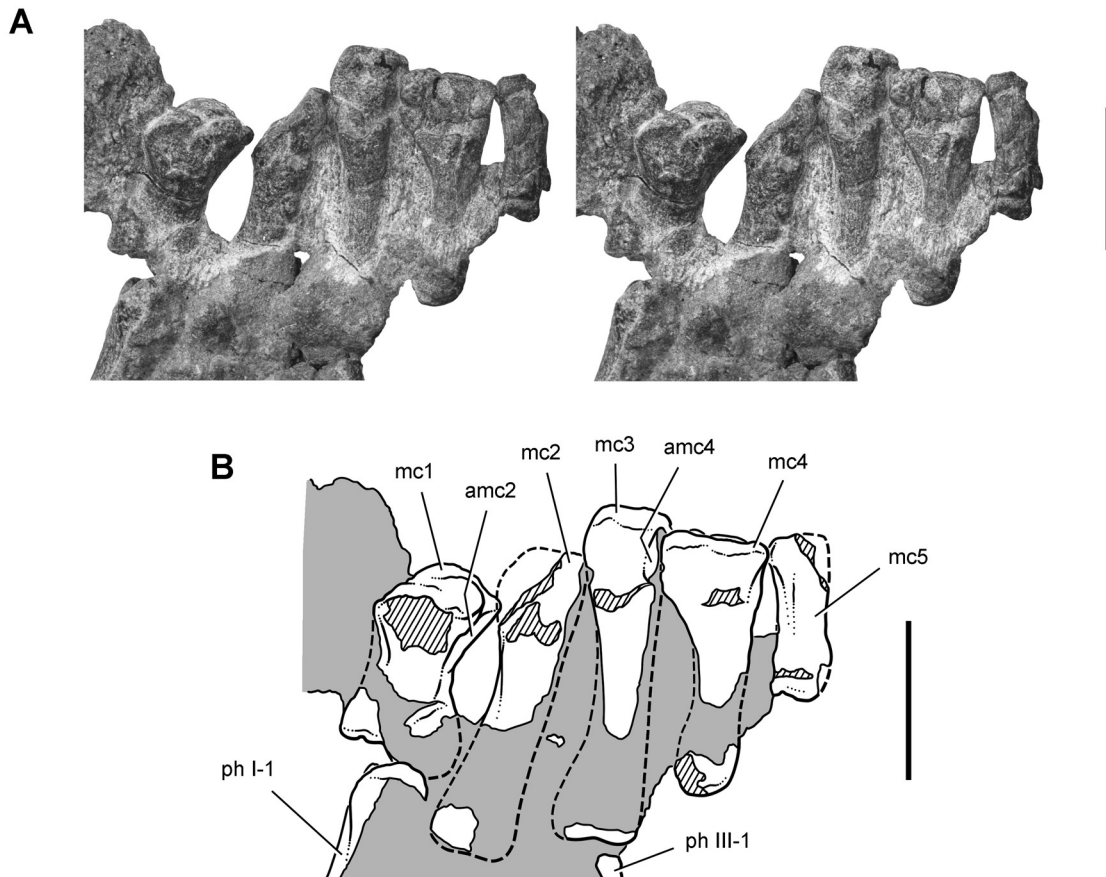


FIGURE 72. Stereopair (A) and drawing (B) of the right metacarpals of *Eoraptor lunensis* (PVSJ 512) in ventral view. **Abbreviations:** I, III, manual digit I, III; amc2, 4, articular surface for metacarpal 2, 4; mc1–5, metacarpals 1–5; ph, phalanx. Dashed line indicates a missing margin; hatching indicates a broken surface; shading indicates matrix. Scale bars equal 1 cm.

the large medial collateral ligament pit is visible in dorsal view of the manus (Fig. 73D). There is no development of an opposing lateral collateral ligament pit. The distal articular surface is subtriangular and has divided distal condyles. A small proximal phalanx may have been present as in *Herrerasaurus* (Sereno, 1994) and *Eodromaeus* (Martínez et al., 2011), although none is preserved (Fig. 73A).

Metacarpal 5 is the shortest metacarpal, with a length approximately two-thirds that of metacarpals 1 and 4 (Table 8). Metacarpal 5 is longer and broader than in *Herrerasaurus* (Figs. 69–74). The proximal articular surface is missing its lateral edge but appears to be deeper than it is broad (Fig. 73B, C). The rod-shaped shaft has a concave medial edge and tapers toward a rounded distal end, which lacks collateral ligament pits. The rudimentary form of the distal end could indicate the absence of phalanges in manual digit V (Fig. 73A, D, 74).

**Manual Phalanges**—The phalangeal formula, based on the well-preserved right manus of the holotype, is 2\*-3\*-4\*-(1)-0, in which parentheses indicate estimation; a zero indicates that the respective metacarpal is present but lacks phalanges; and an asterisk indicates that the digit has a terminal ungual (Figs. 73A, D, 74; Table 8). Although no phalanges are present in manual digit IV, the well-formed medial collateral ligament pit and distal articular surface on metacarpal 4 sug-

gest that at least a single rudimentary phalanx was probably present.

Except for the unguals, phalangeal length decreases distally within manual digits I–III (Figs. 73A, D, 74; Table 8). This is the primitive dinosaurian condition common in larger-bodied basal sauropodomorphs such as *Plateosaurus*. In theropods, in contrast, the penultimate phalanges are longer than the preceding phalanx, as seen in *Herrerasaurus* (Sereno, 1994) and *Eodromaeus* (Martínez et al., 2011). The manual unguals are also less trenchant than those in the basal theropods *Herrerasaurus* (Sereno, 1994) and *Eodromaeus* (Martínez et al., 2011), or those in heterodontosaurid ornithischians (Sereno, 2012).

The proximal manual phalanges of manual digits I–III have shorter, more robust proportions than in *Herrerasaurus* and *Eodromaeus* and, in general, are shorter relative to the metacarpus (Figs. 73D, 74). The relative length of phalanx 1 within digit I, however, is more variable in basal saurischians from Ischigualasto. In *Eoraptor*, phalanx 1 of digit I is equal to that of metacarpal 1; in *Eodromaeus* it is shorter (Martínez et al., 2011), and in *Herrerasaurus* it is longer than metacarpal 1 (Sereno, 1994).

The proximal articular surface of phalanx 1 of digit I is subtriangular, with prominent dorsal and ventral intercondylar processes and an expanded socket laterally to accommodate the large lateral distal condyle of metacarpal 1 (Fig. 75C). The shape of the

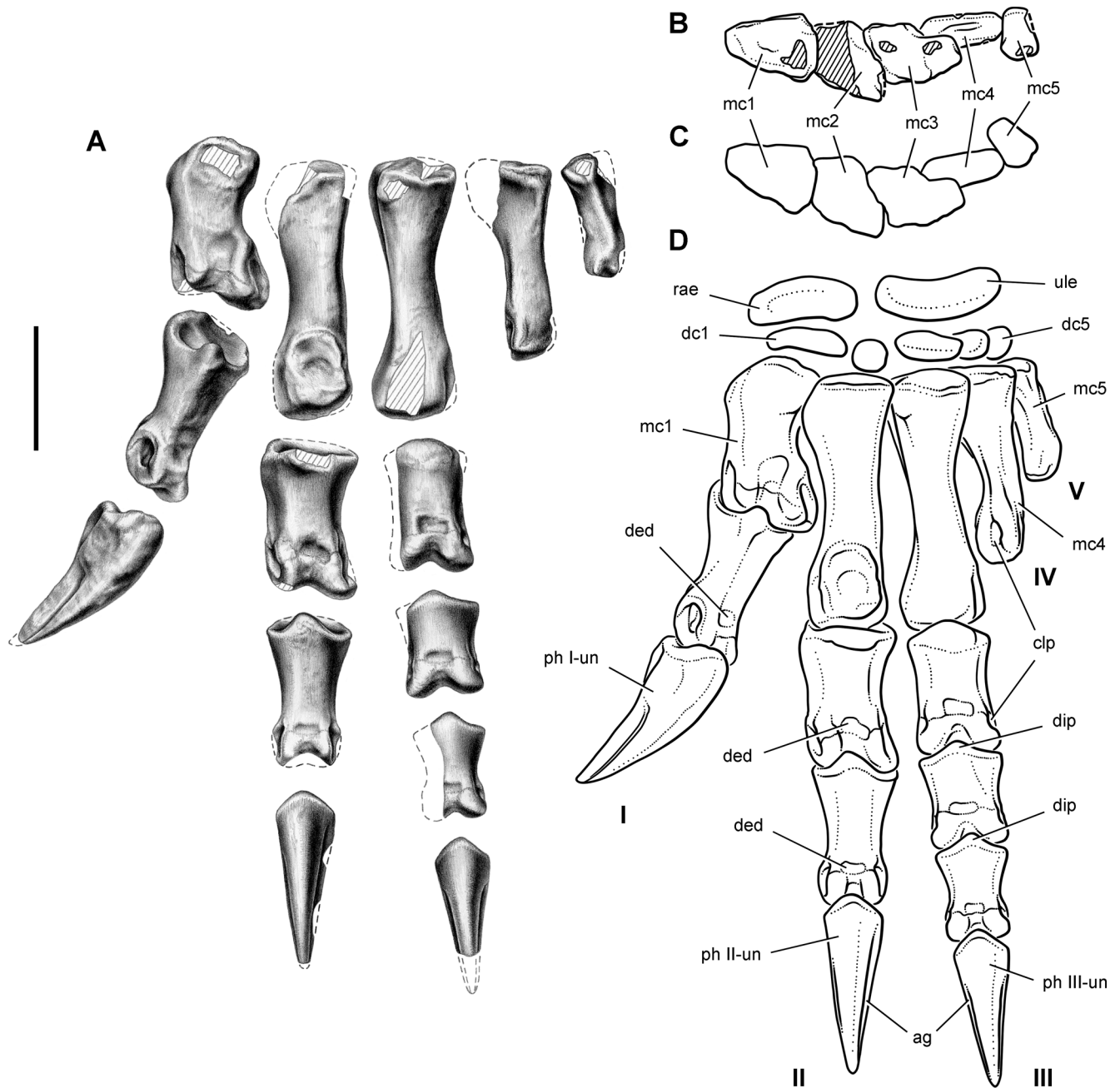


FIGURE 73. Left manus of *Eoraptor lunensis* (PVSJ 512). **A**, left manus (reversed from right) in exploded dorsal view with phalanges of digit I rotated so their sagittal plane is vertical. **B**, left metacarpus (reversed from right) in proximal view (dorsal toward bottom of page). **C**, reconstruction of articulated left metacarpus in proximal view showing metacarpal arch. **D**, reconstruction of articulated left carpus and manus in dorsal view showing articulated orientation of digit I. **Abbreviations:** I–V, manual digits I–V; **ag**, attachment groove for ungual sheath; **clp**, collateral ligament pit; **dc1**, 5, distal carpal 1, 5; **ded**, dorsal extensor depression; **dip**, dorsal intercondylar process; **mc1–5**, metacarpal 1–5; **ph**, phalanx; **rae**, radiale; **ule**, ulnare; **un**, ungual. Dashed line indicates a missing margin; hatching indicates a broken surface. Scale bar equals 1 cm in **A** and **B**.

proximal end is similar to that in *Herrerasaurus*, but the intercondylar processes are more prominent and pointed. With the intercondylar processes held along a vertical axis, the distal condyles are rotated approximately  $35^\circ$  (Fig. 75B), such that the lateral distal condyle is positioned dorsal to the medial condyle in neutral pose. In *Eodromaeus*, in contrast, there is negligible rotation of the distal condyles (Martínez et al., 2011:fig. 1G). In *Her-*

*rerasaurus*, there is approximately  $15^\circ$  of rotation in the same direction as in *Eoraptor* (Sereno, 1994:fig. 14A). In larger-bodied basal sauropodomorphs such as *Massospondylus*,  $45\text{--}60^\circ$  of rotation are present within phalanx 1 of digit I (Sereno, 2007b:fig. 9D–F). The condition in *Eoraptor* bears a striking resemblance to that in basal sauropodomorphs. Maximum extension of manual digit I in *Eoraptor* positions the ungual vertically (Fig. 76C, top),

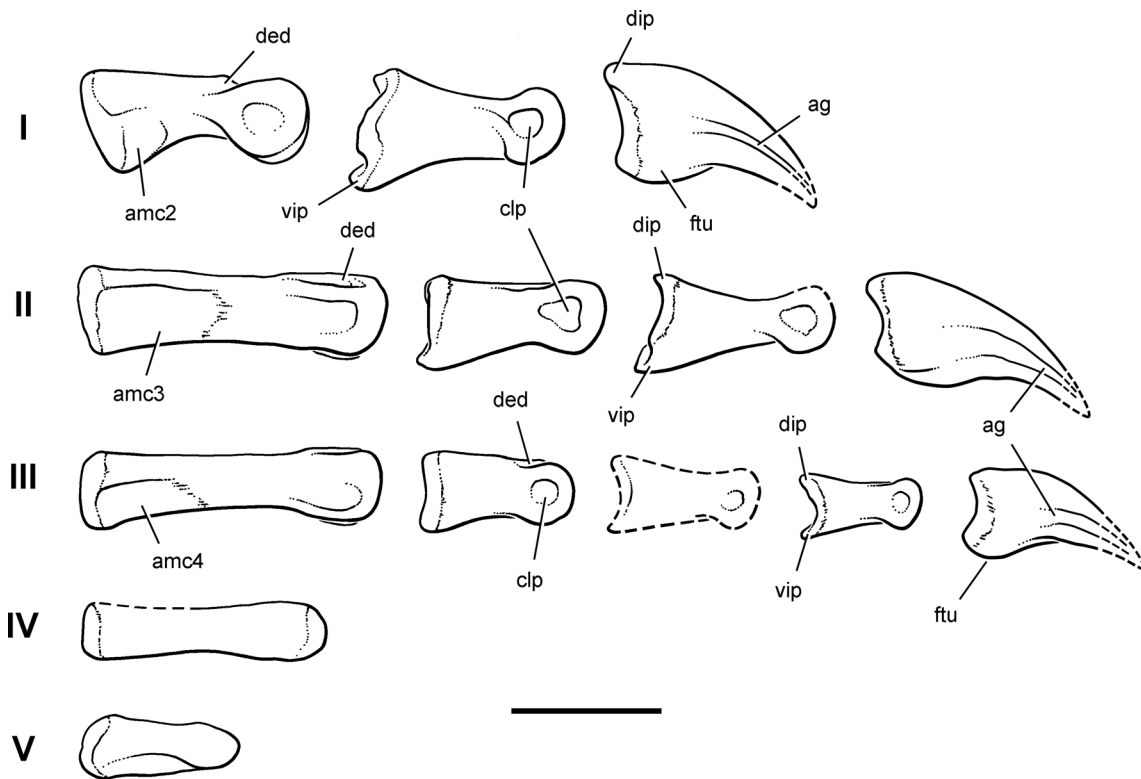


FIGURE 74. Right manus of *Eoraptor lunensis* (PVSJ 512) in exploded lateral view. **Abbreviations:** I–V, manual digits I–V; ag, attachment groove for ungual sheath; amc2–4, articular surface for metacarpals 2–4; clp, lateral collateral ligament pit; ded, dorsal extensor depression; dip, dorsal intercondylar process; ftu, flexor tubercle; vip, ventral intercondylar process. Dashed line indicates a missing margin. Scale bar equals 1 cm.

with the plane through the ungual canted at approximately 45°, as seen in dorsal view (Fig. 76B). Maximum flexion of manual digit I in *Eoraptor* positions the ungual past the vertical and at an angle of 90° to the axis of the penultimate phalanx (Fig. 76C, bottom). Throughout this rotary arc, the ungual of manual digit I in *Eoraptor* is canted so that its medial side is exposed in dorsal view (Fig. 76).

The direction of rotation of the distal condyles relative to the phalangeal base is opposite to the direction of rotation in metacarpal 1, as is also the case in *Herrerasaurus* (Sereno, 1994:fig. 14A). The greater degree of rotation in *Eoraptor*, however, directs the ungual medially, exposing the medial aspect of the ungual in dorsal view (Figs. 73A, D, 76A), which is not the case in *Herrerasaurus* (Sereno, 1994:fig. 15, left), *Eodromaeus* (Martínez et al., 2011:fig. 1G), or *Lesothosaurus* (Fig. 77C). The distal ginglymus in *Eoraptor* is transversely narrow, deeply cleft, and rounded dorsally (Figs. 75B, 76A). The medial collateral ligament pit is shallower than the lateral pit, and the dorsal extensor depression is well developed. In dorsal view, the lateral distal condyle extends farther distally than the medial distal condyle, deflecting the ungual medially (Fig. 76A).

Phalanx 1 of digit II (Figs. 69, 70, 73A, 74) is shorter than the proximal phalanx of digit I but longer than that of digit III, as in *Herrerasaurus* (Sereno, 1994:table 4). In *Eodromaeus*, in contrast, phalanx 1 of digit II is slightly longer than the proximal phalanx of digit I (Martínez et al., 2011). The subtriangular proximal articular surface is asymmetrical; the medial edge is nearly vertical, whereas the lateral edge has an expanded socket laterally for the lateral distal condyle of metacarpal 2,

as in *Herrerasaurus* and *Eodromaeus*. A prominent dorsal intercondylar process is present and associated with a dorsal extensor depression; the ventral intercondylar process is not exposed. The medial collateral ligament pit is shallower than the lateral, and the distal ginglymus is deeply cleft, as in *Herrerasaurus* and *Eodromaeus*.

Phalanx 1 of digit III is the shortest of the proximal phalanges (Figs. 69, 70, 73A, 74). The proximal articular surface, which is partially exposed, appears to be the most symmetrical and has a transversely broad ventral intercondylar process, as in *Herrerasaurus* and *Eodromaeus*. Distally, the lateral collateral ligament pit is deeper than the medial pit, and the lateral distal condyle extends farther distally than the medial distal condyle, as in *Herrerasaurus* and *Eodromaeus*.

The intermediate manual phalanges include phalanx 2 of digit II and phalanges 2 and 3 of digit III (Figs. 69, 70, 73A, 74). The proximal end of phalanx 2 of digit II is proportionately deep, with pointed dorsal and ventral intercondylar processes and an asymmetrical subtriangular articular surface that accommodates the larger lateral distal condyle of the proximal phalanx. There is little torsion in the shaft, and thus the phalanx is very similar to intermediate phalanges in *Herrerasaurus* and *Eodromaeus*. The distal condyles are prominent dorsally, but their dorsal edges and the dorsal extensor depression are damaged. The intermediate phalanges in digit III are badly crushed and preserve few details. Each has a dorsal intercondylar process, collateral ligament pits, and a distal ginglymus (Fig. 70).

The manual unguals are relatively broader transversely and less recurved than in the theropods *Herrerasaurus* (Sereno, 1994) and

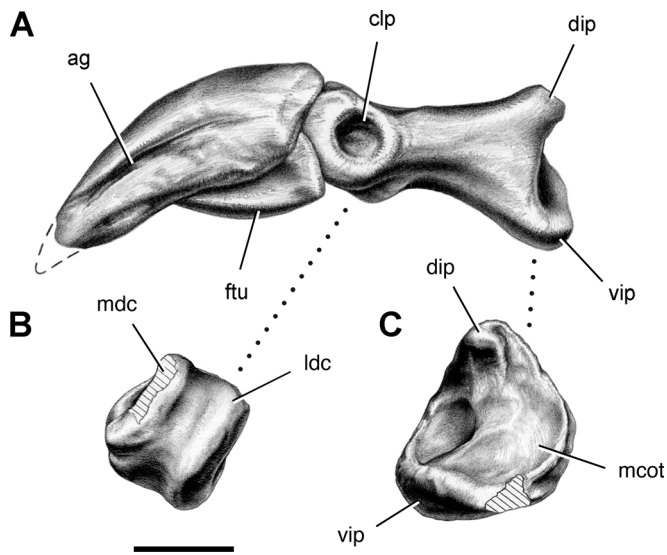


FIGURE 75. Drawings of phalanges of manual digit I in *Eoraptor lunensis* (PVSJ 512). **A**, proximal phalanx and unguis of right manual digit I in medial view. **B**, proximal phalanx of right manual digit I in distal view. **C**, proximal phalanx of right manual digit I in proximal view. **Abbreviations:** **ag**, attachment groove for unguis sheath; **clp**, collateral ligament pit; **dip**, dorsal intercondylar process; **ftu**, flexor tubercle; **ldc**, lateral distal condyle; **mdc**, medial cotylus; **mdc**, medial distal condyle; **vip**, ventral intercondylar process. Dashed line indicates a missing margin; hatching indicates a broken surface; dotted line indicates location in A of other views. Scale bar equals 5 mm.

*Eodromaeus* (Martínez et al., 2011). In *Eoraptor*, the distal tip of the unguis does not extend far below the base, when the base is held vertically (Fig. 74). In nearly all theropods including *Herrerasaurus* (Sereno, 1994) and *Eodromaeus* (Martínez et al., 2011), the distal tip of the unguis is located considerably ventral to the proximal articular surface, when that surface is oriented vertically. For each of the best-preserved unguis (digits I and II), maximum depth is only 150% of maximum width. In *Herrerasaurus* (Sereno, 1994:figs. 14, 15), *Allosaurus* (Madsen, 1976:pl. 44), and nearly all theropods, the manual unguis have a maximum depth ranging from 200–300% of maximum width.

The unguis of digits I and II are subequal in length and nearly identical in form (Figs. 69, 70, 73A, D, 74). The main difference between these two unguis lies in the depth of the proximal end, that of digit I being slightly greater than that of digit II (Fig. 74). The unguis of digit III resembles the other unguis but is smaller in all dimensions, measuring about 75–85% of their length. The tips of all three unguis are broken away.

### Pelvic Girdle

The pelvic girdle is partially obscured in right and left lateral views by the articulated hind limbs (Figs. 78, 79, 83; Table 9). The only missing portions include the distal end of the left ilium, which was eroded at the surface, and the distal end of the right pubis, which was fractured and abraded prior to final burial of the skeleton. The pelvic girdle has been transversely compressed, such that the pubic blades overlap one another in the midline, and sheared anteroposteriorly, such that the left side is shifted about 1 cm anterior to the right side (Fig. 78).

The sutures are not closed between the sacral ribs and ilia or between the three bones on each side of the pelvic girdle. The distal ends of the ischia, however, appear to be coossified, although this

TABLE 9. Measurements (in mm) of the pelvic girdle of *Eoraptor lunensis* (PVSJ 512).

Dimension	Measurement
<b>Ilium</b>	
Blade length (pre- to postacetabular process)	82
Blade maximum depth (from supraacetabular lip)	34
Pubic peduncle length	24
Pubic peduncle, maximum transverse width, distal end	12
Pubic peduncle, maximum dorsoventral depth, distal end	16
Acetabulum, anteroposterior diameter	30L
Brevis shelf, transverse width of distal end, outside	12
Brevis shelf, transverse width of distal end, inside	9
<b>Ischium</b>	
Length (pubic peduncle to foot)	114
Midshaft, dorsoventral shaft diameter	7
Midshaft, transverse shaft diameter	5
Distal end, maximum anteroposterior width	16
Distal end, maximum transverse width	6
<b>Pubis</b>	
Maximum length (from iliac peduncle)	121
Iliac peduncle, transverse width of distal end	8
Blade length	95
Blade, proximal transverse width	27
Blade, midlength transverse width	21
Blade, distal transverse width	17
Maximum diameter of pubic fenestra	10

Measurements are from the right side except as indicated otherwise (L, left).

also may be the result of plastic deformation or diagenesis during fossilization (Fig. 81).

**Ilium**—Relative to the vertebral column, the ilium is as long as in *Herrerasaurus* (Novas, 1994:fig. 3A), spanning approximately four and one-half centra from anterior to posterior extremities (Fig. 79). The iliac blade is more than twice the maximum depth above the acetabulum (Fig. 82A) and closely resembles the proportions in *Panphagia* (Martínez and Alcober, 2009) and *Saturnalia* (Langer, 2003). Among herrerasaurids, the ilium is closer in form to *Chindesaurus* (Long and Murry, 1995:fig. 181) than *Herrerasaurus* (Novas, 1994:fig. 5) or *Staurikosaurus* (Colbert, 1970:fig. 8A), given the planar form and subtriangular shape of the preacetabular process. The low profile and short preacetabular process differ from the deeper preacetabular process in the theropod *Eodromaeus* (Martínez et al., 2011). The thin blade, which is only 1 mm thick, is concave laterally as seen in dorsal view (Fig. 54). In lateral view, its dorsal margin is also arched (Fig. 82A).

A raised attachment scar is present on the lateral aspect of the preacetabular process opposite the attachment of the first sacral rib (Figs. 78, 79, 82A), which is similar to that in *Plateosaurus* (Huene, 1926b), *Staurikosaurus*, and *Chindesaurus*. The ventral margin of the preacetabular process is not continuous with the anterior margin of the pubic peduncle of the ilium. As in *Panphagia*, *Saturnalia*, and *Herrerasaurus*, rather, it joins the peduncle on its lateral side, creating a narrow medial fossa (Fig. 82A). A similar configuration is present in *Staurikosaurus*, *Chindesaurus*, and in tetanuran theropods such as *Allosaurus*, *Tyrannosaurus*, and *Deinonychus*.

The postacetabular process is longer than the preacetabular process in lateral view of the ilium (Fig. 82A). It tapers distally to a squared end, the posterodorsal corner of which is rounded. As in the sauropodomorphs *Panphagia* and *Saturnalia*, an arched brevis fossa is present in *Eoraptor*, unlike the herrerasaurids *Herrerasaurus*, *Staurikosaurus*, and *Chindesaurus*. Partially exposed

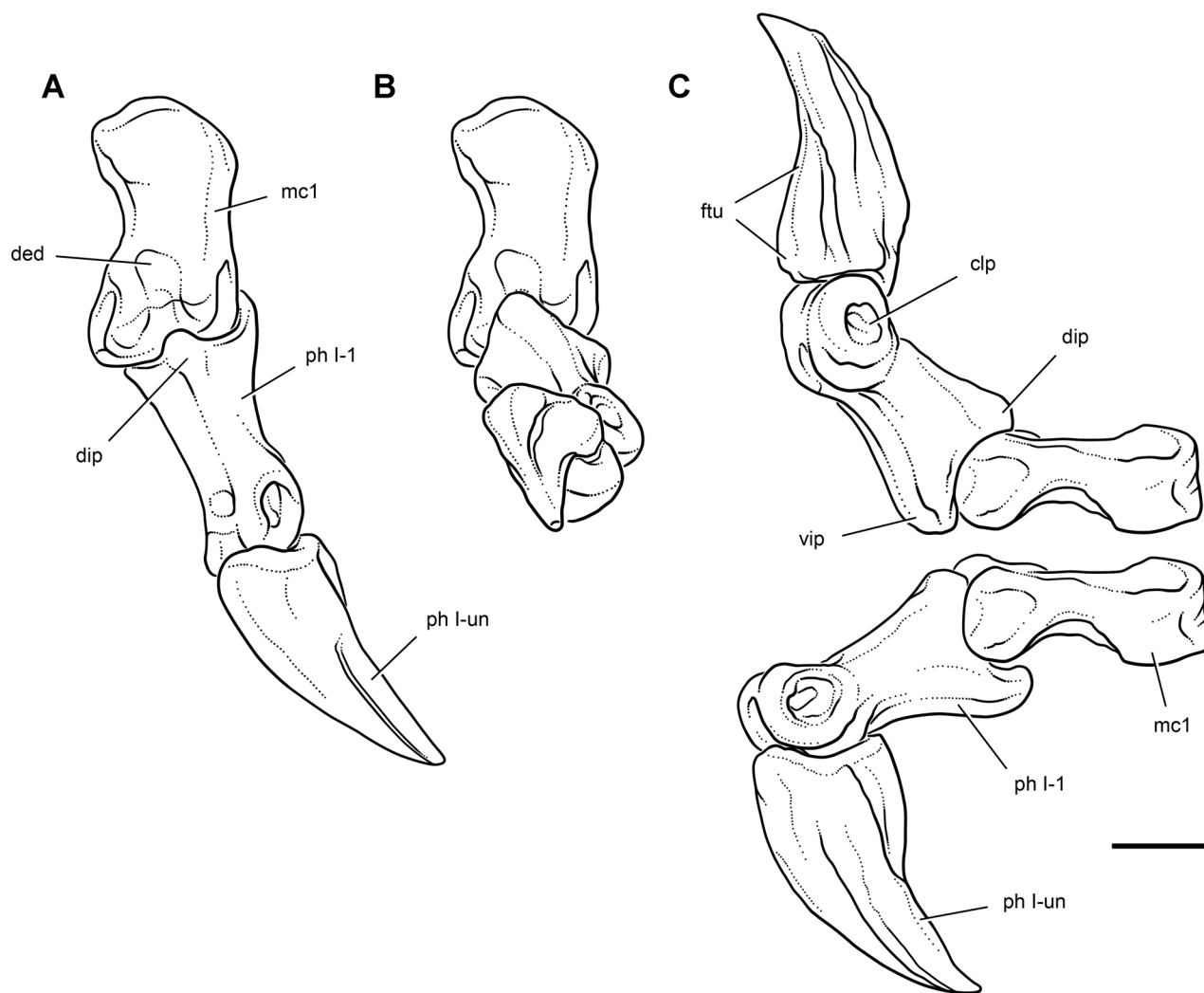


FIGURE 76. Drawings of right manual digit I of *Eoraptor lunensis* (PVSJ 512) in various poses based on manipulations of cast bones. **A**, neutral pose in dorsal view. **B**, fully extended pose in dorsal view. **C**, fully extended (above) and fully flexed (below) poses in medial view. **Abbreviations:** I, manual digit I; **clp**, collateral ligament pit; **ded**, dorsal extensor depression; **dip**, dorsal intercondylar process; **ftu**, flexor tubercle; **mc1**, metacarpal 1; **ph**, phalanx; **un**, ungual; **vip**, ventral intercondylar process. Ungual tip reconstructed. Scale bar equals 5 mm.

on the right side, the arched brevis fossa has lateral and medial walls of equal depth (Fig. 82D). In ventral view, the width of the fossa is constant, and the third sacral rib attaches along the ventral margin of the medial wall. In coelophysoids, in contrast, the width of the fossa expands distally, and the sacral rib attachments rise across the postacetabular process to its posterodorsal corner.

The supraacetabular crest is strongly developed but does not overhang most of the acetabular space as in *Panphagia* (Martínez and Alcober, 2009:fig. 8A). It has a sigmoidal external margin that is continuous anteroventrally with the posterior margin of the pubic peduncle (Fig. 82A).

The stout pubic peduncle angles about 20° below the horizontal (Figs. 78, 79, 82A). It has a subquadrate shape in lateral view and a subtriangular cross-section and distal articular surface (Fig. 82B). The medial side of the peduncle is slightly convex dorsoventrally, whereas the lateral, acetabular, and distal surfaces are gently concave. In distal view of the peduncle, the dorsoven-

tral height (16 mm) is greater than the width of the acetabular surface (12 mm). The ischial peduncle is exposed only on the left side, where it has slid anteriorly on its contact with the ischium (Fig. 79). In lateral view, the posterior margin of the ischial peduncle is concave, which separates the peduncle more distinctly from the postacetabular process than in herrerasaurids (Fig. 82A). The ventral-most portion of the posterior margin is not exposed. A broad antitrochanteric surface is exposed within the acetabulum (Fig. 82A).

**Ischium**—Nearly all of the ischium is exposed in either right or left lateral view, from which a composite reconstruction was made (Figs. 78–82). In lateral view, the broad, plate-shaped proximal end has a shallow acetabular embayment closer to that in *Panphagia* (Martínez and Alcober, 2009) than the deeper embayment partially preserved in *Saturnalia* (Langer, 2003). The posterior margin of the iliac peduncle is convex, and a lateral crest passes from the peduncle down the shaft. The acetabular margin of the ischium is best exposed on the right side; only the posterior

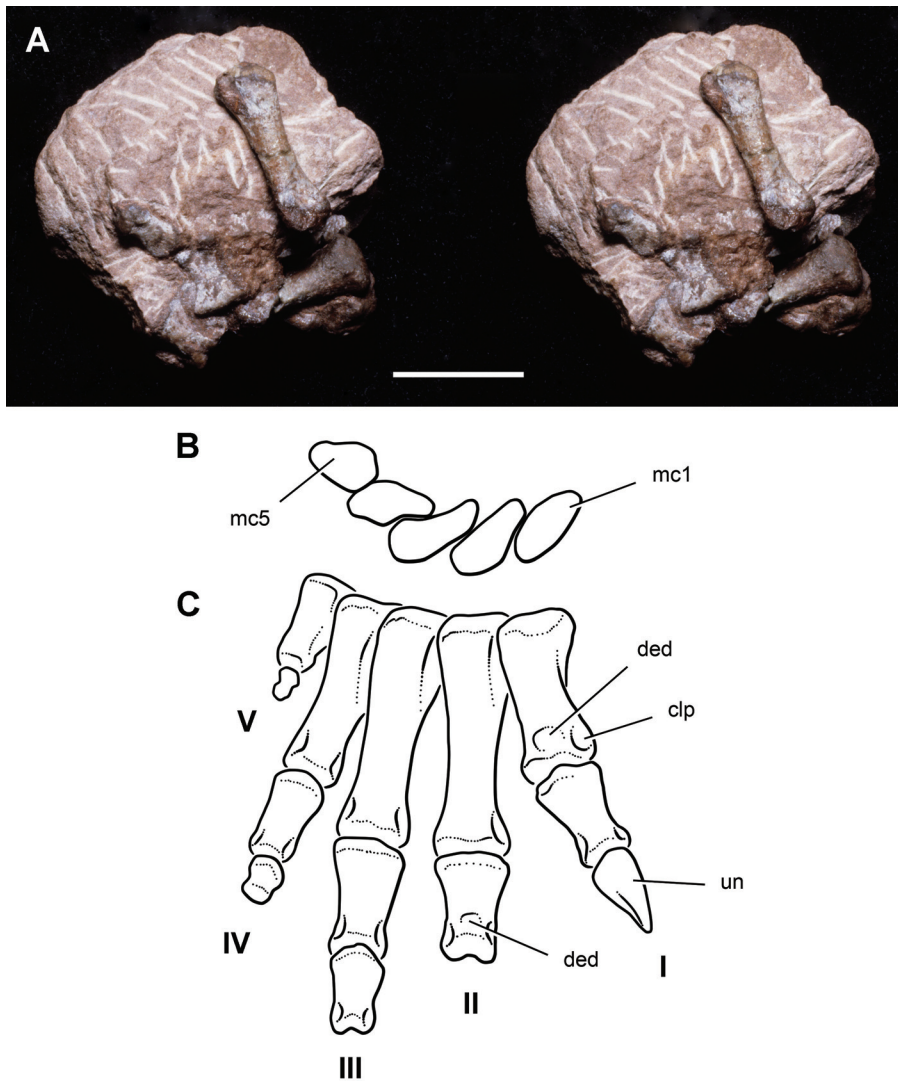


FIGURE 77. Right manus of *Lesothosaurus diagnosticus* (NHMUK RU B17). **A**, stereopair of right manus as preserved in partial articulation, showing metacarpal 2 (above) and the proximal portion of digit III (below). **B**, reconstruction of the articulated right metacarpus in proximal view. **C**, reconstruction of the preserved bones of the right manus in dorsal view. **Abbreviations:** I–V, manual digits I–V; **clp**, collateral ligament pit; **ded**, dorsal extensor depression; **mc1**, 5, metacarpal 1, 5; **un**, ungual. Scale bar equals 1 cm in **A**.

portion is covered by the femur (Figs. 78, 83). The raised anterior corner of the ischial antitrochanter is exposed, anterior to which is a non-articular margin at least 7 mm long. The posterior portion of the ischial antitrochanter is exposed on the left side (Fig. 79). The short pubic peduncle (9 mm) has a subtriangular cross-section that is dorsoventrally deeper (12 mm) than transversely broad (8 mm).

Proximally, the shaft is plate-shaped, with a sinuous ventral margin along which there is no development of an obturator process. The ischial symphysis extends along most of the length of the bone, beginning proximally at the base of the pubic peduncle and continuing to the distal end of the shaft (Fig. 82E, G, I). At midlength the shafts are hollow and have a subtriangular cross-section that is dorsoventrally deeper (7 mm) than transversely broad (5 mm) (Figs. 81, 82G). Distally, the ischium expands gradually in depth and, to a lesser extent, in width (Figs. 81, 82A).

The distal end of the ischium has a depth of 17 mm and a width of 7 mm and is truncated at a high angle (ca. 60°) to the horizontal in lateral view (Figs. 80, 81, 82A). A subtriangular distal end (Fig. 82I) is typical of basal sauropodomorphs, such

as *Saturnalia* (Langer, 2003), *Plateosaurus* (Huene, 1926b), and *Adeopapposaurus* (Martínez, 2009). In *Panphagia*, the distal end has a more crescentic shape, although the shaft does have a lateral ridge offset to its dorsal margin (Martínez and Alcober, 2009). In both *Panphagia* and *Saturnalia*, the distal end of the ischium is expanded to a greater degree than in *Eoraptor*. In theropods, in contrast, the distal end of the ischium is rounded or truncated roughly horizontally, as in *Herrerasaurus* (Novas, 1994) and various basal neotheropods (e.g., *Carnotaurus*, Bonaparte et al., 1990; *Dilophosaurus*, Welles, 1984; *Coelophysis*, Colbert, 1989; *Allosaurus*, Gilmore, 1920; Madsen, 1976).

**Pubis**—The pubis, the longest element in the pelvic girdle, projects anteroventrally from the acetabulum and is best exposed in right lateral view (Figs. 78, 79, 82A, C, F, H). The proximal end is divided between the articular surfaces for the ilium and ischium and an intervening acetabular margin (Fig. 82A). Of the three, the iliac articular surface is the longest and thickest portion of the proximal end. The acetabular margin and iliac peduncle are plate-shaped, and both angle medially toward the median symphysis, which seems to run the entire length of the bone. A shallow

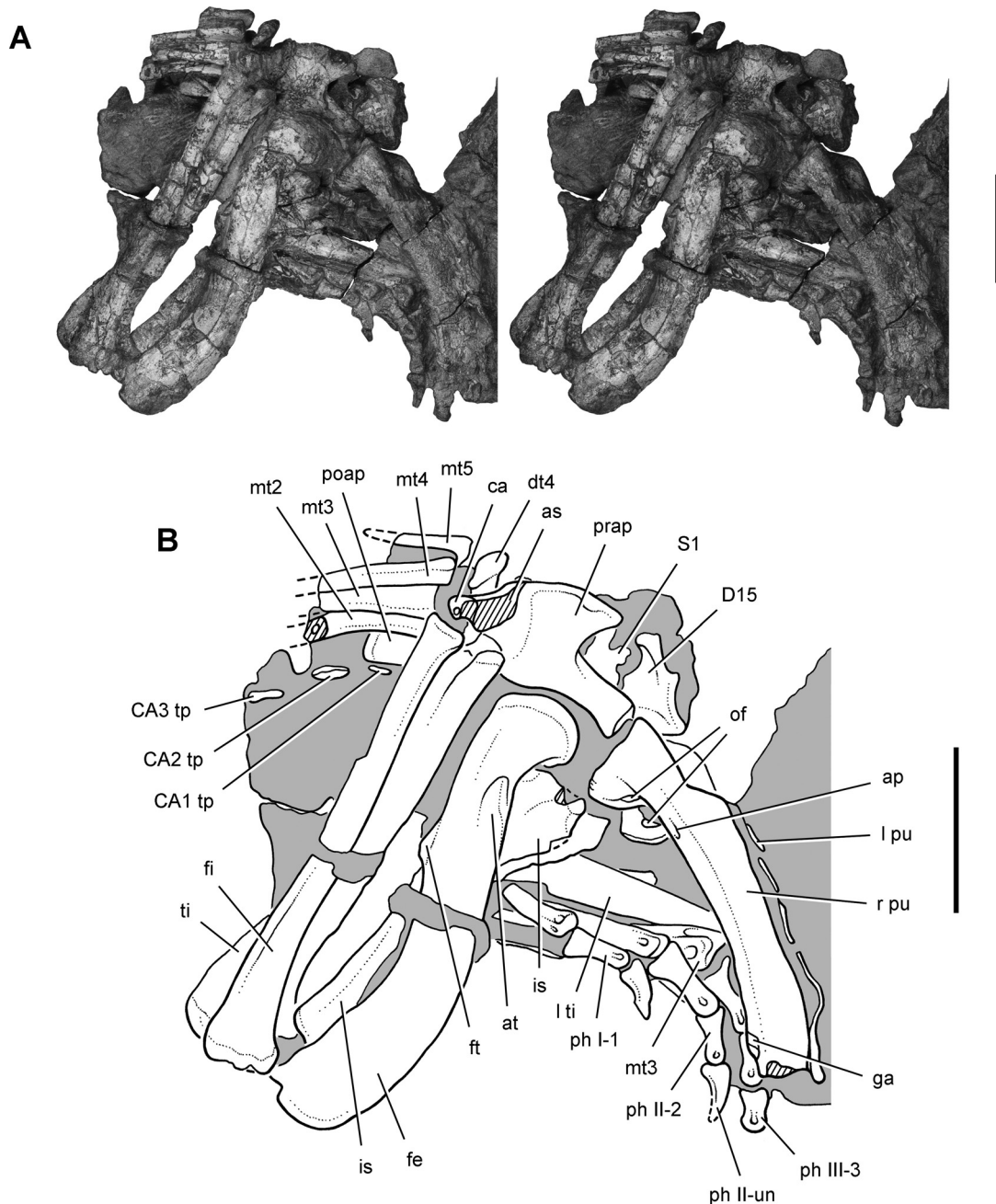


FIGURE 78. Stereopair (A) and drawing (B) of the pelvic girdle and right hind limb of *Eoraptor lunensis* (PVSJ 512) in lateral view. **Abbreviations:** I–III, pedal digits I–III; ap, ambiens process; as, astragalus; at, anterior trochanter; ca, calcaneum; CA1–3, caudal vertebrae 1–3; D15, dorsal vertebra 15; dt4, distal tarsal 4; fe, femur; fi, fibula; ft, fourth trochanter; ga, gastralgia; is, ischium; l, left; mt2–5, metatarsals 2–5; of, obturator foramen; ph, phalanx; poap, postacetabular process; prap, preacetabular process; pu, pubis; r, right; S1, sacral vertebra 1; ti, tibia; tp, transverse process; un, ungual. Dashed line indicates a missing margin; hatching indicates a broken surface; shading indicates matrix. Scale bars equal 5 cm.

groove passes out of the acetabulum. A large oval obturator foramen, with an anteroposterior diameter of approximately 10 mm, is located in the thin medial portion of the proximal end of the pubis and would have had only a narrow medial margin separating it from its opposite (Figs. 78, 82A). There are no additional openings in the proximal end of the pubis.

The plate-shaped blade faces anteriorly (Figs. 78, 82A). Along with its opposite, it is gently arched transversely. The thickened

lateral edge of the proximal blade curls posteriorly (Fig. 82C), whereas the majority of the blade is composed of a nearly planar sheet of bone only 2 mm thick (Fig. 82H). Proximally, a prominent, dorsoventrally compressed ambiens process is present along the lateral margin (Fig. 82A). In anterior view, the width of the blade decreases gradually such that the distal end is 60% the width of the proximal end (Fig. 82C, H). The distal end, which is well preserved on the left side, is slightly swollen along its ventral margin

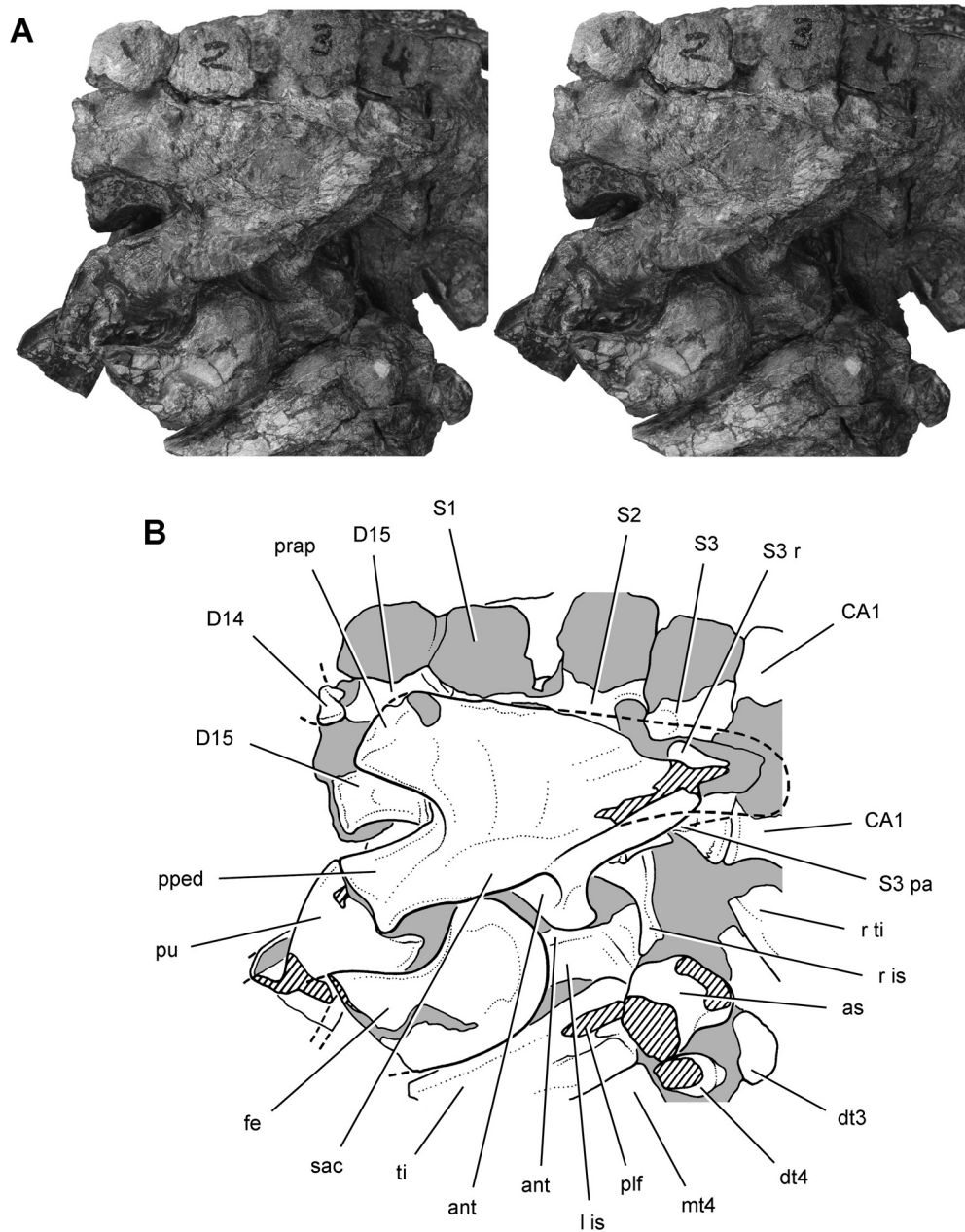


FIGURE 79. Stereopair (A) and drawing (B) of the pelvic girdle and left hind limb of *Eoraptor lunensis* (PVSJ 512) in lateral view. **Abbreviations:** *ant*, antitrochanter; *as*, astragalus; *CA1*, caudal vertebra 1; *D14*, *15*, dorsal vertebra 14, 15; *dt3*, *4*, distal tarsal 3, 4; *fe*, femur; *is*, ischium; *l*, left; *mt4*, metatarsal 4; *pa*, parapophysis; *plf*, posterolateral flange; *pped*, pubic peduncle; *prap*, preacetabular process; *pu*, pubis; *r*, rib or right; *S1–3*, sacral vertebra 1–3; *sac*, supraacetabular crest; *ti*, tibia. Dashed line indicates a missing margin; hatching indicates a broken surface; shading indicates matrix. Scale bars equal 3 cm.

(Fig. 82A). There is no development of a pubic foot as occurs in *Herrerasaurus*, *Eodromaeus*, and other theropods.

#### Hind Limb

The elongate long bones in the distal segments of the hind limb in *Eoraptor* are consistent with the proportions of a cursorial biped (Carrano, 1999). The tibia exceeds the femur in

length, and metatarsal 3 is greater than one-half the length of the tibia (Table 10). All of the long bones, including all non-ungual phalanges, and at least the proximal tarsals are hollow. Although the following description of the hind limb is based primarily on the holotypic skeleton (Figs. 83, 87, 89, 90), many aspects of the femur and tibia are better preserved in referred material (Table 1). A partial, articulated right hind limb (PVSJ 559) was found in the wall of the excavation trench around the

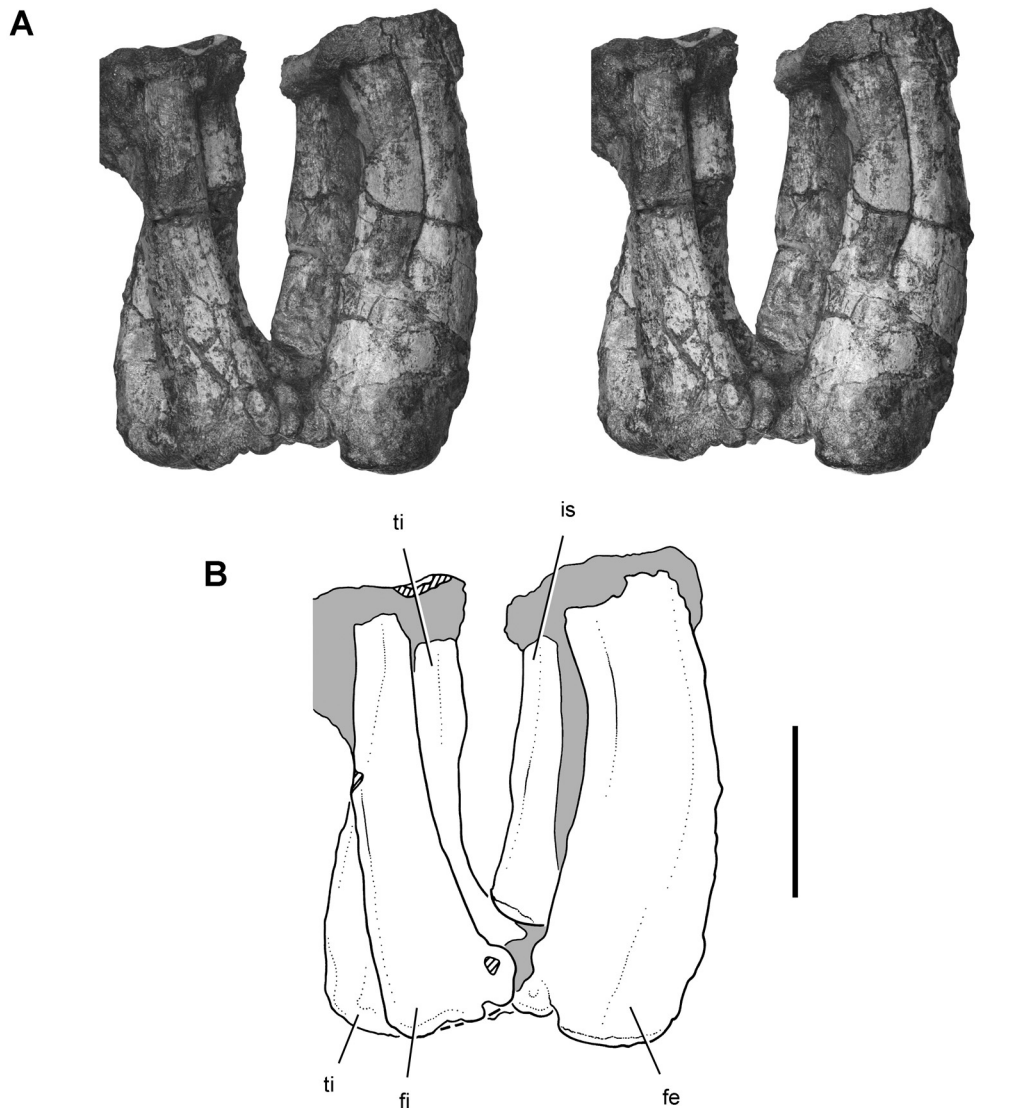


FIGURE 80. Stereopair (A) and drawing (B) of the distal right ischium, distal right femur, and proximal right tibia of *Eoraptor lunensis* (PVSJ 512) in lateral view. **Abbreviations:** *fe*, femur; *fi*, fibula; *is*, ischium; *ti*, tibia. Dashed line indicates a missing margin; hatching indicates a broken surface; shading indicates matrix. Scale bars equal 3 cm.

holotypic skeleton and provides the most complete information for the femur, tibia, distal fibula, and proximal tarsals (Figs. 84–86, 88).

**Femur**—The maximum length of the proximal end of the femur is approximately twice its minimum width. With the axis through the distal condyles oriented transversely, the long axis of the proximal end projects anteromedially toward the acetabulum at about 50° from a transverse axis. In this regard, *Eoraptor* resembles *Saturnalia* (Langer, 2003:fig. 4), *Herrerasaurus* (Novas, 1994:fig. 7E), *Staurikosaurus* (Colbert, 1970:fig. 11A), and basal neotheropods (e.g., *Coelophysis*; Padian, 1986:fig. 5.4C). The head, which is partially exposed, forms the hemispherical medial extremity of the proximal end (Fig. 83). The lateral rim of the head is very prominent as in *Saturnalia* (Fig. 83). On the medial side of the proximal end, the head is delimited posteriorly by a sulcus for the ligament

of the head, posterior to which is a rounded medial tuberosity and trough.

The anterior trochanter is developed as a vertical process, most of which is attached to the anterolateral margin of the proximal shaft (Figs. 83, 86). The anterior surface of the femoral shaft adjacent to the anterior trochanter is flattened as in *Saturnalia* and less than the extent that occurs in herrerasaurids (Novas, 1994). An additional vertical rugosity seems to be present on the posterior margin of the shaft, opposite and slightly proximal to the anterior trochanter (Fig. 83).

The trochanteric shelf (Fig. 84E, F) and its associated sigmoidal rugosity are similar in general form and position to that in the basal dinosauriforms *Marasuchus* (Sereno and Arcucci, 1994a) and *Silesaurus* (Dzik, 2003) and in other basal dinosaurs such as *Saturnalia* (Langer, 2003), *Herrerasaurus* (Novas, 1994),

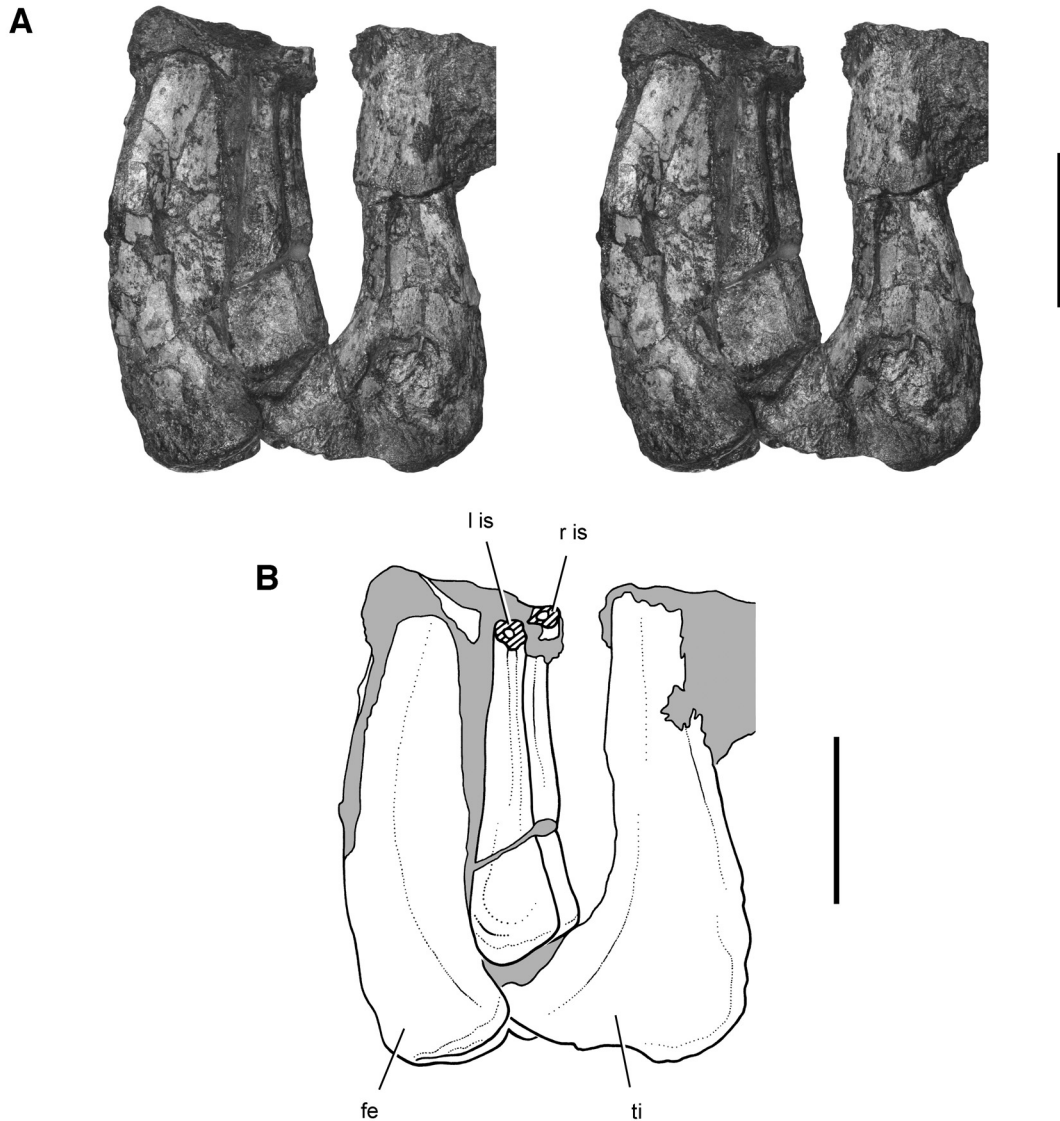


FIGURE 81. Stereopair (A) and drawing (B) of the distal ischia, distal right femur and proximal right tibia and fibula of *Eoraptor lunensis* (PVSJ 512) in medial view. **Abbreviations:** fe, femur; is, ischium; l, left; r, right; ti, tibia. Hatching indicates a broken surface; shading indicates matrix. Scale bars equal 3 cm.

and coelophysoids (Rowe, 1989; Tykoski and Rowe, 2004). The crest descends and then traverses the proximal femoral shaft as a trough with a raised rugose external ridge, attenuating as a low rugose scar on the posterolateral aspect of the shaft (Figs. 84D, F, 86A), presumably for attachment of the ischiotrochanteric muscle (Carrano and Hutchinson, 2002). At that point, the rugosity diverges, with one branch continuing posteroventrally to join the proximal end of the fourth trochanter and the other joining a ridge passing down the lateral aspect of the femoral shaft as an intermuscular line (Figs. 84F, 86A).

The fourth trochanter, located on the posteromedial side of the shaft one-third of the distance from the head along the femur, is developed as a prominent subrectangular flange, measuring about 22 mm along its external margin and 7 mm wide (Fig. 84F). As the flange expands from the shaft, a subtle proximal corner is present that is more prominent than in *Saturnalia* (Langer, 2003:fig.4B,

E). The distal corner of the flange, likewise, is more prominent than in *Saturnalia*, such that it is slightly pendant at its apex. In general, however, the fourth trochanter in *Eoraptor* resembles the subquadrate, hatchet-shaped fourth trochanter in basal sauropodomorphs (e.g., *Massospondylus*, Cooper, 1981; *Adeopapposaurus*, Martínez, 2009) and *Herrerasaurus* (Novas, 1994) than the more symmetrical, crescentic flange typical of theropods, such as *Eodromaesus* (Martínez et al., 2011) and *Tawa* (Nesbitt et al., 2009). Scars indicate the likely attachment areas for caudofemoralis brevis and longus muscles (Fig. 84C, F).

The anterior aspect of the distal end of the femur is marked by a large, subtriangular rugose area for attachment of the femorotibialis musculature (Figs. 84H, 86A). In *Herrerasaurus* (Novas, 1994), *Eodromaesus* (Martínez et al., 2011), and other theropods (e.g., *Allosaurus*; Gilmore, 1920), this attachment area is often depressed to form a shallow fossa. The distal articular surface of the

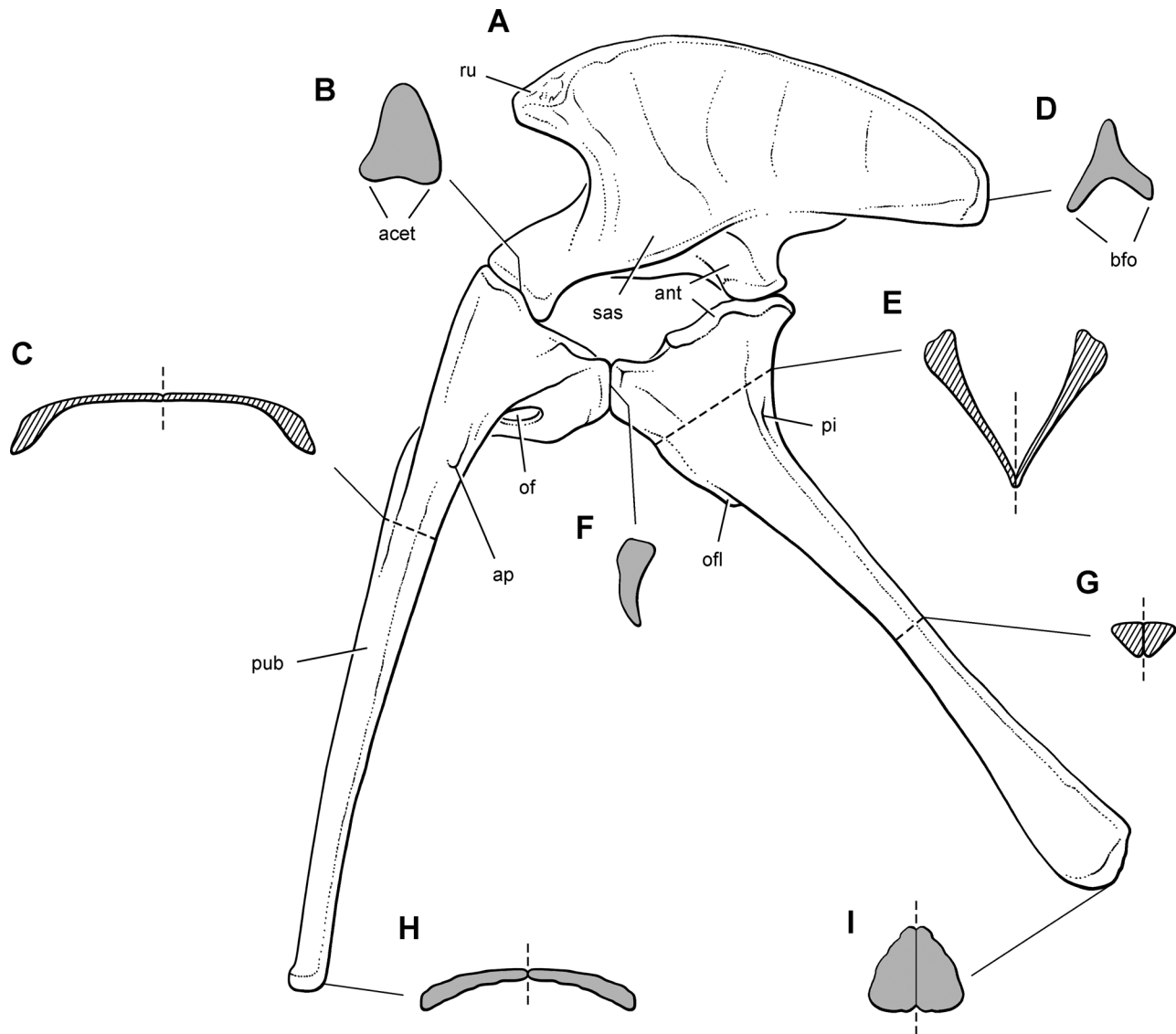


FIGURE 82. Reconstruction of the pelvic girdle of *Eoraptor lunensis* (PVSJ 512) in left lateral view with cross-sections. **A**, pelvic girdle. **B**, distal articular end of pubic peduncle. **C**, cross-section of the proximal end of the pubic blades. **D**, distal end of the iliac postacetabular process. **E**, cross-section of the proximal end of the ischia. **F**, distal articular end of pubic peduncle of ischium. **G**, cross-section of ischial shafts at midlength. **H**, distal ends of pubes. **I**, distal ends of the ischia. **Abbreviations:** acet, acetabulum; ant, antitrochanter; ap, ambiens process; bfo, brevis fossa; of, obturator foramen; ofl, obturator flange; pi, pit; pub, pubic blade; ru, rugosity; sas, supraacetabular shelf. Dashed line in **A** indicates position of cross-sections and in **C**, **E**, and **C**, **G–I** indicates the midline; hatching indicates a cross-sectional view; shading indicates view of distal end.

femur has subequal anteroposterior and transverse maximum dimensions (Fig. 84G). There is no anterior intercondylar groove, but the posterior intercondylar groove is well developed and separates the medial condyle from the smaller lateral condyle. The fibular condyle is located anterior to the lateral condyle, separated distally and laterally by shallow troughs (Fig. 84D, G). There is no development of a sharp tibiofibular crest on the rounded lateral condyle, which is well developed in ceratosaurian theropods and birds (Rowe, 1989:fig. 4F). A broad area in the center of the distal articular surface is concave (Fig. 84G), as in *Saturnalia* (Langer, 2003) and herrerasaurids (*Herrerasaurus*, Novas, 1994; *Staurikosaurus*, Bittencourt and Kellner, 2009). The distal end of the femur is nearly indistinguishable from that in *Saturnalia*.

**Tibia**—The proximal articular end of the tibia is subtriangular, about one-third longer than wide (Fig. 85F). The cnemial crest forms the rounded anterior apex of the articular surface and in lateral view projects a short distance above the remainder of the proximal end (Fig. 85E), as in *Panphagia* (Martínez and Alcober, 2009:fig. 9A) and *Herrerasaurus* (Novas, 1994:fig. 8B). In *Saturnalia*, the central portion of the proximal end is more prominent than that over the cnemial crest (Langer, 2003:fig. 5A).

Two condyles are developed on the remainder of the proximal articular surface. The medial condyle is the largest (12 mm width) and is separated from the lateral condyle (7 mm width) by a shallow notch (Fig. 85B, F). The lateral condyle is set anterior to the medial condyle and has a distinct beveled posterolateral edge

TABLE 10. Measurements (in mm) of the femur, tibia, fibula, and proximal tarsals of *Eoraptor lunensis* (PVSJ 512).

Dimension	Measurement
<b>Femur</b>	
Length	152L
Head, maximum anteroposterior width	27
Head, maximum transverse width	14
Head to apex of fourth trochanter (distal notch)	55
Midshaft, anteroposterior diameter	21
Midshaft, transverse diameter	21
Distal end, maximum transverse width	25
Distal end, maximum anteroposterior depth	25
<b>Tibia</b>	
Length	156
Proximal end, maximum anteroposterior width	30
Proximal end, maximum transverse width	21L
Midshaft, anteroposterior diameter	13
Midshaft, transverse diameter	12
Distal end, maximum distal width	19
Distal end, posterolateral flange thickness	6
<b>Fibula</b>	
Length	154
Proximal end, maximum anteroposterior width	21L
Proximal end, maximum transverse width	7L
Midshaft, anteroposterior diameter	10
Midshaft, transverse diameter	8
Distal end, maximum width (oblique axis)	15
<b>Astragalus</b>	
Maximum transverse width	27
Tibial depression, minimum thickness	9
Ascending process, height to apex	6
<b>Calcaneum</b>	
Maximum transverse width	11
Maximum dorsoventral depth (posterior portion)	8
<b>Distal tarsal 3</b>	
Maximum transverse width	(12)
Maximum dorsoventral depth	6
<b>Distal tarsal 4</b>	
Maximum transverse width	13
Body, maximum dorsoventral depth (medial edge)	6
Heel, maximum dorsoventral depth	7

Measurements are from the right side except as indicated otherwise (L, left). Parentheses indicate estimated measurement.

(Fig. 85E, F). In lateral view of the proximal end, the shaft bears a strong fibular crest (Fig. 85E). At midlength the shaft is subcylindrical. The transversely expanded distal end curves slightly anteriorly and medially, as seen in medial and posterior views, respectively (Fig. 85B, C).

The subquadrate distal end of the tibia is approximately 20% broader transversely than deep anteroposteriorly (Fig. 85H). In distal view, a curving articular surface accommodates the wedge-shaped ascending process of the astragalus (Fig. 85H), which is very similar to that in *Saturnalia* (Langer, 2003). A relatively thin posterolateral flange (6 mm) projects laterally, backing the ascending process of the astragalus and approaching, but not contacting, the fibula (Figs. 85G, H, 87, 88B, F). A groove that separates the posterolateral flange from the remainder of the tibia curves from the distal end onto the lateral aspect of the shaft (Figs. 86B, 87A, C). The form of the distal end of the tibia is nearly identical in *Eoraptor*, *Panphagia*, and *Saturnalia* (Langer, 2003).

**Fibula**—The fibula is exposed in lateral view in the holotypic skeleton (PVSJ 512), the left side preserving the proximal end, and the right side preserving the central shaft and distal end. A disarticulated distal end of the fibula is also available (PVSJ 559).

The proximal articular surface of the fibula is crescentic, with an anteroposterior length that is three times its maximum width. The external margin is slightly convex and the internal concave. The anterior trochanter, if present at all, is a low rugosity on the anterior margin of the proximal shaft. The cross-section of the shaft is cylindrical at midlength.

The distal end has an elliptical articular surface, the long axis of which angles posterolaterally (Figs. 85K, 88C). In lateral view, the distal end of the fibula angles posteroventrally at approximately 25° (Fig. 85I, J). The posterolateral margin of the distal end projects as a prominent posterior tuberosity, which overhangs the calcaneum posteriorly (Figs. 85I–K, 88B, C). The distal end of the fibula extends ventral to the tibia in articulation, where it contacts the calcaneum and astragalus (Fig. 88A, B). Fibular contact with the astragalus occurs on the lateral aspect of the ascending process, a configuration that closely matches that in basal sauropodomorphs (Cooper, 1981).

**Astragalus**—The astragalus is partially exposed in the holotypic skeleton (Fig. 87) and fully exposed in two referred specimens (PVSJ 534, 862). In the holotype, the posterior one-half of the bone has sheared off, exposing hollow pockets in the body of the astragalus (Fig. 87). That cross-section also shows that the astragalus is nearly three times as wide transversely as it is thick dorsoventrally. In dorsal view (Fig. 88G), the astragalus is transversely broad, its maximum anteroposterior depth measuring only 65% of its transverse width, compared with 75% in *Panphagia* (Martínez and Alcober, 2009:fig. 9D) and *Saturnalia* (Langer, 2003:fig. 6A).

The anterolateral corner of the astragalus is very prominent in dorsal or ventral view in *Eoraptor*, as in *Panphagia*, *Saturnalia*,



FIGURE 83. Stereopair of right ilium, proximal femur, distal tibia and fibula, and ankle of *Eoraptor lunensis* (PVSJ 512) in lateral view. Scale bar equals 5 cm.

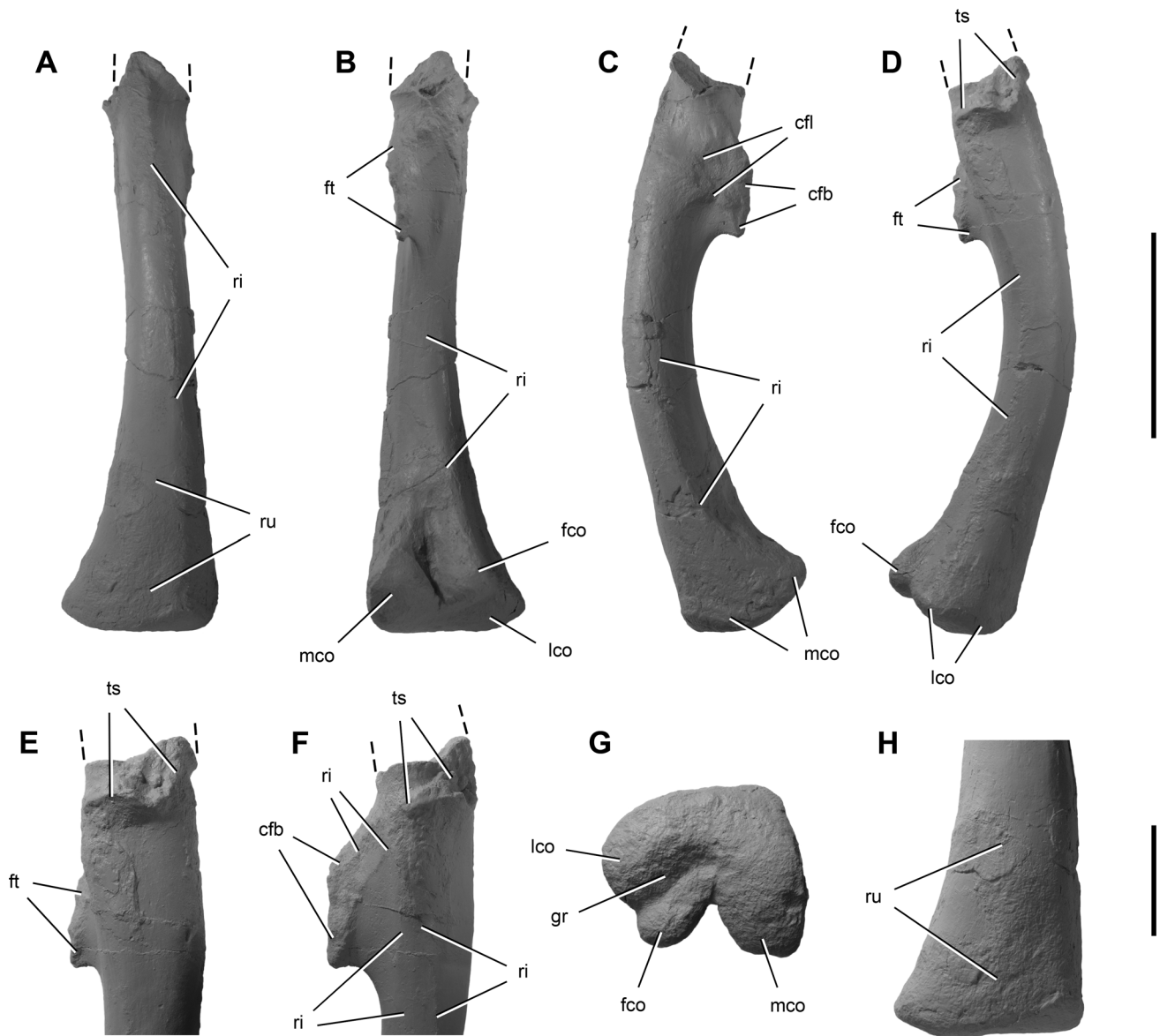


FIGURE 84. Partial right femur of *Eoraptor lunensis* (cast of PVSJ 559). **A**, anterior view. **B**, posterior view. **C**, medial view. **D**, lateral view. **E**, lateral view (close-up) of trochanteric shelf and fourth trochanter. **F**, posterolateral view (close-up) of fourth trochanter. **G**, distal view. **H**, anterior view (close-up) of distal end. **Abbreviations:** **cfb**, m. caudofemoralis brevis scar; **cfl**, m. caudofemoralis longus scar; **fco**, fibular condyle; **ft**, fourth trochanter; **gr**, groove; **lco**, lateral condyle; **mco**, medial condyle; **ri**, ridge; **ru**, rugosity; **ts**, trochanteric shelf. Dashed line indicates a missing margin. Scale bar equals 5 cm in **A–D** and 2 cm in **E–H**.

and other basal sauropodomorphs (Fig. 88G, H). The dorsal surface of the astragalus is predominated by the tibial articular surface, which articulates against all but the anteromedial corner and posterior fossa. The posterior fossa provides vascular supply to the astragalus via a large foramen (Fig. 88E). The posterolateral flange of the tibia extends across this region (Fig. 88B), but a gap separates the flange from the surface of the fossa (Fig. 88C). In dorsal view, the anteromedial corner of the astragalus can be seen extending beyond the tibia (Fig. 88C). In medial view (Fig. 88F), the ventral articular surface of the astragalus is beveled parallel to the surface of the ascending process, which reduces the thickness of the posterior portion of the astragalus. In ventral view, the articular surface is saddle-shaped, with a dis-

tinct bulge ventral to the anterolateral corner. That bulge is separated from the distal articular surface by a low, rounded diagonal crest.

A small anterior fossa is present, within which are situated a few small foramina (Fig. 88A, D). The ascending process is wedge-shaped, and has a concave articular facet laterally for contact with the fibula. Laterally, the astragalus meets the calcaneum along a complex suture. As seen in dorsal view (Fig. 88G), the astragalus projects laterally over the calcaneum along its anterior and posterior margins and receives in return a short, subtriangular process of the calcaneum (Fig. 88D, E, H). The concave articular socket for the distal end of the fibula faces laterally and undercuts the upper portion of the ascending process.

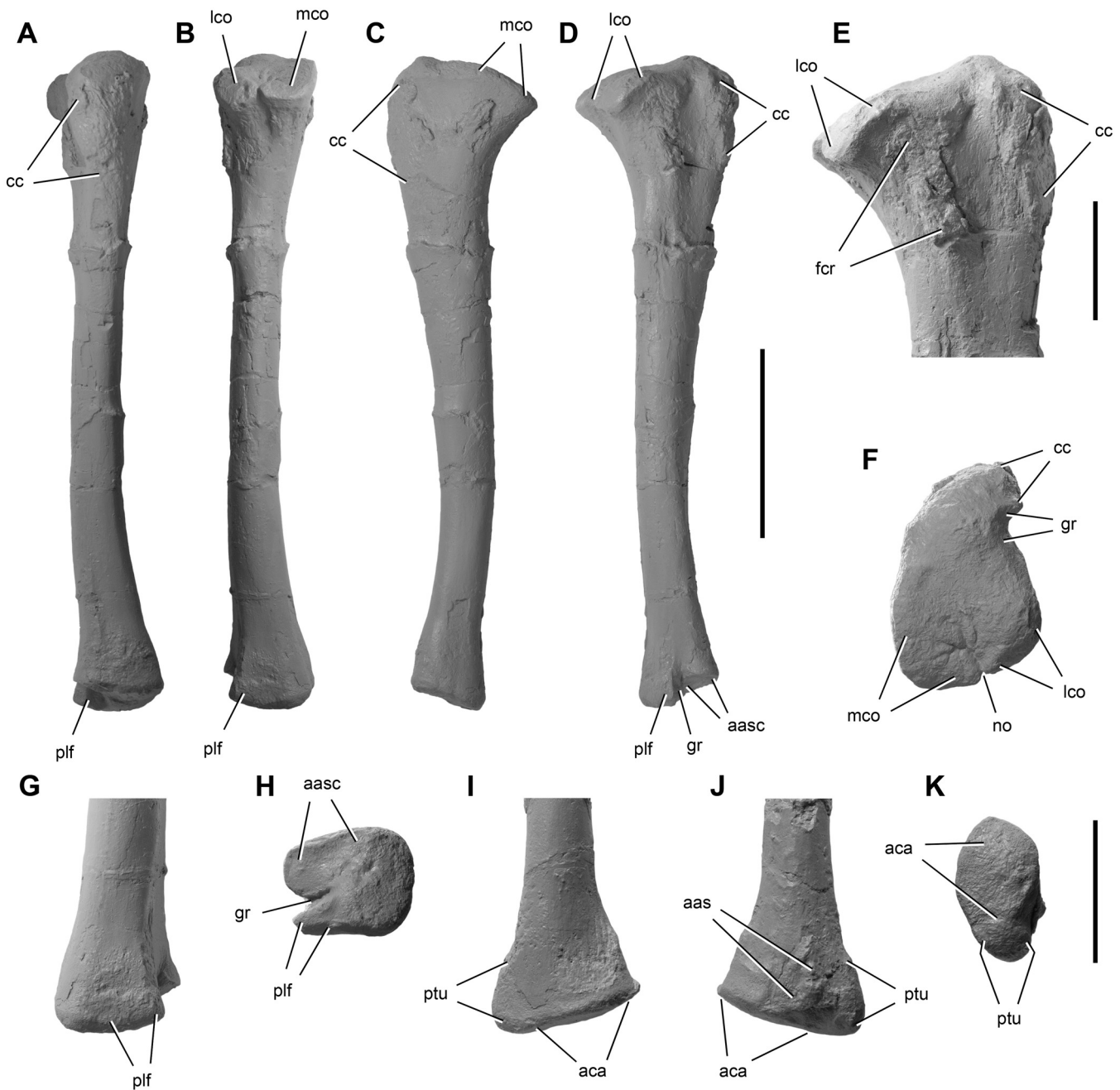


FIGURE 85. Right tibia and distal fibula of *Eoraptor lunensis* (cast of PVSJ 559). Right tibia in anterior (A), posterior (B), medial (C), and lateral (D) views. Proximal end of the right tibia in lateral (E) and proximal (F) views. Distal end of the right tibia in posterior (G) and distal (H) views. Distal end of the right fibula in lateral (I), medial (J), and distal (K) views. **Abbreviations:** aas, articular surface for the astragalus; aasc, articular surface for the astragalus ascending process; aca, articular surface for the calcaneum; cc, cnemial crest; fcr, fibular crest; gr, goove; lco, lateral condyle; mco, medial condyle; no, notch; plf, posterolateral flange; ptu, posterior tuberosity. Scale bar equals 5 cm in A–D, 2 cm in E–H, and 2 cm in I–K.

A wedge-shaped ascending process projects dorsally from the lateral portion of the astragalus (Fig. 88D–I). Its anterodorsal face is flat; its posterior face is gently concave and bordered dorsally by a rounded posteriorly protruding edge of the process; its lateral face is deeply concave to receive the medial edge of the distal end of the fibula (Fig. 88A, I). The ascending process, which is identical

in form to that in *Panphagia* and *Saturnalia*, inserts into the distal end of the tibia.

**Calcaneum**—The subtriangular calcaneum is nearly identical to that in *Saturnalia* (Langer, 2003:fig. 6G, H). It is partially preserved in articulation in the holotypic skeleton, with the posterior portion of the bone sheared off (Fig. 87). As with the astragalus,

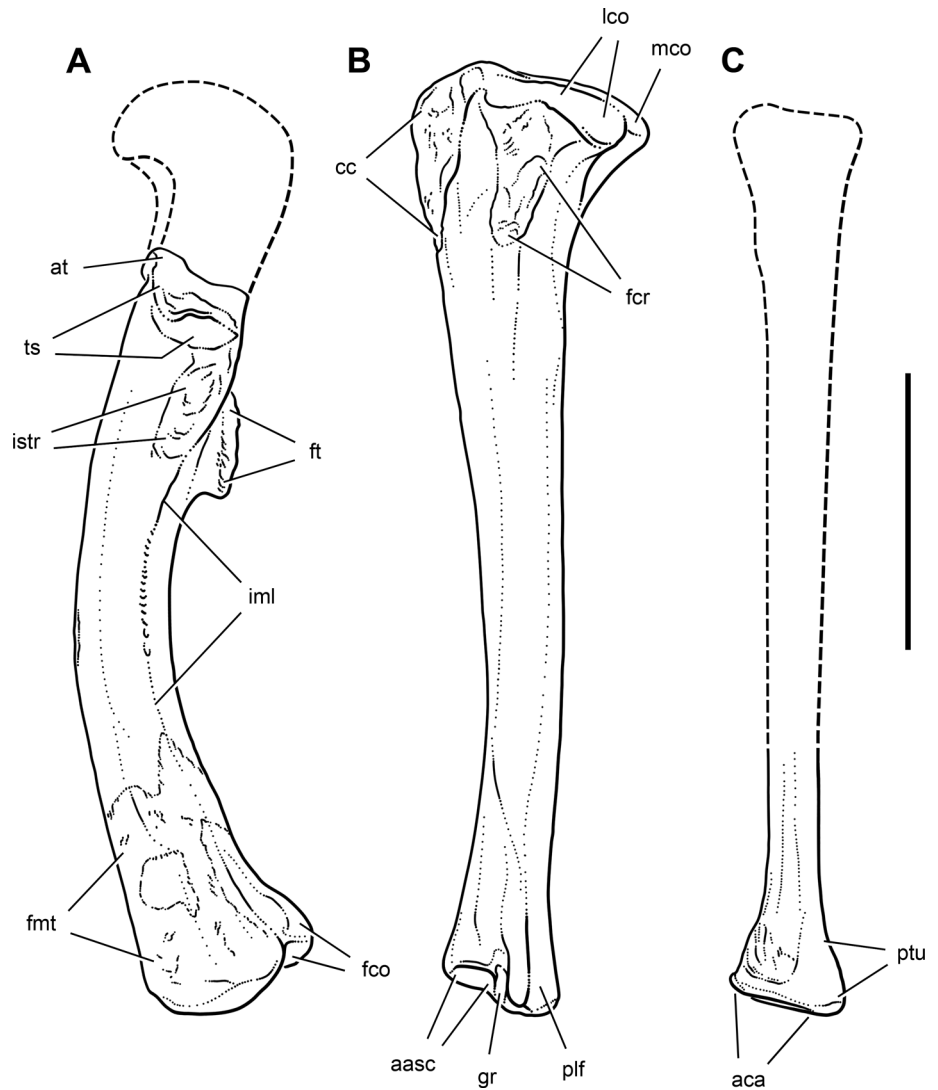


FIGURE 86. Drawing of the left femur, tibia, and fibula of *Eoraptor lunensis* in left lateral view based on PVSJ 512 and 559. **A**, femur. **B**, tibia. **C**, fibula. **Abbreviations:** aasc, articular surface for the astragalus ascending process; aca, articular surface for the calcaneum; at, anterior trochanter; cc, cnemial crest; fco, fibular condyle; fcr, fibular crest; fmt, m. femorotibialis attachment; ft, fourth trochanter; gr, groove; iml, intermuscular line; istr, m. ischio-trochanteric scar; lco, lateral condyle; mco, medial condyle; plf, posterolateral flange; ptu, posterior tuberosity; ts, trochanteric shelf. Dashed line indicates bone margins based on PVSJ 512. Scale bar equals 5 cm.

there is a hollow space within the body of the calcaneum exposed on the breakage surface.

The subtriangular articular surface for the fibula is slightly concave anteroposteriorly and transversely and elevated above the smaller, subtriangular, rugose surface of the posterior tuberosity (Fig. 88G). The articulation with the astragalus is complex but precisely similar to that in *Saturnalia* (Langer, 2003). There is a pair of short, subtriangular medial articular processes for the astragalus, one above and one below a wedge-shaped lateral process on the astragalus (Fig. 88G, H). As seen in dorsal view, the smaller dorsomedial calcaneal process is positioned just posterior to the middle of the astragalus, where it overlaps the astragalus as part of the articular surface for the fibula (Fig. 88G). As seen in ventral view, the larger ventromedial process is situated more posteriorly, extending under the astragalus to articulate within a well-defined notch (Fig. 88H). Together these processes appear to lock the calcaneum to the astragalus, eliminating the possibility of rotary movement of one against the other.

The distal articular surface is moderately convex. In ventral view, however, a substantial portion of the calcaneum is devoted to a concave, irregular non-articular surface between the posterior

tuberosity and the medial process (Fig. 88H). In dorsal view, the posterior margin of the calcaneum also forms an irregular, non-articular surface between the contact with the astragalus and the posterior tuberosity (Fig. 88G). The fibula clearly articulates over this entire area (Fig. 88C). In lateral view, there are two depressions, the larger of the two here termed a fossa and the smaller a pit (Fig. 88I).

**Distal Tarsals**—Distal tarsal 3, best exposed in the right ankle of the holotype (Fig. 89C, D), is a lozenge-shaped bone that articulates proximally with the astragalus and distally with metatarsals 2 and 3. It becomes thicker dorsoventrally toward its posterior edge.

Distal tarsal 4 articulates with the astragalus and calcaneum proximally and metatarsals 4 and 5 distally (Figs. 87, 89). As preserved in the hyperextended right ankle, it is dislodged from its natural articulation over the lateral side of the metatarsus and partially overlaps distal tarsal 3. As in basal dinosauromorphs (e.g., *Lagerpeton*, *Marasuchus*; Sereno and Arcucci, 1994a, 1994b), *Herrerasaurus* (Novas, 1994), and *Saturnalia* (Langer, 2003), the dorsal (anterior) portion of distal tarsal 4 is proximodistally compressed. The concave proximal surface of this portion of the bone articulates with the convex distal surface of the astragalus

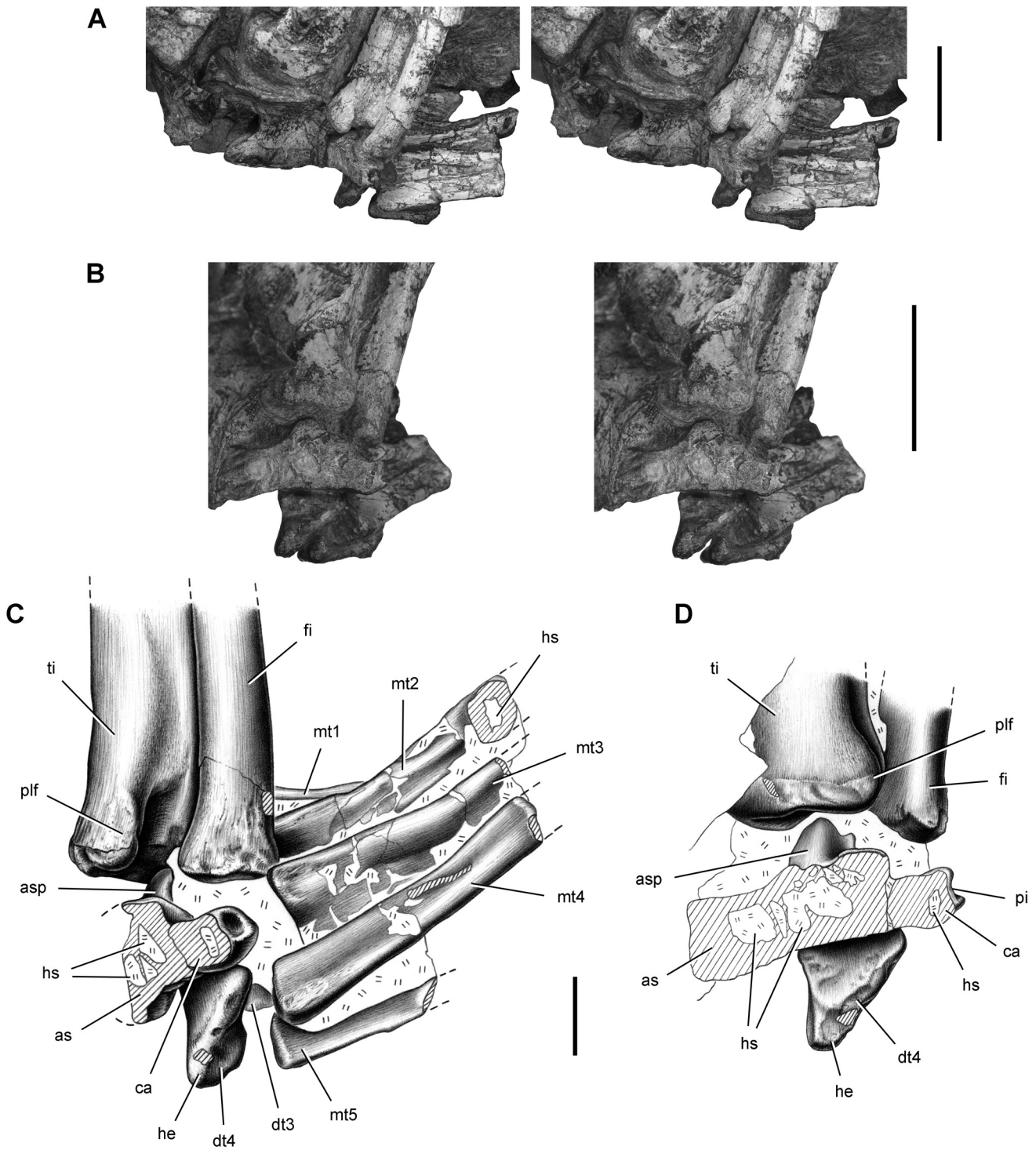


FIGURE 87. Stereopairs (A, B) and drawings (C, D) of the right ankle of *Eoraptor lunensis* (PVSJ 512) in anterolateral (A, C) and posterior (B, D) views. **Abbreviations:** as, astragalus; asp, ascending process; ca, calcaneum; dt3, 4, distal tarsal 3, 4; fi, fibula; he, heel; hs, hollow space; mt1–5, metatarsals 1–5; pi, pit; plf, posterolateral flange; ti, tibia. Dashed line indicates a missing margin; hatching indicates a broken surface; double hatch marks indicate matrix. Scale bars equal 3 cm in A and B and 1 cm in C and D.

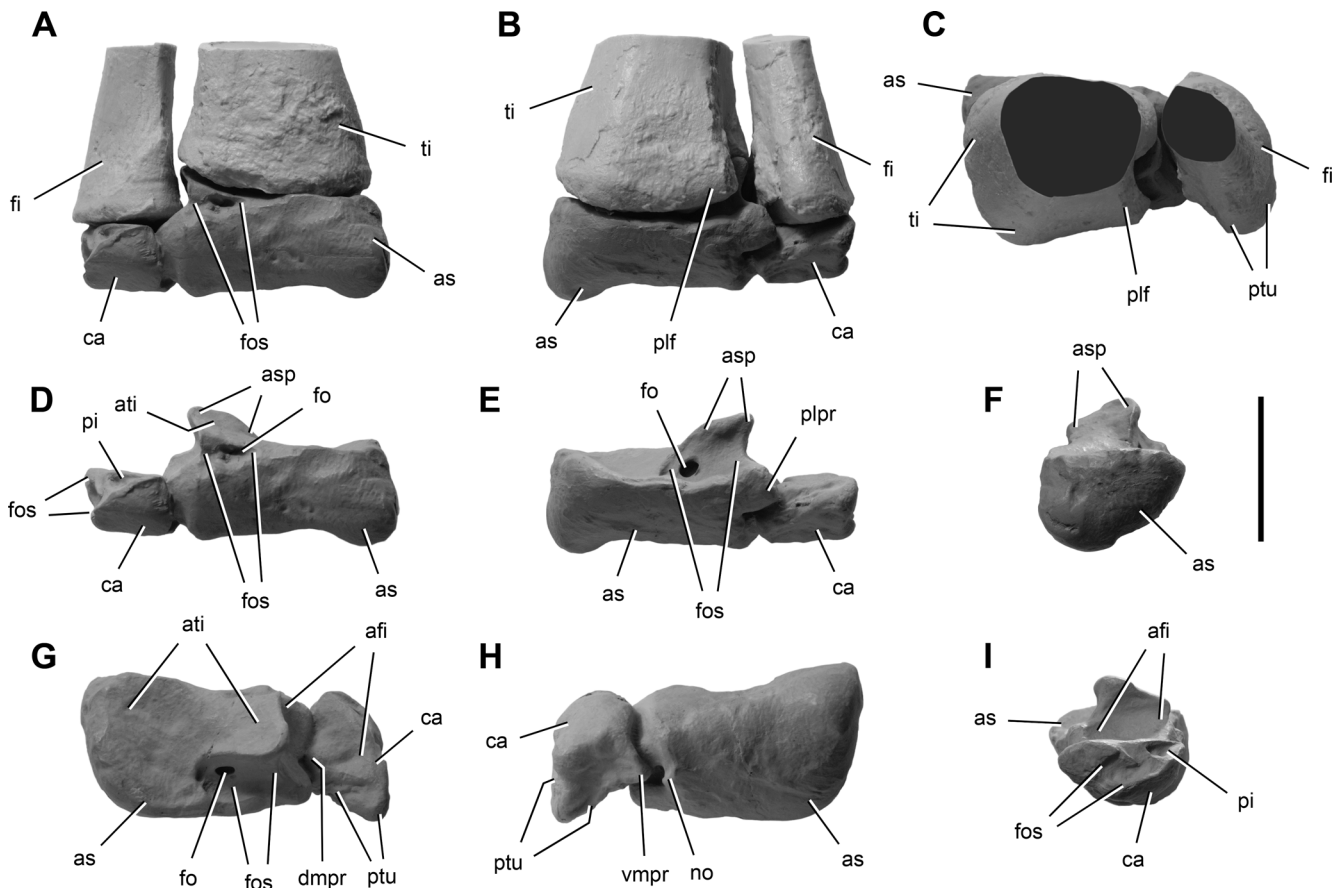


FIGURE 88. Right distal tibia, distal fibula, astragalus, and calcaneum of *Eoraptor lunensis* (cast of PVSJ 559). Right tibia, fibula, astragalus, and calcaneum in articulation in anterior (A), posterior (B), and dorsal (C) views. Astragalus and calcaneum in articulation in anterior (D), posterior (E), medial (F), dorsal (G), ventral (H), and lateral (I) views. **Abbreviations:** afo, articular surface for the fibula; as, astragalus; asp, ascending process; ati, articular surface for the tibia; ca, calcaneum; dmp, dorsomedial process; fi, fibula; fo, foramen; fos, fossa; no, notch; pi, pit; plf, posterolateral flange; plpr, posterolateral process; ptu, posterior tuberosity; ti, tibia; vmp, ventromedial process. Dark shading in C indicates the cross-section of the tibial and fibular shafts. Scale bar equals 2 cm.

and calcaneum; the convex distal surface articulates with the concave proximal end of metatarsal 4. The ventral (posterior) portion comprises a transversely compressed, non-articular heel, which projects ventrally (posteriorly). There is a rounded trough laterally at the proximal end of the heel. This trough, which faces laterally and distally, constitutes the articular surface for the medial portion of the proximal end of metatarsal 5 (Fig. 89D).

**Metatarsus**—Although not fully visible on either side, the metatarsus is complete and articulated on both sides (Figs. 87, 89, 90; Table 11). The proximal one-half of the more fully exposed right metatarsus has undergone some dorsoventral compression. Here the proximal articular ends of metatarsals 4 and 5 are exposed (Fig. 89). The proximal articular ends of metatarsals 1–3 are covered on both sides, so the shape and articulation of these metatarsals was estimated from dorsal and ventral views of the right metatarsus (Fig. 91A). At midshaft, metatarsals 1–4 are cylindrical and hollow (Figs. 87A, C, 89A, B).

Although metatarsal 1 is preserved on both sides, it is partially obscured by matrix and other bones (Fig. 89). It is the shortest and most slender of the four fully formed metatarsals, with a relative length (56% that of metatarsal 3) identical to that in *Saturnalia* (Langer, 2003). Relative to metatarsals 2 and 3, metatarsal 1 in *Eoraptor* is proportionately shorter than in *Herrerasaurus*

(63% and 54%, respectively, in *Eoraptor*; 70% and 61%, respectively, in *Herrerasaurus*). The proximal one-half of the shaft is transversely compressed and fitted against the shaft of metatarsal 2. It extends proximally as far as the other metatarsals and covers most of the medial aspect of metatarsal 2. As in *Saturnalia* (Langer, 2003) and *Herrerasaurus* (Novas, 1994), metatarsal 1 would have contributed to the proximal articular surface of the metatarsus (Fig. 91).

The distal one-half of the shaft of metatarsal 1 becomes rounded and then dorsoventrally compressed. The distal end is asymmetrical, the medial condyle shorter and narrower than the lateral condyle. It is also rotated such that the medial condyle is shifted posteriorly relative to the lateral condyle. The functional significance of this asymmetry is that the phalanges in pedal digit I are directed posteromedially during flexion. As in metatarsals 2–4, the division of the distal articular surface into discrete condyles occurs only on the ventral aspect of the distal end. The dorsal aspect of the distal end is marked by a shallow dorsal extensor depression, as in metatarsals 2–4. A collateral ligament pit is present medially. The presence of a lateral ligament pit cannot be determined, because that surface is not exposed.

Metatarsal 2 is 89% of the length of metatarsal 3 and slightly shorter than metatarsal 4, the reverse of the condition in

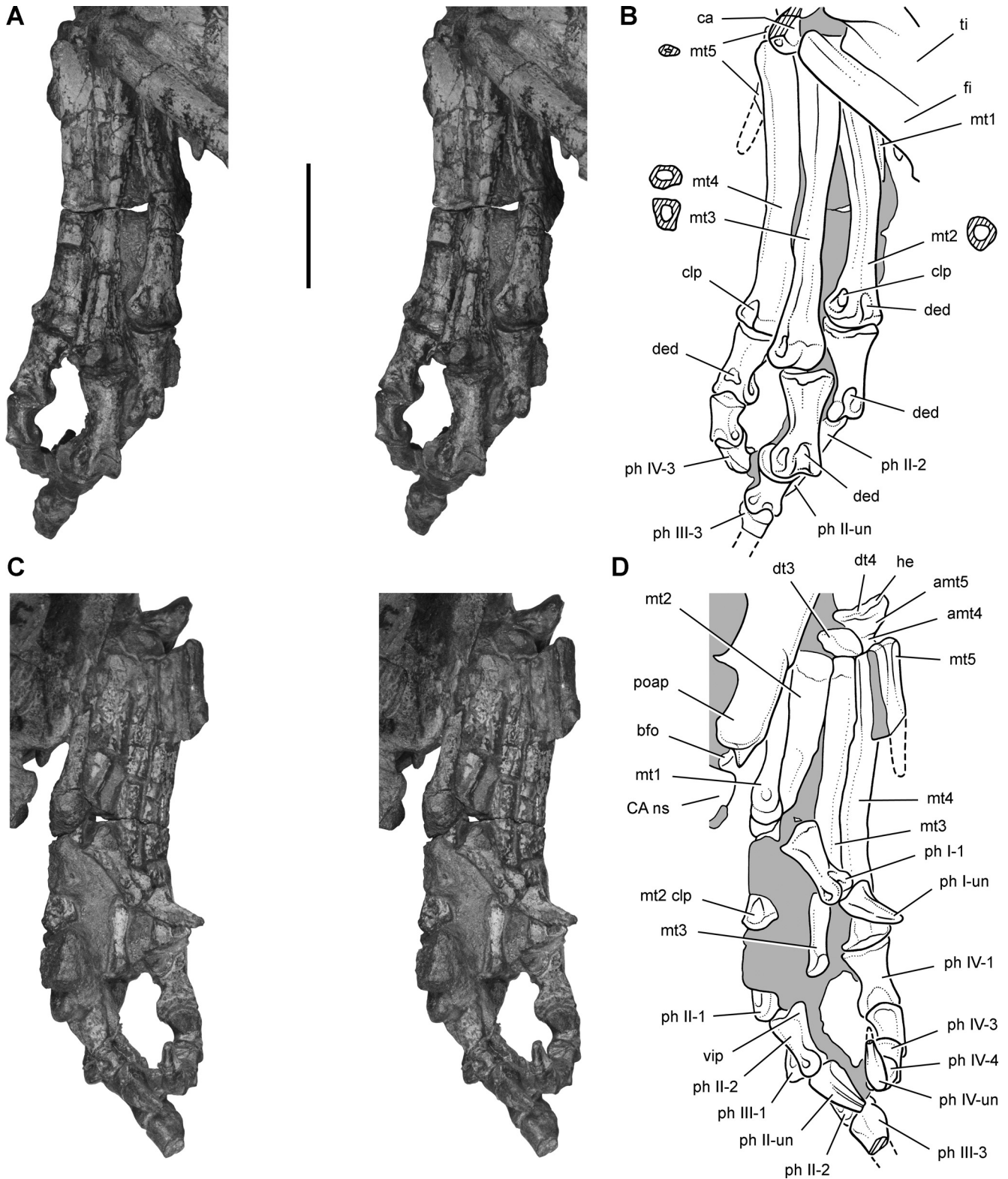


FIGURE 89. Stereopairs (A, C) and drawings (B, D) of right pes of *Eoraptor lunensis* (PVSJ 512) in dorsal (A, B) and ventral (C, D) views. Midshaft cross-sections are shown (in B) for metatarsals 2–5. **Abbreviations:** I–IV, pedal digits I–IV; **amt4, 5**, articular surface for metatarsal 4, 5; **bfo**, brevis fossa; **ca**, calcaneum; **CA**, caudal vertebra; **clip**, collateral ligament pit; **ded**, dorsal extensor depression; **dt3, 4**, distal tarsal 3, 4; **fi**, fibula; **he**, heel; **mt1–5**, metatarsals 1–5; **ns**, neural spine; **ph**, phalanx; **poap**, postacetabular process; **ti**, tibia; **un**, ungual; **vip**, ventral intercondylar process. Dashed line indicates a missing margin; hatching indicates a broken surface; shading indicates matrix. Scale bar equals 3 cm.

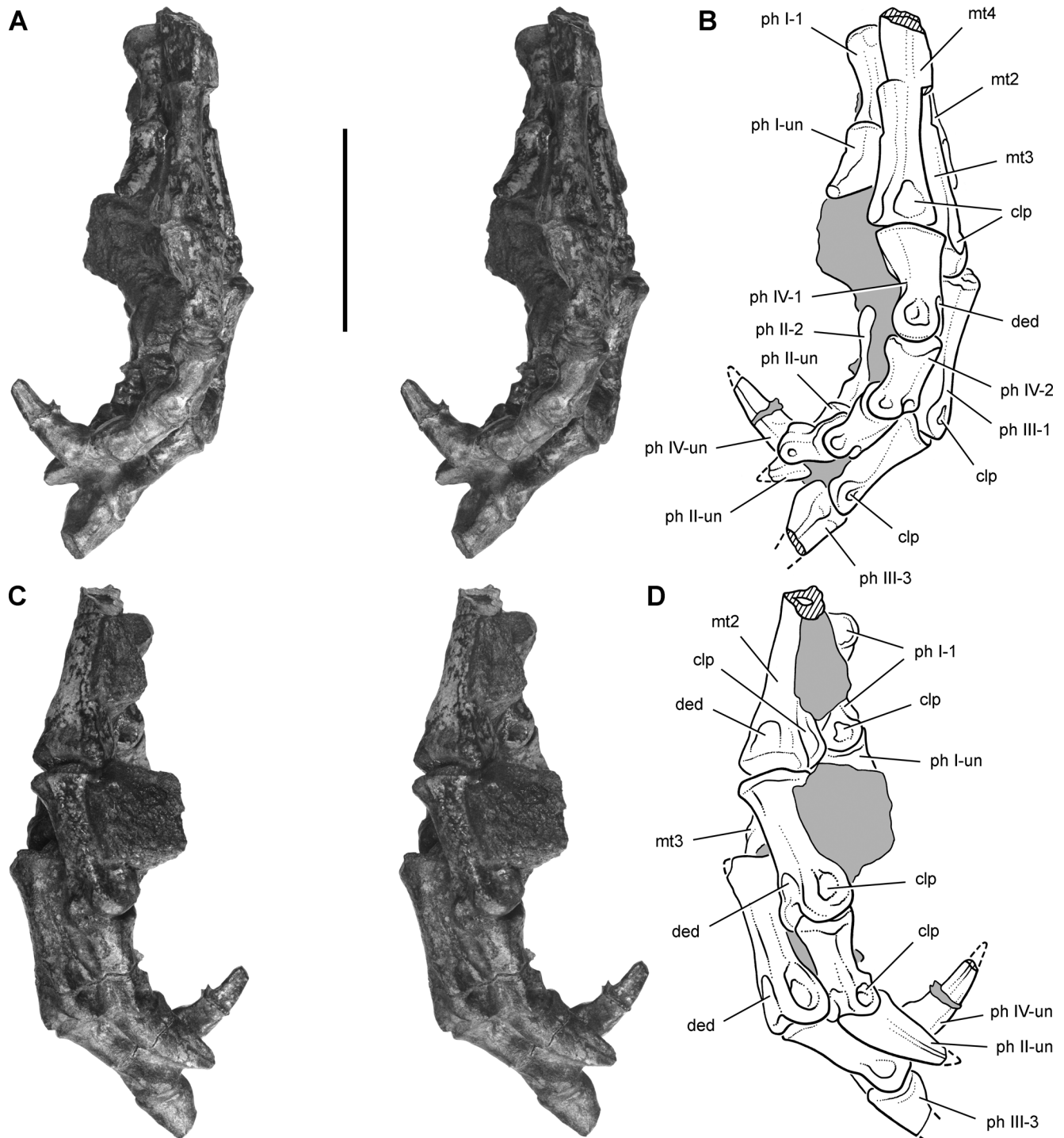


FIGURE 90. Stereopairs (A, C) and drawings (B, D) of right pedal phalanges of *Eoraptor lunensis* (PVSJ 512) in lateral (A, B) and medial (C, D) views. **Abbreviations:** I–IV, pedal digits I–IV; **clp**, collateral ligament pit; **ded**, dorsal extensor depression; **mt2–4**, metatarsals 2–4; **ph**, phalanx; **un**, unguis. Dashed line indicates a missing margin; hatching indicates a broken surface; shading indicates matrix. Scale bar equals 3 cm.

*Saturnalia* (Langer, 2003). Much of the proximal one-half of the bone (Fig. 89) is transversely compressed and articulates against the shafts of adjacent metatarsals. The base of the bone, however, appears to be quite deep, slightly deeper than broad (Fig. 91). The

distal one-half becomes dorsoventrally compressed (Figs. 89, 90). Subtle curvature in the shaft and the precise orientation of the distal condyles cannot be determined because of postmortem crushing. The distal ginglymus is asymmetrical as in metatarsal 1, with a

TABLE 11. Measurements (in mm) of the pes of *Eoraptor lunensis* (PVSJ 512).

Bone	Maximum length
Digit I	
Metatarsal 1	45
Phalanx 1	21
Ungual	15
Digit II	
Metatarsal 2	72
Phalanx 1	25
Phalanx 2	19
Ungual	17
Digit III	
Metatarsal 3	81
Phalanx 1	27
Phalanx 2	22
Phalanx 3	18
Ungual	(18)
Digit IV	
Metatarsal 4	74
Phalanx 1	18
Phalanx 2	14
Phalanx 3	12
Phalanx 4	11
Ungual	16L
Digit V	
Metatarsal 5	35L

Measurements are from the right side except as indicated otherwise (L, left). Ungual length is measured perpendicular to a chord across the proximal articular end. Parentheses indicate estimated measurement.

larger lateral condyle that extends farther distally. The lateral collateral ligament pit is considerably more deeply incised than the medial pit. The dorsal extensor depression is shallow as in *Saturnalia*, rather than the incised arcuate trough that occurs in *Herrerasaurus*.

Metatarsal 3, the longest metatarsal (Figs. 89, 91), measures 53% of the length of the tibia, which is indistinguishable from the proportions in *Saturnalia* (54%; Langer, 2003) and slightly greater than that in *Herrerasaurus* (48%) (Table 13). The transversely compressed proximal half of the bone is deeper dorsoventrally than the other metatarsals with subequal dorsal and ventral widths, as in *Herrerasaurus* (PVSJ 373). It has a flat articular surface for metatarsal 4. In the right metatarsus, the long axis of the shaft of metatarsal 3 appears to curve slightly laterally, as in *Herrerasaurus* (PVSJ 373). The distal end shows the same asymmetry as in metacarpals 1 and 2, namely that the lateral condyle extends farther distally than the medial condyle and is slightly broader, as in *Saturnalia* (Langer, 2003) and *Herrerasaurus* (PVSJ 373). Unlike metatarsals 1 and 2, however, the condyles and collateral ligament pits are subequal in size.

Metatarsal 4 is slightly longer than metatarsal 2 (measuring 91% of the length of metatarsal 3) (Figs. 89, 91). The subtriangular proximal end has medial, dorsal, and ventral surfaces. The proximal third of the shaft is flattened for contact with metatarsal 3. The dorsal surface of the proximal end is broader transversely than in other metatarsals. The ventral surface lies adjacent to the shaft of metatarsal 5 but does not form an articulation with it. The shaft is bowed slightly laterally, remaining dorsoventrally compressed throughout its length. The distal condyles are also broader than deep, a primitive proportion also present in *Herrerasaurus* (Novas, 1994). The asymmetry of the distal end is opposite that in metatarsals 1–3; the medial condyle is larger and extends farther distally than the lateral condyle. The ventral edge of the lateral condyle projects laterally, broadly exposing the lateral collateral ligament pit in dorsal view. Medial and lateral collateral ligament

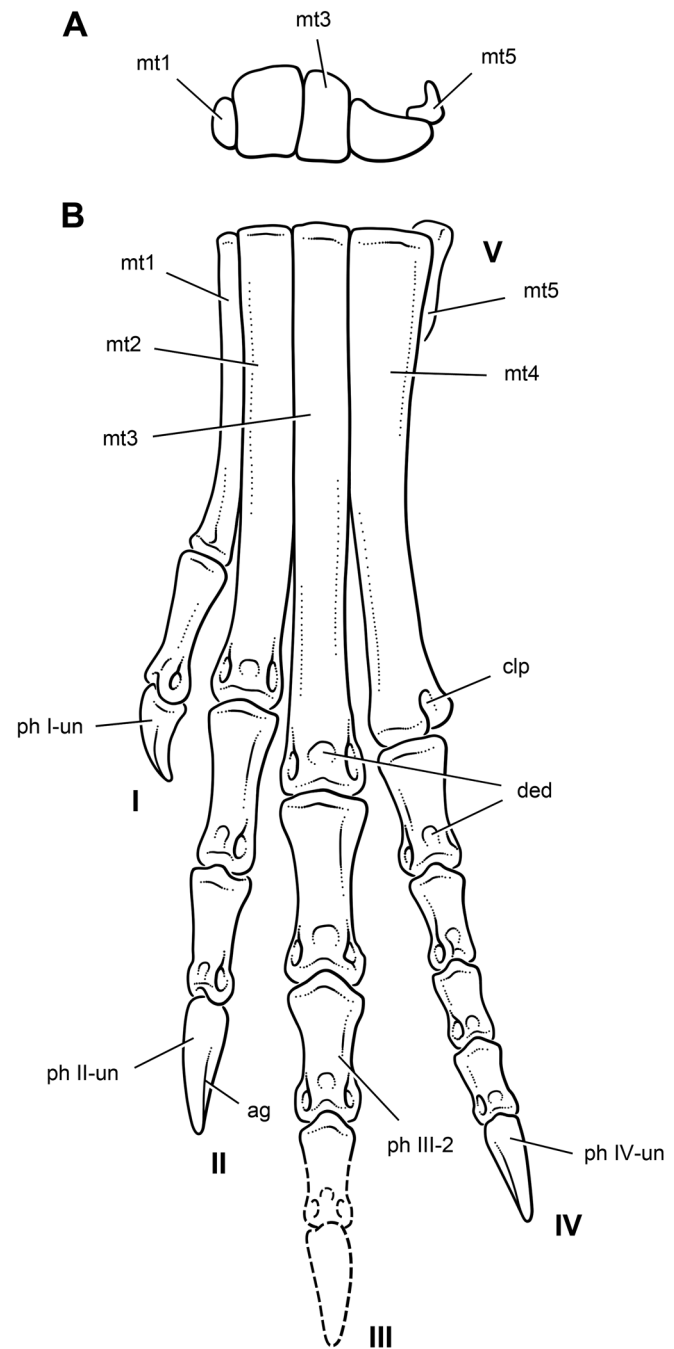


FIGURE 91. Reconstruction of the left pes of *Eoraptor lunensis* (PVSJ 512). **A**, metatarsals 1–5 in proximal view. **B**, pes in dorsal view. **Abbreviations:** I–V, pedal digits I–V; **ag**, attachment groove for unguis sheath; **clp**, collateral ligament pit; **ded**, dorsal extensor depression; **mt1–5**, metatarsals 1–5; **ph**, phalanx; **un**, unguis. Dashed lines indicate bones not preserved in either right or left pes.

pits are developed equally, and no dorsal extensor depression is visible.

Metatarsal 5 is the shortest metatarsal (43% of the length of metatarsal 3), with a relative length similar to that in *Saturnalia* (45%; Langer, 2003) (Figs. 89, 91). Its full length is preserved on

TABLE 12. Maximum length (in mm), comparative ratios of metacarpals 3–5, and manual phalangeal formula in *Eoraptor lunensis* (PVSJ 512), *Eodromaeus murphi* (PVSJ 562), *Herrerasaurus ischigualastensis* (Sereno, 1994), *Coelophysis bauri* (MCZ 4329), *Massospondylus carinatus* (Cooper, 1981), *Adeopapposaurus* (Martínez, 2009), *Lesothosaurus diagnosticus* (Sereno, 1991), *Heterodontosaurus tucki* (Santa Luca, 1980), and *Camptosaurus dispar* (Gilmore, 1909).

Taxon	mc3	mc4	mc5	mc4/3	mc5/3	Phalangeal formula
<i>Eoraptor lunensis</i>	21	16	10	0.76	0.48	2*-3*-4*-(1)-0
<i>Eodromaeus murphi</i>	28	21	10	0.75	0.36	2*-3*-4*-1-1
<i>Herrerasaurus ischigualastensis</i>	62	33	15	0.53	0.24	2*-3*-4*-1-0
<i>Coelophysis bauri</i>	105	68	—	0.65	—	2*-3*-4*-1-X
<i>Massospondylus carinatus</i>	(49)	(44)	(27)	0.90	0.55	2*-3*-4*-3-2
<i>Lesothosaurus diagnosticus</i>	13	9	5	0.69	0.39	2*?-?-?-1
<i>Heterodontosaurus tucki</i>	21	15	8	0.75	0.38	2*-3*-4*-2-1
<i>Camptosaurus dispar</i>	76	60	40	0.79	0.53	2*-3*-4*-2-1

Metacarpal measurements for *Massospondylus* are estimated from Cooper (1981:fig. 35). Parentheses indicate estimated measurement; dash indicates unknown measurement. **Abbreviations:** \*, terminal phalanx is an ungual; **mc3–5**, metacarpals 3–5; **X**, digit absent (i.e., metacarpal and phalanges absent).

the left side, although the form of the proximal end is better shown on the right side. The proximal end is 'L'-shaped, composed of a broad, dorsoventrally compressed main shaft and a narrow lateral flange that tapers distally and disappears at midshaft. The proximal articular surface is confined to the main shaft, which is beveled medioventrally and articulates against a trough on the lateral side of the distal tarsal 4. The shaft narrows in width from midshaft, which is dorsoventrally compressed, to the distal end, which is cylindrical.

**Pedal Phalanges**—The phalangeal formula of the pes is 2\*-3\*-4\*-5\*-0 (Fig. 91). The ungual of pedal digit III is the only phalanx missing on both sides. The absence of phalanges in pedal digit V is based on the left side, where metatarsal 5 is complete and articulated; the distal end of the right metatarsal 5 is broken away (Fig. 89). A single rudimentary phalanx is present in pedal digit V in *Herrerasaurus* and in some other saurischians (e.g., *Plat-*

*teosaurus*; Huene, 1926b), and it is possible that a similar small phalanx was originally present in *Eoraptor*.

Except for the ungual in pedal digit IV and probably the ungual in digit III, phalangeal length decreases distally within pedal digits I–IV (Fig. 92; Table 11). The non-ungual pedal phalanges have slightly deeper proportions and narrower midshafts than in *Herrerasaurus* (PVSJ 373), which appears to be an allometric consequence of larger body size in *Herrerasaurus* and more so in *Allosaurus* (Madsen, 1976:pl. 54). The transverse width of the proximal and distal ends are subequal, except for the proximal phalanx of pedal digit I, which is narrower distally.

The proximal phalanges in pedal digits II–IV are noticeably more robust than succeeding non-ungual phalanges (Figs. 89–92). Their proximal articular ends are deeper dorsoventrally than broad transversely. In pedal digit I, the subtriangular base of phalanx 1 is deeper than broad in *Eoraptor*, whereas the opposite is

TABLE 13. Skull and long bone lengths (in mm, upper part of table) and limb proportions (in%, lower part of table) of *Eoraptor lunensis* (PVSJ 512), *Saturnalia tupiniquim* (MCP 3844-PV; Langer, 2003; Langer et al., 2007), *Adeopapposaurus mognai* (Martínez, 2009), *Eodromaeus murphi* (Martínez et al., 2011), *Herrerasaurus ischigualastensis* (Sereno, 1994), and *Heterodontosaurus tucki* (Sereno, 2012).

Measure or ratio	<i>Eoraptor</i>	<i>Saturnalia</i>	<i>Adeopapposaurus</i>	<i>Herrerasaurus</i>	<i>Eodromaeus</i>	<i>Heterodontosaurus</i>
Skull <sup>a</sup>	114	—	165	282 <sup>e</sup>	(120)	115
Humerus	85	98 <sup>d</sup>	167	(175)	85	83
Radius	63	61	106	153	64	58
Metacarpal 3	21	—	44	62	28	22
Femur	152	155	227	345	160	112
Tibia	156	158	210	315	165	145
Metatarsal 3	81	84	153	165	(100)	68
Humerus/forelimb <sup>b</sup>	50%	—	53%	45%	48%	51%
Radius/forelimb	37%	—	33%	39%	36%	36%
Metacarpal 3/forelimb	12%	—	14%	16%	16%	14%
Tibia/femur	103%	102%	93%	91%	106% <sup>f</sup>	130%
Metatarsal 3/femur	53%	54%	67%	49%	(63%)	61%
Femur/hind limb <sup>c</sup>	39%	39%	39%	42%	38%	35%
Tibia/hind limb	40%	40%	36%	38%	39%	45%
Metatarsal 3/hind limb	21%	21%	26%	20%	24%	21%
Humerus/femur	56%	63%	74%	51%	53%	74%
Forelimb/hind limb	43%	—	54%	47%	42%	50%

Parentheses indicate estimate. Measurements represent the average of right and left long bone lengths when both are available.

<sup>a</sup>Skull length is measured between the anterior tip of the premaxilla and posterior extremity of the occipital condyle.

<sup>b</sup>Forelimb length equals sum of humerus, radius, and metacarpal 3.

<sup>c</sup>Hind limb length equals sum of femur, tibia, and metatarsal 3.

<sup>d</sup>Humerus length is from the similar-sized paratypic specimen (MCP 3845-PV).

<sup>e</sup>Skull length is based on the comparably sized specimen PVSJ 407, because the skull is not preserved in the specimen with the most complete long bones (PVSJ 373).

<sup>f</sup>Average of 103% and 109%, based on PVSJ 560 and 562, respectively.

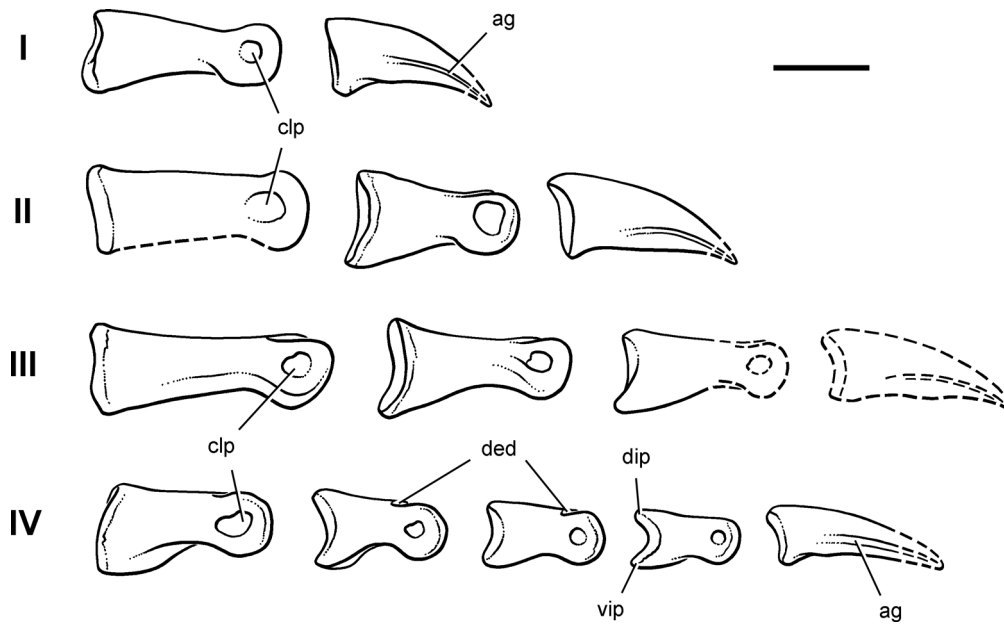


FIGURE 92. Right pedal phalanges of *Eoraptor lunensis* (PVSJ 512) in exploded lateral view. **Abbreviations:** I–IV, pedal digits I–IV; **ag**, attachment groove for unguis; **clp**, collateral ligament pit; **ded**, dorsal extensor depression; **dip**, dorsal intercondylar process; **vip**, ventral intercondylar process. Dashed line indicates a missing margin. Scale bar equals 1 cm.

true in *Herrerasaurus* (PVSJ 373). This proportional difference is not simply an allometric consequence of larger body size in *Herrerasaurus*, because *Allosaurus* has intermediate (subequal) proportions (Madsen, 1976) at a considerably larger body size. The distal condyles of this phalanx are rotated such that the medial collateral ligament pit is broadly exposed in dorsal view when the major axis of the proximal end is held vertically. This rotation, which directs the unguis more posteriorly than laterally, is opposite that in metatarsal 1, in which the medial collateral ligament pit faces ventrally. The same torsion is present in phalanx 1 of pedal digit I in *Herrerasaurus* (Novas, 1994:410). The distal ginglymus is unequally divided; the lateral distal condyle is broader and more rounded than the medial as in *Herrerasaurus* (PVSJ 373; contra Novas, 1994:410).

The length of phalanx 1 of pedal digit I is proportionately the same in *Eoraptor* and *Herrerasaurus* (29% and 30%, respectively, of the length of metatarsal 2) (Fig. 89). However, because metatarsal 1 is more than 5% shorter in *Eoraptor* as described above, the joint between the proximal phalanx and unguis is more proximally located. In *Eoraptor*, this joint is positioned proximal to the end of metatarsal 2, whereas in *Herrerasaurus* it is coincident with the distal end and would place the unguis closer to, and perhaps lightly in contact with, the substrate. In *Eoraptor*, the unguis of pedal digit I could not have effectively engaged the substrate during locomotion. In both cases, nonetheless, pedal digit I is located too far proximally to have borne significant weight.

Except in phalanx 1 of pedal digit I, there is no development of ventral intercondylar processes among the proximal phalanges. Dorsal intercondylar processes are rudimentary as well, although distal extensor depressions are marked particularly in the proximal phalanges. The proximal articular surfaces of the proximal phalanges in pedal digits II–IV are broader than deep, especially so in pedal digits III and IV (Figs. 89, 90). Although in theropods phalanx 1 of pedal digit III always has a subrectangular proximal articular surface (modified in deinonychosaurids by strong

intercondylar processes; Ostrom, 1969:fig. 75), the same surface in pedal digit IV in ceratosaurians and tetanurans is deeper than broad to accommodate the narrowed, subtriangular distal articular surface of metatarsal 4 (e.g., *Liliensternus*, Huene, 1932; *Allosaurus*, Madsen, 1976). In *Eoraptor* and *Herrerasaurus*, in contrast, the proportions of the distal end of metatarsal 4 and proximal end of phalanx 1 remain broader than deep.

Except in phalanx 1 of pedal digit I, deep dorsal extensor depressions are present dorsal to the distal condyles (Figs. 89–91). The distal ginglymi are slightly asymmetrical, following closely similar asymmetries in *Herrerasaurus* (PVSJ 373). In phalanx 1 of pedal digits II and III, the lateral distal condyle is broader and extends farther distally than the medial condyle. In phalanx 1 of pedal digit III, the lateral condyle is canted away from the vertical, exposing the lateral collateral ligament pit in dorsal view (also present in *Allosaurus*; Madsen, 1976:pl. 53). In phalanx 1 of pedal digit IV, a reverse asymmetry is present in which the medial distal condyle is broader and extends slightly farther distally. These asymmetries have the effect of spreading the toes from the center of the metatarsus and positioning a greater area of condylar surface perpendicular to the axis of the distal phalanges.

The intermediate phalanges in pedal digits II–IV are more symmetrical than the proximal phalanges (Figs. 89–92). The dorsal intercondylar process is better formed than the ventral process. The ginglymi are well developed and appear to be symmetrical. All have dorsal extensor depressions and medial and lateral collateral ligament pits of approximately equal depth.

The pedal unguis (Figs. 91, 92), like the manual unguis, are noticeably less recurved than common among theropods such as *Herrerasaurus* (PVSJ 373), *Eodromaes* (PVSJ 560), and *Allosaurus* (Madsen, 1976). When the proximal articular surface is oriented along a vertical axis, the distal tip of the unguis is not positioned very far ventrally. In *Herrerasaurus* (PVSJ 373) or *Allosaurus* (Madsen, 1976), in contrast, the tip of the unguis is displaced ventrally beneath the base by a distance greater than the

TABLE 14. Measurements (in mm) of the right manus of *Lesothosaurus diagnosticus* (NHMUK RU B17).

Bone	Maximum length
Digit I	
Metacarpal 1	8.9*
Phalanx 1	6.0*
Ungual	5.0
Digit II	
Metacarpal 2	12.2*
Phalanx 1	5.4
Digit III	
Metacarpal 3	12.1
Phalanx 1	6.3
Phalanx 2	5.3
Digit IV	
Metacarpal 4	9.6*
Phalanx 1	3.9
Phalanx 2	2.2*
Digit V	
Metacarpal 5	4.8
Phalanx 1	1.8

Measurements marked with an asterisk differ from, and supersede, those in Sereno (1991:table 1). Metacarpals 2 and 3 were identified in Sereno (1991) as metacarpals 3 and 2, respectively.

vertical depth of the base. All of the unguals, including the unguual of pedal digit I, lack flexor tubercles ventral to the proximal articular surface. The ventral surface is flat, and the cross-section at midlength is subtriangular. The unguual of pedal digit III is not preserved; it was probably slightly longer than the unguuals of pedal digits II and IV, or about 18 mm in length.

## DISCUSSION

### Autapomorphies of *Eoraptor lunensis*

Below we list seven features that we regard as diagnostic (autapomorphic) for *Eoraptor*, because they are generally absent in other basal dinosaurs. All of these features are treated in the description above.

- (1) Premaxilla with slender posterolateral process with distal expansion. In *Eoraptor*, the posterolateral process of the premaxilla is a ribbon-shaped bone that terminates in a pointed tongue-shaped lobe (Figs. 22, 40). The form of this process is unique among dinosaurs.
- (2) Deep lateral nasal shelf overhanging antorbital fossa. Although the nasal usually forms a prominent edge along the dorsal margin of the antorbital fossa in saurischians, in *Eoraptor* the nasal is further developed as a thin horizontal shelf that overhangs the antorbital fossa (Fig. 20). This was originally preserved on both sides in the holotypic skull (PVSJ 512), but some damage has occurred to one of the edges after it was molded. In dorsal view, the lateral margin of the nasal is convex (Figs. 14, 15, 41). Such a strongly projecting nasal margin is exceptional among saurischians, although data are currently lacking from closely related basal sauropodomorphs (e.g., *Panphagia*, *Pampadromaeus*, *Saturnalia*).
- (3) Pterygoid-ectopterygoid synovial joint on posterior margin of palate. In *Eoraptor*, the pterygoid has a robust lateral process that extends along the posterior margin of the palate, terminating in an articular head that fits into a socket on the ectopterygoid (Figs. 29, 30). Such an articulation has not been reported in other dinosaurs, in which the pterygoid and ectopterygoid contact one another along butt or scarf joints. Re-

cently, the pterygoid of the closely related sauropodomorph *Pampadromaeus* has been figured and may have a similar pterygoid process (Cabeira et al., 2011:fig. 2g). If that proves to be the case, this feature may unite these genera or a subset of basal sauropodomorphs.

- (4) Narrow premaxilla-maxilla diastema (rounded posterior margin on premaxilla, small first maxillary tooth). In *Eoraptor*, a short diastema is present between premaxillary and maxillary tooth rows due to a short edentulous margin at the anterior end of the maxilla under the subnarial foramen (Figs. 20, 35). The first tooth in the maxilla is shorter than adjacent teeth in the premaxilla and maxilla. The third dentary tooth that opposes the diastema is slightly enlarged. Some functional differentiation is strongly suggested by the diastema and the change in crown size between premaxillary and maxillary tooth rows (see below, Form and Function, Dental Specialization).
- (5) Maxillary crowns with a prominent lateral eminence or crest. All maxillary crowns in *Eoraptor* have a prominent linear eminence, or rounded crest, on the labial side of the crown (Figs. 20, 36). A discrete linear crest of this prominence is not present in other basal sauropodomorphs (*Panphagia*, *Saturnalia*, *Pampadromaeus*) or basal theropods (*Herrerasaurus*, *Eodromaeus*, *Tawa*). A linear crest of this sort is not known in sauropodomorphs and basal ornithischians (*Pisanosaurus*, Bonaparte, 1969; *Lesothosaurus*, Sereno, 1991; *Huayangosaurus*, Sereno and Dong, 1992).
- (6) Extreme hollowing of the axial column. In *Eoraptor*, all of the long bones of the skeleton, as well as the shafts of the ischium, ribs, and chevrons, are hollow. Although marked hollowing of at least the long bones is common to all theropods, hollowing of the axial column is carried to an extreme in *Eoraptor*. The walls of the centra and neural arches are very thin, in some places as thin as 0.5 mm. The hollow space in the neural arch and centrum is not partitioned or filled with cancellous bone, has no external communicating diverticuli, and therefore was not pneumatic.
- (7) Accessory prezygapophyseal process in middle cervical vertebrae. At least some of the middle cervical vertebrae in *Eoraptor* have a small accessory process on the medial side of the prezygapophysis (Fig. 44). It articulates with the medial portion of the postzygapophysis of the next anterior vertebra. This accessory articular process, the function of which remains obscure, has not been reported elsewhere among dinosaurs.

### Phylogenetic Relationships

*Eoraptor lunensis* was placed by Sereno et al. (1993) and Sereno (1999) as the basal member of Theropoda on the basis of phylogenetic analyses that identified synapomorphies uniting *Eoraptor* with *Herrerasaurus* and other theropods. In the years following the debut of *Eoraptor*, opinion varied regarding the phylogenetic interpretation of *Eoraptor*. In a short note, Padian and May (1993) suggested that neither *Eoraptor* nor *Herrerasaurus* are theropods (or possibly even dinosaurs), although there was no analysis or supporting character evidence. Other authors examined the fossil material and drew conclusions similar to those we suggested in 1993—that *Eoraptor* was a basal theropod (Novas, 1994; Tykoski, 2005; Nesbitt et al., 2009; Ezcurra, 2010; Nesbitt, 2011). An opposing camp emerged with the view that *Eoraptor* was a more basal saurischian, outside both Theropoda and Sauropodomorpha (Langer, 2004; Martínez and Alcober, 2009; Brusatte et al., 2010; Langer et al., 2010). We now regard *Eoraptor* as a basal sauropodomorph (Martínez et al., 2011), and there are important events that led us to this new understanding.

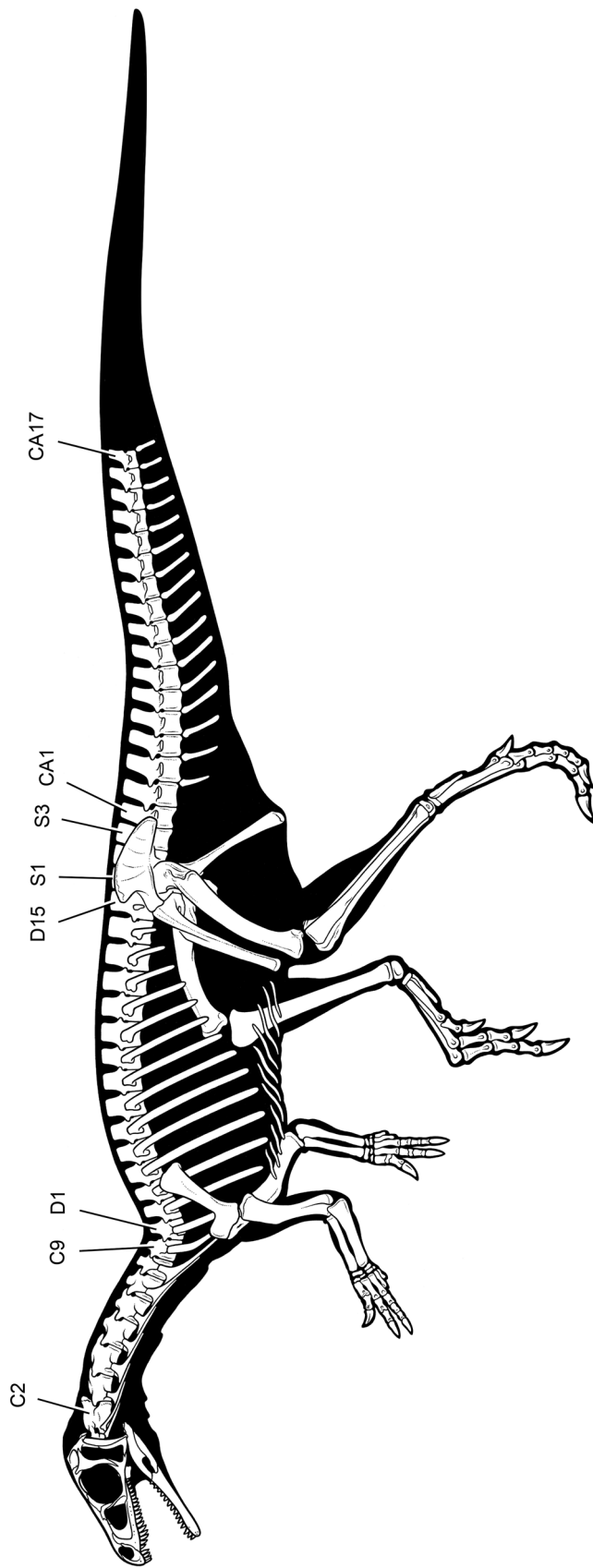


FIGURE 93. Skeletal silhouette of *Eoraptor lunensis* based principally on the holotypic skeleton (PVSJ 512). Estimated tail length distal to caudal vertebra 17 is based on the proportions of three mid-caudal vertebrae in the closely related basal sauroptomorph *Panphagia protos* (Martínez and Alcober, 2009;fig. 6H). **Abbreviations:** C2, 9, cervical vertebra 2, 9; D1, 15, dorsal vertebra 1, 15; S1, 3, sacral vertebra 1, 3; CA1, 17, caudal vertebra 1, 17.

Firstly, the material basis for phylogenetic assessment has changed markedly (Sereno and Martínez, in review). When originally described in 1993, the holotypic specimen of *Eoraptor* (PVSJ 512) was only partially exposed. Important referred specimens that include well-preserved proximal tarsals had yet to be prepared and identified (PVSJ 559, 862; Table 1). Isolated bones thought to pertain to *Eoraptor* are now known to belong to a similar-sized contemporary—a basal theropod later named *Eodromaeus murphi*. It was not until excellent remains of this dinosaur were discovered in 1996 and prepared several years later that its distinction from *Eoraptor* was revealed (Martínez et al., 2011). In the 20 years since the discovery of *Eoraptor*, the dinosaurian fauna in the Cancha de Bochas Member of the Ischigualasto Formation is now understood to include several small-bodied basal saurischians (*Eoraptor*, *Panphagia*, Martínez and Alcober, 2009; *Chromogisaurus*, Ezcurra, 2010; *Eodromaeus*, Martínez et al., 2011).

Secondly, two key discoveries came to light while working on the holotypic skeleton of *Eoraptor* for this monograph. We discovered that, prior to its final fossilization, slight disarticulation of digit I in the well-preserved right manus of *Eoraptor* (Fig. 69) had obscured a remarkable derived feature known only among large-bodied basal sauropodomorph dinosaurs (Sereno, 2007b)—the medial rotation in the shaft of proximal phalanx of manual digit I that directs the tip of the unguis inward (Fig. 73D). The rotation of this digit in natural articulation was removed incidentally during burial (Fig. 69). We reassembled manual digit I in natural articulation using bone casts as part of our reinterpretation of the relationships of *Eoraptor* (Martínez et al., 2011).

We also realized that the lower jaws of *Eoraptor* seemed slightly short relative to the upper jaws (Figs. 16, 17) and that the anterior end of the dentaries also had vascular openings (Fig. 23) similar to those of many larger-bodied basal sauropodomorphs thought to have a small keratinous lower bill (Sereno, 2007b; Martínez, 2009). By preparing between the premaxillary teeth, we were able to verify evidence from the computed tomography (CT) data that the first dentary tooth in *Eoraptor*, as in *Panphagia* (Martínez and Alcober, 2009), is inset a short distance from the anterior end of the dentary.

Thirdly, the discovery of *Panphagia* in Ischigualasto (Martínez and Alcober, 2009) and *Saturnalia* in southeastern Brazil (Langer et al., 1999, 2007; Langer, 2003) highlighted postcranial features in the girdles and hind limb shared with later sauropodomorphs. The new material also documented the relatively short length of the centra in the distal half of the tail, in contrast to the condition in the contemporaneous theropods *Herrerasaurus* (Novas, 1994) and *Eodromaeus* (Martínez et al., 2011). The striking similarities between *Eoraptor* and *Panphagia* and *Saturnalia* became apparent. More recently, the discovery in southeastern Brazil of well-preserved cranial remains of *Pampadromaeus* (Cabeira et al., 2011) has extended the striking similarities between *Eoraptor* and Brazilian genera to include the skull.

We reconsider the relationships of *Eoraptor* and other basal dinosaurs elsewhere (Sereno and Martínez, in review). Evidence is mounting that *Eoraptor* and several other taxa from the Ischigualasto and Santa Maria formations (*Panphagia*, *Saturnalia*, *Pampadromaeus*) are basal sauropodomorphs.

### Form and Function

**Cranial Pneumaticity**—The antorbital fossa in *Eoraptor* appears to have been occupied by one large air sac emanating from the nasal cavity, as in living birds (Witmer, 1990). The maxilla and lacrimal form most of the osseous medial wall of the fossa, which is smooth and bounded by a prominent external rim (Figs. 20, 40). The dorsal portion of this rim is particularly pronounced, with the

nasals extending laterally as a sharp-edged, horizontal shelf that overhangs the antorbital fossa. In dorsal view, the convex contour of the nasal shelf (Figs. 14, 15, 41) resembles the comparable margin in the snout of *Plateosaurus* (Sereno, 2007b). The posterodorsal corner of the antorbital fossa, which is slightly invaginated, is formed by the lacrimal, with a small contribution from the anterior ramus of the jugal (Figs. 24, 40). A much broader portion of the osseous medial wall of the fossa is formed by the anterior ramus of the palatine, the everted ventral rim of which appears to have cupped the edge of the pneumatic sac (Fig. 21).

Unlike most theropods, there is no evidence in *Eoraptor* of any accessory diverticuli into the maxilla anteriorly (Fig. 22), the lacrimal dorsally (Fig. 25), the jugal posteriorly (Fig. 24), or the palatine medially (Fig. 21). Recently, a fossa of some depth was described in the maxilla at the anterior end of the antorbital fossa in the closely related Brazilian sauropodomorph *Pampadromaeus* (Cabeira et al., 2011:fig. 2). In a similar position in the maxilla, a small fenestra was described recently in the basal theropods *Herrerasaurus* (Sereno, 2007a) and *Eodromaeus* (Martínez et al., 2011), although another basal theropod shows no discrete fossa or fenestra in this location (*Tawa*; Nesbitt et al., 2009). Similarly, a small blind depression was recently described in the maxilla of the early ornithischian *Heterodontosaurus* (Sereno, 2012), although other basal ornithischians show no evidence of a depression in this region (*Lesothosaurus*; Sereno, 1991). These openings or fossae correspond in location with the promaxillary diverticulum common among neotheropods. Whether they are homologous or not is an open question, given their variable expression and distribution at the base of Dinosauria.

In theropods, additional pneumatic spaces are present in the quadrate and articular (diverticulae of the middle ear sac in living birds), the basisphenoid, and the ectopterygoid (diverticulae of the nasopharynx). Because the quadrate and articular are in contact and the distal end of the quadrate is not exposed in anterior view, the pneumaticity of these bones cannot be evaluated. In ventral view, the basisphenoid is gently concave, with a small pit near its junction with the basioccipital. There is no development of a deep median fossa, as characterizes *Eodromaeus* (Martínez et al., 2011) and most neotheropods. Other portions of the braincase, such as the parasphenoid, are hidden by matrix or broken. There is no development of an invaginated fossa on the ectopterygoid, as is well developed in many tetanuran theropods.

In summary, cranial pneumaticity in *Eoraptor* appears to be limited to a simple, single antorbital diverticulum of the nasal cavity, as is typical of most basal sauropodomorphs and ornithischians. None of the accessory diverticuli of the antorbital sinus that characterize theropods is present in *Eoraptor*.

**Cranial Kinesis**—Distortions of the cranial skeleton during feeding in living vertebrates are reflected in the form and position of osseous joints within the skull (Versluys, 1910, 1912). Despite a literature rich in descriptive models, accurate measurement of cranial distortion in living animals has been achieved only recently (Smith and Hylander, 1985; Condon, 1987; Iordansky, 2011). In the Nile monitor (*Varanus*), it now is clear that cranial kinesis does occur during feeding, with several degrees of angular rotation about several joints in the skull (Condon, 1987). The timing of these movements suggests that they play a role in seizing, subduing, and swallowing prey (Frazzetta, 1962, 1986; Bolt and Ewer, 1964; Rieppel, 1979), rather than serving only as a shock absorbing mechanism during the strike.

Proposed models for cranial kinesis in dinosaurs have recently come under criticism for lack of sufficient lines of evidence, including integrated kinematic linkages within the cranium and evidence of musculature that could have driven or controlled intracranial movement (Holliday and Witmer, 2008). This long-overdue

critique has yet to address kinesis within the lower jaws, where the most interesting joint morphology is located in *Eoraptor* (Fig. 33).

In the cranium of *Eoraptor*, most of the synovial joints are fairly typical and plesiomorphic for dinosaurs (Holliday and Witmer, 2008). The quadrate head inserts into a deep cup on the ventral aspect of the squamosal (Fig. 27), forming a joint that is disarticulated on the right side of the cranium (Fig. 26). In *Eoraptor*, the cotylus would have covered the entire head of the quadrate, which has the usual smooth and bounded articular surface of a synovial joint. In other basal dinosaurs, the squamosal cotylus is not as deep as in *Eoraptor*. In *Herrerasaurus*, for example, a portion of the quadrate head is exposed in lateral view (Sereno and Novas, 1994). There is no evidence, therefore, to suggest significant movement at the squamosal-quadrate joint ('dorsal quadrate joint' in lepidosaur models).

The basiptyergoid processes are unusually robust in *Eoraptor*. They project as stout columns that are expand slightly toward their articular ends (Figs. 29, 30). These processes are approximately twice the diameter and length of those of in *Herrerasaurus* and *Lesothosaurus*, relative to the length of the braincase or skull (Sereno, 1991; Sereno and Novas, 1994) and may have provided extra support to the posterior palate, which has broad mandibular flanges for the attachment of pterygoideus musculature (Fig. 33A, B). They most closely resemble the stout basiptyergoid processes in larger-bodied basal sauropodomorphs, such as *Adeopapposaurus* (Martínez, 2009:fig. 10). By contrast, the basiptyergoid processes in the similar-sized contemporaneous theropod *Eodromaemus* terminate as expanded, but thin, plates (Martínez et al., 2011).

The posterior margin of the broad, triangular mandibular flange in *Eoraptor* has an unusual pterygoid-ectopterygoid joint (Figs. 29, 30). The pterygoid forms as a robust ventrolaterally projecting strut that expands distally to an articular head lodged in an articular socket in the ectopterygoid. The pterygoid head is smooth and appears to have been enclosed in a synovial capsule, judging from the disarticulated view of the process on the left side of the palate (Fig. 29). *Pampadromaemus* may have had a similar joint in the posterior palate (Cabreira et al., 2011:fig. 2g). The function of this apparently synovial joint on the posterior palate is unknown.

Other articulations within the cranium in *Eoraptor* include tongue-and-groove joints (maxilla-jugal, jugal-quadratojugal, prefrontal-frontal, postorbital-frontal, squamosal-postorbital), scarf joints (lacrimal-prefrontal, jugal-postorbital), squamous joints (nasal-frontal, lacrimal-jugal, quadrate-quadratojugal, pterygoid-quadrate, pterygoid-palatine) (Figs. 10–17), and butt joints (jugal-ectopterygoid, maxilla-palatine). The frontal-parietal suture, which is the 'mesokinetic' hinge in lepidosaur models, is not well preserved (Figs. 14, 15).

The form of most of these sutures is common among theropods across a wide range of body size. Along the ventral margin of the cranium, tongue-and-groove articulations predominate (quadratojugal-jugal-maxilla), suggesting that very minor telescoping may have occurred in the posterior one-half of the skull as described in *Syntarsus* (Raath, 1977:160). Along the dorsal orbital margin, the frontal is notched for the postorbital and slotted for the prefrontal, the functional significance of which remains obscure. A large prefrontal is much more common in basal sauropodomorphs and ornithischians than in theropods, which eventually eliminate the prefrontal as a separate bone (lost or fused to the posterior aspect of the lacrimal).

The potential for kinetic premaxillae in *Eoraptor* (Tykoski, 2005) was an important line of evidence supporting the position of *Eoraptor* within Theropoda (Nesbitt et al., 2009). In the coelophysoids *Dilophosaurus*, *Coelophysus*, and *Syntarsus*, the unusual

overhanging premaxillary dental arcade may not have been anchored immovably to the maxilla (Tykoski, 2005; Sereno, 2012:fig. 91). In those forms, the premaxilla-maxilla articular contact is very reduced laterally, which is indicated by extreme reduction of the premaxillary posterolateral process and an arched diastema that has eliminated the subnarial foramen, whereas interpremaxillary contact is broadened (external nares and narial fossa retracted). In *Eoraptor*, in contrast, the premaxillary posterolateral process is long and slender, the diastema is short and shallow, a subnarial foramen is present between the premaxilla and maxilla for passage of neurovascular structures, and interpremaxillary contact is not expanded (Figs. 23, 35, 40). There is no evidence to suggest kinesis at the anterior end of the snout in *Eoraptor*.

**Intramandibular Kinesis**—An intramandibular joint with dorsal and ventral articulations is present in *Eoraptor* (Sereno, 2007a); the ventral articulation is better exposed (Fig. 33). Although the tapering, tongue-shaped posterior end of the splenial is broken away, its form is shown by the articular trough on the ventromedial edge of the angular. In *Herrerasaurus*, this ventral joint is better developed than in *Eoraptor*, with the tongue-shaped end of the splenial fitted ventrally to the polished hook-shaped anterior end of the angular. Also in *Herrerasaurus*, the dorsal joint between the toothed anterior moiety (dentary, splenial) and bones that compose the remainder of the lower jaw is fully exposed (Sereno and Novas, 1994). This two-part construction of the lower jaw is well known among small- and large-bodied theropods (Brochu, 2002) and may have been managed by spring ligaments rather than muscles (Sampson and Witmer, 2007).

Except for *Eoraptor*, an intramandibular joint has not been described outside Theropoda, if one accepts herrerasaurids as basal theropods. Interestingly, the concavoconvex polarity of the joint differs in the earliest saurischians to exhibit this morphology—*Herrerasaurus* and *Eoraptor*. In the former and its close relative *Staurikosaurus* (P.C.S., pers. observ.), the splenial has a concave surface fitted to a convex surface on the angular. The conformation of these surfaces is reversed in *Eoraptor* and neotheropods.

In *Eoraptor*, the ventral joint is not as well developed as in herrerasaurids or neotheropods (Fig. 33). Nonetheless, the splenial does not contact the angular medially along a broad scarf joint, but rather tapers in width and twists under the angular, its tip residing in a smooth trough on the angular. That trough is slightly dorsoventrally convex, suggesting that whatever intramandibular flexure the ventral joint allowed would have occurred in a vertical plane. It would not have facilitated transverse bending of the mandible to widen the gape as occurs in some snakes (Sereno and Novas, 1994). In *Eoraptor*, the dorsal intramandibular joint between the anterior (dentary, splenial) and posterior (surangular, coronoid, prearticular, angular) moieties is not well exposed laterally. In medial view, its anterior location relative to the ventral joint suggests limited intramandibular flexion (Fig. 33). In theropods with enhanced intramandibular flexion, such as the abelisaurid *Majungasaurus*, dorsal and ventral joints are positioned over one another (Sampson and Witmer, 2007). In addition, the dentary is shortened, the external mandibular fenestra is enlarged, the dorsal joint is reduced to peg-in-socket articulations, and the ventral sliding joint is expanded (Sampson and Witmer, 2007). None of these features is present in *Eoraptor*.

Yet, the form of the ventral joint and the portion of the dorsal joint exposed in medial view suggest limited intramandibular flexion was possible. There is no additional information on the intramandibular joint in available specimens pertaining to *Panphagia*, *Pampadromaemus*, or *Saturnalia*. This condition may be plesiomorphic for Saurischia and subsequently reduced and lost among herbivorous sauropodomorphs and enhanced among carnivorous theropods.

**Dental Specialization**—The dentition in *Eoraptor* has recently been compared with teeth of a similar-sized contemporaneous basal theropod *Eodromaeus*, the carnivorous diet of which is not in dispute (Martínez et al., 2011:fig. 1D, E). The comparison is particularly revealing in terms of crown shape and size and orientation of the marginal ornamentation. In *Eoraptor*, the distal margin of the crown is straight or only slightly concave in labial view, rather than consistently concave and contributing to the recurvature of the crown (Fig. 37). In *Eoraptor*, the marginal ornamentation, particularly that on the mesial margin, resembles ornithischian denticles that project toward the crown apex rather than strictly perpendicular to the crown edge (Fig. 37C). Such ornamentation on the maxillary crowns in *Eoraptor*, which is similar to that of the dentary crowns of *Panphagia* and *Pampadroameus*, suggests a pulping function suitable for plant matter, rather than a meat-cutting function suitable for slicing. Theropod crowns suitable for the latter function tend to be more finely serrate, transversely compressed, and recurved (Martínez et al., 2011:fig. 1D, E). In *Eoraptor*, there are approximately six denticles per millimeter, whereas there are nine serrations per millimeter in *Eodromaeus* (Martínez et al., 2011). The comparison of ornamentation size we regard here as particularly suitable, given the similar body size in *Eoraptor* and *Eodromaeus*.

The first dentary tooth in *Eoraptor*, in addition, is retracted from the anterior end of the dentary, which is marked by a pair of conspicuous neurovascular foramina—features that characterize plant-eating basal sauropodomorphs (Sereno, 2007b; Martínez, 2009). These features and the short length of the lower jaws suggest that there may have been a small keratinous beak at the anterior end of the lower jaws in *Eoraptor* and *Panphagia*. Recently, the closely related basal sauropodomorph *Pampadromaeus* was described as lacking the inset at the anterior end of the tooth row (Cabreira et al., 2011). Close-up images of the anterior end of the dentary, however, suggest that the first alveolus is inset in *Pampadromaeus* as in *Eoraptor*. In *Pampadromaeus*, the first dentary tooth is partially dislodged from its alveolus and shifted mesially, giving the impression that the tooth row extended to the anterior end of the dentary (Cabreira et al., 2011:Suppl. Info.).

Crown recurvature, particularly when weakly expressed as in *Eoraptor*, cannot stand alone as an arbiter of diet. Sauropodomorph and ornithischian herbivores often retain some recurvature in their crowns, especially in the premaxillary series. Likewise, a short upper diastema that opposes a dentary crown does not necessarily indicate carnivorous habits.

Heterodontosaurid ornithischians present some similarities to *Eoraptor* in that both upper and lower teeth are inset from the ends of the jaws and replaced by keratinous beaks. In the case of the lower jaw, a specialized bone (the predentary) supports the beak. Although there is no such specialized bone among basal sauropodomorphs, there is increasing evidence that many have small lower (and upper) beaks to support a cropping or plucking function (Sereno, 2007b; Martínez, 2009). We have yet to discover a carnivorous dinosaur—or for that matter a carnivorous extant lizard—that has retained teeth for predation and that has inset these teeth from the anterior end of the lower or upper jaws (Sereno, 2012). This favors *Eoraptor* as a herbivore.

Crown morphology by itself is not decisive in this case, nor is the presence or absence of palatal teeth, which are now known in both *Eoraptor* and *Eodromaeus*. Claiming that *Eoraptor* might be an omnivore or insectivore at a subadult or adult body length of ca. 1–1.5 m are hypotheses in need of supporting evidence. Dietary inferences, including the proposition of omnivory (Barrett et al., 2011), must be based on a broader array of information tied to extant analogs (Zanno and Makovicky, 2011).

**Hollowing of the Axial Column**—A striking feature of the axial column is the extreme hollowing of the centra and neural arches

that has reduced the external walls of the vertebrae to a thickness of less than 1 mm. The hollowing is accomplished by internal cavities apparently without any pneumatic communication to the exterior of the bone. Non-vertebral elements of the axial skeleton, such as rib and chevron shafts, are solid in many theropods but have central cavities in *Eoraptor*. The function of this extreme skeletal hollowing, comparable to that in any theropod, is unknown. Because *Eoraptor* is among the smallest of dinosaurs, it is difficult to suppose that reduction of skeletal weight as a primary driving factor.

The observed hollowing is very difficult to explain away as an artifact of diagenesis. The spaces and sometimes-uniform wall thicknesses do not appear to be a random artifact or some bone-destroying process, which would likely have created openings to the exterior.

**Axial Column Function**—The cervical centra in basal dinosaurs, such as *Eoraptor* and *Herrerasaurus*, do not have the tightly fitted, concavoconvex articular surfaces present in neotheropods. Judging from the shape of the centra and their preserved articulation, nevertheless, the cervical column in *Eoraptor* followed a sigmoid curve in neutral articulation that elevates the skull significantly above the level of the dorsal column (Figs. 43, 93). Several aspects of the cervical vertebrae suggest that the cervical column was capable of significant dorsoventral and lateral flexion. The low, plate-shaped neural spines in the mid-cervical vertebrae would allow significant dorsoventral flexion by muscles attaching between the neural spines and well-developed epiphyses, as occurs in living birds (principally the longus colli dorsalis muscle: Harvey et al., 1968; Raath, 1977). The zygapophyseal facets in anterior and middle cervical vertebrae are broad, with a shallow inclination (20–30° from the horizontal) that would have permitted extensive lateral flexion (Fig. 43). In this regard, the function of the unique accessory prezygapophyseal process in the middle cervical vertebrae of *Eoraptor* remains unknown. All of the cervical ribs are joined by overlapping spines and rib shafts to form a slender, flexible rod, positioned ventrolateral and parallel to the cervical series. The slender form of the cervical column and its associated ribs (Figs. 49, 60) would have permitted significant dorsoventral and lateral flexion.

Anterior and middle caudal vertebrae have prominent blade-shaped neural spines, substantial transverse processes, and long chevrons, which increase in length in that order in each vertebra (Fig. 59; Tables 5, 6). These processes indicate that the dorsal, lateral, and ventral musculature of the tail was well developed and that significant dorsoventral and lateral excursion of the tail was possible. Because the caudal series is not preserved posterior to the 17th caudal vertebra, it cannot be determined in *Eoraptor* if the distal caudal vertebrae had elongate centra stiffened in articulation by elongate prezygapophyses, as occurs in *Herrerasaurus*, *Eodromaeus*, and nearly all neotheropods. The absence of such distal caudal vertebrae in close relatives (*Panphagia*, Martínez and Alcober, 2009; *Pampadromaeus*, Cabreira et al., 2011) suggests that the tail of *Eoraptor* was similar to that in large-bodied basal sauropodomorphs (Fig. 93)—long and muscular but not stiffened as a narrow beam.

**Forelimb Function**—In general form and proportions, the forelimb of *Eoraptor* closely resembles that in *Saturnalia* (Langer et al., 2007) and large-bodied basal sauropodomorphs, such as *Platiosaurus* (Huene, 1926b). In *Eoraptor*, the forearm was composed of stout long bones with a substantial interosseous gap (Fig. 93), as preserved in articulation in the holotypic skeleton (Fig. 9) and in the basal sauropodomorph *Adeopapposaurus* (Martínez, 2009:fig. 18K, L). In *Herrerasaurus* (Sereno, 1994), *Eodromaeus* (Martínez et al., 2011), and other theropods, in contrast, the forearm bones are appressed along their shafts, ostensibly as an enhancement of raptorial function.

Although the carpals are not well preserved, there is evidence of a radiale, ulnare, and possibly a large distal carpal 1 (Figs. 68, 73D). The base of metacarpal 1 may be inset into the carpus. Both of these features are consistent with the carpus in basal sauropodomorphs (Sereno, 2007b). The well-preserved carpi in the theropods *Herrerasaurus* and *Eodromaeus* also have a substantial radiale and ulnare, but distal carpal 1 is small and metacarpal 1 is not inset into the carpus (Sereno, 1994; Martínez et al., 2011).

The twisted form of phalanx 1 of manual digit I in *Eoraptor* directs the tip of the ungual medially (Figs. 73D, 76A), a unique adaptation of the manus previously known only in large-bodied basal sauropodomorphs (Sereno, 2007b; Martínez, 2009). The function of the unusual basal sauropodomorph pollex is unknown. The relatively short length of the forelimb compared with the hind limb in *Eoraptor* (43%, see below) and metacarpal 3 compared with the forelimb (12%, see below) suggests that the manus and its modified pollex probably were not specialized for a locomotor function.

Digital proportions within the manus and the manual phalangeal formula, in general, resemble those in other basal dinosaurs in the retention of five manual digits and the reduction or elimination of the phalanges in manual digits IV and V (Table 12). In *Eoraptor*, metacarpals 4 and 5 are longer relative to metacarpal 3 than in *Herrerasaurus*, a theropod with a well-developed raptorial manus (Sereno, 1994). In later larger-bodied basal sauropodomorphs such as *Massospondylus* that were probably using the manus periodically in locomotion, metacarpals 4 and 5 become relatively even stronger than in *Eoraptor*, the former attaining a length 90% that of metacarpal 3 (Table 12).

**Limb Proportions**—In *Eoraptor*, forelimb length is 43% that of the hind limb (Fig. 93; Table 13). In this proportion, *Eoraptor* most closely resembles the basal theropod *Eodromaeus* (42%) among the genera tabulated for comparison. The large-bodied sauropodomorph *Adeopapposaurus* (54%), the basal theropod *Herrerasaurus* (47%), and the long-armed ornithischian *Heterodontosaurus* (50%) have forelimbs that are longer relative to their hind limbs (Table 13). Within the forelimb, the manus is particularly short in *Eoraptor* relative to forelimb length (12%; using metacarpal 3 as a proxy for manual length). In other taxa sampled, manual length is at least 14% or more of forelimb length.

The hind limb in *Eoraptor* has exactly the same proportions as *Saturnalia* (Table 13). In both genera, the tibia is slightly longer than the femur, and metatarsal 3 is slightly more than one-half femoral length. The larger-bodied *Adeopapposaurus* is typical for more derived basal sauropodomorphs, with a tibia slightly shorter than the femur (93%), as is also the case in *Herrerasaurus* (91%). *Eodromaeus* (106%) and particularly *Heterodontosaurus* (130%) have more cursorial proportions in the hind limb.

The picture that emerges from the limb proportions of *Eoraptor* is that it has a somewhat shorter forelimb and manus and less cursorial hind limb proportions than the contemporaneous, similar-sized theropod *Eodromaeus*. Individual long bones of adult specimens of these dinosaurs are distinguishable on the basis of their relative robustness; for long bones of equal length, *Eoraptor* has more robust long bones than *Eodromaeus*. The larger predator *Herrerasaurus* has a longer forearm and manus (as a proportion of forelimb length) than in *Eoraptor*, which along with trenchant claws is clearly an adaptation for grasping prey. In the hind limb, *Eoraptor* has exactly the same proportions as in *Saturnalia*, both of which would have been less fleet of foot than *Eodromaeus*.

## CONCLUSIONS

*Eoraptor lunensis* provides the most complete view so far of the skeletal anatomy of a dinosaur from the dawn of the dinosaur

era in mid-Carnian time (ca. 230 Ma). Although its skull and postcranial skeleton are remarkably similar to the contemporaneous theropod *Eodromaeus*, telltale signs of an entirely different way of life are preserved in its dentition, skull, and postcranial anatomy.

In the dentition, a suite of characters is related to the acquisition of a predominantly or wholly herbivorous diet. These include a gentle swelling of the crown base and rise of a rounded eminence leading to the crown apex in maxillary teeth, the suppression of crown recurvature, the greater inclination of denticles on the anterior crown margin, and the retraction of the first dentary tooth from the anterior end of the lower jaw. The lower jaws, which have closed in natural articulation in the holotypic skull, end short of the premaxillary arcade, suggesting that there may have been a small keratinous lower beak as in many large-bodied basal sauropodomorphs.

Elsewhere in the skull, there are features supportive of a relationship at the base of Sauropodomorpha, most notably the enlarged external naris, a distinctive linear pattern of vascular openings on the maxilla below the antorbital fossa, and the slender ventral process on the squamosal. The lower jaw has an intramandibular joint with limited mobility between the splenial and angular; the polarity of the sliding joint is similar to that seen in neotheropods (angular concave, splenial process convex). Other cranial sutures and joints do not support a particularly kinetic skull, which otherwise is notable for the retention of approximately 100 rudimentary palatal teeth and the presence of an unusual pterygoid-ectopterygoid joint along the posterior margin of the palate. *Pampadromaeus*, a similar-sized basal sauropodomorph from southeastern Brazil, preserves cranial bones that are strikingly similar to *Eoraptor*.

In the postcranium, the axial column and hind limbs remain remarkably primitive and have identical proportions to another similar-sized basal sauropodomorph from southeastern Brazil, *Saturnalia*. Differences between *Eoraptor* and the contemporaneous basal theropod *Eodromaeus* are most apparent in the skull, forelimb, and pelvis. Unlike *Eoraptor*, *Eodromaeus* has a promaxillary fenestra and laterally compressed, recurved, and serrated teeth. In the forelimb, *Eodromaeus* (and *Herrerasaurus*) have appressed the shafts of the radius and ulna and specialized the inner three manual digits for grasping. In contrast to *Eoraptor*, the manus in these forms is longer relative to other forelimb segments and is tipped with elongate penultimate phalanges and trenchant unguals. In the pelvic girdle, *Eoraptor* shows the classic broad pubic apron common to large-bodied basal sauropodomorphs, whereas *Eodromaeus* (and *Herrerasaurus*) have narrowed distal pubes, turning them posteriorly to form a pubic foot common to later theropods.

An outstanding adaptation in the manus of *Eoraptor* is the specialized 'twisted' pollex that characterizes all larger-bodied basal sauropodomorphs ('prosauropods'). The distal condyles of the first phalanx of the pollex are rotated approximately 35°, directing the ungual medially. The modified pollex is unlikely to have appeared as a locomotor adaptation, given that *Eoraptor* has a relatively short forelimb and has hind limb proportions (tibia slightly longer than the femur) that are consistent with bipedal posture at speed.

## ACKNOWLEDGMENTS

We are deeply indebted to C. Abraczkas for her skillful renderings from bones, and for the arrangement and labeling of all figures and final drafts of reconstructions. We thank S. Nesbitt and M. Carrano for their detailed reviews of the manuscript, which resulted in many improvements, and C. Abraczkas, J. Fronimos and E. Moacdieh for proofing portions

of the text and figures. We also thank R. Masek, I. Morrison, and W. Simpson for their skill in preparation and molding of the holotypic skeleton of *Eoraptor lunensis*, the Field Museum of Natural History and the Royal Ontario Museum for providing laboratory facilities, and the High-Resolution X-ray Computed Tomography Facility at The University of Texas at Austin for CT imaging. This research was supported by the National Science Foundation research grant BSR 8722586 (to P.C.S.), Petroleum Research Fund of the American Chemical Society (grant ACS-PRF 22637-G8) (to P.C.S.), the David and Lucile Packard Foundation (to P.C.S.), National Geographic Society (to P.C.S.), Whitten-Newman Foundation, and the Island Fund of the New York Community Trust (to P.C.S.), and Universidad Nacional de San Juan (to R.N.M. and O.A.A.).

## LITERATURE CITED

- Alcober, O. A., and R. N. Martínez. 2010. A new herrerasaurid (Dinosauria, Saurischia) from the Upper Triassic Ischigualasto Formation of northwestern Argentina. *ZooKeys* 63:55–81.
- Barrett, P. M., R. J. Butler, and S. J. Nesbitt. 2011. The roles of herbivory and omnivory in early dinosaur evolution. *Earth and Environmental Science Transactions of the Royal Society of Edinburgh* 101:383–396.
- Bittencourt, J. S., and A. W. A. Kellner. 2009. The anatomy and phylogenetic position of the Triassic dinosaur *Staurikosaurus pricei* Colbert, 1970. *Zootaxa* 2079:1–56.
- Boltt, R. E., and E. F. Ewer. 1964. The functional anatomy of the head of the puff adder, *Bitis arietans* (Merr.). *Journal of Morphology* 114:1–42.
- Bonaparte, J. F. 1966. Una nueva “fauna” Triásica de Argentina (Therapsida: Cynodontia, Dicynodontia). *Ameghiniana* 4:243–295.
- Bonaparte, J. F. 1976. *Pisanosaurus mertii* Casamiquela and the origin of the Ornithischia. *Journal of Paleontology* 50:808–820.
- Bonaparte, J. F., and A. W. Crompton. 1994. A juvenile probainognathid cynodont skull from the Ischigualasto Formation and the origin of mammals. *Museo Argentino de Ciencias Naturales “Bernardino Rivadavia” y Instituto Nacional de Investigación de las Ciencias Naturales* 5:1–12.
- Bonaparte, J. F., F. E. Novas, and R. A. Coria. 1990. *Carnotaurus sastrei* Bonaparte, the horned, lightly built carnosaur from the middle Cretaceous of Patagonia. *Contributions in Science, Natural History Museum of Los Angeles County* 416:1–42.
- Brochu, C. A. 2002. Osteology of *Tyrannosaurus rex*: insights from a nearly complete skeleton and high-resolution computed tomographic analysis of the skull. *Memoir of the Society of Vertebrate Paleontology* 7:1–138.
- Brown, B., and E. M. Schlaikjer. 1940. A new element in the ceratopsian jaw with additional notes on the mandible. *American Museum Novitates* 1092:1–13.
- Brusatte, S. L., S. J. Nesbitt, R. B. Irmis, R. J. Butler, M. J. Benton, and M. A. Norell. 2010. The origin and early radiation of dinosaurs. *Earth-Science Reviews* 101:68–100.
- Bryant, H. N., and A. P. Russell. 1993. The occurrence of clavicles within Dinosauria: implications for the homology of the avian furcula and the utility of negative evidence. *Journal of Vertebrate Paleontology* 13:171–184.
- Cabreira, S. F., C. L. Schultz, J. S. Bittencourt, M. B. Soares, D. C. Fortier, L. R. Silva, and M. C. Langer. 2011. New stem-sauropodomorph (Dinosauria, Saurischia) from the Triassic of Brazil. *Naturwissenschaften* 938:1035–1040.
- Carrano, M. T. 1999. What, if anything, is a cursor? Categories versus continua for determining locomotor habit in mammals and dinosaurs. *Journal of Zoology* 247:29–42.
- Carrano, M. T., and J. R. Hutchinson. 2002. Pelvic and hindlimb musculature of *Tyrannosaurus rex* (Dinosauria: Theropoda). *Journal of Morphology* 253:207–228.
- Casamiquela, R. M. 1967. Un nuevo dinosaurio ornitisquio Triásico (*Pisanosaurus mertii*; Ornithopoda) de la formación Ischigualasto, Argentina. *Ameghiniana* 4:47–64.
- Colbert, E. H. 1970. A saurischian dinosaur from the Triassic of Brazil. *American Museum Novitates* 2405:1–39.
- Colbert, E. H. 1989. The Triassic dinosaur *Coelophysis*. *Museum of Northern Arizona Bulletin* 57:1–160.
- Condon, K. 1987. A kinematic analysis of mesokinesis in the Nile monitor (*Varanus niloticus*). *Experimental Biology* 47:73–87.
- Cooper, M. R. 1981. The prosauropod dinosaur *Massospondylus carinatus* Owen from Zimbabwe: its biology, mode of life and phylogenetic significance. *Occasional Papers of the National Museum of Rhodesia* (B), *Natural Sciences* 6:689–840.
- Cox, C. B. 1965. New Triassic dicynodonts from South America, their origins and relationships. *Philosophical Transactions of the Royal Society of London, Series B* 248:457–516.
- Currie, B. S., C. E. Colombi, N. J. Tabor, T. C. Shipman, and I. P. Montañez. 2009. Stratigraphy and architecture of the Upper Triassic Ischigualasto Formation, Ischigualasto Provincial Park, San Juan, Argentina. *Journal of South American Earth Sciences* 27:74–87.
- Dzik, J. 2003. A beaked herbivorous archosaur with dinosaur affinities from the early Late Triassic of Poland. *Journal of Vertebrate Paleontology* 23:556–574.
- Ezcurra, M. D. 2010. A new early dinosaur (Saurischia: Sauropodomorpha) from the Late Triassic of Argentina: a reassessment of dinosaur origin and phylogeny. *Journal of Systematic Palaeontology* 8:371–425.
- Frazzetta, T. H. 1962. A functional consideration of cranial kinesis in lizards. *Journal of Morphology* 3:287–319.
- Frazzetta, T. H. 1986. The origin of amphikinesis in lizards: a problem in functional morphology and the evolution of adaptive systems; pp. 419–461 in M. K. Hecht, B. Wallace, and G. T. Prance (eds.), *Evolutionary Biology*. Plenum Press, New York.
- Galton, P. M. 1984. Cranial anatomy of the prosauropod dinosaur *Plateosaurus* from the Knollenmergel (Middle Keuper, Upper Triassic) of Germany. I. Two complete skulls from Trossingen/Württemberg, with comments on the diet. *Geologica et Palaeontologica* 18:139–171.
- Gauthier, J. 1986. Saurischian monophyly and the origin of birds; pp. 1–55 in K. Padian (ed.), *The Origin of Birds and the Evolution of Flight*. *Memoirs of the California Academy of Sciences* 8.
- Gilmore, C. W. 1909. Osteology of the Jurassic reptile *Camptosaurus*, with a revision of the species and of the genus, and descriptions of two new species. *Proceedings of the United States National Museum* 36:197–332.
- Gilmore, C. W. 1920. Osteology of the carnivorous Dinosauria in the United States National Museum, with special reference to the genera *Antrodemus* (*Allosaurus*) and *Ceratopsaurus*. *Bulletin of the United States National Museum* 110:1–159.
- Gore, R. 1993. Dinosaur. *National Geographic* 1993(January):2–53.
- Gradstein, F. M., and J. G. Ogg. 2009. The geologic time scale; pp. 26–34 in S. B. Hedges and S. Kumar (eds.), *The Timetree of Life*. Oxford University Press, Oxford, U.K.
- Harvey, E. B., H. E. Kaiser, and L. E. Rosenberg. 1968. *An Atlas of the Domestic Turkey (Meleagris gallopavo): Myology and Osteology*. U.S. Atomic Energy Commission, Germantown, Maryland, 247 pp.
- Holliday, C. M., and L. M. Witmer. 2008. Cranial kinesis in dinosaurs: intracranial joints, protractor muscles, and their significance for cranial evolution and function in diapsids. *Journal of Vertebrate Paleontology* 28:1073–1088.
- Huene, F. v. 1926a. The carnivorous Saurischia in the Jura and Cretaceous formations, principally in Europe. *Revista del Museo de La Plata* 29:35–167.
- Huene, F. v. 1926b. Vollständige Osteologie eines Plateosauriden aus dem schwäbischen Trias. *Geologische und Paläontologische Abhandlungen, Neue Folge* 15:129–179.
- Huene, F. v. 1932. Die fossile Reptil-Ordnung Saurischia, ihre Entwicklung und Geschichte. *Monographien zur Geologie und Paläontologie* 4:1–361.
- Iordansky, N. N. 2011. Cranial kinesis in lizards (Lacertilia): origin, biomechanics, and evolution. *Biology Bulletin* 38:868–877.
- Langer, M. C. 2003. The pelvic and hind limb anatomy of the stem-sauropodomorph *Saturnalia tupiniquim* (Late Triassic, Brazil). *PaleoBios* 23:1–30.
- Langer, M. C. 2004. Basal Saurischia; pp. 25–46 in D. B. Weishampel, P. Dodson, and H. Osmólska (eds.), *The Dinosauria*, second edition. University of California Press, Berkeley, California.

- Langer, M. C. 2005. Studies on continental Late Triassic tetrapod biochronology. II. The Ischigualastian and a Carnian global correlation. *Journal of South American Earth Sciences* 19:219–239.
- Langer, M. C., and M. J. Benton. 2006. Early dinosaurs: a phylogenetic study. *Journal of Systematic Palaeontology* 4:309–358.
- Langer, M. C., M. A. G. Franca, and S. Gabriel. 2007. The pectoral girdle and forelimb anatomy of the stem-sauropodomorph *Saturnalia tupiniquim* (Upper Triassic, Brazil); pp. 113–137 in P. M. Barrett and D. J. Batten (eds.), *Evolution and Paleobiology of Early Sauropodomorph Dinosaurs*. Special Papers in Palaeontology 77.
- Langer, M. C., F. Abdala, M. Richter, and M. J. Benton. 1999. A sauropodomorph dinosaur from the Upper Triassic (Carnian) of southern Brazil. *Comptes Rendus de l'Academie des Sciences, Paris, Sciences de la Terre et des Planètes* 329:511–517.
- Langer, M. C., M. D. Ezcurra, J. S. Bittencourt, and F. E. Novas. 2010. The origin and early evolution of dinosaurs. *Biological Reviews* 85:55–110.
- Long, R. A., and P. A. Murry. 1995. Late Triassic (Carnian and Norian) tetrapods from the southwestern United States. *Bulletin of the New Mexico Museum of Natural History and Science* 4:1–254.
- Madsen, J. H., Jr. 1976. *Allosaurus fragilis*: a revised osteology. *Bulletin of the Utah Geological and Mineral Survey* 109:1–163.
- Marshall Faux, C., and K. Padian. 2007. The opisthotonic posture of vertebrate skeletons: postmortem contraction or death throes? *Paleobiology* 33:201–226.
- Martínez, R. N. 2009. *Adeopapposaurus mognai*, gen. et sp. nov. (Dinosauria: Sauropodomorpha), with comments on adaptations of basal Sauropodomorpha. *Journal of Vertebrate Paleontology* 29:142–164.
- Martínez, R. N., and O. A. Alcober. 2009. A basal sauropodomorph (Dinosauria: Saurischia) from the Ischigualasto Formation (Triassic, Carnian) and the early evolution of Sauropodomorpha. *PLoS ONE* 4:e4397. doi: 4310.1371/journal.pone.0004397.
- Martínez, R. N., and C. A. Forster. 1996. The skull of *Probesodon sanjuanensis*, sp. nov., from the Late Triassic Ischigualasto Formation of Argentina. *Journal of Vertebrate Paleontology* 16:285–291.
- Martínez, R. N., C. L. May, and C. A. Forster. 1996. A new carnivorous cynodont from the Ischigualasto Formation (Late Triassic, Argentina), with comments on eucynodont phylogeny. *Journal of Vertebrate Paleontology* 16:271–284.
- Martínez, R. N., P. C. Sereno, O. A. Alcober, C. E. Colombi, P. R. Renne, I. P. Montañez, and B. S. Currie. 2011. A basal dinosaur from the dawn of the dinosaur era in southwestern Pangaea. *Science* 331:206–210.
- Martínez, R. N., C. Apaldetti, O. A. Alcober, C. Colombi, P. C. Sereno, E. Fernandez, P. Santi Malnis, G. Correa, and D. Abelín. 2013. Vertebrate succession in the Ischigualasto Formation; pp. 10–30 in P. C. Sereno (ed.), *Basal sauropodomorphs and the vertebrate fossil record of the Ischigualasto Formation (Late Triassic: Carnian–Norian) of Argentina*. Society of Vertebrate Paleontology Memoir 12.
- Nesbitt, S. J. 2011. The early evolution of archosaurs: relationships and the origin of major clades. *Bulletin of the American Museum of Natural History* 352:1–292.
- Nesbitt, S. J., N. D. Smith, R. B. Irmis, A. H. Turner, A. Downs, and M. A. Norell. 2009. A complete skeleton of a Late Triassic saurischian and the early evolution of dinosaurs. *Science* 326:1530–1533.
- Norell, M. A., and P. J. Makovicky. 1999. Important features of the dromaeosaurid skeleton II: information from newly collected specimens of *Velociraptor mongoliensis*. *American Museum Novitates* 3282:1–45.
- Novas, F. E. 1994. New information on the systematics and postcranial skeleton of *Herrerasaurus ischigualastensis* (Theropoda: Herrerasauridae) from the Ischigualasto Formation (Upper Triassic) of Argentina. *Journal of Vertebrate Paleontology* 13:400–423.
- Ostrom, J. H. 1969. Osteology of *Deinonychus antirrhopus*, an unusual theropod from the Lower Cretaceous of Montana. *Bulletin of the Peabody Museum of Natural History* 30:1–165.
- Owen, R. 1842. Report on British fossil reptiles. Report of the British Association for the Advancement of Science 11 (for 1841):60–294.
- Padian, K. 1986. On the type material of *Coelophys* (Saurischia: Theropoda), and a new specimen from the Petrified Forest of Arizona (Late Triassic, Chinle Formation); pp. 45–60 in K. Padian (ed.), *The Beginning of the Age of Dinosaurs*. Cambridge University Press, Cambridge, U.K.
- Padian, K., and C. L. May. 1993. The earliest dinosaurs; pp. 379–381 in S. G. Lucas and M. Morales (eds.), *The Nonmarine Triassic*. New Mexico Museum of Natural History and Science, Albuquerque, New Mexico.
- Raath, M. A. 1977. The anatomy of the Triassic theropod *Syntarsus rhodesiensis* (Saurischia: Podokesauridae) and a consideration of its biology. Ph.D. dissertation, Rhodes University, Grahamstown, South Africa, 233 pp.
- Reig, O. 1963. La presencia de dinosaurios sauriscuios en los “Estratos de Ischigualasto” (Mesotriásico superior) de las provincias de San Juan y La Rioja (República Argentina). *Ameghiniana* 3:3–20.
- Rieppel, O. 1979. A functional interpretation of the varanid dentition (Reptilia, Lacertilia, Varanidae). *Gegenbaurs Morphologie Jahrbuch* 125:797–817.
- Rogers, R. R., C. C. Swischer III, P. C. Sereno, A. M. Monetta, and R. N. Martínez. 1993. The Ischigualasto tetrapod assemblage (Late Triassic, Argentina) and  $^{40}\text{Ar}/^{39}\text{Ar}$  dating of dinosaur origins. *Science* 260:794–797.
- Romer, A. S. 1956. *Osteology of the Reptilia*. University of Chicago Press, Chicago, Illinois, 772 pp.
- Rowe, T. 1989. A new species of the theropod dinosaur *Syntarsus* from the Early Jurassic Kayenta Formation of Arizona. *Journal of Vertebrate Paleontology* 9:125–136.
- Sampson, S. D., and L. M. Witmer. 2007. Craniofacial anatomy of *Majungasaurus crenatissimus* (Theropoda: Abelisauridae) from the Late Cretaceous of Madagascar. *Memoir of the Society of Vertebrate Paleontology* 8:32–102.
- Santa Luca, A. P. 1980. The postcranial skeleton of *Heterodontosaurus tucki* (Reptilia, Ornithischia) from the Stormberg of South Africa. *Annals of the South African Museum* 79:159–211.
- Seeley, H. G. 1887. The classification of the Dinosauria. *Proceedings of the Royal Society London* 43:165–171.
- Sereno, P. C. 1991. *Lesothosaurus*, “fabrosaurids,” and the early evolution of Ornithischia. *Journal of Vertebrate Paleontology* 11:168–197.
- Sereno, P. C. 1994. The pectoral girdle and forelimb of the basal theropod *Herrerasaurus ischigualastensis*. *Journal of Vertebrate Paleontology* 13:425–450.
- Sereno, P. C. 1997. The origin and evolution of dinosaurs. *Annual Review of Earth and Planetary Sciences* 25:435–489.
- Sereno, P. C. 1999. The evolution of dinosaurs. *Science* 284:2137–2147.
- Sereno, P. C. 2007a. The phylogenetic relationships of early dinosaurs: a comparative report. *Historical Biology* 19:145–155.
- Sereno, P. C. 2007b. Basal Sauropodomorpha: historical and recent phylogenetic hypotheses, with comments on *Ammosaurus major* (Marsh, 1889); pp. 261–289 in P. M. Barrett and D. J. Batten (eds.), *Evolution and Paleobiology of Early Sauropodomorph Dinosaurs*. Special Papers in Palaeontology 77.
- Sereno, P. C. 2012. Taxonomy, morphology, masticatory function and phylogeny of heterodontosaurid dinosaurs. *ZooKeys* 226:1–225.
- Sereno, P. C., and A. B. Arcucci. 1994a. Dinosaurian precursors from the Middle Triassic of Argentina: *Marasuchus lilloensis*, gen. nov. *Journal of Vertebrate Paleontology* 14:53–73.
- Sereno, P. C., and A. B. Arcucci. 1994b. Dinosaurian precursors from the Middle Triassic of Argentina: *Lagerpeton chanarensis*. *Journal of Vertebrate Paleontology* 13:385–399.
- Sereno, P. C., and Z. Dong. 1992. The skull of the basal stegosaur *Huayangosaurus taibaii* and a cladistic diagnosis of Stegosauria. *Journal of Vertebrate Paleontology* 12:318–343.
- Sereno, P. C., and F. E. Novas. 1992. The complete skull and skeleton of an early dinosaur. *Science* 258:1137–1140.
- Sereno, P. C., and F. E. Novas. 1994. The skull and neck of the basal theropod *Herrerasaurus ischigualastensis*. *Journal of Vertebrate Paleontology* 13:451–476.
- Sereno, P. C., C. A. Forster, R. R. Rogers, and A. M. Monetta. 1993. Primitive dinosaur skeleton from Argentina and the early evolution of Dinosauria. *Nature* 361:64–66.
- Sill, W. D. 1974. The anatomy of *Saurosuchus galilei* and the relationships of the rauisuchid thecodonts. *Bulletin of the Museum of Comparative Zoology* 146:317–362.

- Smith, K. K., and W. L. Hylander. 1985. Strain gauge measurement of mesokinetic movement in the lizard *Varanus exanthematicus*. *Journal of Experimental Biology* 114:53–70.
- Sues, H.-D., R. R. Reisz, S. Hinic, and M. A. Raath. 2004. On the skull of *Massospondylus carinatus* Owen, 1854 (Dinosauria: Sauropodomorpha) from the Elliot and Clarens Formations (Lower Jurassic) of South Africa. *Annals of the Carnegie Museum* 73:239–257.
- Sullivan, C., D. W. E. Hone, X. Xu, and F. Zhang. 2010. The asymmetry of the carpal joint and the evolution of wing folding in maniraptoran theropod dinosaurs. *Proceedings of the Royal Society B* 277:2027–2033.
- Tykoski, R. S. 2005. Anatomy, ontogeny, and phylogeny of coelophysoid theropods. Ph.D. dissertation, University of Texas, Austin, Texas, 553 pp.
- Tykoski, R. S., and T. Rowe. 2004. Ceratosauria; pp. 47–70 in D. B. Weishampel, P. Dodson, and H. Osmólska (eds.), *The Dinosauria*, second edition. University of California Press, Berkeley, California.
- Versluys, J. 1910. Streptostylie bei Dinosauriern. *Zoologische Jahrbuch Abhandlungen für Anatomie* 30:177–258.
- Versluys, J. 1912. Das Streptostylie-Problem und die bewegung im Schädel bei Sauropsida. *Zoologische Jahrbuch, Supplement* 15 2:545–716.
- Welles, S. P. 1984. *Dilophosaurus wetherilli* (Dinosauria, Theropoda) osteology and comparisons. *Palaeontographica, Abteilung A* 185:85–180.
- Wilson, J. A. 2006. Anatomical nomenclature of fossil vertebrates: standardized terms or ‘lingua franca’? *Journal of Vertebrate Paleontology* 26:511–518.
- Wilson, J. A. 1999. A nomenclature for vertebral laminae in sauropods and other saurischian dinosaurs. *Journal of Vertebrate Paleontology* 19:639–653.
- Wilson, J. A. 2011. Anatomical terminology for the sacrum of sauropod dinosaurs. University of Michigan Museum of Paleontology, Contributions 32:59–69.
- Wilson, J. A., M. D. D’Emic, T. Ikejiri, E. M. Moacdieh, and J. A. Whitlock. 2011. A nomenclature for vertebral fossae in sauropods and other saurischian dinosaurs. *PLoS ONE* 6:e17114. doi: 17110.11371/journal.pone.0017114.
- Witmer, L. M. 1990. The craniofacial air sac system of Mesozoic birds (Aves). *Zoological Journal of the Linnean Society* 100:327–378.
- Witmer, L. M. 1997. The evolution of the antorbital cavity of archosaurs: a study in soft-tissue reconstruction in the fossil record with an analysis of the function of pneumaticity. *Memoir of the Society of Vertebrate Paleontology* 3:1–73.
- Zanno, L. E., and P. J. Makovicky. 2011. Herbivorous ecomorphology and specialization patterns in theropod dinosaur evolution. *Proceedings of the National Academy of Sciences of the United States of America* 108:232–237.

Submitted January 8, 2013; revisions received June 8, 2013; accepted June 23, 2013.

Handling editor: Jeffrey Wilson.